AD-772 065

ELECTROMAGNETIC PULSE SOUNDING FOR GEOLOGICAL
SURVEYING WITH APPLICATION IN ROCK MECHANICS
AND THE RAPID EXCAVATION PROGRAM

OHIO STATE UNIVERSITY

PREPARED FOR
ADVANCED RESEARCH PROJECTS AGENCY
BUREAU OF MINES

SEPTEMBER 1973

ELECTROMAGNETIC PULSE SOUNDING FOR GEOLOGICAL SURVEYING
WITH APPLICATION IN ROCK MECHANICS AND THE
RAPID EXCAVATION PROGRAM

D.L. Moffatt
R.J. Puskar
L. Peters, Jr.

AD772065

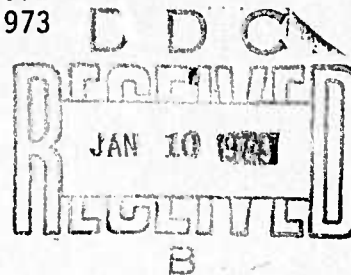**The Ohio State University**

ElectroScience Laboratory

Department of Electrical Engineering
Columbus, Ohio   43212
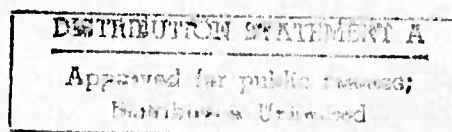
Final Technical Report 3408-2

September 1973

The views and conclusions contained in this document are those
of the authors and should not be interpreted as necessarily
representing the official policies, either expressed or implied,
of the Advanced Research Projects Agency or the U.S. Government.

U. S. Dept. of Interior
Bureau of Mines
Advanced Research Projects Agency
Denver, Colorado 80225

DOCUMENT CONTROL DATA - R & D

Security classification of title, body of abstract and indexing annotation must be entered when the overall report is classified

1. ORIGINATING ACTIVITY (Corporate author)	2a. REPORT SECURITY CLASSIFICATION
ElectroScience Laboratory Department of Electrical Engineering, The Ohio State University, Columbus, Ohio 43212	Unclassified
	2b. GROUP

3. REPORT TITLE

ELECTROMAGNETIC PULSE SOUNDING FOR GEOLOGICAL SURVEYING WITH APPLICATION IN ROCK MECHANICS AND THE RAPID EXCAVATION PROGRAM

4. DESCRIPTIVE NOTES (Type of report and inclusive dates)

Final Technical Report

5. AUTHOR(S) (First name, middle initial, last name)

Moffatt, D.L., Puskar, R.J., Peters, L., Jr.

6. REPORT DATE	7a. TOTAL NO. OF PAGES	7b. NO. OF REFS
September 1973	169	20

8a. CONTRACT OR GRANT NO.	9a. ORIGINATOR'S REPORT NUMBER(S)
H0230009	
b. PROJECT NO.	ElectroScience Laboratory 3408-2
c.	9b. OTHER REPORT NO(S) (Any other numbers that may be assigned this report)
d.	

10. DISTRIBUTION STATEMENT

Distribution of this document is unlimited.

11. SUPPLEMENTARY NOTES	12. SPONSORING MILITARY ACTIVITY
	Advanced Research Projects Agency 1400 Wilson Blvd. Arlington, Va. 22209

13. ABSTRACT

Research on Contract H0230009 for the period 1 September 1972 to 6 August 1973 is summarized. A full scale version of an electromagnetic pulse sounding probe is described with attendent experimental data. Propagation and scattering measurements in limestone and dolomite media are presented. The scattering measurements are for targets consisting of faults, joints and lithologic contrasts in a dolomite medium. Measured frequency-dependent constitutive parameters for the limestone and dolomite media are given and realistic pulse propagation calculations using these data are shown. Probe calibration procedures are described and illustrated.

14	KEY WORDS	LINK A		LINK B			
		ROLE	WT	ROLE	WT		
	Electromagnetic						
	Pulse						
	Subsurface						
	Sounder						
	Rock						

1C

ELECTROMAGNETIC PULSE SOUNDING FOR GEOLOGICAL SURVEYING
WITH APPLICATION IN ROCK MECHANICS AND THE
RAPID EXCAVATION PROGRAM

Final Technical Report 3408-2

ElectroScience Laboratory
The Ohio State University

D D C

JAN 10 1974

B

/d

ABSTRACT

Research on Contract H0230009 for the period 1 September 1972 to 6 August 1973 is summarized. A full scale version of an electromagnetic pulse sounding probe is described with attendent experimental data. Propagation and scattering measurements in limestone and dolomite media are presented. The scattering measurements are for targets consisting of faults, joints and lithologic contrasts in a dolomite medium. Measured frequency-dependent constitutive parameters for the limestone and dolomite media are given and realistic pulse propagation calculations using these data are shown. Probe calibration procedures are described and illustrated.

TABLE OF CONTENTS

I. TECHNICAL REPORT SUMMARY

A unique electromagnetic pulse sounding probe for the detection, diagnosis and identification of geological and man-made anomalies within the earth is being developed. The immediate application of the probe is as a hazard detection device in advance of hard rock rapid tunneling operations. Numerous other applications in geophysical exploration, geophysical prospecting, mining, agriculture, civil engineering, earthquake engineering and archeology can be envisioned. While applications in geophysical prospecting and mining are apparent, many other more subtle applications appear to be feasible. Location of archaeological features in soil prior to digging would save the archaeologist a great deal of labor. Evaluating the effectiveness of grouting procedures in construction of dams or nuclear power plants would save much time and money. Detection of and the monitoring of sub surface fault structures would present new information to the earthquake engineer. The probe is basically an active remote sensor capable of interrogating a material medium from the surface of the medium. Within limits imposed by the electrical properties of the medium in question, the probe has both a detection and identification capability and this capability suggests an ever-widening range of applications. The identification capability of the system stems from the use of a periodic video-type pulse as the interrogating signal. This basically means that the spectrum of the returned signal from the target spans a sufficient frequency range to permit classification. The system can also be operated in two modes, one of which does not "see" symmetrical targets such as the air-rock interface. Thus the horrendous difficulties caused by layering in seismic or acoustical work can be avoided. At the same time, the layering can be "seen" using the system in its other mode.

The main goals of the program during this contract period are: 1) to obtain full scale field measurements of the type of geological hazards likely to be encountered in deep tunneling such as faults, joints and lithologic contrasts, 2) to devise techniques for estimating in situ the frequency-dependent electrical properties of a rock medium and 3) to complete theoretical analyses and computer programs which will permit realistic calculations of pulse propagation and pulse scattering by geological-type targets.

This Final Technical Report has four main sections covering design of the antenna geometries and computer control of the measurements, realistic pulse propagation calculations and measurements, system calibration and experimental target response measurements. The most interesting data, the target response measurements, are presented in Section VII. Here successful electromagnetic pulse soundings of

1

faults, joints and lithological contrasts in dolomite, a large cylindrical void in limestone, and selected measurements of man-made targets in the overburden are given. All of the remote field measurements have been made in limestone or dolomite quarries. Dolomite and limestone are not igneous-type rocks but their electrical properties are quite similar to those of an igneous rock such as granite. The primary difference is a reduction in conductivity for the igneous rock in so far as the characteristics of an electromagnetic probe are concerned. To make the measurements in igneous rock would have required prohibitive travel from our Ohio site. It is felt however that at this stage the system is fully ready for demonstration in a true igneous-rock tunnel and that the experimental results reported herein fully justify this conclusion. Supplemental funding for igneous rock measurements was requested but was rejected.

The deepest reported measurement is 45 feet for a lithologic contrast in dolomite (conductivity $\approx 10^{-3}$ mhos/meter). This does not necessarily represent the system limit however. For an igneous rock medium at great depths where conductivities of the order of 10^{-4} to 10^{-6} mhos/meter can be anticipated, it is felt that the present system may well meet the suggested 200 foot range.

In summary, remarkable progress has been achieved in the development of an electromagnetic video pulse sounding system. Measurements have been made, in the field, of those geological anomalies defined to be of interest for a hazard detection device in hard rock tunneling. At the same time, the operation and performance of the system and certain preliminary measurements suggest a number of other applications many of which can be related to national needs. The remote sensing of subterranean features is a difficult task regardless of the sensor type or potential application. The results in this report strongly support arguments that electromagnetic sensors have not yet been fully exploited and further research in this area would prove fruitful.

II.   PURPOSE

A unique electromagnetic pulse sounding system using periodic video pulse signals for the detection and diagnosis of hazards in advance of rapid tunneling operations is being developed. The tunneling is assumed to be in hard igneous-type rock and the hazards considered are planar and include faults, joints and lithologic boundaries of infinite extent. The research program during this contract period has the following objectives:

1) Obtain full scale electromagnetic pulse soundings of faults, gouge-filled faults, joints and lithologic contrasts in a rock medium with electromagnetic properties similar to hard rock. These measurements were made in Plum Run Quarry near Peebles, Ohio approximately 120 miles from the ElectroScience Laboratory. The quarry rock is basically dolomite and the above mentioned geological features exist in abundance. The quarry rock is a soft rock medium but because of the abundance of the desired geological features has been studied for economic reasons. The essential difference between hard and soft rock media is the difference in the conductivity which in essense implies that the operating range in hard rock will be increased.

2) Construct a smaller and lighter version of the full scale probe (antennas) geometry which can be easily supported against a vertical rock face. The smaller probe will greatly facilitate certain of the measurements in 1 and at the same time permit some experimentation with end terminations and synthetic aperture-type signal processing.

3) Obtain estimates of the frequency-dependent relative dielectric constant and conductivity of the dolomite quarry rock via in situ video pulse propagation measurements. Certain measurements of this type are useful in interpretation of measured time and spectral target signatures.

4) Complete the theoretical analysis and computer programs for adding an air-rock interface correction to a previously developed computer program for an arbitrary wire antenna (bare, insulated or partially insulated) in an infinite, lossy, homogeneous medium. This result will add a system calibration and theoretical probe design capability to an existing capacity for realistic (frequency-dependent constitutive parameters) pulse propagation calculations.

5) Devise new signal processing schemes for electromagnetic pulse sounding data to enhance the detection and identification capabilities of the system. Basically, improved estimates of the target's impulse response waveform are to be obtained. Given the calibration capability listed in objective 4, it will then be possible to calculate the transfer function of the probe from measurements of a known target geometry. Improved impulse response waveforms will then be possible.

3

III. INTRODUCTION

Historically, electrical or electromagnetic methods in geophysical applications have been restricted to very low frequencies (< 5000 Hz) because of the severe attenuation and dispersion effects of the medium (the earth). There are, however, numerous practical subsurface problems where either the required penetration depth or the electrical properties of the medium make the use of electromagnetic video pulse signals feasible. These problem areas span applications in civil and mining engineering, agriculture, water resources, archeology, quarrying and hard rock tunneling. Basically, the very broad spectral content of video pulse signals yields an unprecedented diagnostic and identification capability. No single study can hope to explore all the ramifications of this capability. The results of this study, however, firmly establish the use of electromagnetic video pulse interrogating signals as a viable new tool in subsurface applications.

In recent years, numerous papers on the theory of transient electromagnetic sounding have been published[1-2]. Most of the theory has been developed by assuming a time harmonic, single frequency solution, then applying Fourier Transform theory to obtain the transient fields. It is a transient electromagnetic method that is described in this report, in which the transient signal is a short periodic video-type pulse with frequency content spanning a wide spectral range.

The choice of a periodic video pulse as the interrogating signal is based on the fact that "target" identification is an ultimate system objective. Since tremendous advances have been made in the areas of target identification in free space via radar interrogation over a proper spectral range[3-4], it follows that data spanning as wide a spectral range as possible is essential. A broadband video pulse is one effective means of obtaining the spectral information.

Previous successful research at this laboratory in underground remote sensing for the detection of shallow dielectric objects[5-6] and for surveying underground water and moisture content of the soil[7] has been reported. The present work is concentrated on the detection of hazards in advance of rapid tunneling operations in hard rock[8-11], and the results have application in pipe detection, mining and quarrying as well as hazard detection in tunneling. Numerous other applications can be envisioned in pipe laying, engineering geology, and geophysical exploration. To illustrate certain of these applications, target response data are reported herein for metal and dielectric cylinders in soil, a metal cylinder and a cylindrical void (tunnel) in limestone, and faults, joints, soil-rock interface, and a lithologic contrast in dolomite.

4

Estimates of the frequency dependent dielectric constant and conductivity have been obtained for these media, and are compared to existing tabulated data found in the literature. A theoretical analysis and calibration of the system is presented including an approximation to the radiated fields of the antenna lying on a lossy half-space. Pulse propagation, attenuation, and dispersion in a dissipative medium are also analyzed to obtain data processing methods that maximize the sensitivity of the system to subsurface targets.

An alternative system for deeper probing (hundreds of meters) in low loss media has been developed using a pulse modulated S-band signal and a pair of dielectric loaded horns. Since the actual power output of the video pulse generator is rather low, a means of coupling energy at higher power levels to the medium at a single frequency or a narrow band of frequencies is desired. Amplification of the pulse modulated signal provides this high power, thereby increasing the depth penetration, provided the attenuation at the operating frequency is not excessive.

5

IV. SUBSURFACE PROBE SYSTEM

A. Present Configuration

A block diagram of the video pulse subsurface probing system is shown in Fig. 1, where Fig. 1a is the system with the computer on-line and in control of the measurement, and Fig. 1b is the remote (field) measurement configuration[12]. When the computer is on-line, time domain measurements can be quickly recorded and stored via teletype control of the computer. Remote measurements, however, must be recorded on magnetic tape in the field, then processed at a later time.
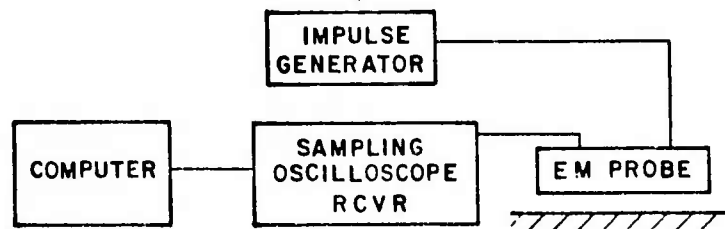
(a) BASIC LABORATORY MEASURMENT SYSTEM
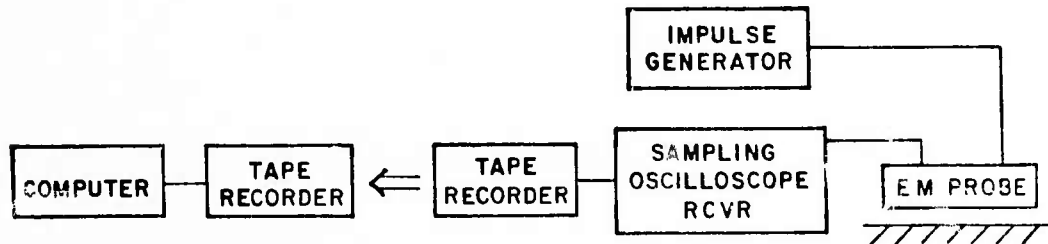
(b) BASIC FIELD MEASURMENT SYSTEM

Fig. 1. Block diagram of electromagnetic pulse
sounding system.

6

Two modes of system operation are possible; 1) direct reflection mode, in which a single antenna acts as both transmitter and receiver, and 2) the orthogonal mode, in which one dipole antenna is used as the transmitter and a second antenna, oriented orthogonally to the transmitter, is used as the receiver. In both modes, the antenna is designed to operate lying flush on the surface of the medium. Figure 2 shows the two antennas currently being used, oriented for orthogonal mode operation. In the direct reflection mode, only one of the dipole arms of either antenna is used. Antenna design will be discussed in more detail in the next section. The large antenna (28 foot dipole) of Fig. 2a consists of two transmission line fed, orthogonally oriented dipoles lying on the surface of the medium. The feed system consists of RG-9 coaxial cable, a broadband balun (50:200Ω unbalanced to balanced transformer) which can be viewed as a broadband impedance matching network and a short length of 300Ω twin lead transmission line. Each dipole arm consists of two linear conducting elements whose spacing is used to control the characteristic impedance of the dipole. Reflections from the ends of the dipole arms are suppressed by a capacitive type coupling provided by solid 4' x 8' conducting sheets at the ends of the dipole arms. This antenna can also be matched to a soil medium by another method. Ground rods driven into the ground at the ends of the dipole arms are a very effective means of controlling end reflections.

The smaller probe of Fig. 2b was originally designed to match a soil medium, where the angle of the V-shaped arms is related to the characteristic impedance of the dipole at the feed point. Modification of the probe for a rock medium simply consisted of lying the probe on approximately 2" of hairflex broadband absorber. The effect of the absorber is to attenuate some of the energy propagating out to the ends of the dipole, thereby reducing the reflections from the antenna ends, and minimizing clutter in the time window of interest.

Both probes find useful application in different situations. While the large probe is a better electrical match to a rock medium, and achieves greater depth penetration due to its longer length, it may not always be practical or possible to use in a small working area. The small probe, on the other hand, can easily be used in a small working area, particularly in the direct reflection mode, and is better suited for use in synthetic aperture-type processing schemes.

Two different interrogating pulses are also currently being used with the system, a 50 volt, 45 nsec pulse (Hewlitt-Packard model 214-A generator) with a 10 KHz rep rate and 15 nsec rise time, and a 1000 volt, 1 nsec pulse (Ikor model R-100) with a rep rate of 250 Hz, and a 150 psec rise time. The bandwidth of the 1000 volt pulse is so wide (D.C. to 10 GHz) that the actual power output at any given frequency is rather low, being roughly 20 mW/MHz. The power output of the H.P. generator on the other hand, is 110 mW/MHz; but contains very little energy above 60 MHz. The pulses and their
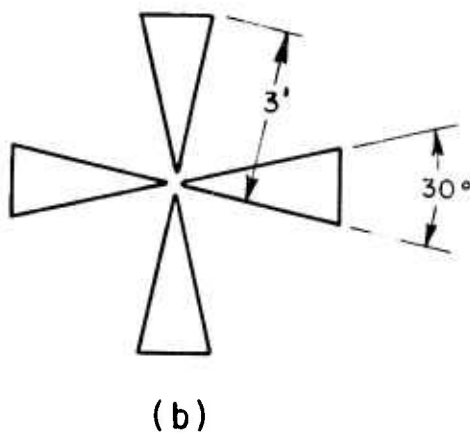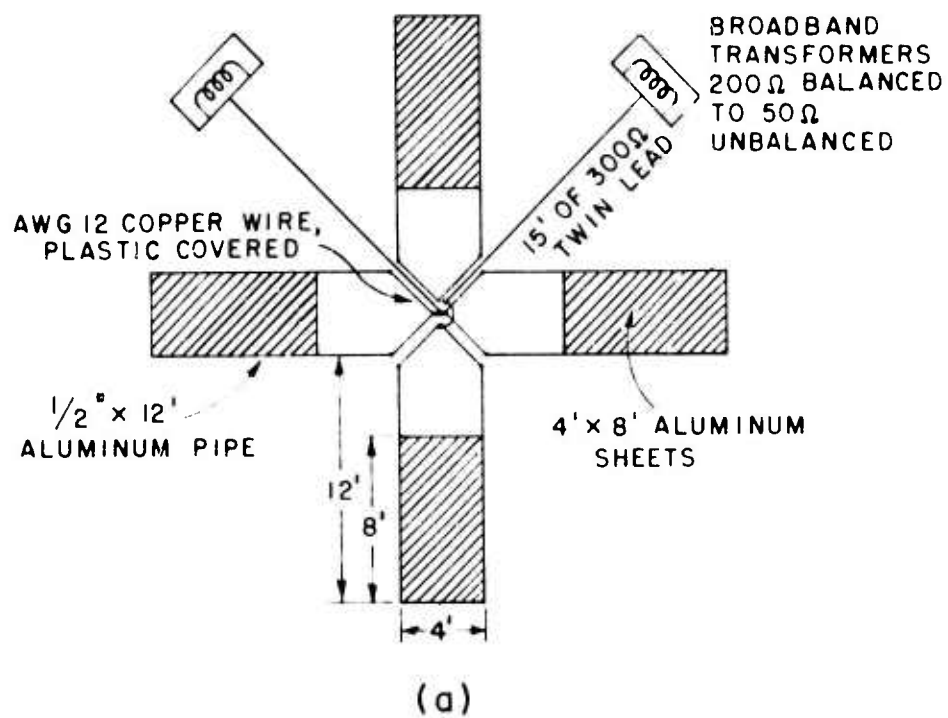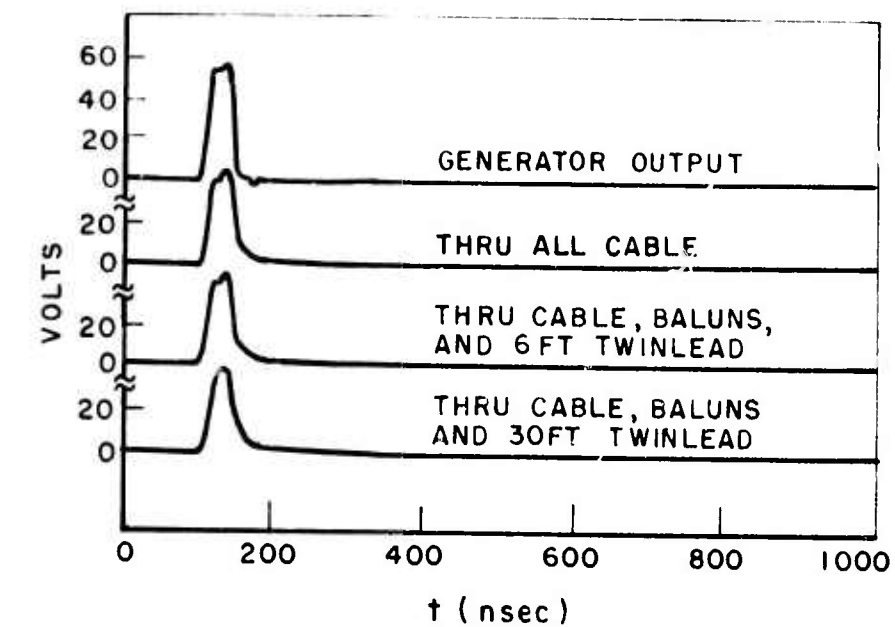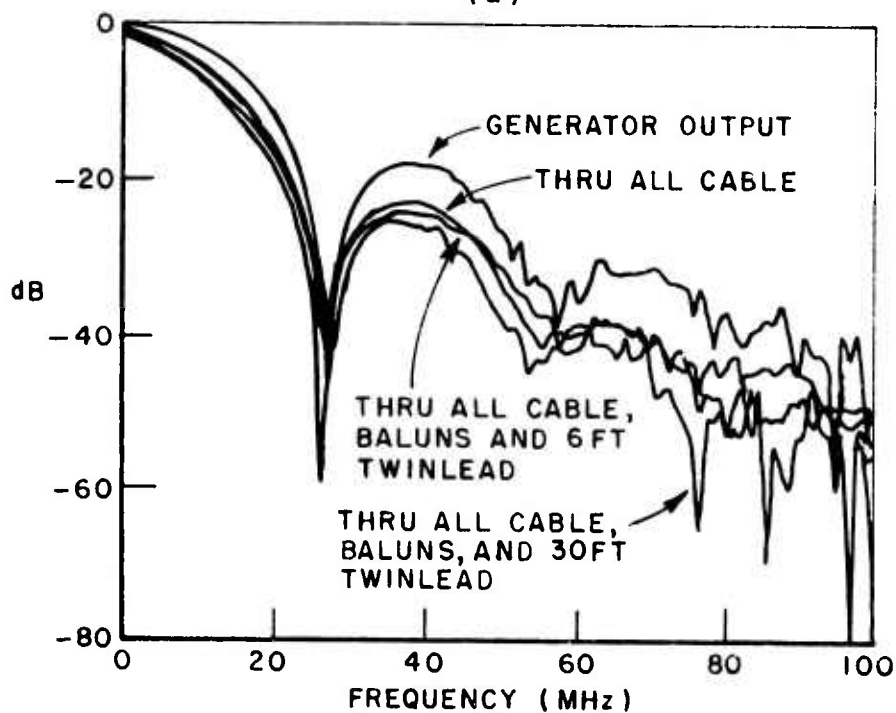
7

BROADBAND
TRANSFORMERS
200 Ω BALANCED
TO 50 Ω
UNBALANCED

15' OF 300 Ω TWIN LEAD

AWG 12 COPPER WIRE,
PLASTIC COVERED

½" × 12'
ALUMINUM PIPE

4' × 8' ALUMINUM
SHEETS

12'

8'

4'

(a)

3'

30°

(b)

Fig. 2.   (a)   Large electromagnetic probe.
          (b)   Small electromagnetic probe.

8

Fig. 3. Hewlett-Packard (H.P.) input pulse and effect
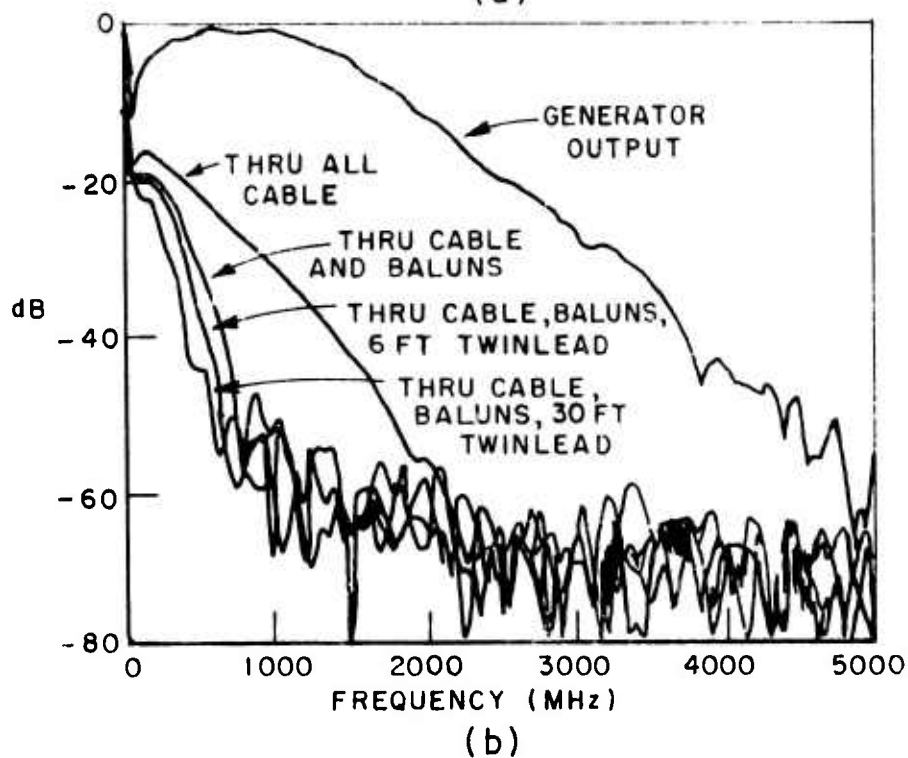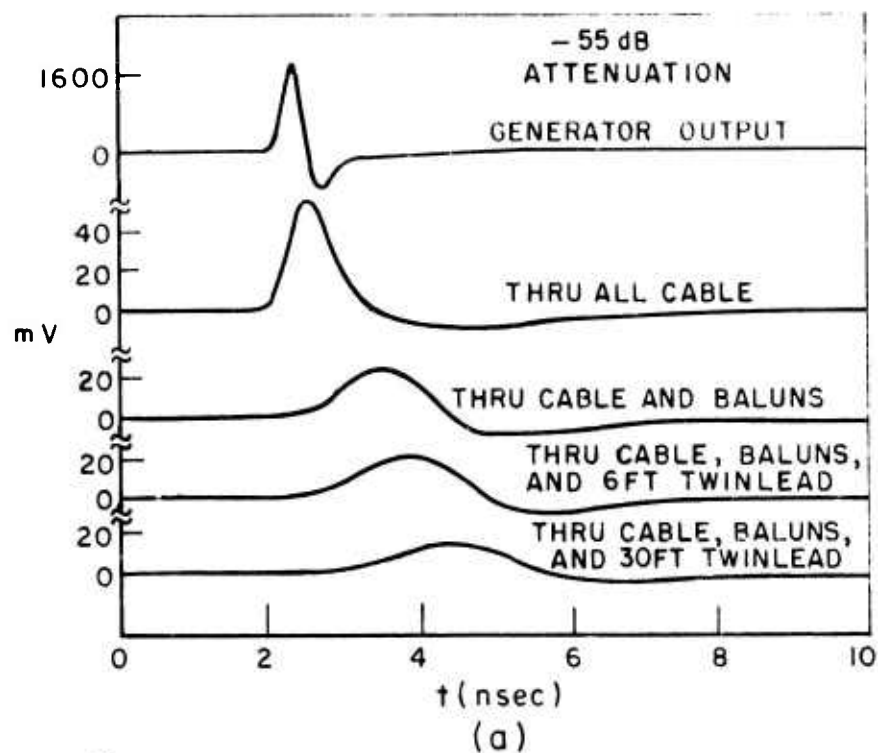of the feed system.
(a) time domain waveforms
(b) amplitude spectra.

9

Fig. 4. Ikor input pulse and effect of the feed system.
(a) time domain waveforms
(b) amplitude spectra.

10

respective amplitude spectra are shown in Figs. 3 and 4.* The figures also show the effect of the feed system on the input pulses and spectra indicating that the cable is the most detrimental component of the feed system. The nominal length of the cables is 400 feet. In some situations the cable length could be reduced to 10 feet, but in many situations, the entire length is necessary. For convenience, the entire length was used for most of the measurements. The severe cable losses indicated by the Ikor waveforms of Fig. 4 are more excessive than one would normally encounter (see Reference [11]) because the cable had been exposed to adverse weather conditions on several occasions. Note that over the low-frequency range of the H.P. pulse, the effect of the baluns and twin lead is negligible, but for the high frequency content of the Ikor pulse, the losses of the twin lead and baluns do become significant. Original probe design called for 15 feet of twin lead for each dipole (bottom waveform), simply to isolate the balun response from the antenna and target response of the large antenna. The twin lead was shortened as much as possible without seriously affecting the coupling and the time window to a total length of approximately 6 feet. The time and frequency domain waveforms thru 6 feet of twin lead are shown in the second waveform from the bottom in Figs. 3a and 4a. Many of the earlier measurements presented herein were recorded with the 30 foot length of twin lead. The amplitude spectra of Figs. 3b and 4b are normalized to the magnitude of the peak harmonic of the respective input pulses.

The twin lead problem has recently been greatly simplified by using a shielded twin lead, consisting of two 72Ω coaxial cables with their outer shields connected. The center conductors are employed as the two elements of the twin lead. The impedance of this arrangement is roughly 144Ω, which is still a mismatch from the 200Ω balun, but the reflection coefficient is reduced from 1/5 to roughly 1/6, and the attenuation is greatly reduced. Using 100Ω cables connected in this manner would eliminate the mismatch. Unfortunately, only the last set (VII-D) of the measurements presented in this report were recorded using this new twin lead.

In the same way that each probe finds application in different situations, each pulse also finds application in different situations. The 1000 volt 1 nsec pulse, for example, is more useful in probing for objects near the surface than the 50 volt, 45 nsec pulse, simply because of its greater resolution capability. The resolution of the Ikor pulse (1000 volt, 1 nsec) is roughly

---

*Throughout this report, phase spectra are only presented in the text when they are deemed meaningful by the authors. To satisfy a contractual obligation, other phase spectra are given in Appendix B.

$$d = \frac{c\Delta\tau}{n} = \frac{.3}{n} \text{ meters,}$$

while the resolution capability of the H.P. (50 volt, 45 nsec) pulse is

$$d = \frac{13.5}{n} \text{ meters,}$$

where

$$n = \sqrt{\epsilon_r}$$

is the effective refractive index of the medium, ϵ_r is the relative dielectric constant, c is the speed of light in free space, and $\Delta\tau$ is the base pulse width of the input pulse. These figures are lower bounds and neglect any dispersive effects of the medium. The H.P. (50 volt, 45 nsec) pulse, meanwhile, is better suited to deeper probing because of the higher power within its spectrum (> 110 mW/MHz) as compared to the broader spectrum of the Ikor pulse (< 20 mW/MHz).

B.   Design of Antenna Geometry

The design of the antenna structure for electromagnetically probing a subsurface medium has two primary objectives; to couple as much electromagnetic energy as possible into the medium, and to provide the clearest "time window" possible by minimizing reflections from the baluns, antenna terminals, antenna ends, the surface of the medium and any objects on or above the surface. The goal is to isolate in time the scattered signal associated with a subsurface target from these reflection mechanisms.

Pulse sounding in the orthogonal mode proceeds in the following manner. An input pulse is periodically fed to the transmitting antenna via RG-9 cable, a 50:200 ohm balun, and a short length of standard 300 ohm T.V. twin lead. The baluns are special broadband balanced to unbalanced transformers that are used to match the 50 ohm impedance of the coaxial cable to the impedance of the twin lead and antenna. A balanced antenna is desired to prevent radiation from the cables and feed system. The purpose of the length of twin lead is simply to isolate the baluns from one another and from the antenna. When the baluns are too close to each other or to the antenna, severe coupling problems arise. The twin lead feeds the pulse directly to the terminals of the transmitting antenna. As the pulse propagates along the arms of the dipole, the fringe fields penetrate deeper into the medium. For shallow targets, the antenna is not being employed as a radiating element since it is the near fields which are being utilized. For this reason, the antenna is often referred to as a probe. For deeper targets, however, the antenna is used as a radiating structure. Reflections from scatterers located within the

12

subsurface medium are received on the orthogonally oriented dipole and fed back through a feed system identical to that of the transmitting dipole to the sampling oscilloscope. The resulting time domain waveform is recorded, either directly by the computer or on magnetic tape, and stored for subsequent processing. The orthogonal mode probe configuration has the interesting advantage of being blind to planar type targets such as the air-medium interface and similar stratifications within a homogeneous isotropic medium. This can be seen by observing that the polarization of the radiated field and reflected fields from a planar stratification is orthogonal to the orientation of the receiving dipole. A typical time domain orthogonal mode waveform using the small probe and the Ikor pulse, is shown in Fig. 5. The initial spike is caused by direct coupling across
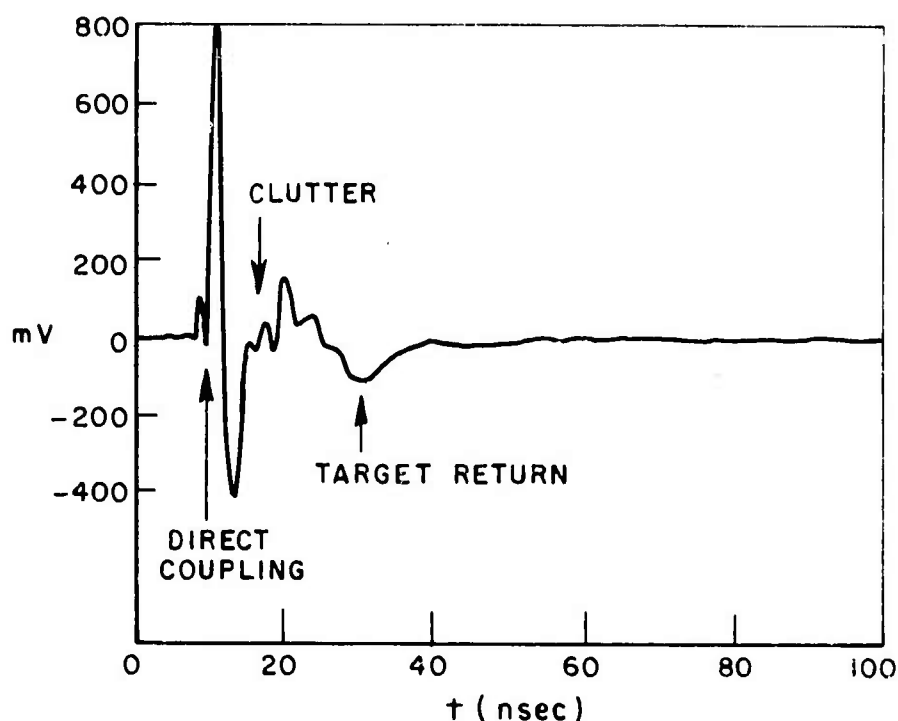
Fig. 5. Sample orthogonal mode waveform.

the feed terminals of the transmit and receive dipoles. This coupling is in general a replica of the input pulse, and provides a means for determining the delay time to a target signature. The next few nanoseconds are usually unpredictable clutter due to surface variations of the medium, such as level, roughness, moisture content, and vegetation. It is the following time interval that is of interest in that reflected signals from underground objects at depths greater than $d = c/n \epsilon$ will be seen in this time window, where c is the speed

13

of light, n is the refractive index of the medium, and Δt is the duration of the clutter. In Fig. 5, the system is "seeing" a buried plastic cylinder at a depth of 2.5 feet at a delay of roughly 20 nsec from the direct coupling.

Direct reflection mode operation is similar to the orthogonal mode in that reflections from underground targets are viewed as a time domain waveform on the sampling scope. In the direct mode, however, a single antenna is used as both transmitter and receiver. Because of this fact, the oscilloscope sampling head must obviously be exposed to the high voltage input pulse. A voltage limiter designed to protect the sampling head from harmful high voltage pulses was built to permit direct reflection mode operation. A pair of step recovery diodes (SRD's), which are used as charge controlled switches, provide the limiting action necessary to protect the sampling heads. When charge is inserted into an SRD by forward bias, the diode appears as a very low impedance (1Ω). When this charge is being removed, the diode continues to appear as a low imoedance until all the stored charge is removed, at which point it quickly switches to a high impedance[13].

In this application, the oncoming high voltage pulse provides the forward bias to an SRD shunted across a small section of 50 ohm microstrip transmission line (Fig. 6b). When the voltage of the input pulse becomes greater than roughly 800 mV, the diode switches to a low impedance causing the limiter to appear as a short circuit, thereby reflecting the incident pulse back down the line. After the trailing edge of the pulse has been reflected, the diode remains a low impedance until all of the stored charge is removed, at which point it switches back to a high impedance which is unnoticable in parallel with the 50Ω transmission line. Any signal that is less than 800 mv in magnitude, as most target returns happen to be, passes through the limiter undistorted. Actually, only one SPD is required to protect the sampling head from the input pulse, however, for added orotection from reflections from accidental short circuits or large magnitude target returns, a second diode was inserted.

Figure 6a shows the direct reflection mode system with the limiter. The length ℓ_1 can be made as short as possible, but ℓ_2 and ℓ_3 must be long enough (have sufficient time delay) so that reflections from the tee junction do not clutter the time window of interest. The stripline limiter simply consists of two parallel plates with a center conductor sandwiched in a dielectric between them (Fig. 6b). The SRD's are shunted between the center conductor and the parallel plates as shown in Fig. 6c. The diodes are Hewlitt-Packard Type 5082-0300 with a maximum breakdown voltage of 100 volts and a maximum transition time of 360 psec. These specifications make the diodes ideal for use with the 50 volt, 45 nsec HP pulse generator.

14
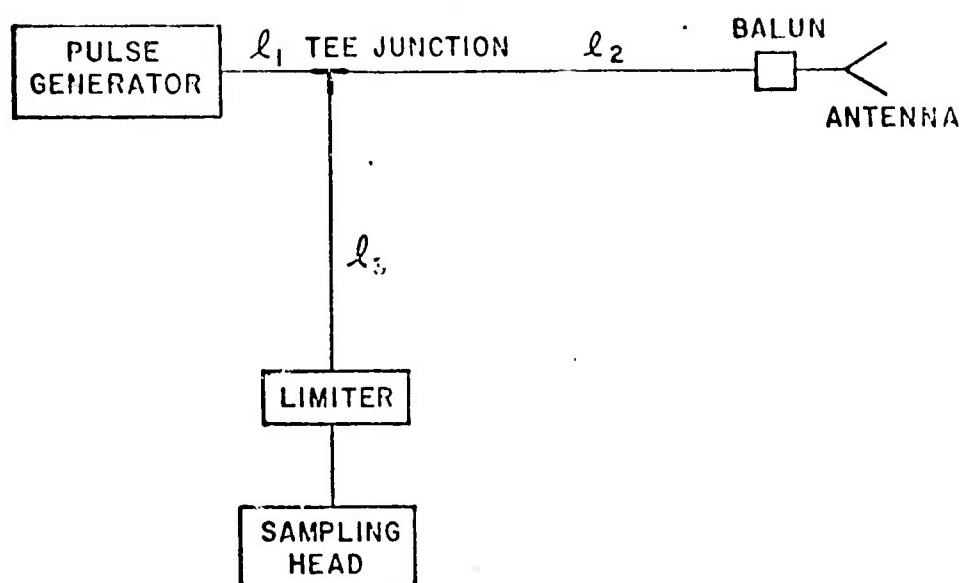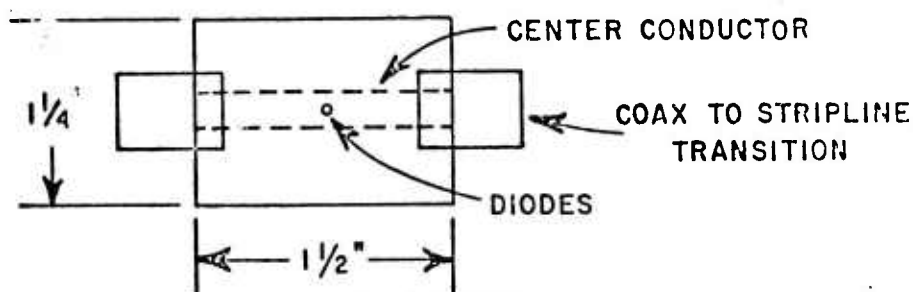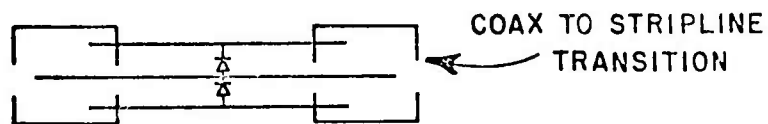
Fig. 6. Limiter for sampling head protection.
   (a) block diagram with limiter
   (b) detail of limiter
   (c) detail of limiter.

15

The waveform shown in Fig. 7 clearly shows the relationship between the time delays involved and the lengths ℓ_2 and ℓ_3. The operation proceeds as follows: A pulse is generated and propagates down the line ℓ_1 to the tee junction. The impedance looking into the junction is 25 ohms, resulting from two 50 ohm cables in parallel, so a portion of the voltage is reflected back to the pulse generator where it is dissipated by the matched 50 ohm output impedance of the pulse generator. The remaining portion of the input pulse power is divided equally between the cables ℓ_2 and ℓ_3. Assuming a 50 volt input pulse, and neglecting the attenuation of the cables, a voltage reflection coefficient of $\rho = -1/3$ at the tee implies that roughly 24 volts is being applied to both the antenna and limiter. The first pulse in Fig. 7 is this 24 volt pulse limited to 800 mV. The second and third pulses are the reflections from the balun and from the antenna and ground, respectively. The antenna was not located over a known target for this measurement, so there is no target signal. Note that the time delay from the input pulse to the balun reflection corresponds to twice the time delay of ℓ_2. The next series of pulses in Fig. 7 are multiple reflections. The second balun and antenna reflections result from the mismatch at the tee junction. A portion of ($\rho = -1/3$) the first balun and antenna reflections are reflected back towards the antenna by the junction, and back again to the junction and sampling scope by the antenna. The last pulse in Fig. 7 is a second reflection of the first pulse which had been reflected toward the tee by the short-circuited limiter, and then back to the limiter by the mismatch at the tee junction. This method admittedly can be more confusing than the orthogonal mode because of the multiple reflections, and slightly inefficient because of the signal power lost at the tee. The clutter problem, however, can be overcome by proper choice of the lengths ℓ_2 and ℓ_3, and the power losses are overshadowed by the advantages for certain targets of working with only one antenna and polarization, and the elimination of the direct coupling. Note that since coupling is not a problem, the section of twin lead can be eliminated. Alternatively, the multiple reflections on ℓ_2 could be eliminated by insertion of a resistance in series with the diodes to dissipate instead of reflecting the input pulse. In fact, special limiting diodes are available* that have this resistance built into the diode package, but these have not yet been adapted to the system. Another possible means for reducing reflections on ℓ_2 would be to choose the characteristic impedance of ℓ_1 and ℓ_2 as 100Ω, and ℓ_2 as 50Ω. The input impedance of the tee junction from ℓ_2 would be 50Ω, which matches the impedance of ℓ_2.

---

*General Semiconductor Transorbs, #1CT5.
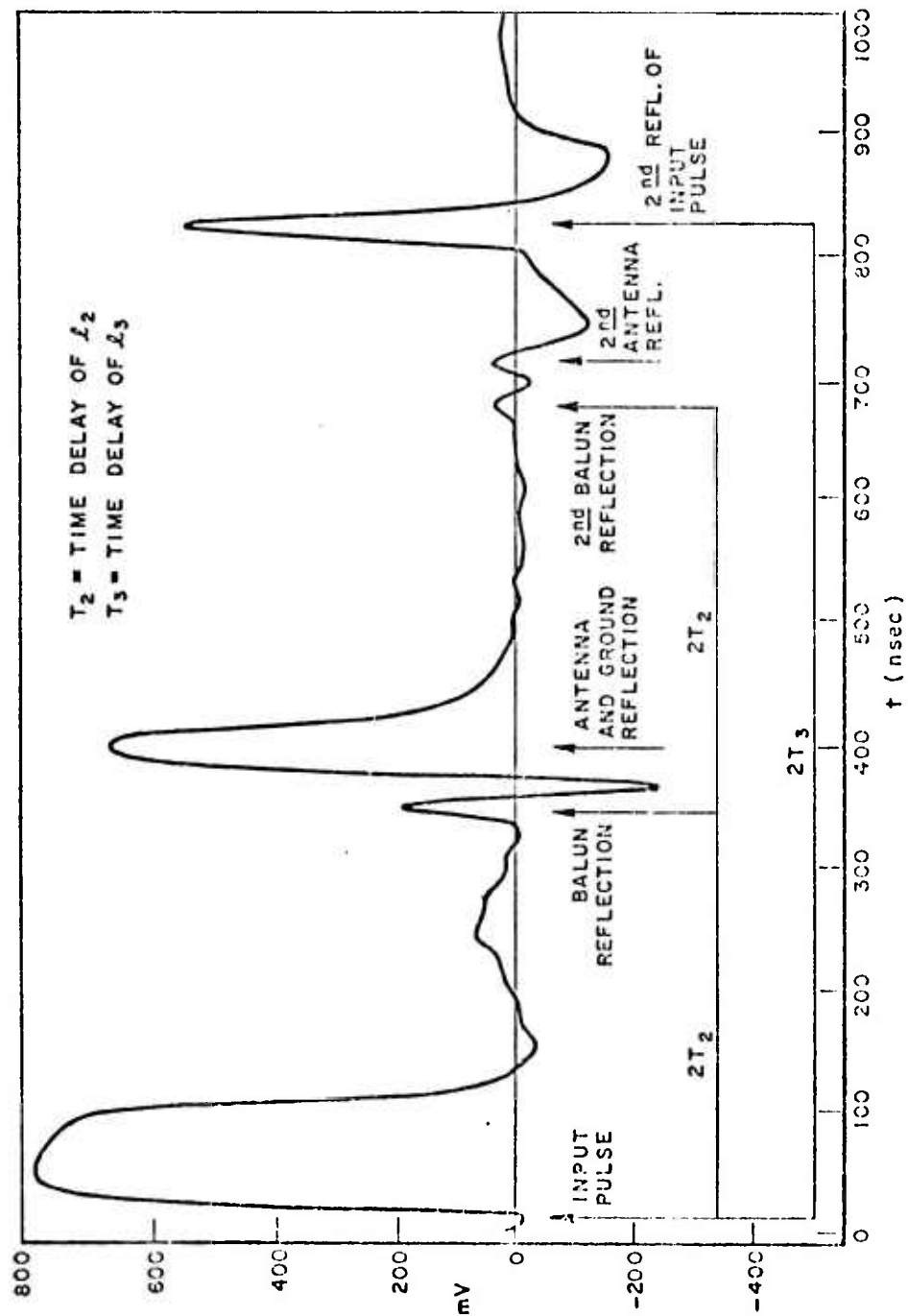
Fig. 7. Sample direct mode waveform.

17

The design of the broadband probe geometry was carried out completely in the time domain as compared to conventional frequency domain antenna design. The entire system consisting of coaxial cable, balun, twin lead, and antenna was viewed as a transmission line with discontinuities in characteristic impedance along the line. In a time domain reflectometry (TDR) direct reflection mode arrangement, the reflection from each discontinuity was minimized without regard to any other point along the line. A long, step function excitation was used to prevent misleading reflections from the trailing edge of the pulse. In this way, the trailing edge of the step is well beyond the time window of interest. The rise time required for the step is determined by the resolution desired, and antenna size. Figure 8 shows the reflections from the large antenna of Fig. 2a (direct
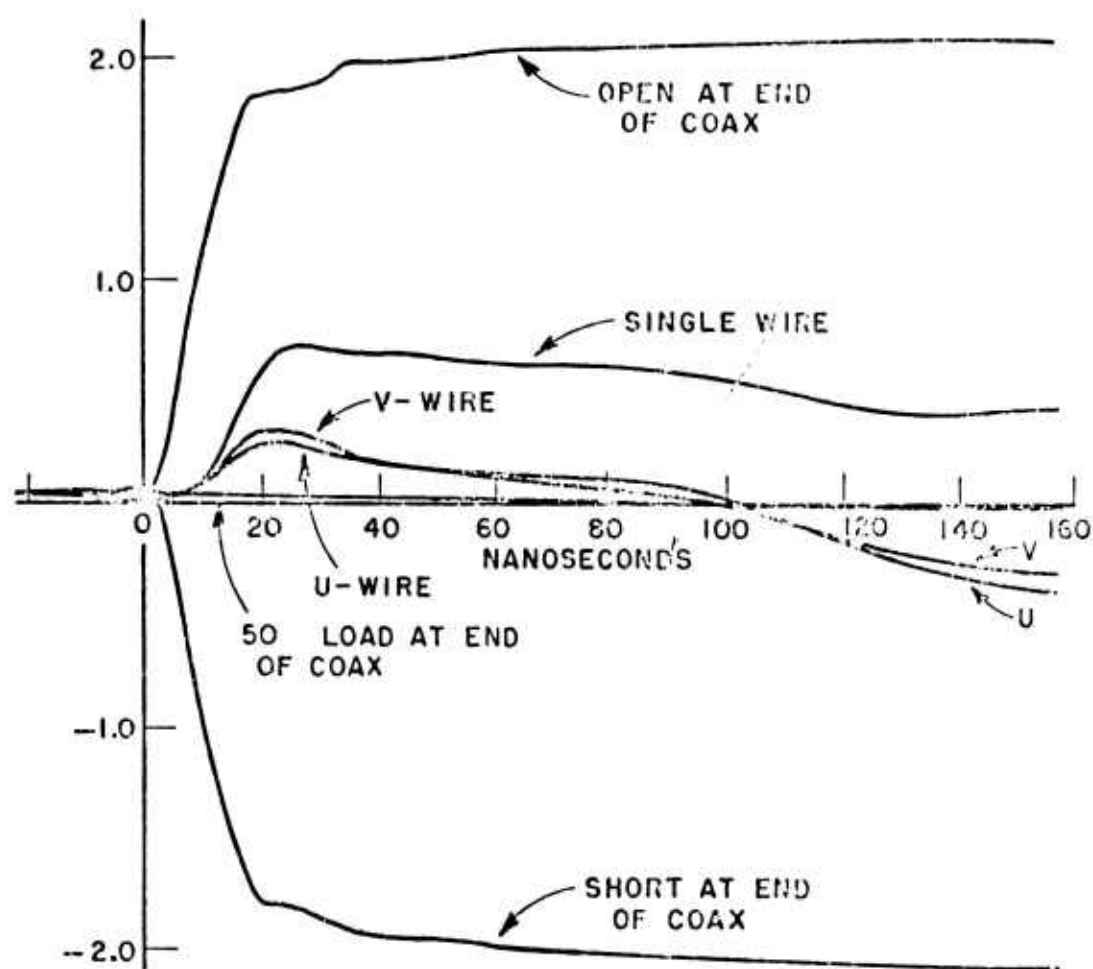
Fig. 8. Direct reflection mode-step input on large dipole on soil medium.

18

reflection mode) lying on a soil medium with a 15 nsec rise time input step. When used on a soil medium, ground rods are used at the ends of the dipole arms instead of the aluminum sheets to obtain a match to the impedance of the medium. For this case, the balun was connected directly to the feed terminals of the antenna, eliminating the twin lead. The open and short circuit waveforms are used as references in determining the reflection coefficient and impedance at the discontinuities. A perfect match (50Ω load) with no dis- continuities would be a straight horizontal line lying on the time axis. The figure demonstrates the advantages of two linear dipole elements, for which a characteristic impedance of 280 ohms is measured, as compared to a single dipole element, which yields a characteristic impedance of 400 ohms. The difference between a U and V type arrange- ment of the feed wires is also illustrated, yielding characteristic impedance values of 257 and 280 ohms at the terminals, respectively.

The direct reflection mode of the large antenna of Fig. 2a on limestone is shown in Fig. 9a. The dashed lines indicate the open and short circuit reflection levels, and the three waveforms clearly display the effect of placing aluminum foil across the arms of the dipole. Note that for very long times, all of the waveforms should approach the open circuit level. Figure 9b shows the same antenna on limestone with the foil replaced by the 4' x 8' conducting sheets, while Fig. 9c shows the same measurement on dolomite. From the reflection magnitudes at the twin lead and antenna of Fig. 9b, the characteristic impedance of the twin lead lying on limestone is found to be 268Ω, and the characteristic impedance of the antenna to be 161Ω. Similarly, for the dolomite medium (Fig. 9c) impedance values of 268Ω and 118Ω were obtained for the twin lead and antenna, respect- ively. Figure 10 shows the reflection mode of the same antenna on limestone, recorded on a different day and with a shorter length of twin lead. During this measurement, it happened to be raining heavily, and there was standing water on the sheets. A 5 nsec rise time step was used, and open and short circuit waveforms were obtained at the cable, baluns, and feed terminals. Note the differences in the waveforms of Figs. 9b and 10. The estimated effective impedance of the twin lead was found to be 256 ohms while the characteristic impedance of the antenna at the terminals was 249 ohms. Since these impedance values are really effective values, and since the constitutive parameters of the medium can be very dependent on the moisture content and temperature of a medium, it is not at all surprising that different impedance values are obtained on different days. Note that reflections are observed that correspond to changes in the characteristic impedance of the twin lead, the U-shaped feed wires, the 12 foot rods and the aluminum sheets.

Figures 11a and b show similar results for the small antenna of Fig. 2b over a soil medium and a limestone medium, respectively. Short circuits at the cable end, the balun, and the feed point are shown in

19
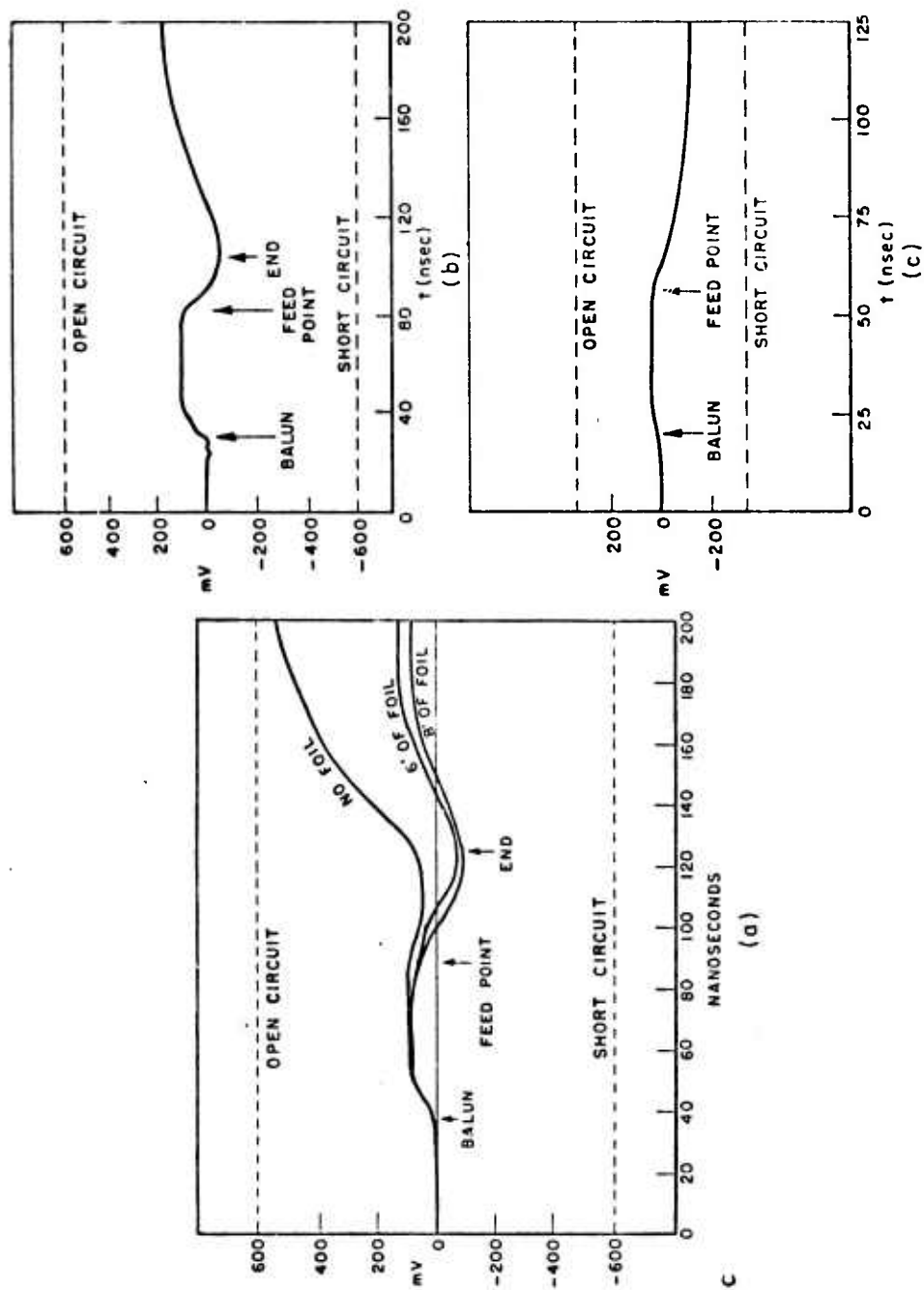
Fig. 9. Direct reflection mode-step input. (a) large dipole with foil on limestone. (b) large dipole with 4' x 8' sheets on limestone. (c) large dipole with 4' x 8' sheets on dolomite.
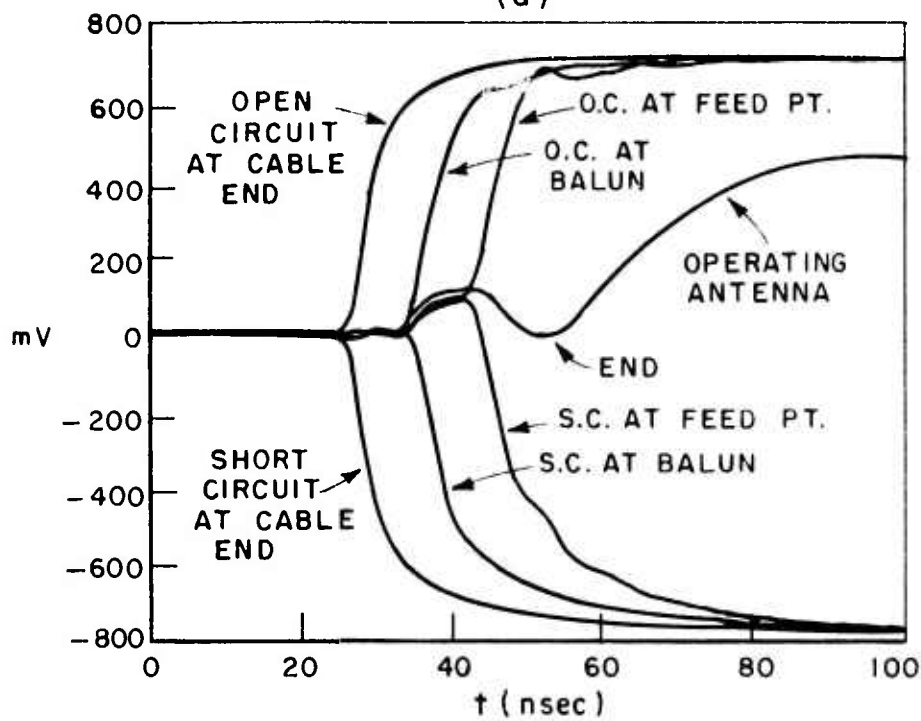
20
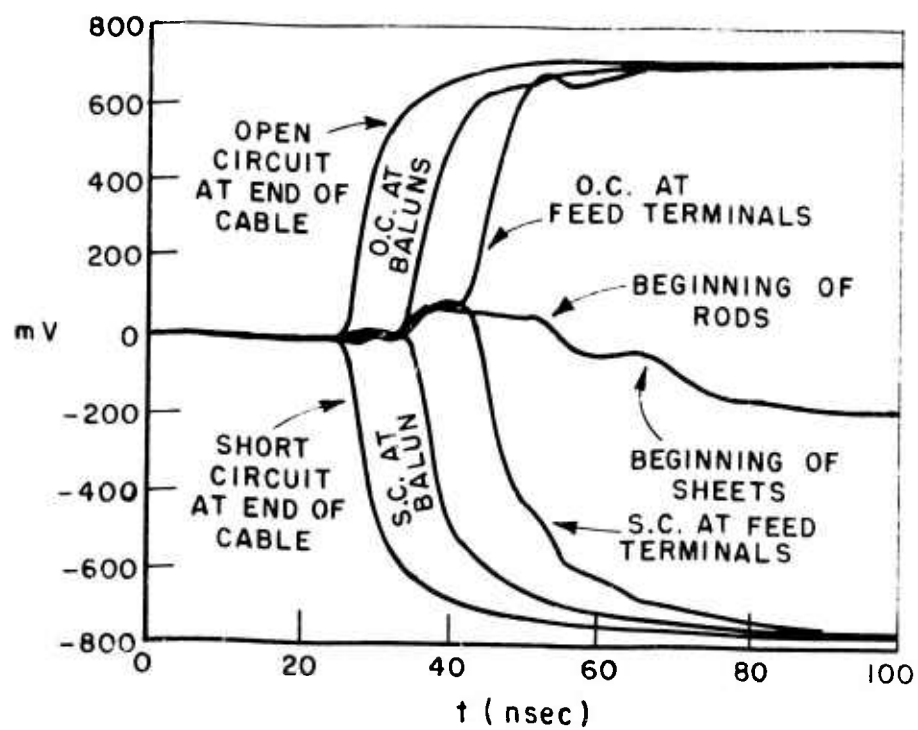
Fig. 10. Direct reflection mode-step input
large dipole on limestone.
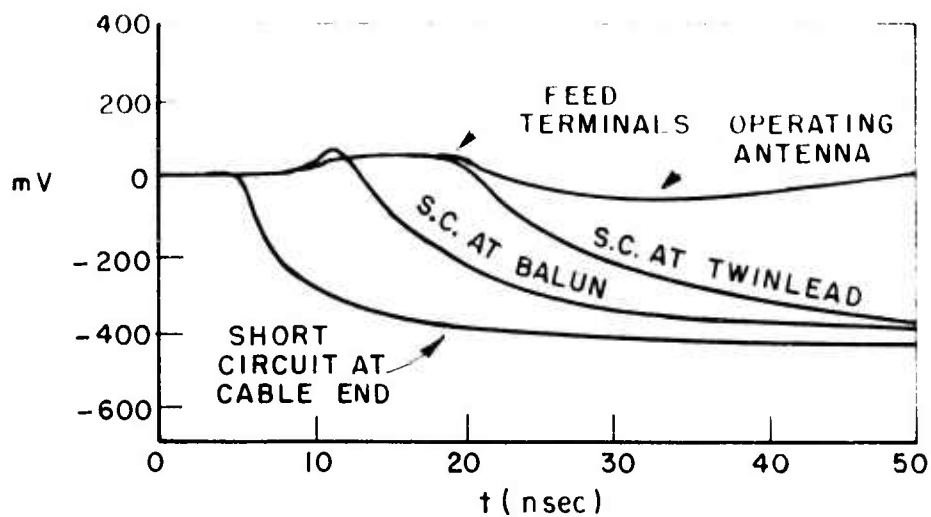
Fig. 11. Direct reflection mode-step input.
(a) small dipole on soil.
(b) small dipole on limestone.

22

both figures, and the corresponding open circuits are shown in Fig. 11b. Note the very good match of the antenna to the soil medium. Impedance values for the twin lead and antenna are 250 ohms and 141 ohms, respectively. With the antenna over limestone, the impedance values are 256 ohms and 199 ohms for the twin lead and antenna, respectively. Note that the voltage level of the input step is not the same in all of the figures, which accounts for the differences in the open circuit and short circuit levels. Note also that the time scales are not the same in all cases, because the rise time of the input step was varied.

To obtain a comparison of energy coupled to a subsurface medium by each of the antennas, a pulse was transmitted through 20 feet of limestone using the large antenna with and without the sheets and the small antenna as the transmitter. The small antenna was used as the receiver for all three measurements. Figure 12 compares the time waveforms and the amplitude spectra for the H.P. pulse of Fig. 3 and Fig. 13 shows similar results for the Ikor pulse. Note from the H.P. spectra that the small antenna transmits 12 dB less at the low frequencies than the large antennas, but does transmit more of the high frequencies, as it should. The same effect can be seen from the Ikor pulse waveforms. The sheets appear to have little effect on the H.P. waveform and spectra at the low frequencies, but above 40 MHz, the spectrum of the pulse transmitted on the antenna with the sheets is down at least 6 dB. From the spectra of the Ikor waveforms, however, the level at frequencies near 40 MHz is lower for the antenna with sheets, but above 60 MHz, the level becomes greater for the antenna with the sheets.

Note the effect of the sheets in the top two waveforms of Figs. 12a and 13a. These figures verify that the first effect observed in the received waveforms is due to the radiation from the feed terminals of the transmitting dipole. In other words, for very early times, the signal is not affected by the addition of the sheets, and it can be seen that the leading edges of the waveforms are not changed. For later times, however, differences are obviously beginning to occur. Note from the direct reflection measurement of Fig. 10 that the time delay from the feed terminals to the beginning of the sheets is roughly 12 nsec, and that the changes between the waveforms of Figs. 12a and 13a for transmission with and without sheets appear to be starting near 12 nsec from the leading edge of the waveform. The discontinuity in characteristic impedance introduced by the addition of the sheets is effectively acting as another point of radiation.
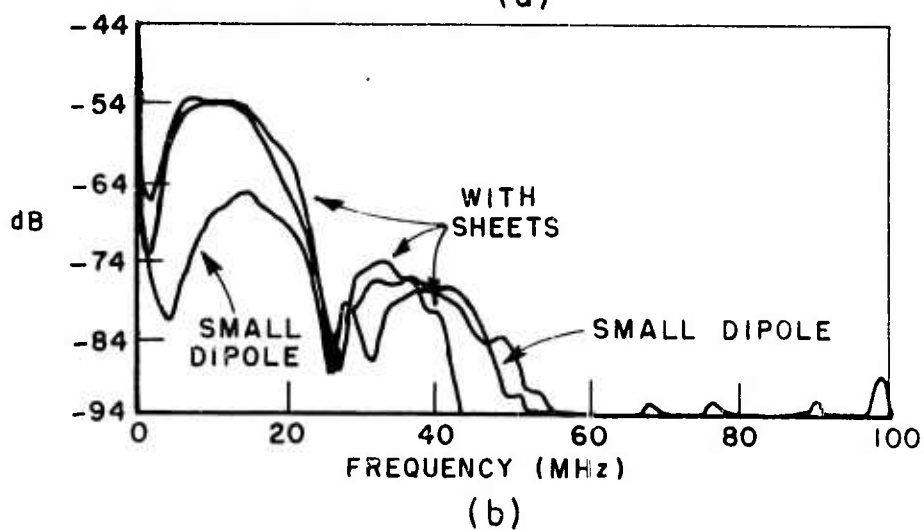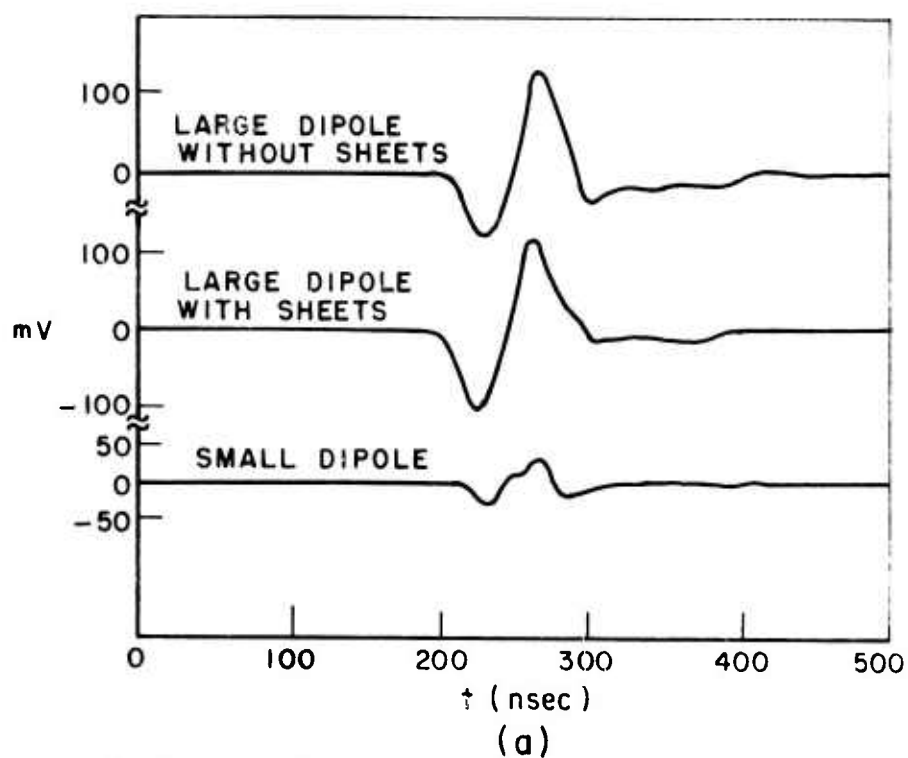
Fig. 12. Comparison of transmitted pulses using different transmitting antennas - H.P. Generator.
(a) time domain waveforms
(b) amplitude spectra.

24
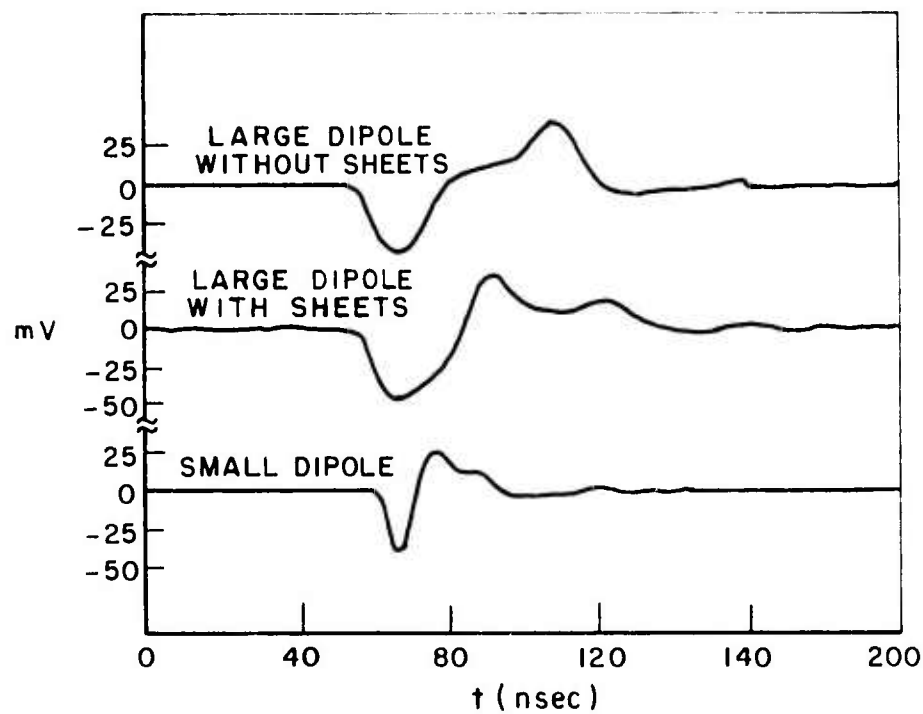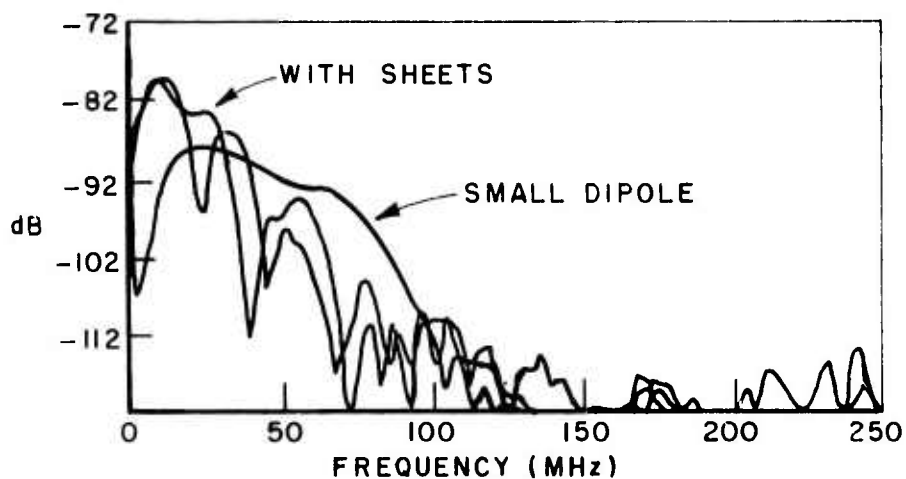
Fig. 13. Comparison of transmitted pulses using different transmitting antennas - Ikor Generator.
(a) time domain waveform
(b) amplitude spectra.

25

C. Computer Control and Processing Techniques

The computerized system of Fig. 1a is used to control the sweep of the sampling oscilloscope, and rapidly record, store, and plot a time domain waveform. A complete description of the computerized operating system is given in Reference [8]. The small instrumentation computer described in this reference is still used for the actual measurement process, but the unprocessed data is now being transferred to a larger, faster computer that services the entire laboratory. Further processing and data analysis is carried out on the new computer, in which a CRT display is useful in viewing and manipulating the data. Briefly, the processing techniques most commonly used are the Fast Fourier Transform and Inverse Transform, ideal bandpass or trapezoidal filtering, time domain gating, averaging and differencing. Proper use of these techniques results in obtaining maximum information from the measured data.

V. PULSE PROPAGATION CALCULATIONS AND MEASUREMENTS

A. Analytical Studies

In order to obtain meaningful information from any subsurface probing measurement, one must first obtain information about the medium in which a target is immersed. Properties such as attenuation, dispersion, signal velocity and the constitutive parameters are extremely important. A study of the effect of the medium on pulse propagation between two wire antennas has been undertaken. Computer programs have been developed to completely analyze arbitrary wire antennas or arrays of antennas embedded in an infinite homogeneous medium[14]. Typical program output consists of self impedance, mutual impedance, current distribution, near zone fields and far zone patterns. Finite conductivity of the wire and insulating dielectric sleeves can also be taken into account. A piecewise sinusoidal expansion is assumed for the unknown current distribution on the antenna, and Galerkin's method is used to reduce the integral equation to a system of simultaneous linear equations. Although the program normally operates in the frequency domain, speed and accuracy are sufficient to permit a Fourier transformation to the time domain. There is one program limitation that is determined by the amount of computer storage available. The antenna must be divided into a finite number of segments which is related to the number of terms in the piecewise continuous expansion for the current. In order to obtain sufficient accuracy, the length of each segment should be less than $\lambda/4$. At high frequencies, therefore, the number of elements could easily become too large for the computer to accommodate. The current limit of the Datacraft 6024 ElectroScience Laboratory computer is 50 elements. Larger computers such as the IBM 370 could accommodate perhaps 250 segments. The Fourier Transform modification has been added to the main program to allow conversion between the time and frequency domains. A time domain voltage pulse signal is applied to the terminals of the transmit antenna, shown in Fig. 14. This antenna is identical to one of the dipoles in Fig. 1c. Note that Fig. 14 shows the antenna divided into 14 segments as needed for the calculation. The radius of the wires is 3/8" and assumed to be perfect conductors. The input pulse is the 50 volt, 45 nsec (H.P.) pulse (Figs. 3 and 15) after it has been passed through the cables, baluns, and twin lead. It can be seen from the amplitude spectrum of Fig. 15b that the most significant frequency content of the pulse is below 50 MHz, (above 50 MHz the amplitude spectra is down 40 dB) so the lengths of the segments in Fig. 32b had to be less than $\ell = \lambda/4 = c/4f\sqrt{\epsilon_r} = 4.45/\sqrt{\epsilon_r}$ feet, which they are for $\epsilon_r \leq 20$. The input time domain pulse (Fig. 15a) is Fourier transformed and the first 50 harmonics of the resulting complex spectrum (Fig. 15b) are applied to the terminals of the transmitting

27
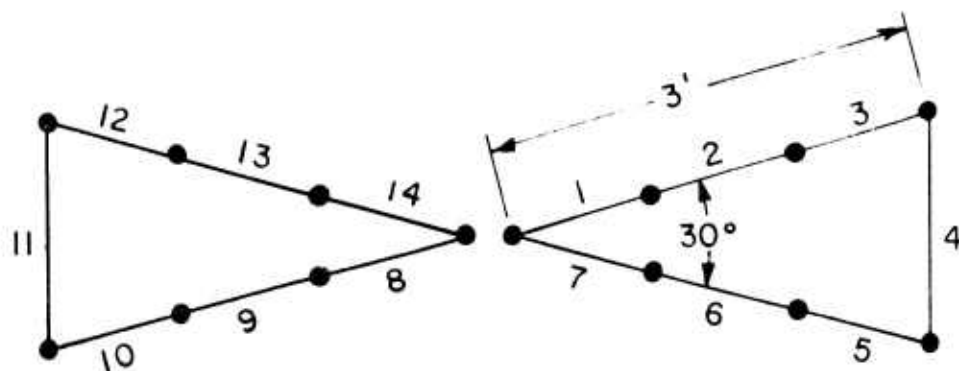
Fig. 14. Antenna used in pulse propagation calculations.

antenna. An induced voltage is calculated at the terminals of an
identical receiving antenna a specified distance away at each of the
fifty harmonics. The receiving antenna is terminated in a 300 load to
agree with the 300Ω twin lead used in the pulse sounding system. This
spectrum of received voltages is then inverse Fourier transformed to
obtain the received time domain waveform. With theoretical pulse
propagation calculations it is a simple matter to correctly reference
the phase of the received waveform to that of the input pulse, thus
phase spectra are shown in this section. With experimental propagation
or scattering measurements, however, a similar reference is extremely
difficult. At this stage, therefore, experimental phase spectra are
simply not meaningful (see References [6] and [11]) and none are
presented in the text of this report.

Figure 16 shows the effect of increasing conductivity on the
transmitted pulse for a relative dielectric constant (ϵ_r) of 10 and
a separation distance of 20 feet. As the conductivity is varied from
$\sigma = .001$ mho per meter to $\sigma = .01$ mho per meter, the attenuation
increases according to the relation

$$(1) \qquad \alpha = \frac{\omega\sqrt{\mu_0\epsilon_0\epsilon_r}}{2}\left[\sqrt{1 + \frac{\sigma^2}{\omega^2\epsilon^2_0\epsilon^2_r}} - 1\right]^{1/2}$$

from .03774 to .16953 at a frequency of 20 MHz. In dB per meter, this
corresponds to roughly .3 dB/m and 1.5 dB/m. The changes in attenu-
ation can best be seen by comparing the amplitude spectra of Fig. 16b.
Note that for very low frequencies ($\leq$ 2 MHz), the received voltage
increases with increasing conductivity, but for high frequencies, the
received voltage decreases with increasing conductivity.

28
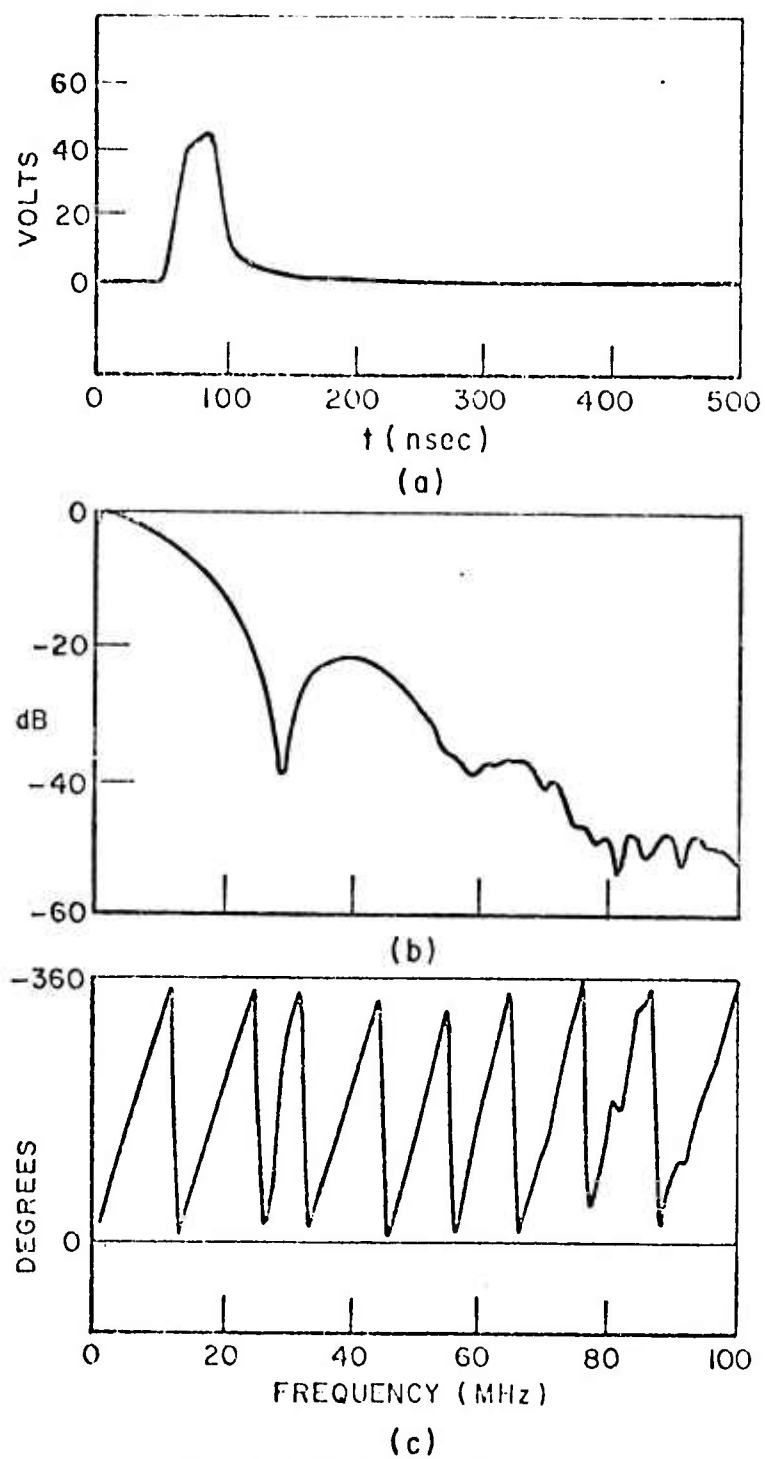
Fig. 15. Input pulse (H.P.) for pulse propagation calculations.
(a) time domain waveform
(b) amplitude spectra
(c) phase spectra.

29
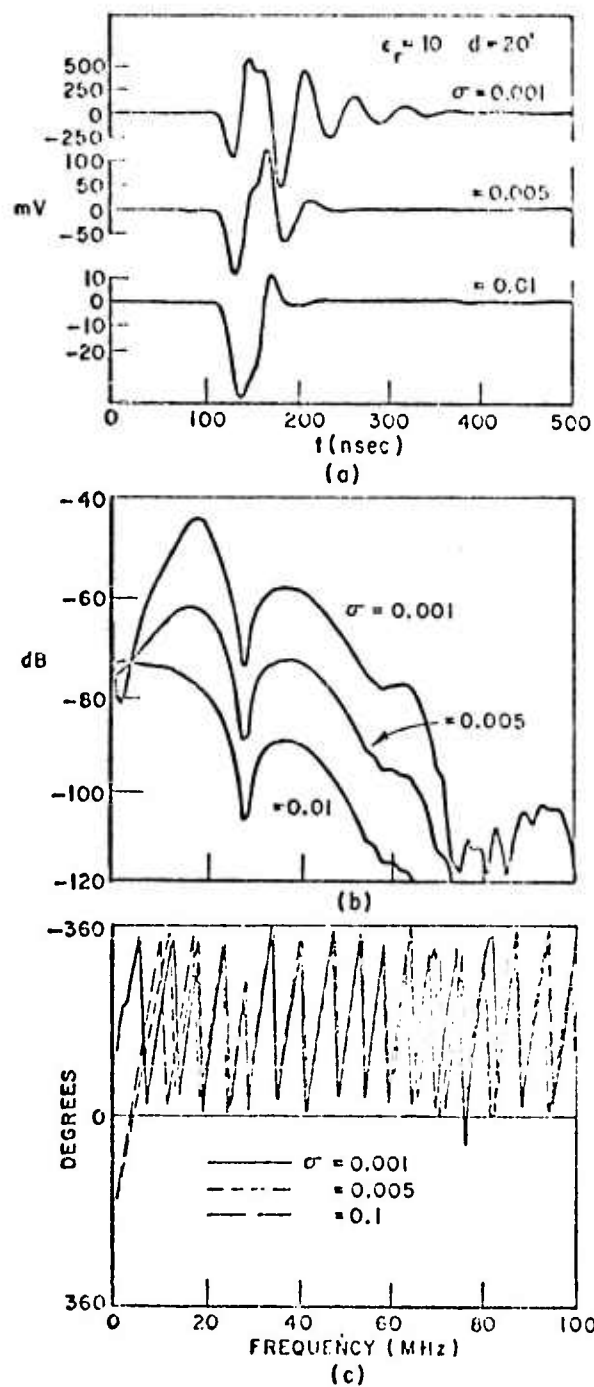
Fig. 16. Effect of conductivity on pulse propagation.
(a) time domain waveforms
(b) amplitude spectra
(c) phase spectra.

Figure 17 demonstrates the effect of the relative dielectric constant, ϵ_r, on the transmitted pulse. An increase in the value of the relative dielectric constant (ϵ_r) results in an increase in magnitude of the received waveform. Since the characteristic impedance $\sqrt{\mu_0/\epsilon_0 \epsilon_r}$ is decreased by an increase in ϵ_r, an increase in the magnitude of the received voltage is to be expected. Note that the start of the waveform for $\epsilon_r = 20$ is delayed 30 nsec from the start of the $\epsilon_r = 10$ waveform. The computer program is also accurately predicting the delay time of the transmitted signal, $\tau = d/v_p = d\sqrt{\epsilon_r}/c$, which obviously increases with increasing ϵ_r. Figure 17b displays the effect of ϵ_r on the amplitude spectra of the transmitted signals, and Fig. 17c shows the phase spectra. Note that the amplitude of the received voltage for $\epsilon_r = 20$ is lower at high frequencies (>50 MHz) than the $\epsilon_r = 10$ case.

The previous calculations were completed assuming a bare wire antenna, which is really not the case when the antenna is resting on absorber. The effect of an insulating dielectric sleeve on the antenna of $\epsilon_r = 1.0$, and 1/16" thickness, is illustrated in Figs. 18 and 19. Figure 18 shows the transmitted pulse and spectra for $\epsilon_r = 10$, $\sigma = .001$ mho/m and d = 20 feet without and with insulation, and Fig. 19 shows the measurements for $\epsilon_r = 10$, $\sigma = .01$ mho/m and d = 20 feet, without and with insulation, respectively. Note the differences between the insulated and uninsulated cases for each conductivity, and compare the differences. Obviously, for low loss media, the effect of the insulation will not be as great as for a high loss medium. Figures 18 and 19 confirm this reasoning. It can be seen from the $\sigma = .01$ case (Fig. 19b) that the coupling between the bare wire antennas is stronger at low frequencies while the coupling for the insulated antennas is stronger at higher frequencies.

Figure 20 shows that for constant values of ϵ_r and σ, the pulse shape does not change by increasing the path length. Only the magnitude of the waveform and amplitude spectrum is decreased. There is also a phase delay in the phase spectrum, which corresponds to a time delay in the time waveform.

Another important factor in determining the received waveform is the load impedance of the receiving antenna. To illustrate the dependence, Fig. 21 compares the differences between pulses transmitted on the same antennas in the same medium with load impedances of 50Ω and 300Ω. All previous waveforms were calculated with a 300Ω load to roughly correspond to the 300Ω twin lead of the measurement system. The impedance of the twin lead is really lower than 300Ω when it is lying on the interface between free space and the ground, but the actual value of the impedance changes with both frequency and the parameters of the medium. The ideal value of load impedance would naturally be a value that matches the impedance of the antenna. Note from Fig. 21 that a change in a purely resistive load only affects the magnitude of the received waveform and the amplitude spectrum. The phase spectrum remains the same.

31
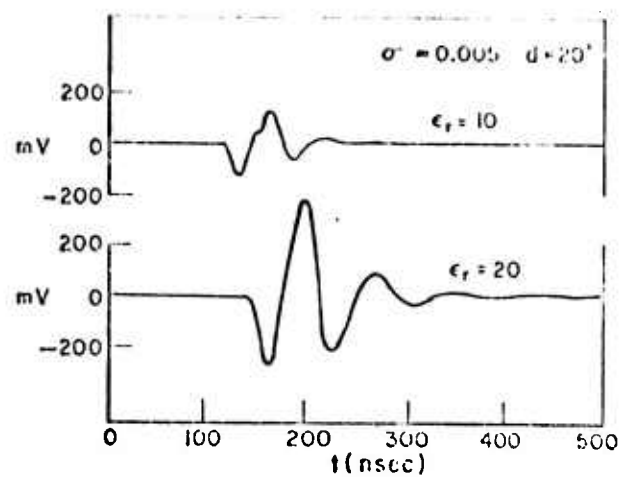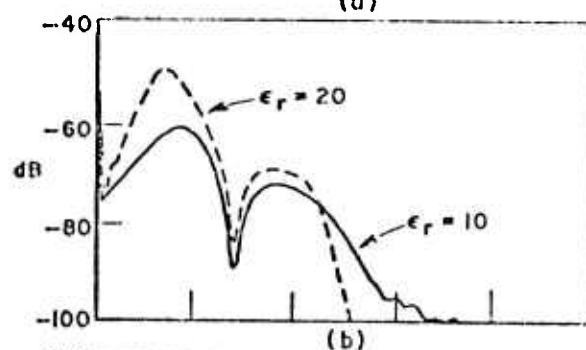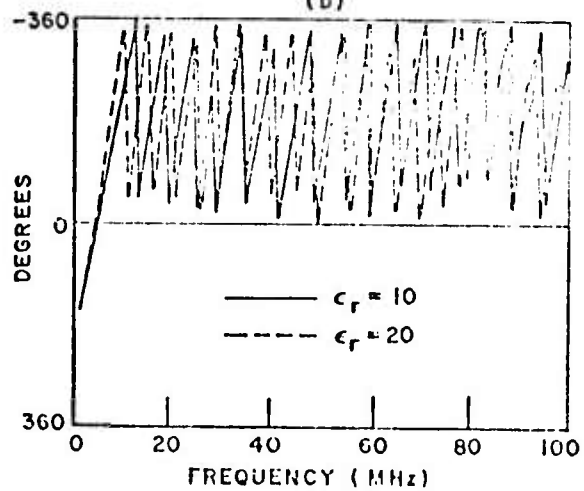
Fig. 17. Effect of relative dielectric constant
on pulse propagation.
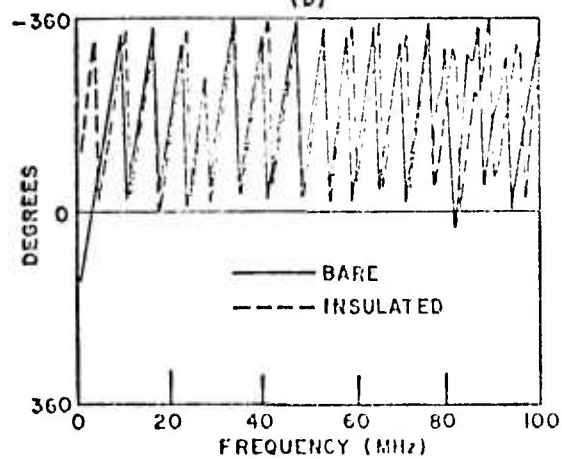(a) time domain waveforms
(b) amplitude spectra
(c) phase spectra.

32
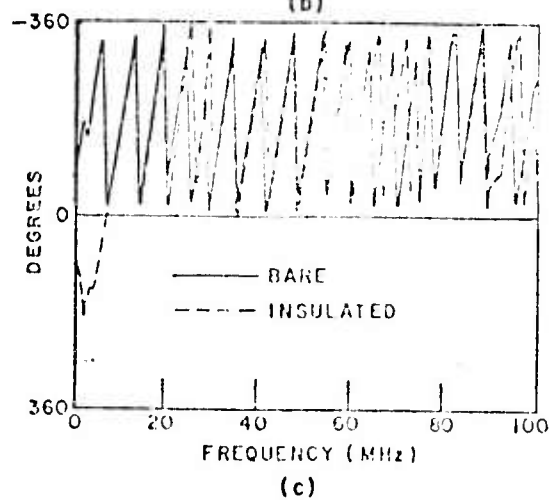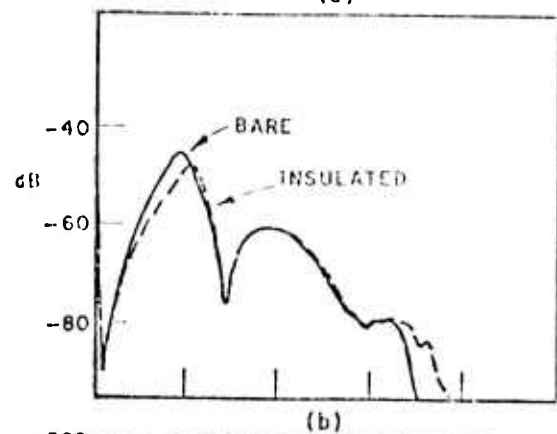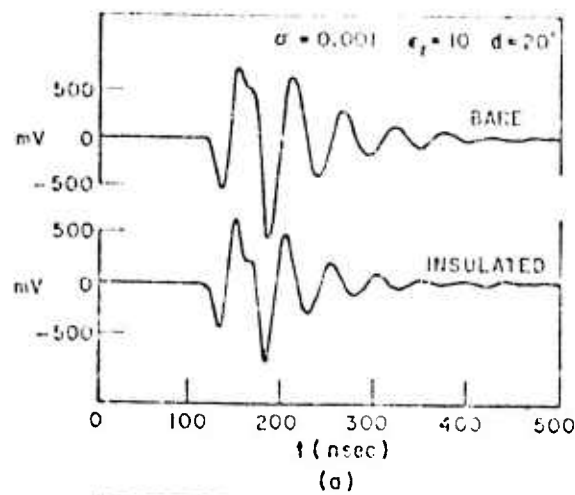
Fig. 18. Effect of antenna insulation - low loss case.
(a) time domain waveform
(b) amplitude spectra
(c) phase spectra

33
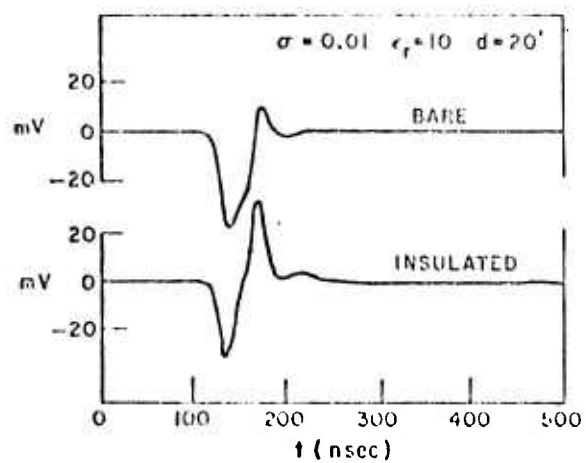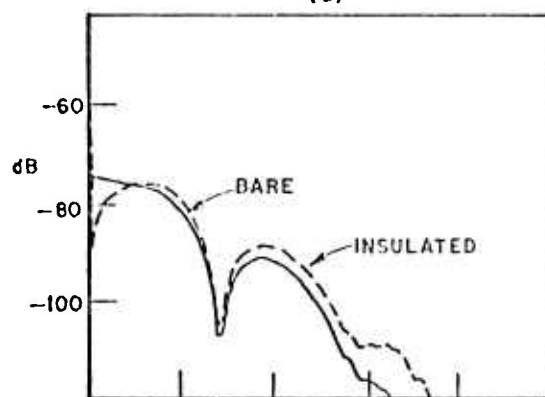
Fig. 19. Effect of antenna insulation - high loss case.
(a) time domain waveform
(b) amplitude spectra
(c) phase spectra

34

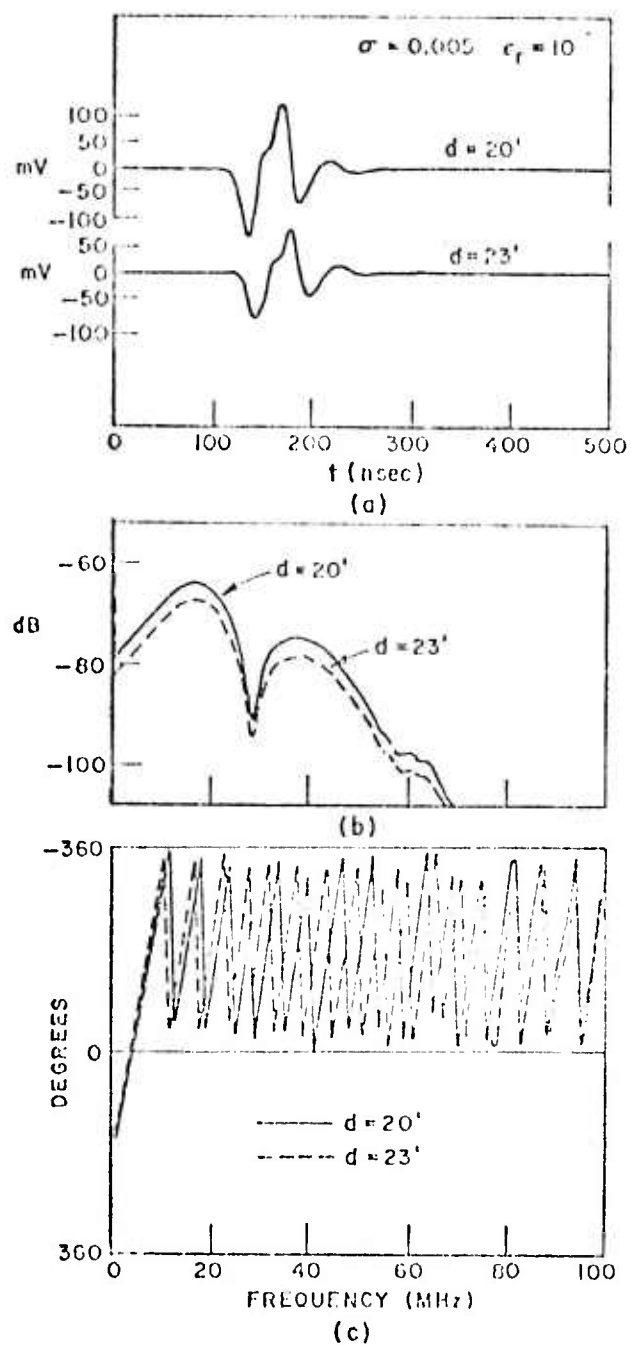Fig. 20. Pulse propagation over two distances.
          (a) time domain waveform
          (b) amplitude spectra
          (c) phase spectra.

35
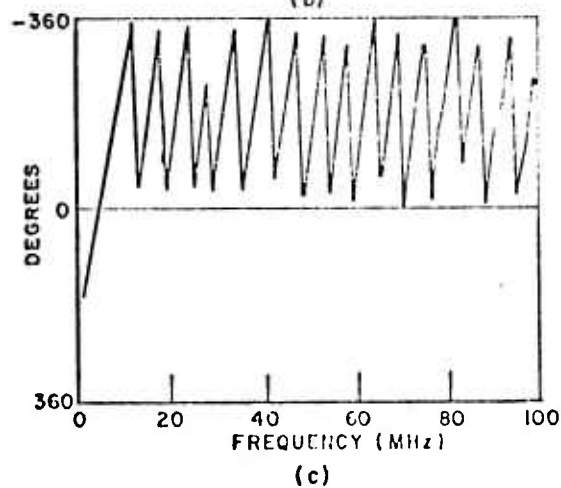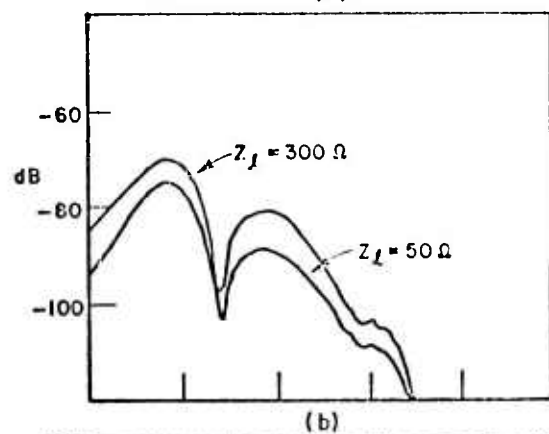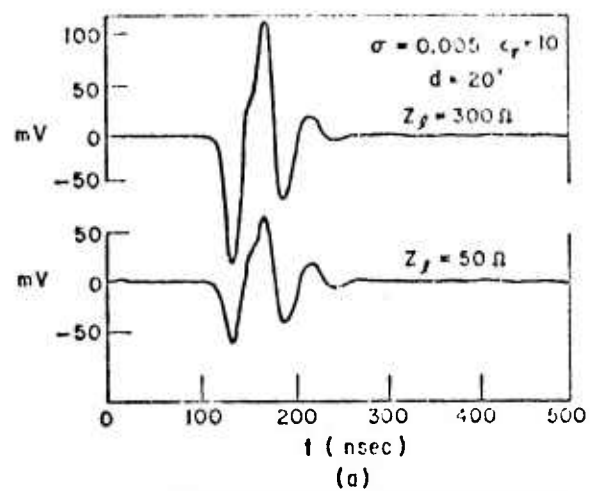
Fig. 21. Effect of receiving antenna load impedance.
(a) time domain waveform
(b) amplitude spectra
(c) phase spectra

36

The relative dielectric constant and conductivity of a sub-surface medium are not constants but functions of frequency. The relative dielectric constant follows a general decreasing trend with increasing frequency, while the conductivity tends to increase with increasing frequency. Just what changes occur in the values is primarily determined by the moisture content of the medium. Figure 22 demonstrates the case of pulse transmission over two path lengths in a dispersive medium. The relative dielectric constant and conductivity were varied linearly over the 2 to 40 MHz range from 20 to 10 and .005 to .015 mho/m, respectively, and then held constant at $\varepsilon_r = 10$ and $\sigma = .015$ from 40 MHz to 100 MHz. While this may not be a realistic frequency dependence, it is helpful simply to demonstrate the effects of dispersive constitutive parameters. From Fig. 22 it is evident that the base width of the time domain signals is greater than the base width of the constant parameter signals. This spreading is one of the primary effects of dispersion. Note also that the waveform for the 25 foot path appears to be spread more than the 20 foot path waveform. The fact that the increased conductivity at higher frequencies causes an increase in attenuation of the higher frequencies accounts for the spreading effect.

It should be stressed that these calculations were completed assuming that the antennas were embedded in an infinite homogeneous medium. In any real situation encountered in underground probing, the air-ground interface would have to be considered. The purpose of this analysis, however, was to study the effects of the medium on pulse propagation.

B. Experimental Studies

A series of propagation measurements has been made through limestone, dolomite and soil media to experimentally determine estimates of the electrical properties of these media. Consider pulse propagation over two path lengths ℓ_1 and ℓ_2. If the received voltage waveforms $v_1(t)$ and $v_2(t)$ are transformed to the frequency domain

(2) $\qquad V_2(\omega) = V_1(\omega) \, e^{-\gamma(\omega)\Delta\ell}$.

In Eq. (2), the propagation constant, $\gamma(\omega) = \alpha + j\beta$ and $\Delta\ell = \ell_2 - \ell_1$, the difference in path length. Since $V_1(\omega)$, $V_2(\omega)$ and $\Delta\ell$ are known (measured) quantities, the constitutive parameters can be found from $\gamma(\omega)$ from the following relationships, where ε_r is the relative dielectric constant and σ is the conductivity.

$$\gamma(\omega) = \alpha + j\beta$$

$$\gamma^2(\omega) = (\alpha^2 - \beta^2) + j2\alpha\beta$$

$$\gamma^2(\omega) = \omega^2 \mu \varepsilon_o \varepsilon_r - j\omega\mu\sigma$$

37
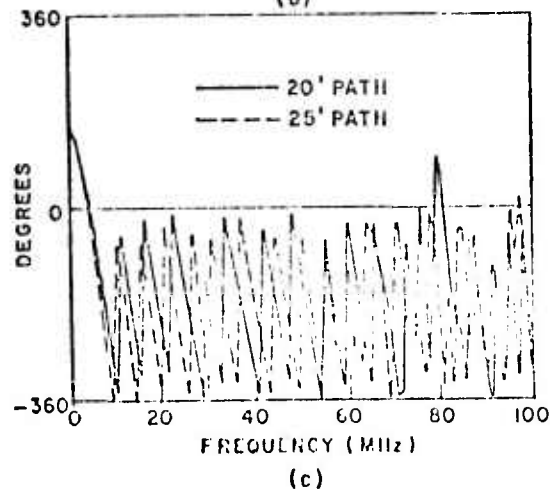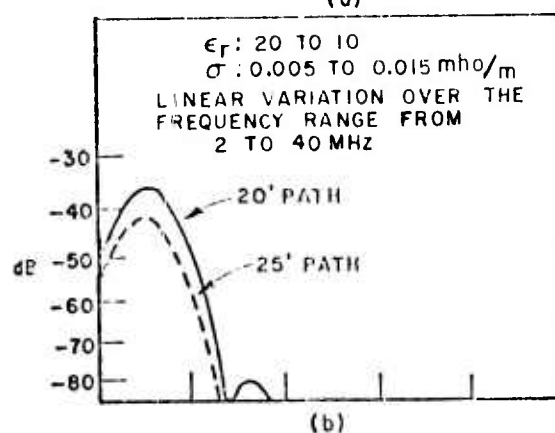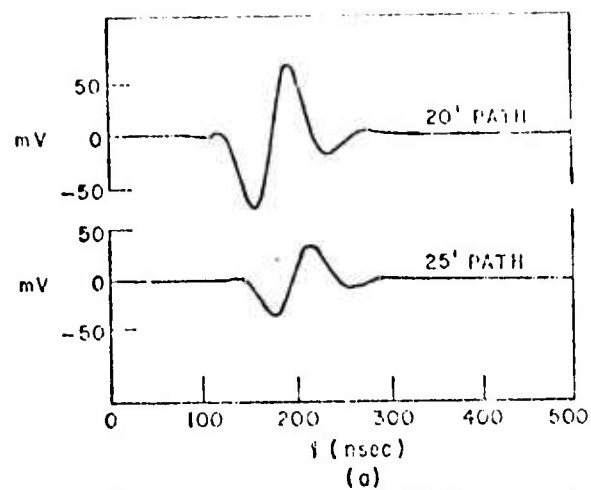
Fig. 22. Effect of dispersion on pulse propagation.
(a) time domain waveform
(b) amplitude spectra
(c) phase spectra.

38

(3) $\quad \therefore \varepsilon_r = \dfrac{(\alpha^2 - \beta^2)}{\omega^2 \mu \varepsilon_o}$

and

(4) $\quad \sigma = \dfrac{-2\alpha\beta}{\omega\mu\sigma}$.*

There are a number of practical limitations to this method for determining the relative dielectric constant and conductivity of a medium. In order to retain significant high frequency content in the received pulse, the propagation path length must be reasonably short. The change in path length, $\Delta\ell$, also presents conflicting needs. If $\Delta\ell$ is very small then it is reasonable to assume approximate cancellation of the near zone terms. The lengths ℓ_1 and ℓ_2 and the size of the antennas must also be considered in this respect. On the other hand, if $\Delta\ell$ is too small, the quantity $\gamma\Delta\ell$ becomes quite small and accuracy problems are encountered. It will be noted in the measured data that for the path lengths used in the experimental measurements, the calculated relative dielectric constant appears to be incorrect for frequencies below 10 MHz. Near 10 MHz, the conductivity term of $\gamma^2 = \omega^2\mu\varepsilon - j\omega\mu\sigma$ is beginning to dominate the propagation effects. This low frequency limitation would tend to increase in frequency as the conductivity is increased, and decrease in frequency as the conductivity is decreased. For very low conductivities (10^{-4}-10^{-5} mho/m), the calculations of conductivity became inaccurate simply because the medium behaves as a dielectric, and the propagation is independent of the conductivity.

The pulse propagation method of estimating the constitutive parameters of a medium was first tested using the calculated waveforms of Fig. 20. These waveforms were calculated with $\varepsilon_r = 10$, $\sigma = .005$ mho/m, and path lengths of 20 feet and 23 feet. The results for ε_r and σ are shown in Fig. 23 in the solid curve. Note the inaccuracy of the dielectric constant at frequencies below 15 MHz, and the inaccuracy of the conductivity above 70 MHz. The dashed curve in Fig. 23 shows similar results when the e^{-jkr}/r dependence is assumed instead of the planewave assumption. The increase in the

---

*Note that if one assumes $\varepsilon = \varepsilon' - j\varepsilon''$, $\mu = \mu' - j\mu''$, $\sigma = \sigma' - j\sigma''$, Eq. (3) and Eq. (4) are interpreted as effective values (Reference 19).
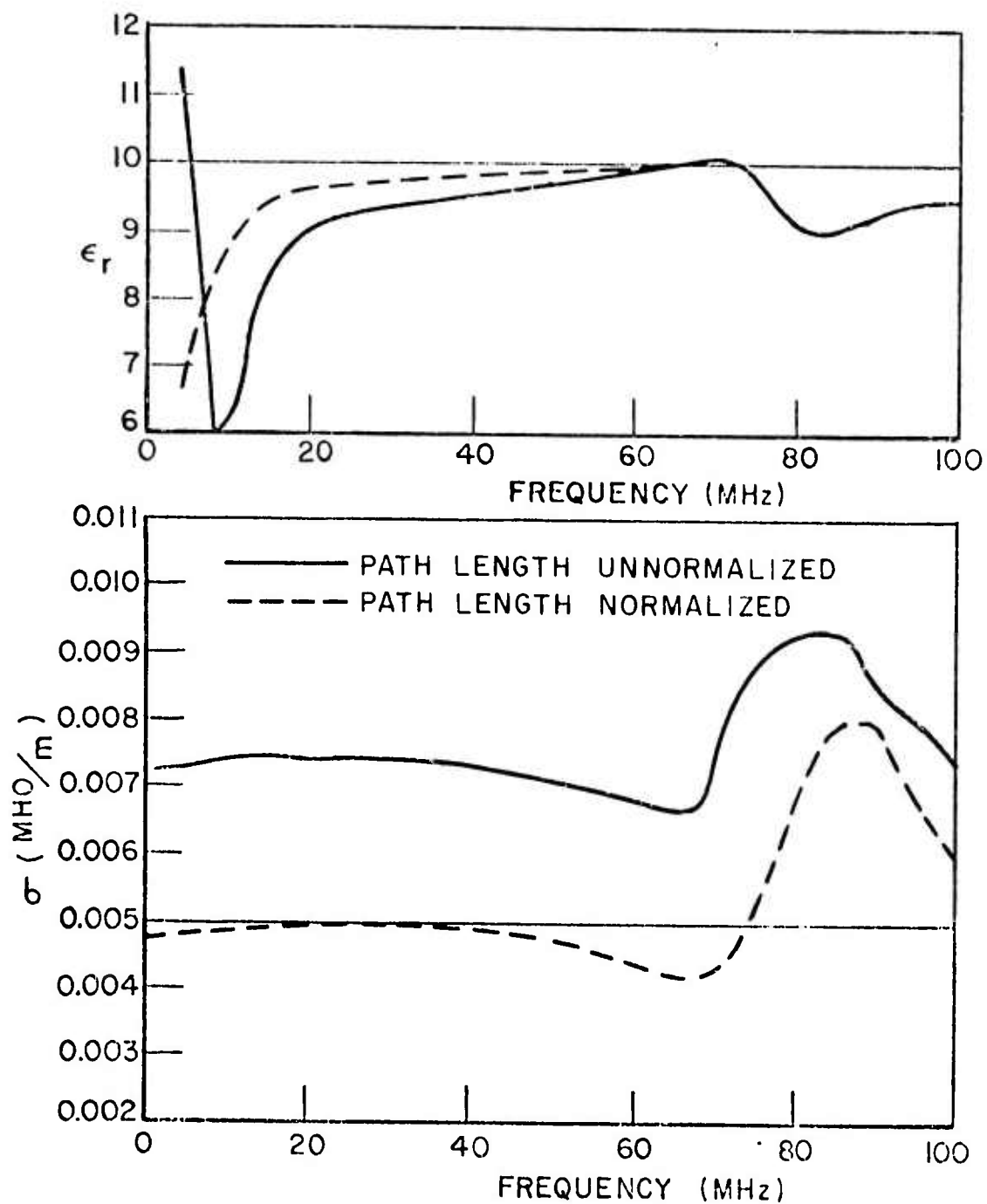
Fig. 23. Relative dielectric constant and conductivity derived from calculated waveforms, $\epsilon_r = 10$, $\sigma = .005$.

accuracy is obvious. Note the relative dielectric constant is still in error below 10 MHz and the conductivity appears to be in error above 70 MHz. The 70 MHz limit is expected since the Hewlitt-Packard pulse (50 volt, 45 nsec) simply does not contain significant energy above 70 MHz.

Although this method is admittedly crude, no better in situ method for estimating the constitutive parameters of a medium over a broad spectral range is available at this time. Unfortunately, nature does not always provide convenient propagation geometries where only the propagation path length can be changed. In these cases it may be necessary to resort to laboratory measurements or to fixed frequency measurements at selected spot frequencies spanning the desired spectral range. Note that with any experimental method, in situ or laboratory, problems will inevitably be encountered when either the displacement currents (ε_r) or the conduction currents (σ) dominate the electrical properties. On the other hand, if either parameter is unimportant to the propagation effects then its value in that frequency range is unimportant for our purpose. For any lossy medium, there will be a span of low frequencies where only the conductivity of the medium is of any consequence.

Figures 24 and 25 show a series of measured pulse waveforms transmitted through 20, 22.4, 28.3, and 36 feet of limestone. The top waveform in both figures is a time reference used to measure the delay and effective refractive index of the medium. It is obtained via a tee at the transmitting balun. Figure 26 shows the geometry of the propagation measurement, where a pulse was transmitted from a ledge above a tunnel to a receiving antenna that was held against the roof of the tunnel. The small dipoles of Fig. 2b were used as transmitter and receiver. The H.P. generator was used to obtain the results of Fig. 24 and the Ikor generator was used for Fig. 25. Note the increase in both attenuation and dispersion as the path length is increased. By differencing the amplitude spectra of Figs. 24b and 25b, the frequency dependent attenuation of the rock is obtained. Figures 27a and b show the attenuation, both magnitude and phase, for the H.P. pulse, and Figs. 27c and d show the attenuation for the Ikor pulse. The 20 foot and 28.3 foot path lengths were used to obtain the attenuation. The phase in Figs. 27b and 27d is obtained by differencing the phase spectra associated with the corresponding amplitude spectra of Figs. 24b and 25b. It is related to the phase constant, β, of the medium by $\beta = -\phi/\Delta\ell$, where ϕ is the phase shown in the figures and $\Delta\ell$ is the difference in path length. Although the first 100 harmonics of the spectral data are shown, only that portion of the data that corresponds to the significant spectral content of the transmitted pulses should be considered valid. For example, in Fig. 27, the attenuation data above 50 MHz for the H.P. and 125 MHz for the Ikor pulses is meaningless. The attenuation data is processed via equations (3) and (4) to obtain a frequency-dependent relative dielectric constant and conductivity. Figures 28

41
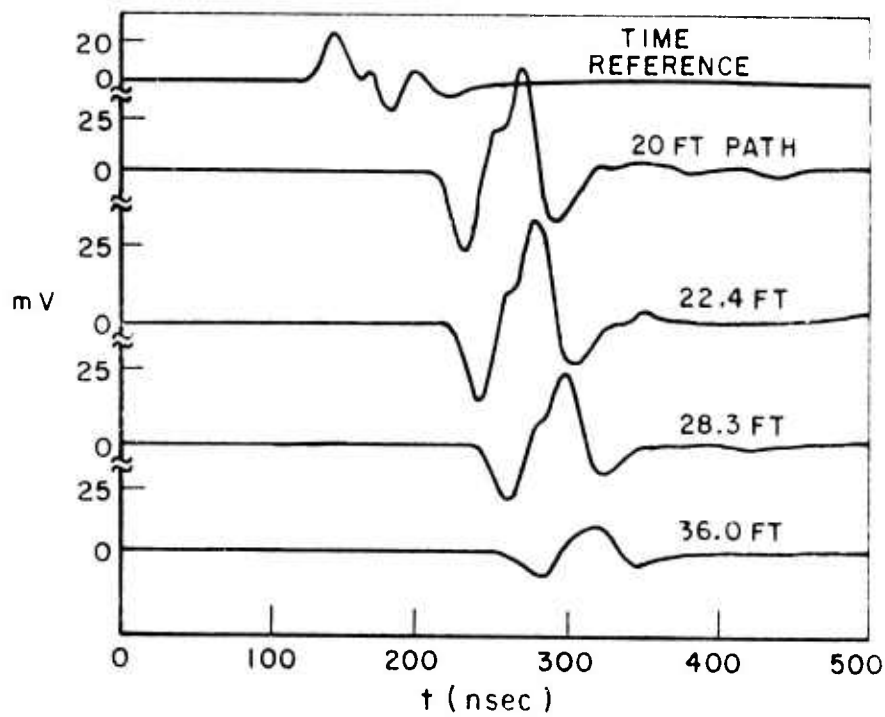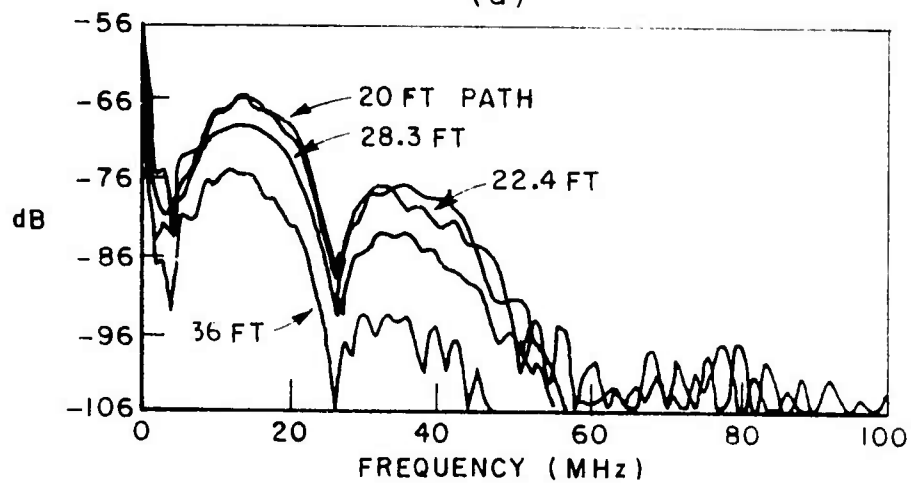
Fig. 24. Transmitted pulses through limestone (H.P.)
(a) time domain waveforms
(b) amplitude spectra.
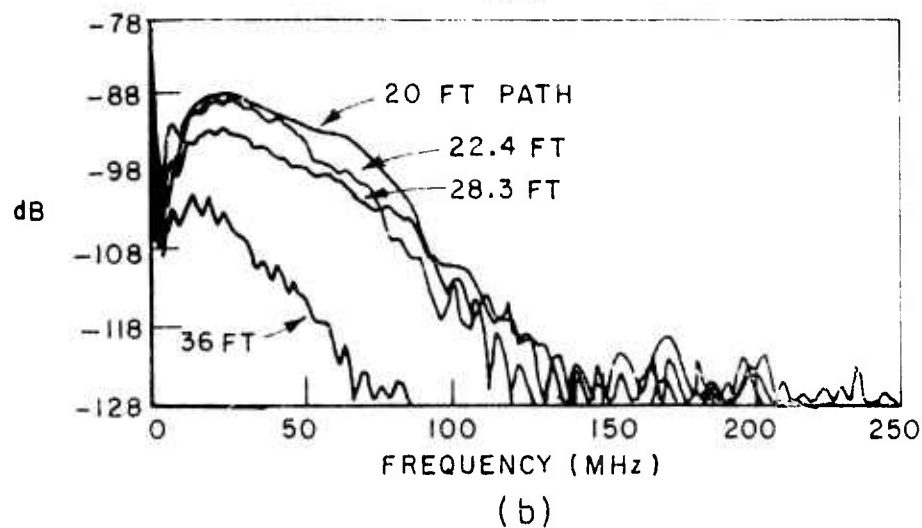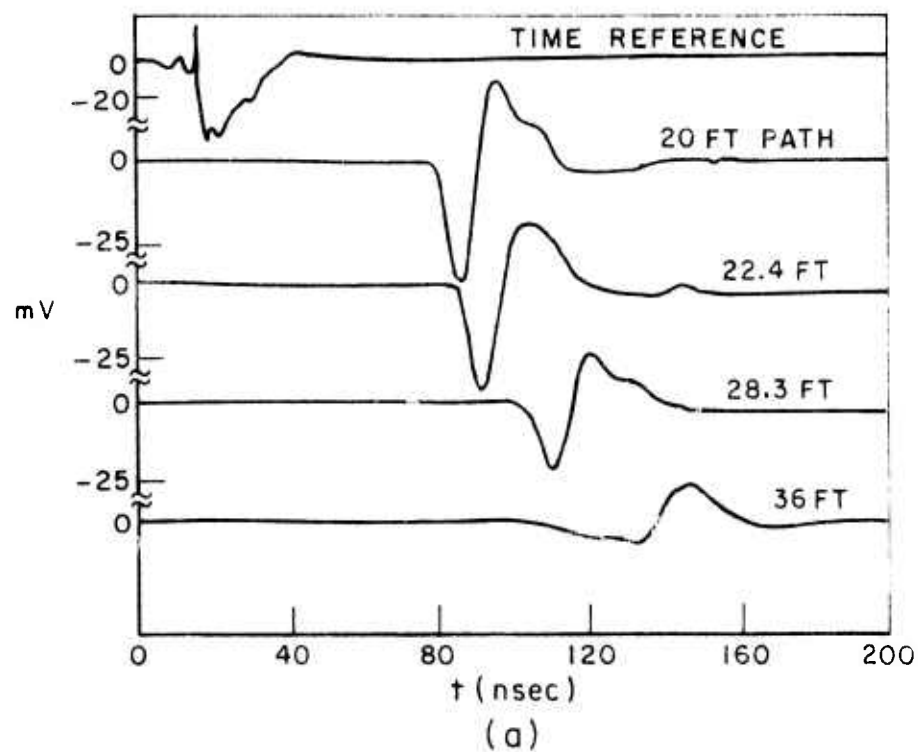
Fig. 25. Transmitted pulses through limestone (Ikor)
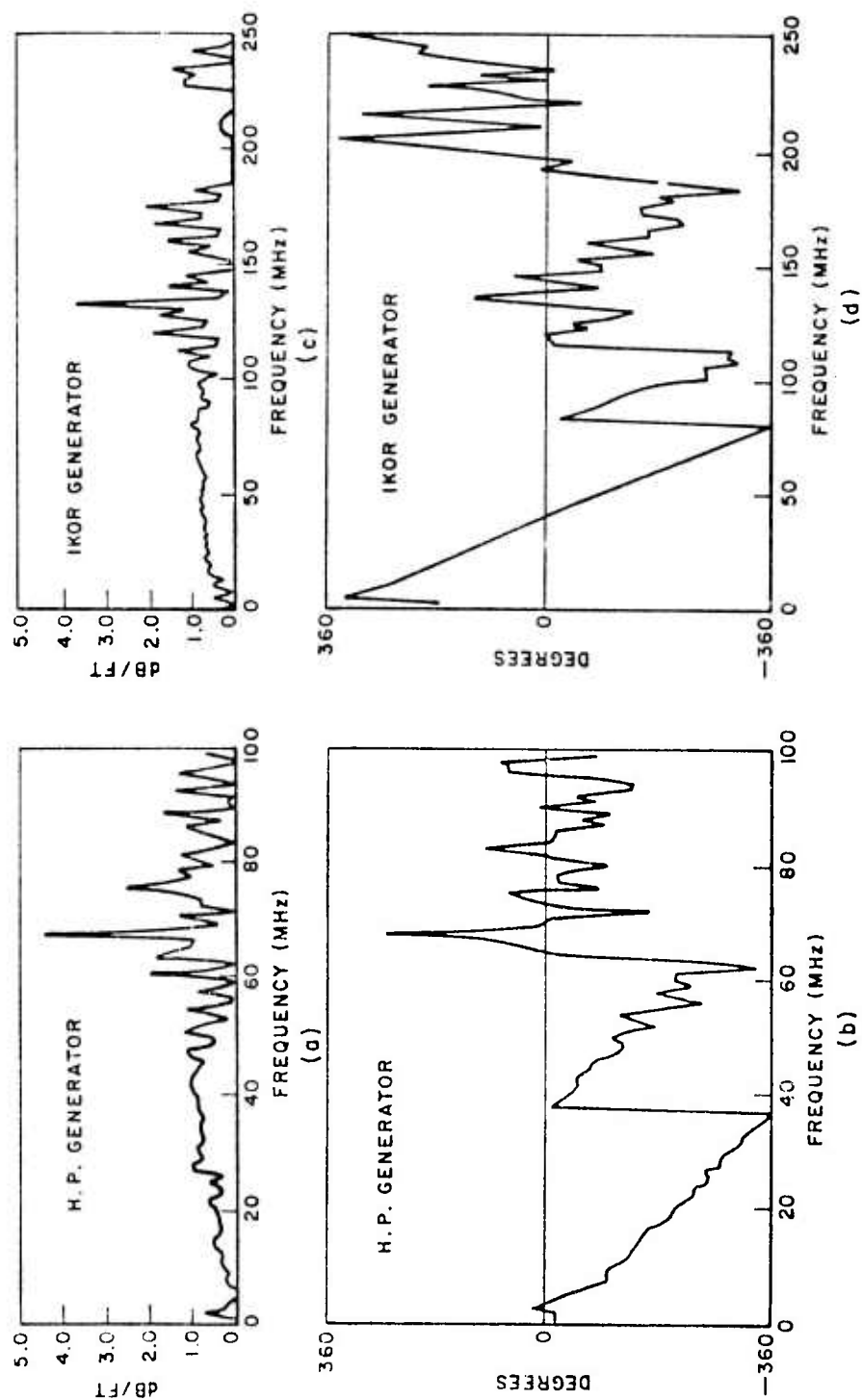(a) time domain waveforms
(b) amplitude spectra.

43

MCKINLEY AVE.

TRANSMITTER

LIMESTONE

20'

10' | 10' | 10'

RECEIVERS

TUNNEL

GROUND LEVEL

Fig. 26.   Geometry of propagation measurement in limestone.

and 29 show the relative dielectric constant and conductivity for both the H.P. and Ikor pulses, respectively.

These data were found to be in reasonable agreement with available data found in the literature[15], which are shown as X's in the figures. Note that the values of the relative dielectric constant appear to be very inaccurate at low frequencies, which corresponds to the point where the conducting term of $\gamma^2 = \omega^2 \mu\epsilon - j\ldots$ begins to dominate the propagation mechanism.

It is also of interest to measure the velocity of a pulse propagating through a medium. By measuring the time delay of the received waveform from the point at which it passes the transmitting antenna, an effective refractive index, $n = \sqrt{\epsilon_r}$ of the medium can be obtained. For the H.P. and Ikor pulses, the refractive indices

44

Fig. 27.   Attenuation of limestone.   (a) H.P. generator, magnitude.
(b) H.P. generator, phase.   (c) Ikor generator, magnitude.
(d) Ikor generator, phase.

45
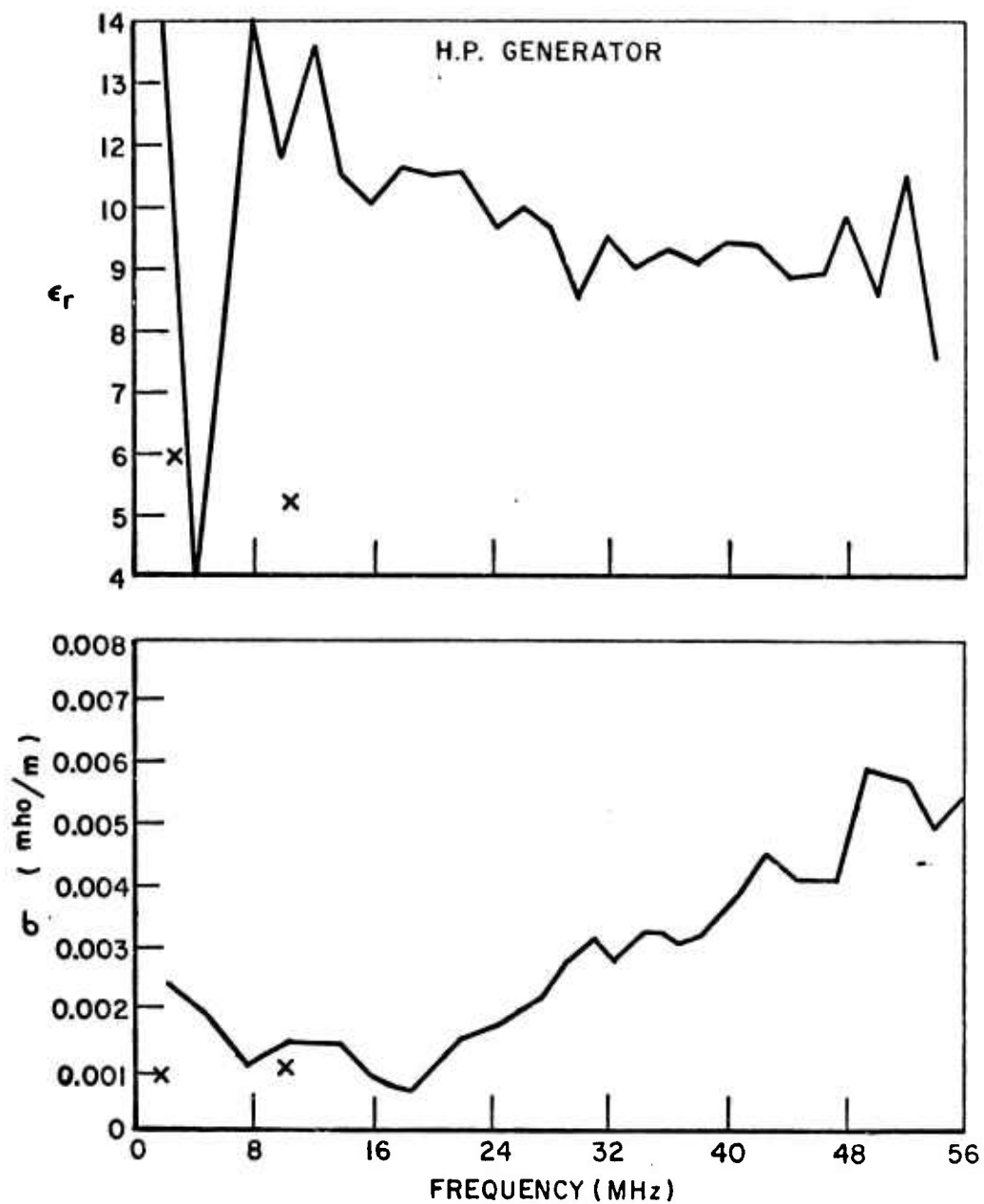
Fig. 28. Constitutive parameters of limestone (H.P.).
(a) relative dielectric constant
(b) conductivity.
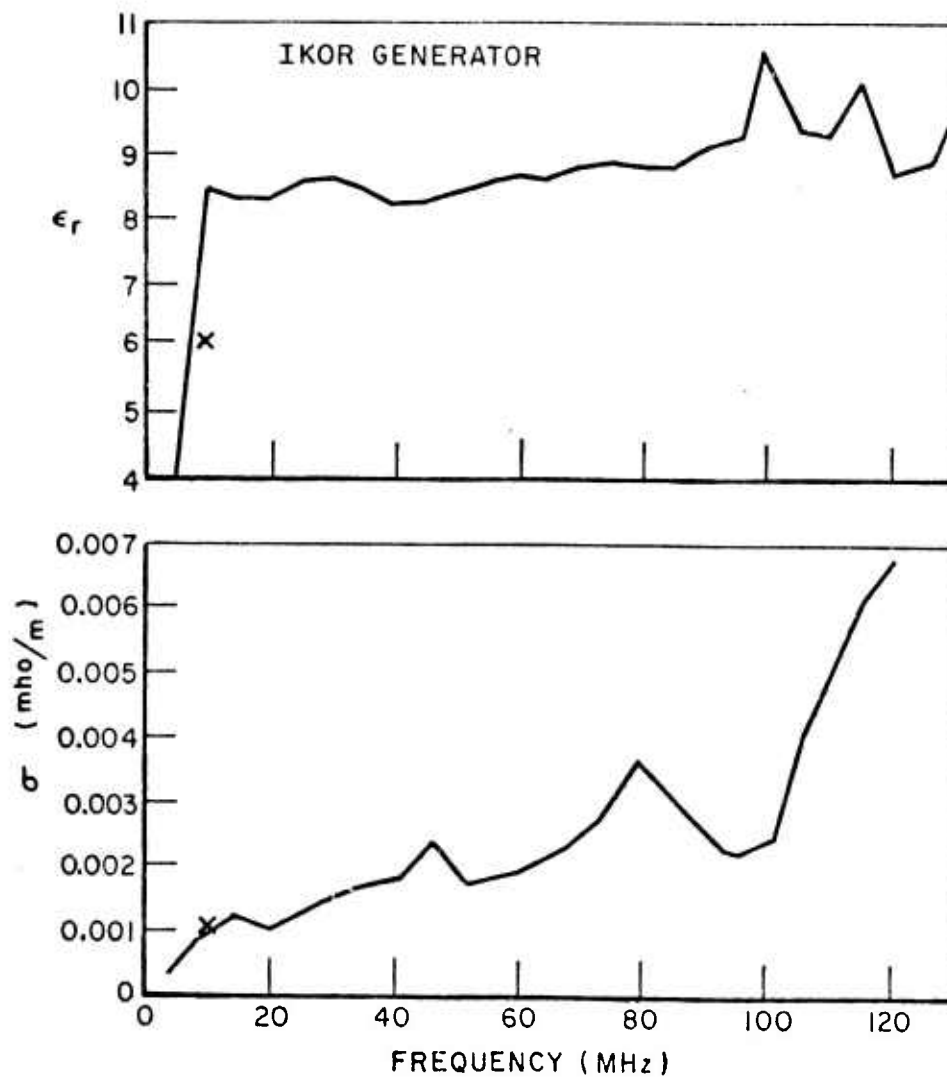
Fig. 29. Constitutive parameters of limestone (Ikor).
(a) relative dielectric constant
(b) conductivity.

obtained were respectively 3.5 and 3.2 for the 20 foot path, and 3.3 and 2.95 for the 28 foot path. Note that the refractive index changes with both distance of propagation and pulse generator. In a dispersive medium, the higher frequency components of the pulse travel faster than the lower frequency components because the relative dielectric constant decreases with increasing frequency. Since the Ikor pulse contains more high frequency energy than the H.P. pulse, it is expected to display a lower refractive index. As the pulse penetrates further into a lossy dispersive medium, more of the high frequency energy is attenuated due to the increasing conductivity. The attenuation of the high frequency components of the pulse leaves behind the slower traveling low frequency components, which should display an increase in refractive index. The fact that the refractive index actually decreases with increasing range may be due to transmission and reception of significant content of the pulse from the ends of the dipoles in addition to that from the feedpoint. The point is that when the propagation range is sufficiently large the transmitter can be considered a point source and the above comments apply. At shorter ranges, however, the received pulse waveform is a complicated combination of feed point and end radiation and apparent anomalous effects can occur.

A similar series of propagation measurements were made in a dolomite quarry near Peebles, Ohio.* Unfortunately a convenient propagation geometry between two parallel faces similar to the tunnel at the limestone quarry was not available. Propagation measurements were made using a 1 foot inverted monopole that was mounted on an 18" diameter circular conducting groundplane. The monopole was inserted in a hole drilled in the rock so that the ground plane rested on the surface of the rock. One of the standard bowtie shaped dipoles (Fig. 2b) was used as the receiver and placed on the ground at distances of 24 feet and 36 feet from the monopole. The geometry of the propagation measurement is shown in the insert in Fig. 30b.

The time and frequency domain waveforms of the transmitted pulses of the H.P. and Ikor pulse generators for the monopole-dipole configuration in dolomite are shown in Figs. 30 and 31, respectively. Note that over a path length of 24', the received H.P. pulse (Fig. 30a) endures for well over 1 μsec while the received Ikor pulse (Fig. 31a) endures for over 2.5 μsec. The excessive dispersion is believed to be due primarily to the moisture content of the rock - it had been raining for at least 24 hours immediately prior to the recording of these measurements. Poor coupling to the rock medium may also be a factor in that the surface (2"-3") of the rock was actually a loose gravel and dirt mixture.

*Plum Run Stone Division, Peebles, Ohio, Richard Bowman - Head Geologist.
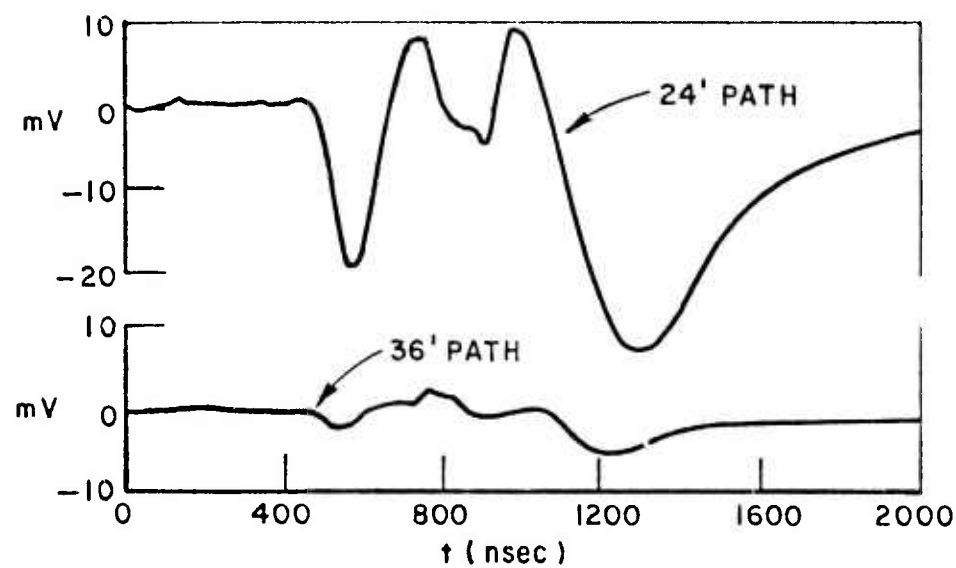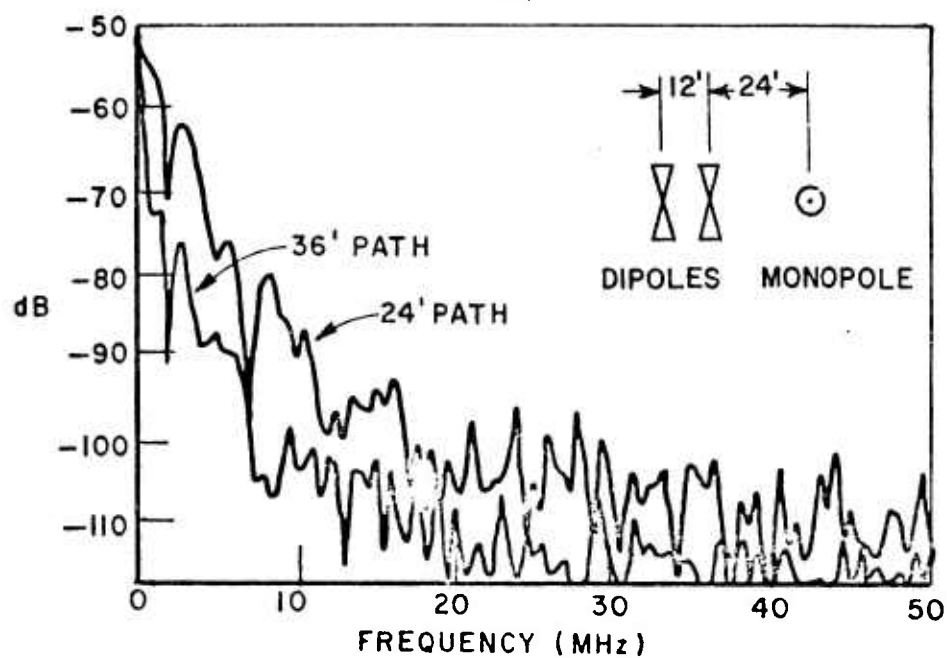
Fig. 30. Transmitted pulses through dolomite (H.P.).
(a) time domain waveform
(b) amplitude spectra.
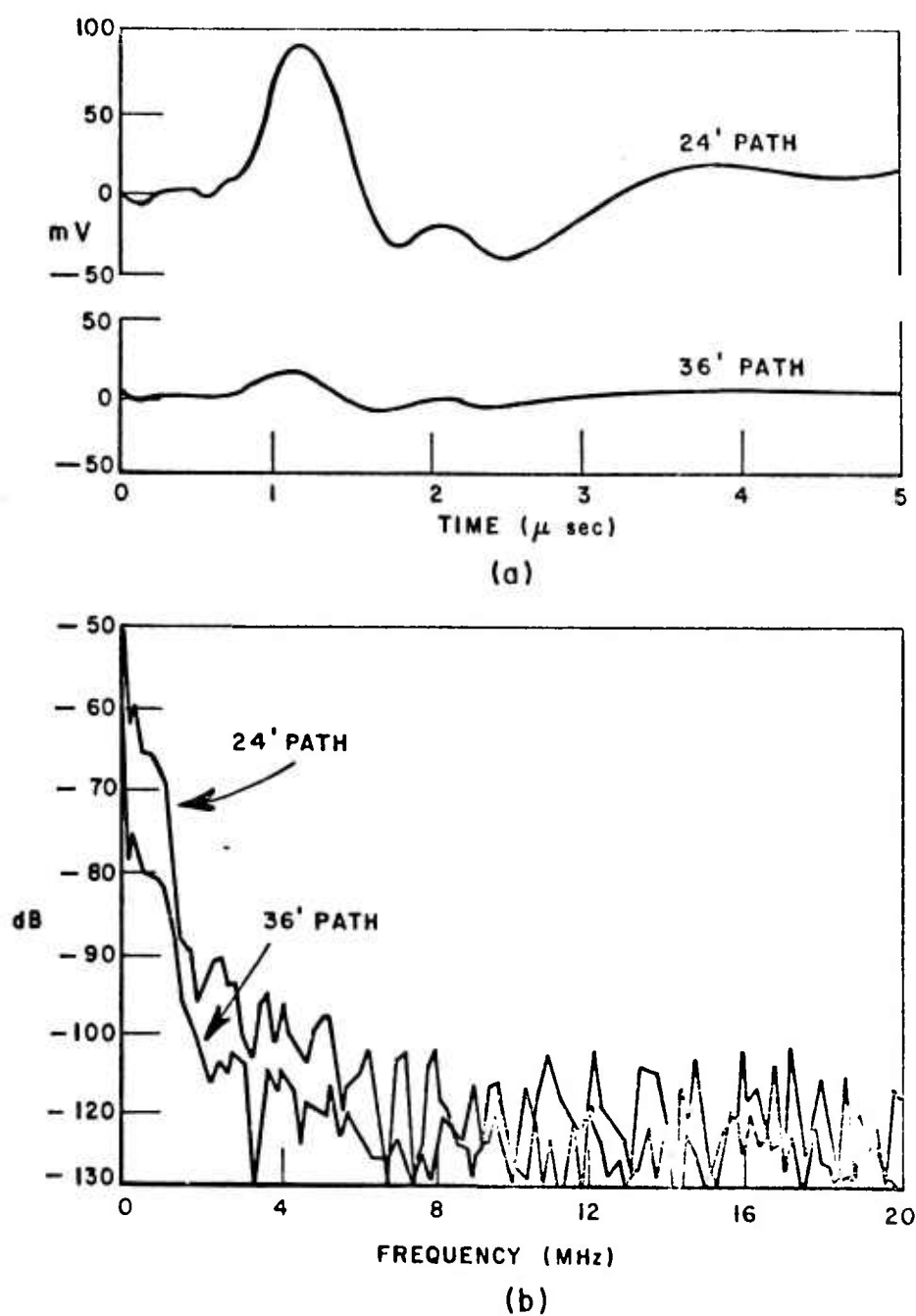
Fig. 31. Transmitted pulses through dolomite (Ikor).
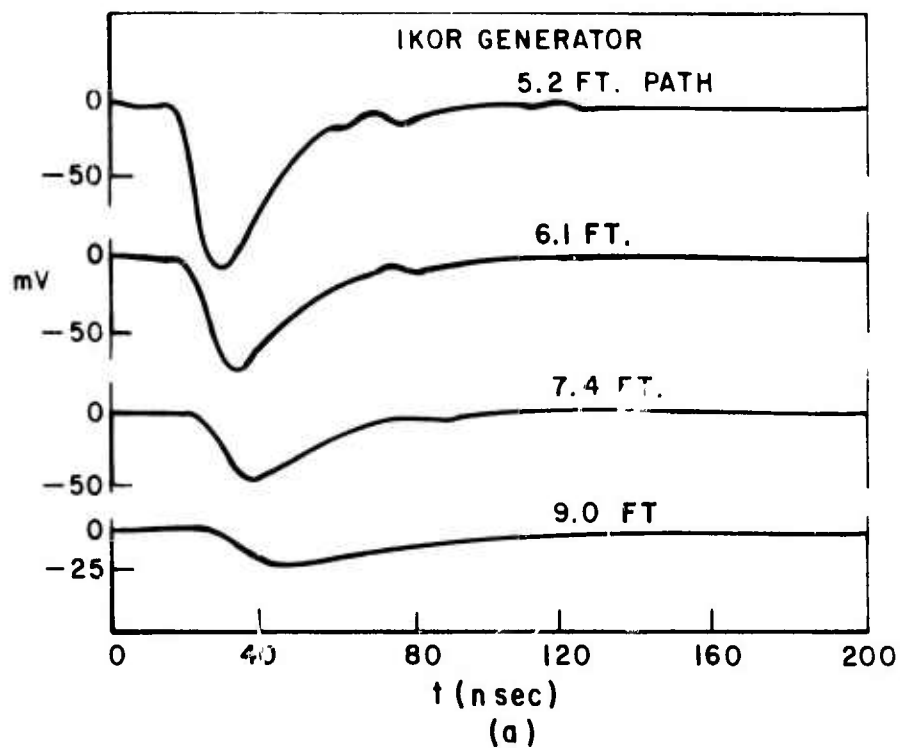(a) time domain waveform
(b) amplitude spectra.

50

The time domain waveforms of Fig. 30a (H.P.) were Fourier transformed to obtain the amplitude spectra shown in Fig. 30b which upon subtraction and normalization by path length yield the attenuation in dB/ft and phase constant of the rock medium as a function of frequency (Figs. 32a and b). This process was repeated for the Ikor pulse waveforms of Fig. 31a to obtain the amplitude and phase spectra (Fig. 31b) and attenuation (Figs. 32c and d). From the Ikor data, it is apparent that frequencies above 6 MHz were lost in the noise over a propagation distance of 24 feet, while from the H.P. data, frequencies above 20 MHz were lost over the same distance. It is important to note that the attenuation vs frequency data in Fig. 32 mean absolutely nothing above these limiting frequencies.

Using the Eq. (3) assumptions, the transmission data were processed to obtain a frequency dependent relative dielectric constant and conductivity for the medium (Fig. 33). Again these data should be considered valid only over the frequency range determined by the significant spectral content of the transmitted pulses. Due to the excessive attenuation and dispersion and the fact that Eqs. (3) and (4) are not strictly valid for this propagation measurement, these data are admittedly very gross estimates, but even so, they are still within an order of magnitude of published results[15]. It should also be recognized that the properties of the rock in a transverse direction along the surface may be quite different from its properties in the vertical direction. The increase in moisture content near the surface (it was raining at the time of the measurement) could have caused the rather high values of conductivity.

On an earlier contract (H0210042) certain initial measurements were made of metal and dielectric cylinders buried in the overburden using a prototype of the pulse sounder(8). Since both a detection and discrimination capability were demonstrated for these targets, it was of interest to obtain the electrical properties of the medium from earlier propagation measurements. The third series of propagation measurements were made in a soil medium[8]. The geometry is shown in Fig. 34. A buried 20 foot dipole was used as the transmitter, and one of the bowtie shaped dipoles (Fig. 2b) was again used as the receiver. The receiver was positioned at distances of 1-1/2, 3-1/2, 5-1/2, and 7-1/2 feet away from directly above the buried dipole, to give total path lengths of 5.2, 6.1, 7.4 and 9.0 feet. Figures 35 and 36 show the received time and frequency domain waveforms for the H.P. and Ikor pulses, respectively. The dispersion and attenuation are naturally much more severe in the soil medium, which can be seen from the attenuation data of Fig. 37. The attenuation data were processed to obtain the frequency-dependent relative dielectric constant and conductivity of Figs. 38 and 39. Since the conductivity dominates the propagation factor, the dielectric constant has little effect on the propagation mechanism, and the resultant relative dielectric constants of Figs. 38 and 39 are seen to be inaccurate. Note the rapid increase

51
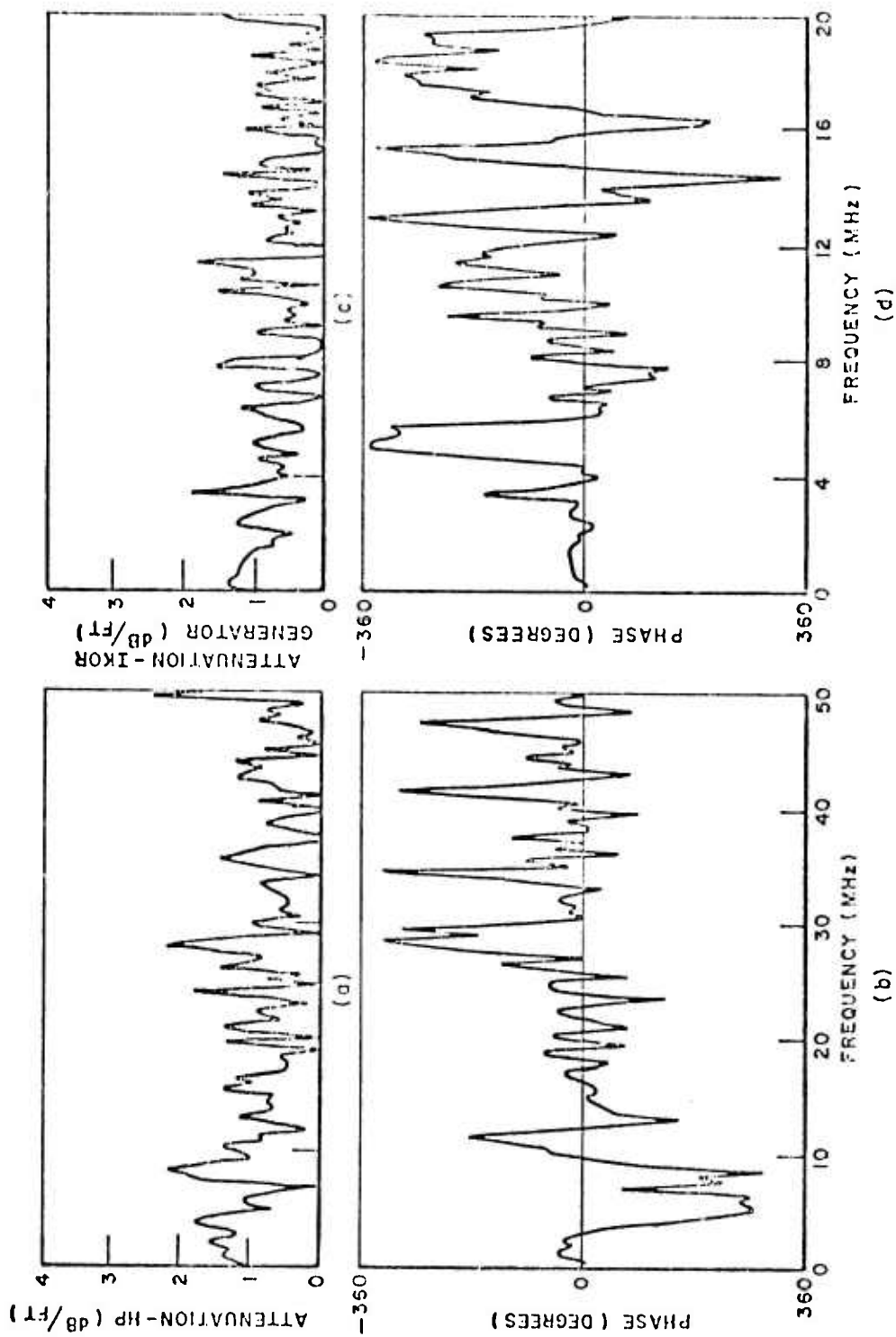
Fig. 32. Attenuation of Dolomite.
(a) magnitude - H.P. generator (b) phase - H.P. generator
(c) magnitude - Ikor generator (d) phase - Ikor generator.
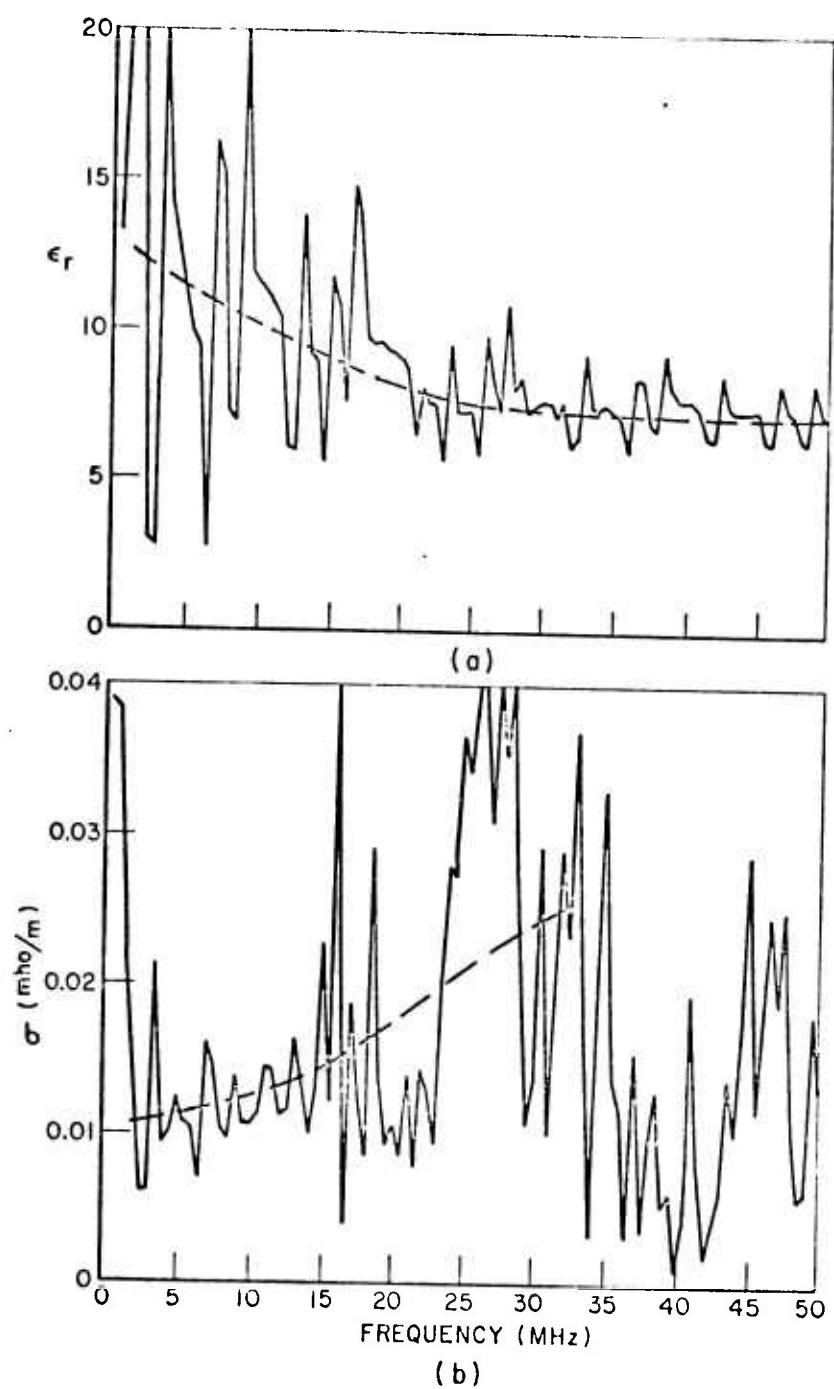
Fig. 33. Constitutive parameters of dolomite.
(a) relative dielectric constant.
(b) conductivity.

53
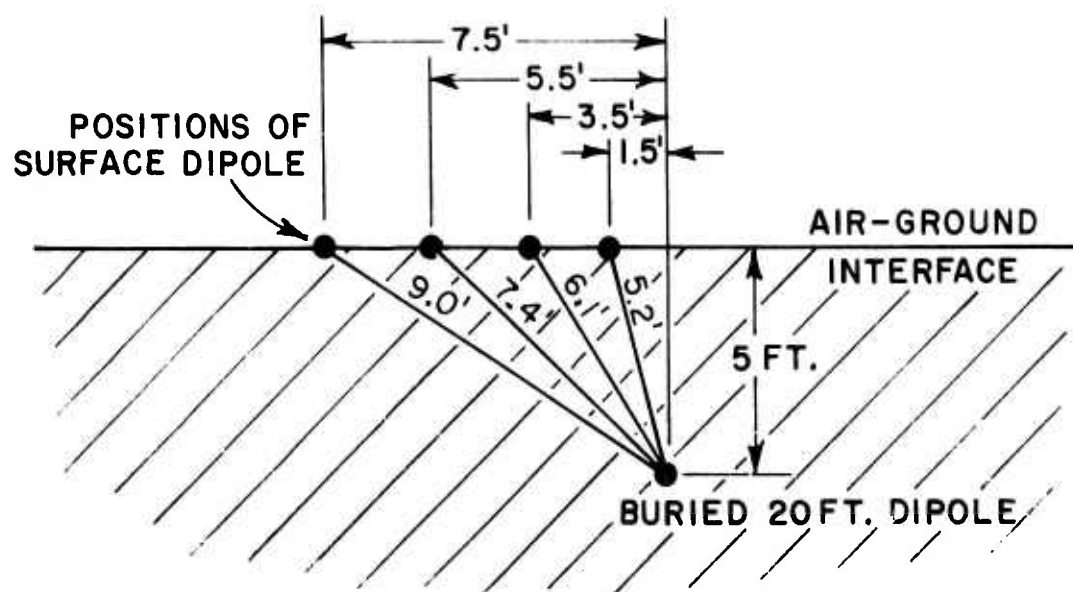
Fig. 34.   Geometry of soil propagation measurement.
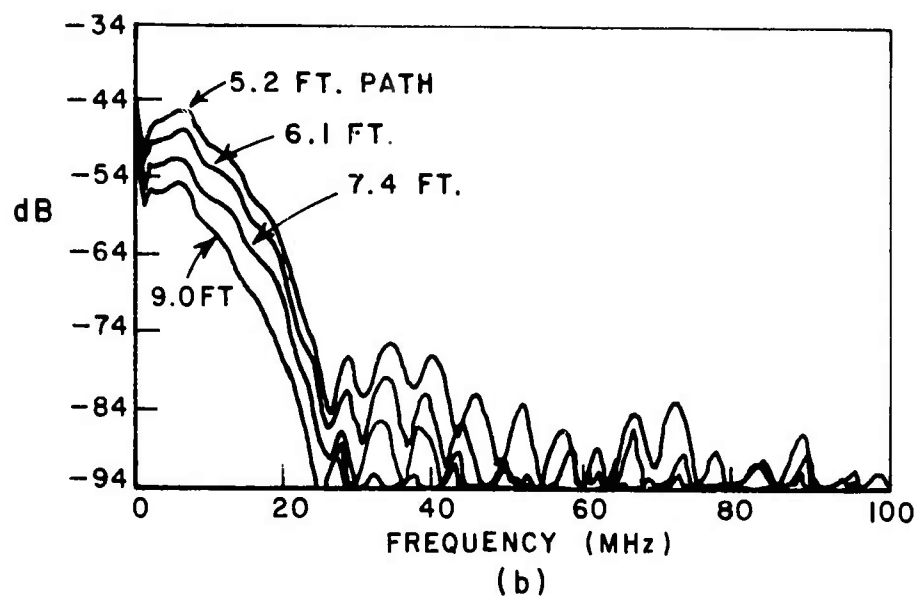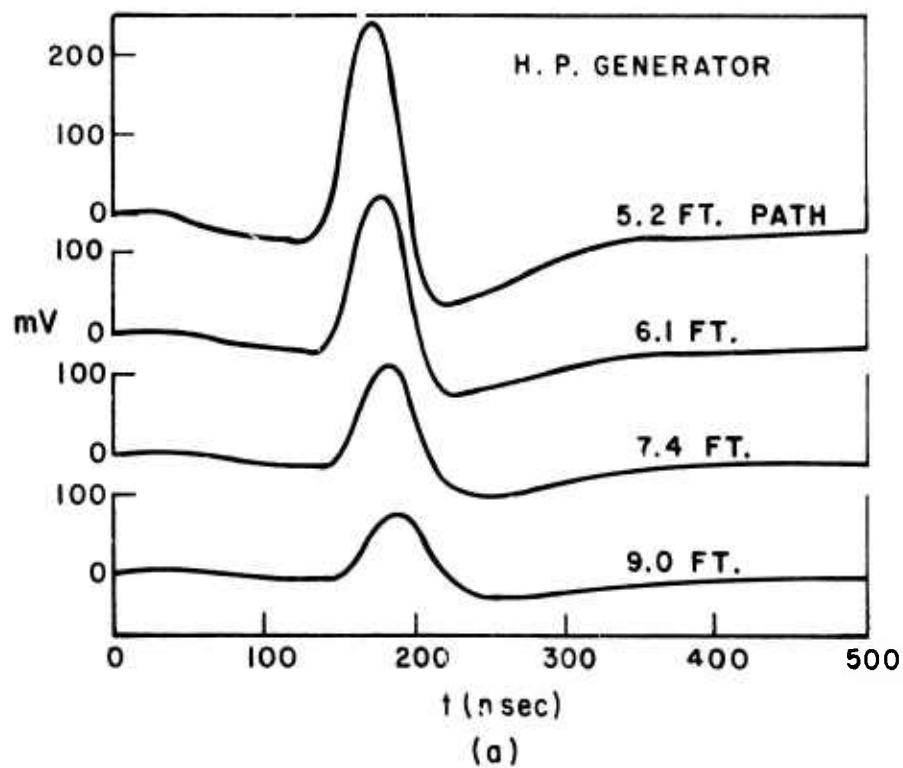
Fig. 35. Transmitted pulses through soil (H.P.)
(a) time domain waveforms
(b) amplitude spectra.
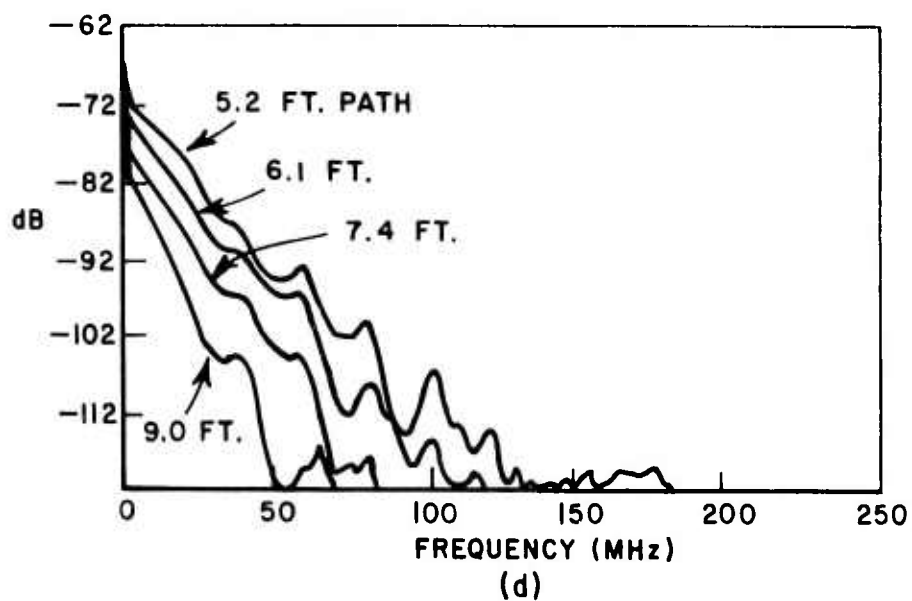
Fig. 36. Transmitted pulses through soil (Ikor).
(a) time domain waveforms
(b) amplitude spectra.

56
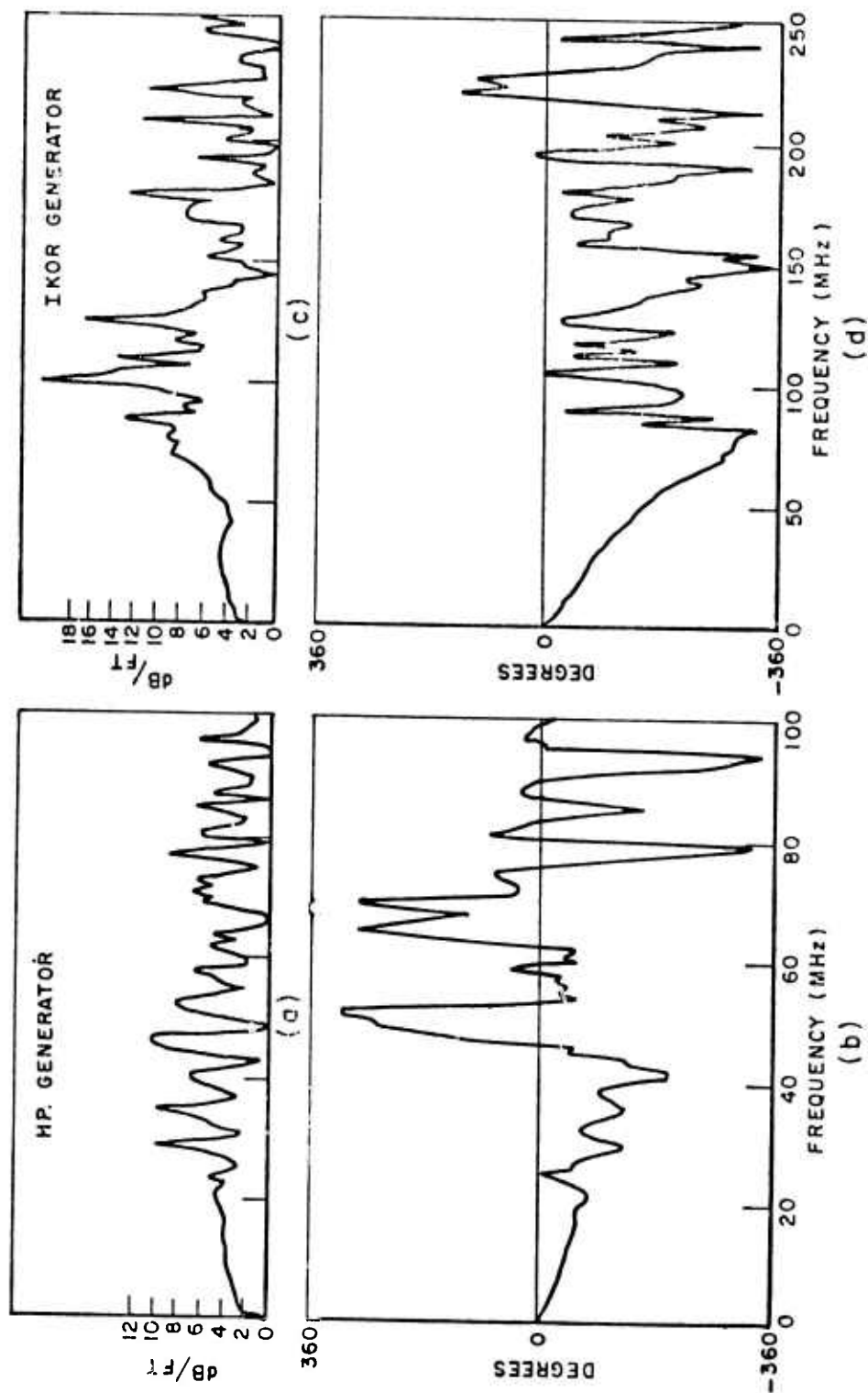
Fig. 37.   Attenuation of soil.
(a) magnitude - H.P.   (b) phase - H.P.
(c) magnitude - Ikor   (d) phase - Ikor.

57
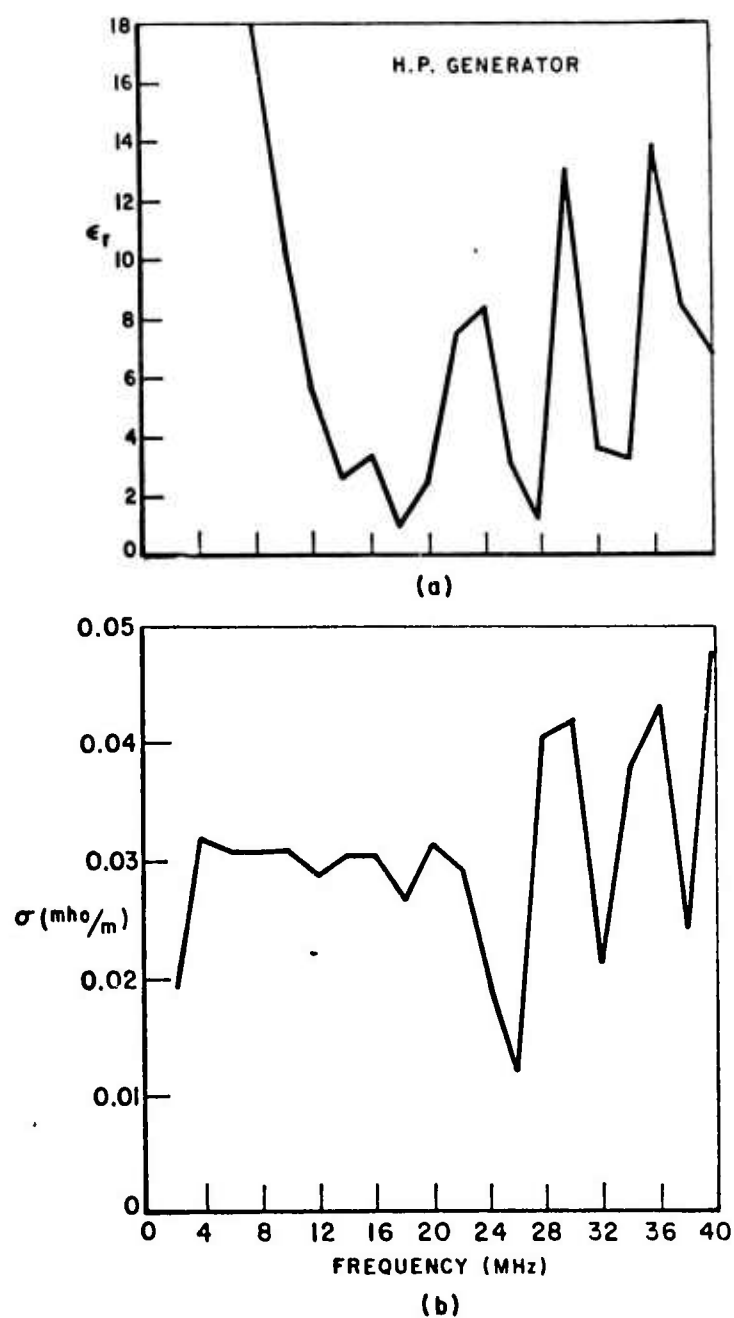
Fig. 38.   Constitutive parameters of soil (H.P.)
(a) relative dielectric constant.
(b) conductivity.
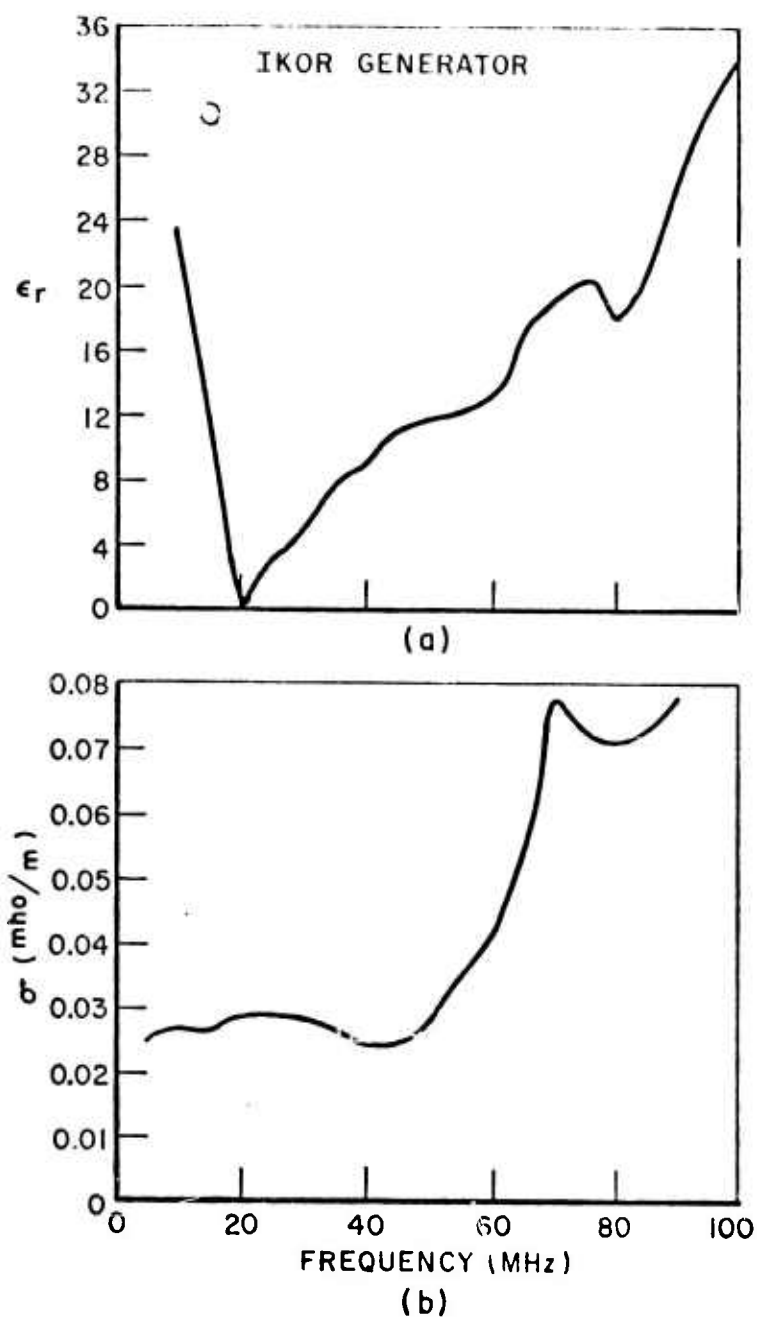
Fig. 39. Constitutive parameters of soil (Ikor).
          (a) relative dielectric constant.
          (b) conductivity.

in conductivity with frequency for the Ikor data. From the delay
measured between the transmitted pulses of Figs. 35 and 36, an
effective refractive index for soil of n = 3.9 was obtained for the
H.P. pulser and n = 3.7 for the Ikor pulse. In a dielectric medium,
these values would correspond to relative dielectric constants of
15.2 and 13.6, respectively for the H.P. and Ikor pulses.

59

VI. CALIBRATION OF SUBSURFACE PROBE SYSTEM

In the previous section on pulse propagation, the attenuation and dispersion properties of realistic subsurface media have been analyzed using state-of-the-art analysis and computer programs[14] for the complete analysis of arbitrary wire antennas in an arbitrary lossy medium. In order to complete a theoretical analysis of the pulse sounding probe, it is necessary to correct the programs to account for the air-surface interface. An exact correction is neither obvious nor simple.

A probe calibration basically means that the transfer function of the dipole antenna lying on the surface of the medium is known. Given this transfer function one can calculate the spectral content of the input signal actually incident on the subsurface target, assuming a homogeneous medium. Once the incident field on a particular target is known, the scattered field spectrum can be calculated for simple targets. A knowledge of the frequency-dependent constitutive parameters of the medium would then permit normalization of the measured response spectrum to obtain the impulse response spectrum of the target. Applying Fourier transform theory would then yield the resultant time domain target impulse response waveform.

A simplified linear system block diagram of the pulse sounding system is shown in Fig. 40a for a propagation measurement. The subscripts T and R refer to the transmitting or receiving components of the system. $P(s)$ is the input pulse spectrum, $C_T(s)$ and $C_R(s)$ are the transfer function of the cables, $B_T(s)$ and $B_R(s)$ are the transfer functions of the baluns. $T_T(s)$ and $T_R(s)$ are the transfer functions of the twin lead transmission line, $A_T(s)$ and $A_R(s)$ are the transfer functions of the antennas, $M(s)$ is the transfer function of the medium, and $R(s)$ is the received spectrum. It is reasonable to assume that the transfer functions of the transmitting and receiving cables, baluns, and twin lead are identical, so that the spectrum of the received waveform $R(s)$ can be written as

$$(4) \qquad R(s) = P(s)C^2(s)B^2(s)T^2(s)A_T(s)M(s)A_R(s).$$

The input pulse spectrum and the transfer functions (attenuation) of the cable, baluns, and twin lead are easily measured (Figs. 3 and 4) and shown in Fig. 41. These can all be lumped into one quantity $G(s)$ to account for the entire feed line.

$$(5) \qquad G(s) = P(s)C^2(s)B^2(s)T^2(s).$$
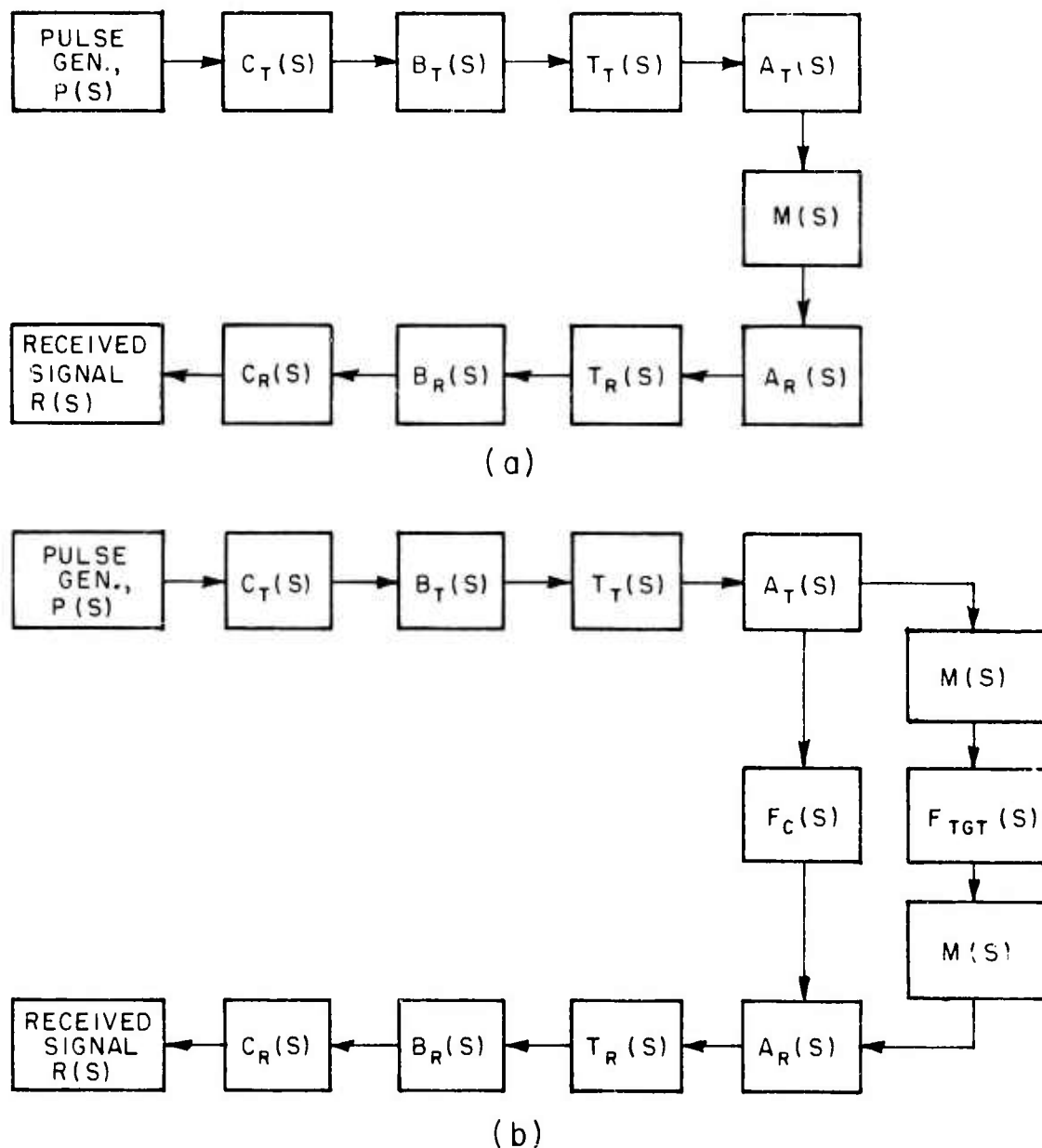
Fig. 40. Linear system block diagram.
(a) propagation measurement
(b) target response measurement,
orthogonal mode.

61
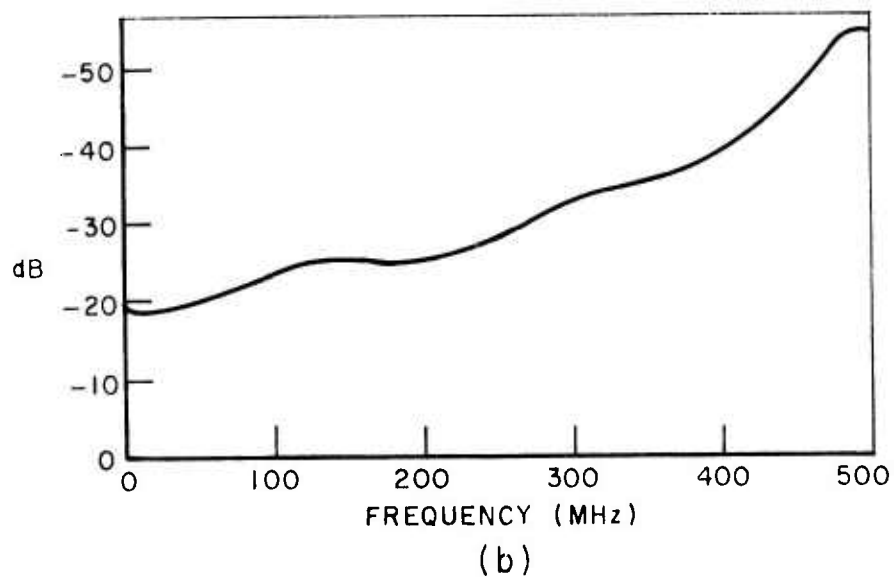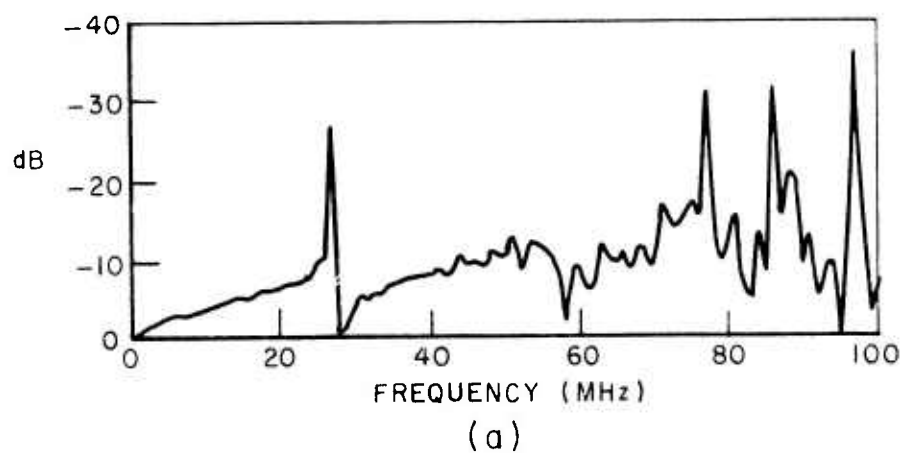
Fig. 41. Transfer function (attenuation) of cables,
baluns, and twin lead.
(a) H.P. pulse.
(b) Ikor pulse.

The transfer function of the antennas cannot be measured directly. It can sometimes be approximately calculated via a propagation measurement, however, which first estimates M(s), the transfer function of the medium.

A second block diagram to account for the presence of a target and coupling between the transmit and receive antennas operating in the orthogonal mode is shown in Fig. 40b. Note that the medium effects of Fig. 40a have been replaced by $F_c(s)$ and $M^2(s) F_{TGT}(s)$, where $F_c(s)$ is the transfer function of the probe when not in the vicinity of a target, and $F_{TGT}(s)$ is the response spectrum of the sub-surface target. $M(s)$ is the transfer function (attenuation) of the medium which is included twice to account for the two way path. The no-target transfer function of the probe, $F_c(s)$, is obviously a function of both probe design and the medium. It is very sensitive to minor changes in the medium and accounts for all of the clutter and coupling mechanisms previously described. When a target is in the near field of the probe, the presence of the target affects the no-target transfer function $F_c(s)$, because of its $\land$, dependence. For those cases, it is difficult to separate the target response from the clutter, which in effect implies that a clear time window is not obtained. R(s) in the presence of a target can be written as

$$(6) \qquad R(s) = P(s)C^2(s)B^2(s)T^2(s)A^2(s)[F_c(s)+M^2(s)F_{TGT}(s)]$$

and an ideal means for processing would be to obtain the impulse response spectrum

$$(7) \qquad F_{TGT}(s) = \left[\frac{R(s)}{P(s)C^2(s)B^2(s)T^2(s)A^2(s)} - F_c(s) \right] \frac{1}{M^2(s)} .$$

In most cases, the term $F_c(s)$ can be eliminated by differencing a target and no-target waveform in the time domain, or simply time window gating to isolate the target response.

Under certain favorable conditions which are not often encountered in the field, it is possible to experimentally estimate the transfer function of the antenna from a propagation measurement. The tunnel geometry in limestone provided such favorable conditions. If two identical antennas are used, one measures via a propagation measurement

$$(8) \qquad R(s) = G(s)A^2(s)M(s).$$

$M(s)$ is obtained by measuring transmitted pulses over two different path lengths, as in Fig. 26. The antenna transfer function $A(s)$ is then calculated by

$$(9) \qquad A(s) = \left[\frac{R(s)}{G(s)M(s)} \right]^{1/2} \quad .$$

The transfer function in the broadside direction of one of the small
bowtie shaped dipoles of Fig. 2b is shown in Fig. 42a. This transfer
function was calculated using the propagation data of Fig. 25 for
the Ikor pulser. Figure 42b shows the results using the H.P.
pulser. An estimate of the actual pulses and spectra transmitted into
the medium are shown in Figs. 43 and 44 for the Ikor and H.P. pulses,
respectively.

Figures 45a and 45b show the experimental transfer functions
of the large 28' dipole with the aluminum sheets. Since the propa-
gation measurements were made with the large dipole transmitting and
the small dipole receiving, it can be seen that the transfer functions
of Fig. 42 were needed to obtain those of the large dipole. The
estimated pulses transmitted to the medium are shown in Figs. 46 and
47 for the Ikor and H.P. pulses, respectively.*

Unfortunately, the dolomite quarry does not contain a similar
tunnel structure that would permit this type of processing. Thus an
experimental determination of the transfer function of the dipole
on the dolomite medium is not feasible. Note, however, that since
the electrical properties of limestone and dolomite were quite
similar, it would not be unrealistic to use the limestone results to
process data from the dolomite quarry. No attempt was made to
estimate the antenna transfer functions for a soil medium. As will
be seen, present applications do not require a calibration capability
for detection and identification.

An experimental determination of the transfer function of the
antennas is not always possible, thus a theoretical analysis is
necessary. A development comparable to the present arbitrary wire
antenna in an infinite medium via numerical evaluation of the
Sommerfeld integrals is not feasible with present funding levels. A
simpler correction to approximately account for the air-medium inter-
face and permit utilization of the existing programs is sought.

In order to obtain an approximation to the subsurface fields
of the antenna lying on a lossy half-space, a simpler image theory
approximation, along with a modification of the antenna currents has
been attempted as a first step. Wait[16] has shown that for an in-
finitely long and infinitely thin wire lying on the interface between
two media of wave numbers k_1 and k_2, that the first term in an
expansion for the wavenumber γ of the current flowing on the wire is

$$\gamma = \sqrt{\frac{k_1^2 + k_2^2}{2}} \quad .$$

*In Figs. 43, 44, 46 and 47, the time waveforms are referenced to the
actual pulse output (Figs. 3 and 4).
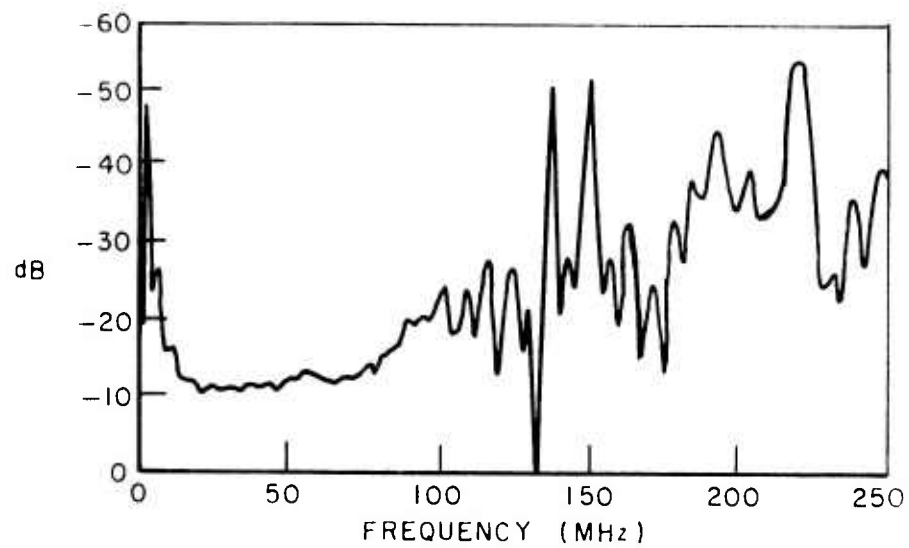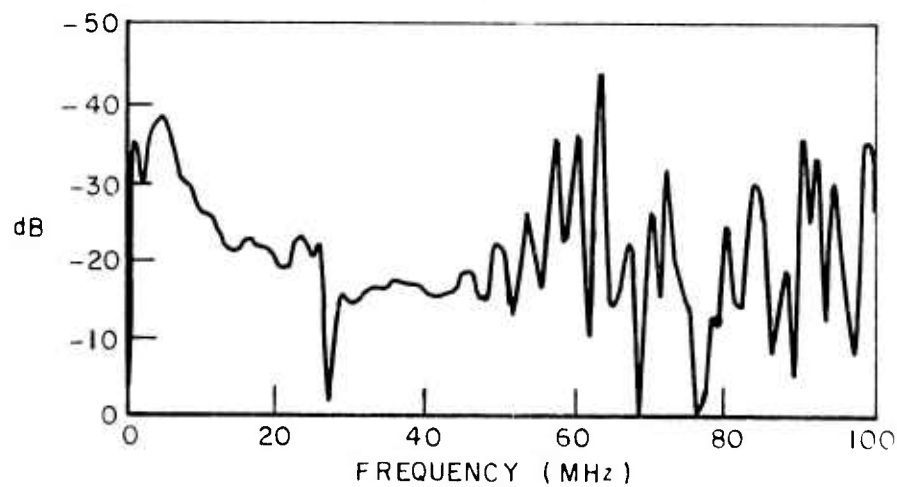
Fig. 42. Transfer function of 6 foot dipole (Fig. 2b)
(a) Ikor pulse.
(b) H.P. pulse.

65
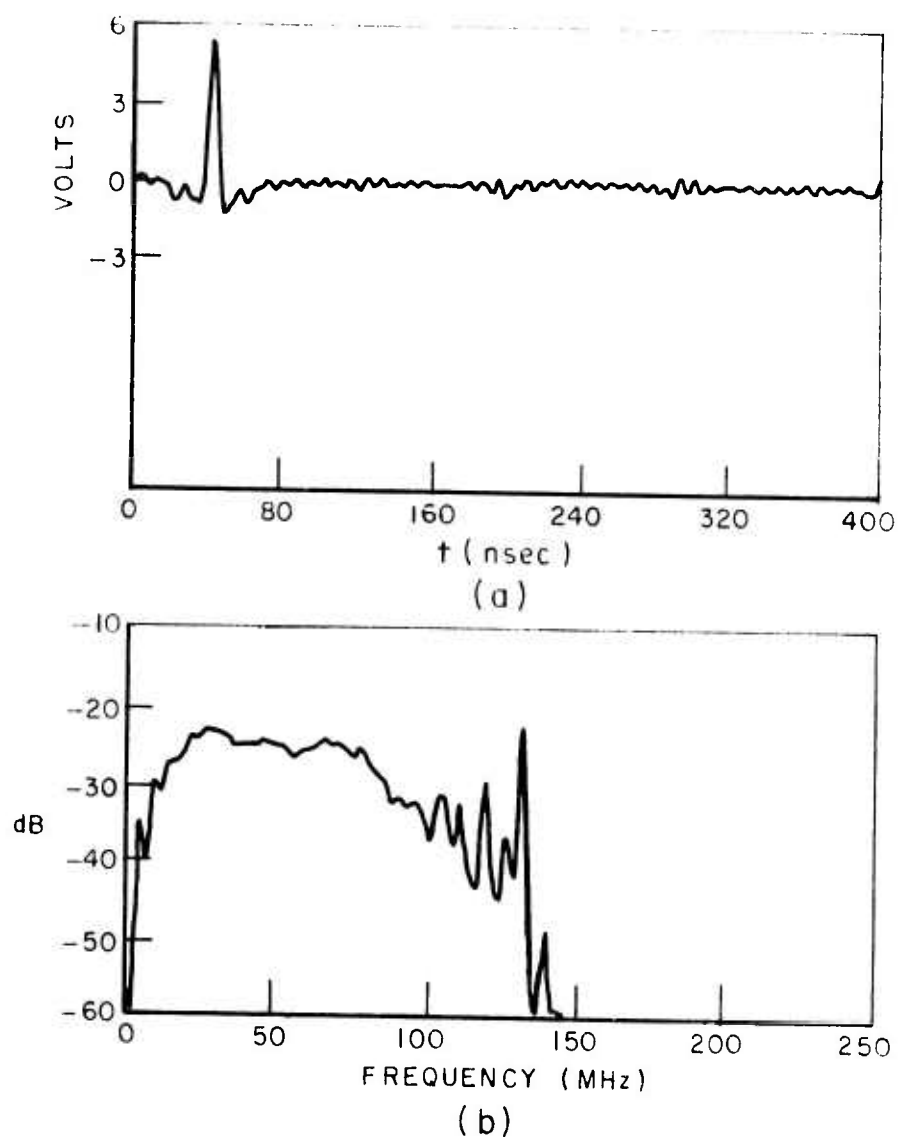
Fig. 43. Pulse transmitted into limestone via 6 foot
dipole - Ikor generator.
(a) time domain waveform.
(b) amplitude spectrum.

66
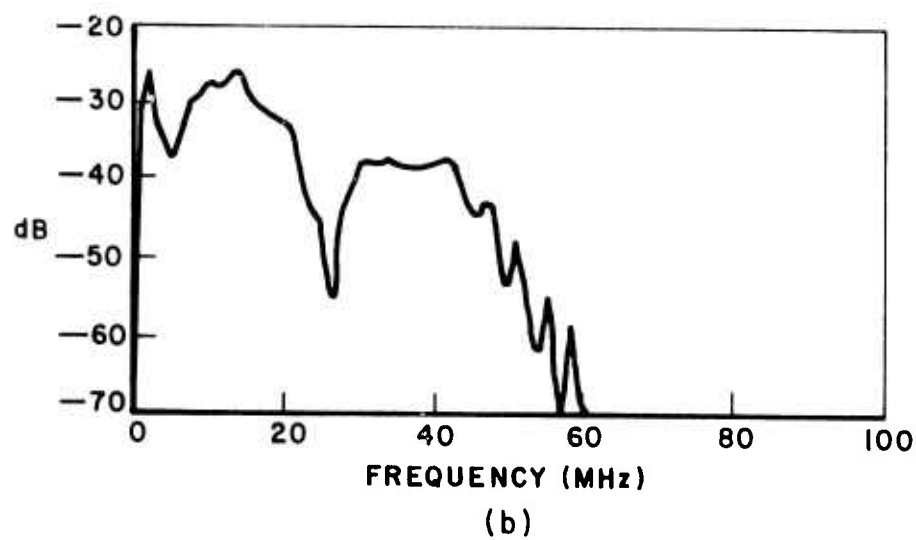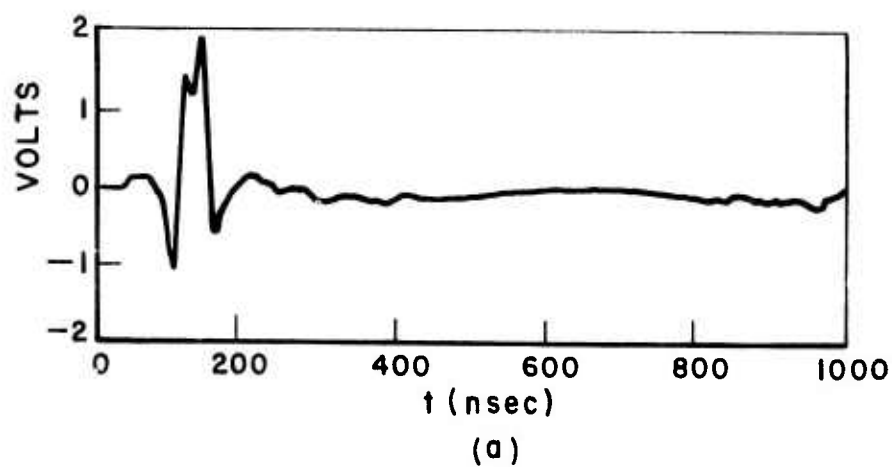
Fig. 44. Pulse transmitted into limestone via 6 foot
dipole - H.P. generator.
(a) time domain waveform
(b) amplitude spectrum.
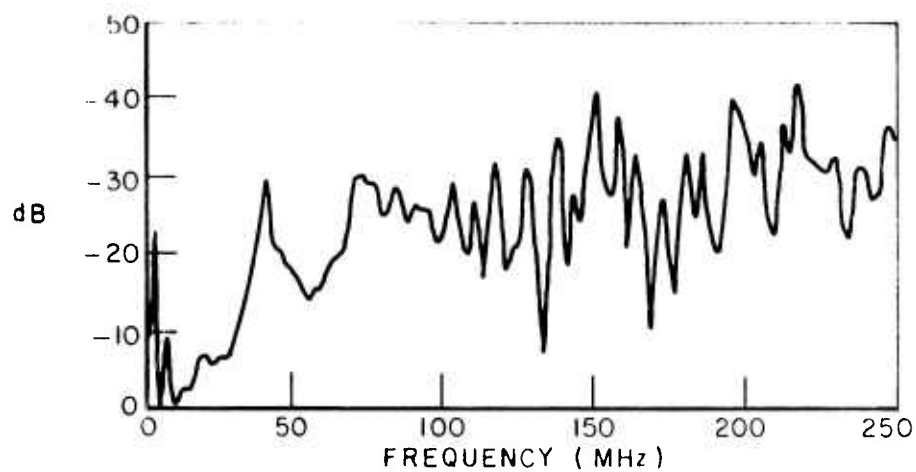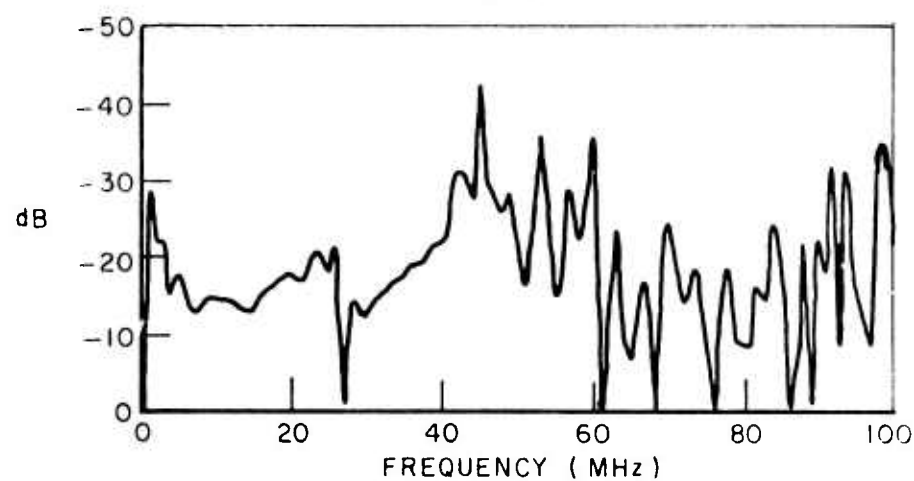
Fig. 45. Transfer function of 28 foot dipole (Fig. 2a).
(a) Ikor pulse
(b) H.P. pulse.
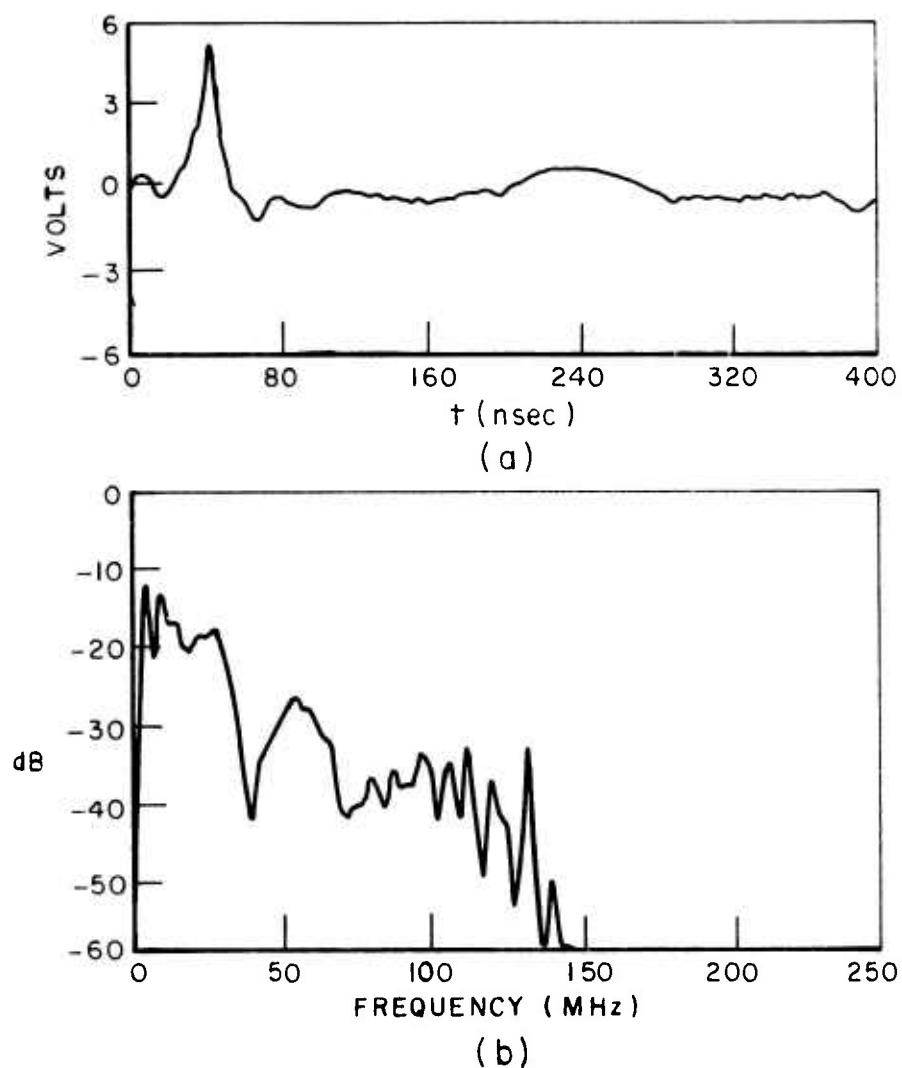
Fig. 46. Pulse transmitted into limestone via 28 foot
dipole - Ikor generator
(a) time domain waveform
(b) amplitude spectrum.

69
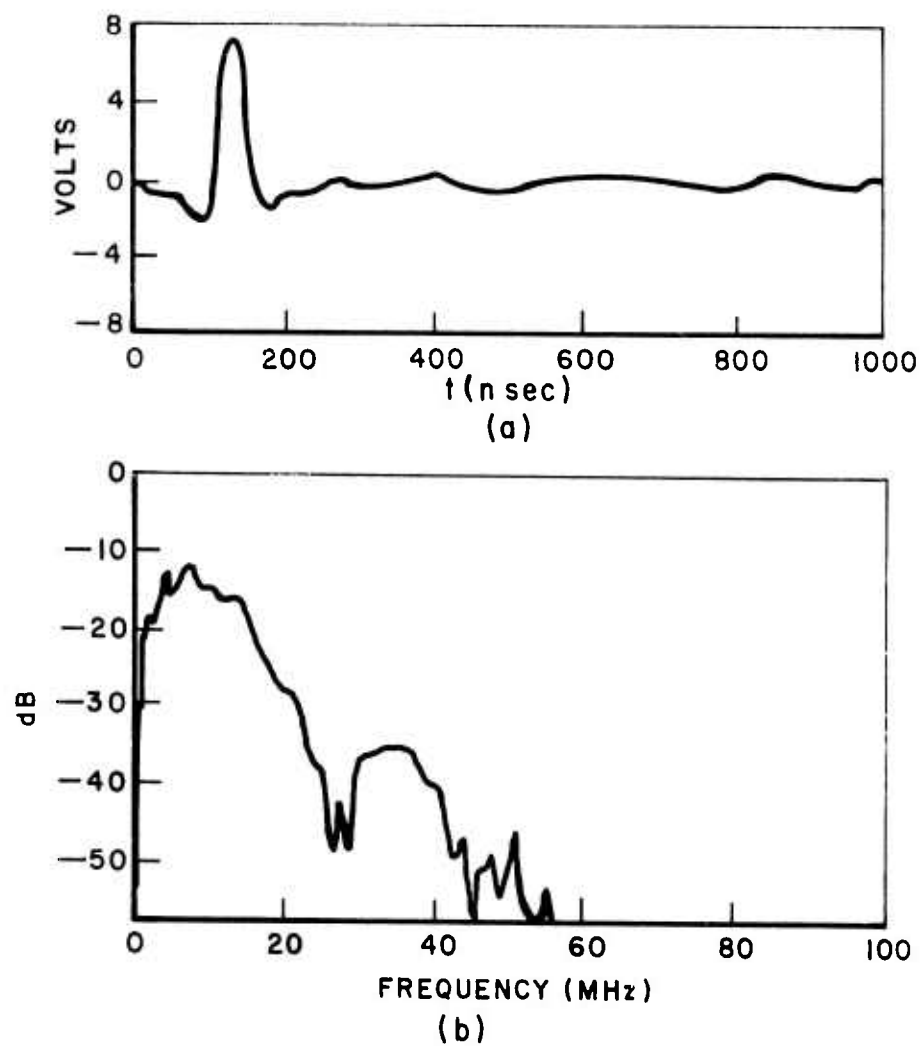
Fig. 47. Pulse transmitted into limestone via 28 foot
dipole - H.P. generator.
(a) time domain waveform
(b) amplitude spectrum.

This approximation in effect assumes an infinite medium with a relative dielectric constant and conductivity equal to the average of the relative dielectric constants and conductivities of the two media. A second approximation applied to the analysis is that of simple plane-wave reflection at the interface. After the currents had been modified by the above equation, the radiated fields were calculated in an infinite medium using the parameters of the subsurface medium of interest. These fields were then modified by the planewave reflection coefficient

$$(10) \qquad \rho = \frac{k_1^2\cos\theta - k_2\sqrt{k_1^2 - k_2^2\sin^2\theta}}{k_1^2\cos\theta + k_2\sqrt{k_1^2 - k_2^2\sin^2\theta}}$$

where $\quad \overline{H}^r = \rho\, \overline{H}^i$

is perpendicular to the plane of incidence, and $\overline{H}^i$ is incident from medium 2. This approximation is valid when the source is distantly removed from the interface in the lossy medium, but is questionable as the source approaches the interface. Despite this fact and the fact that wire antennas of finite radius and finite length are being considered, some interesting results have been obtained. Figures 48 to 51 show the calculated field strength at a distance of 5 feet from the feed terminals of the small dipole of Fig. 2b. The figures cover frequencies of 0.1, 1.0, 10.0, and 100.0 MHz, and show the x and z component magnitudes of the electric field for the configuration shown in the insert of Fig. 48. The fields are shown for the infinite medium, for the infinite medium with only the planewave reflection modification, for the infinite subsurface medium with only the current modification, and finally for the current modification and planewave reflection.

Note from Figs. 48-51 that the planewave reflection modification effectively doubles the magnitude of the x- and z-components at all frequencies and aspect angles for both the modified and unmodified currents. A comparison of the electric field magnitudes for the modified and unmodified currents without planewave reflection is found to agree reasonably well with data presented by Wait[17]. For the quasistatic (neglect displacement currents) case considered by Wait, the magnitude of a transient electric field (x-component) at $\theta=0°$ for the half-space was found to differ from that of the infinite space by the factor 1.75, that is $(E_x)_{H.S.} = 1.75(E_x)_\infty$. Using the planewave reflection approximation, $(E_x)_{H.S.} = 2.0(E_x)_\infty$, and the modified current plane-wave reflection approximation yields

71
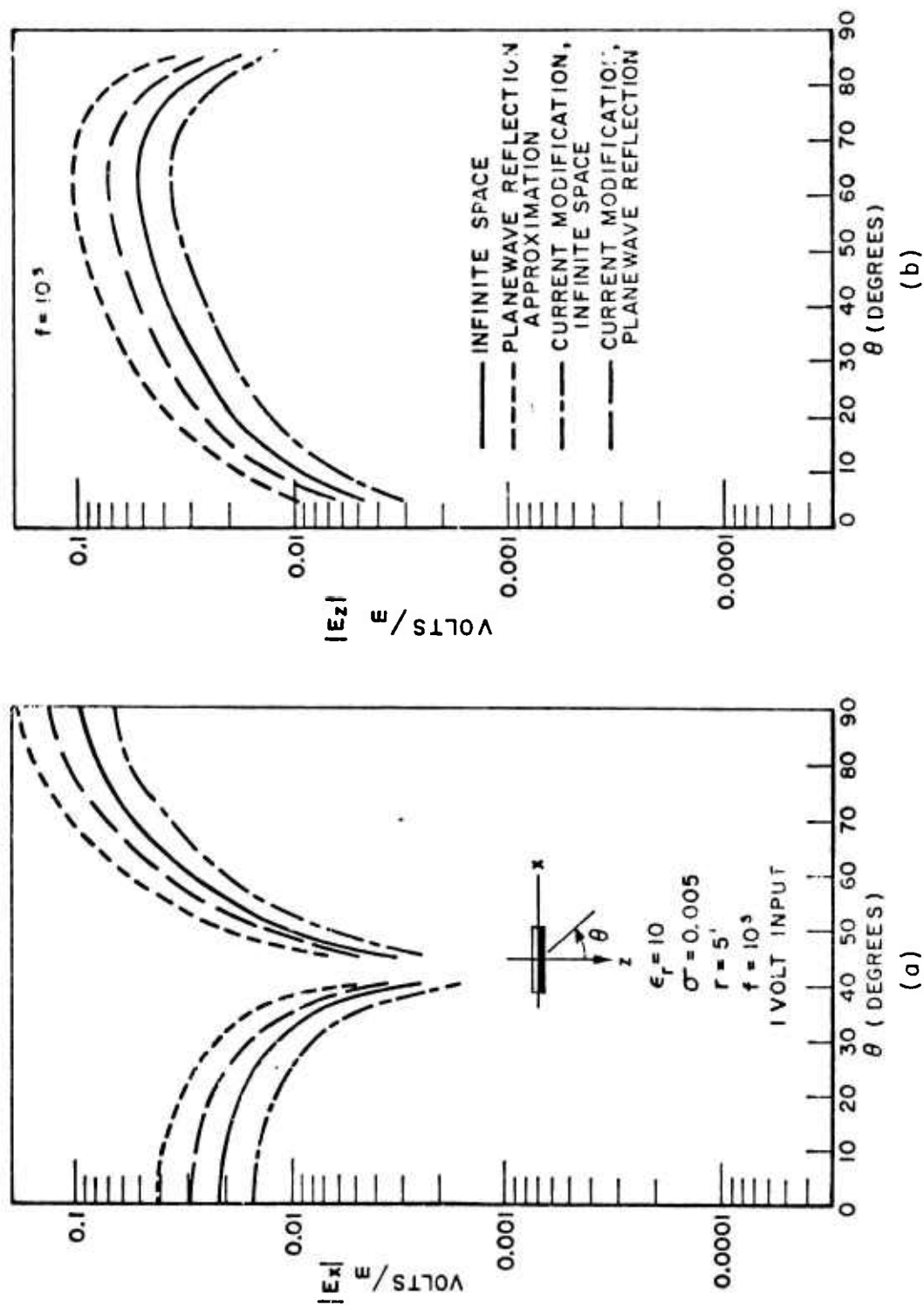
Fig. 48. Subsurface fields of 6 foot dipole, 100 MHz.
(a) x-component   (b) z-component.

72
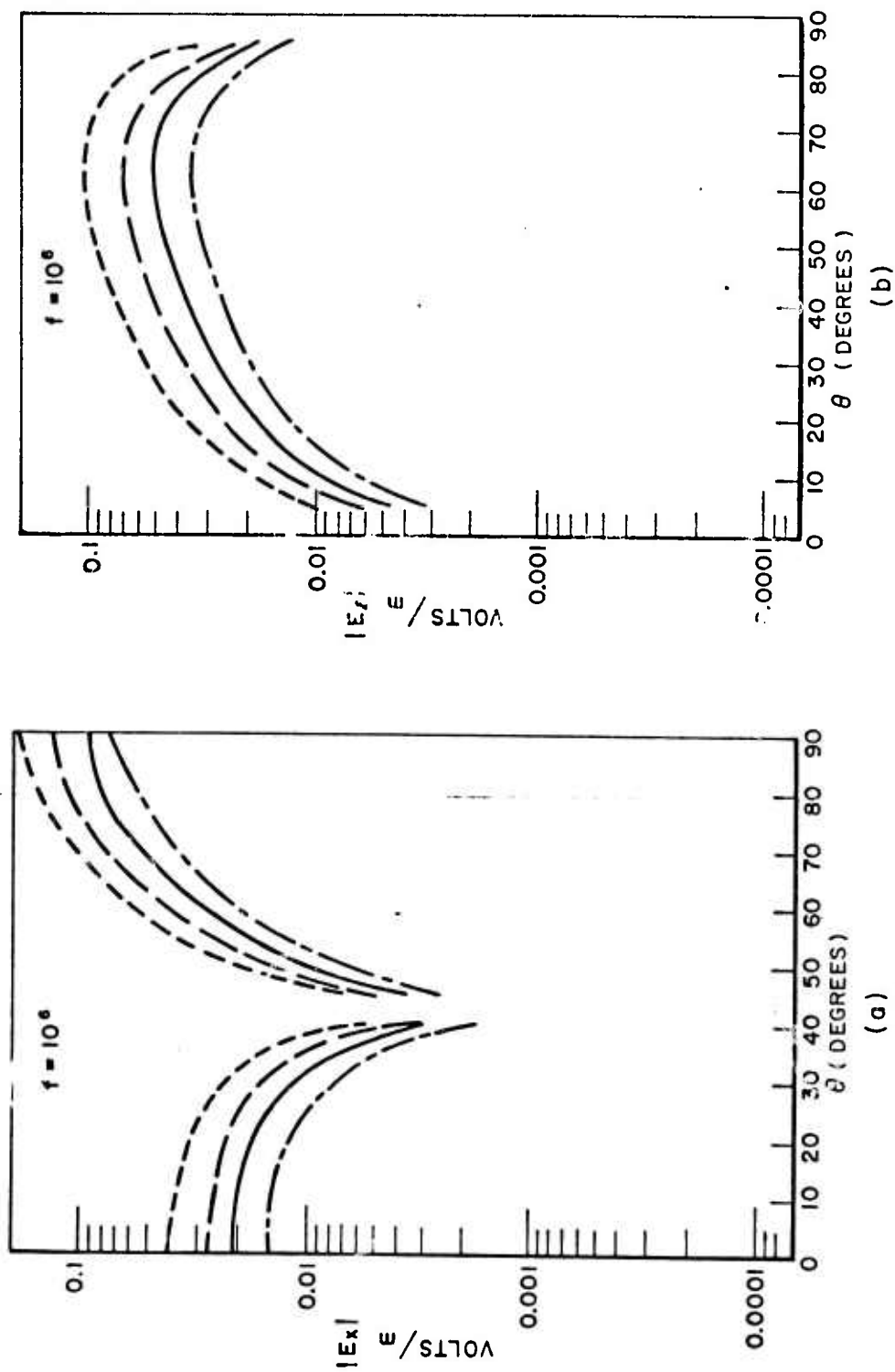
Fig. 29. Subsurface fields of 6 foot dipole, 1 MHz. (a) x-component (b) z-component.

73
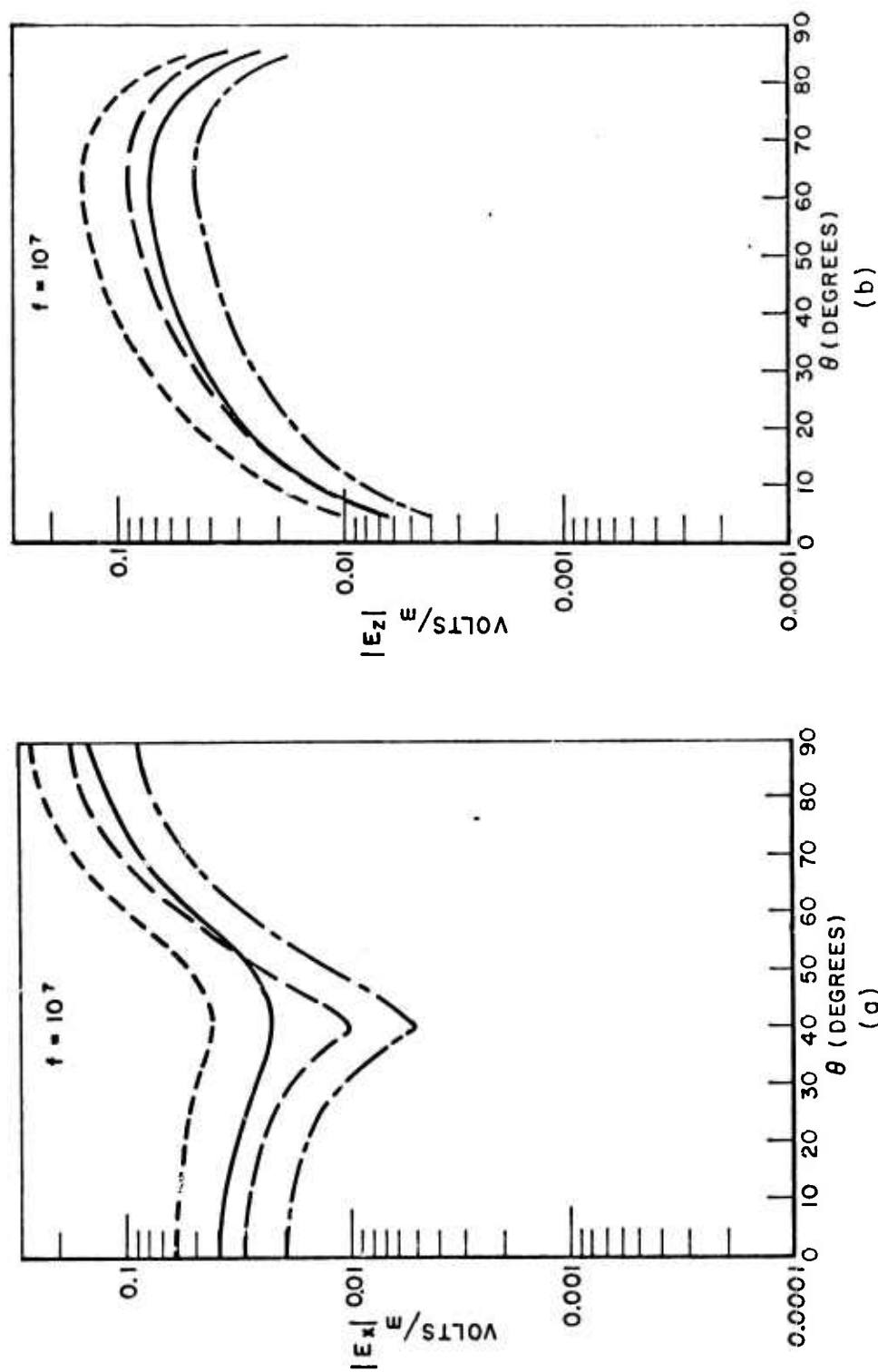
Fig. 50. Subsurface fields of 6 foot dipole, 10 MHz.
(a) x-component (b) z-component.

74
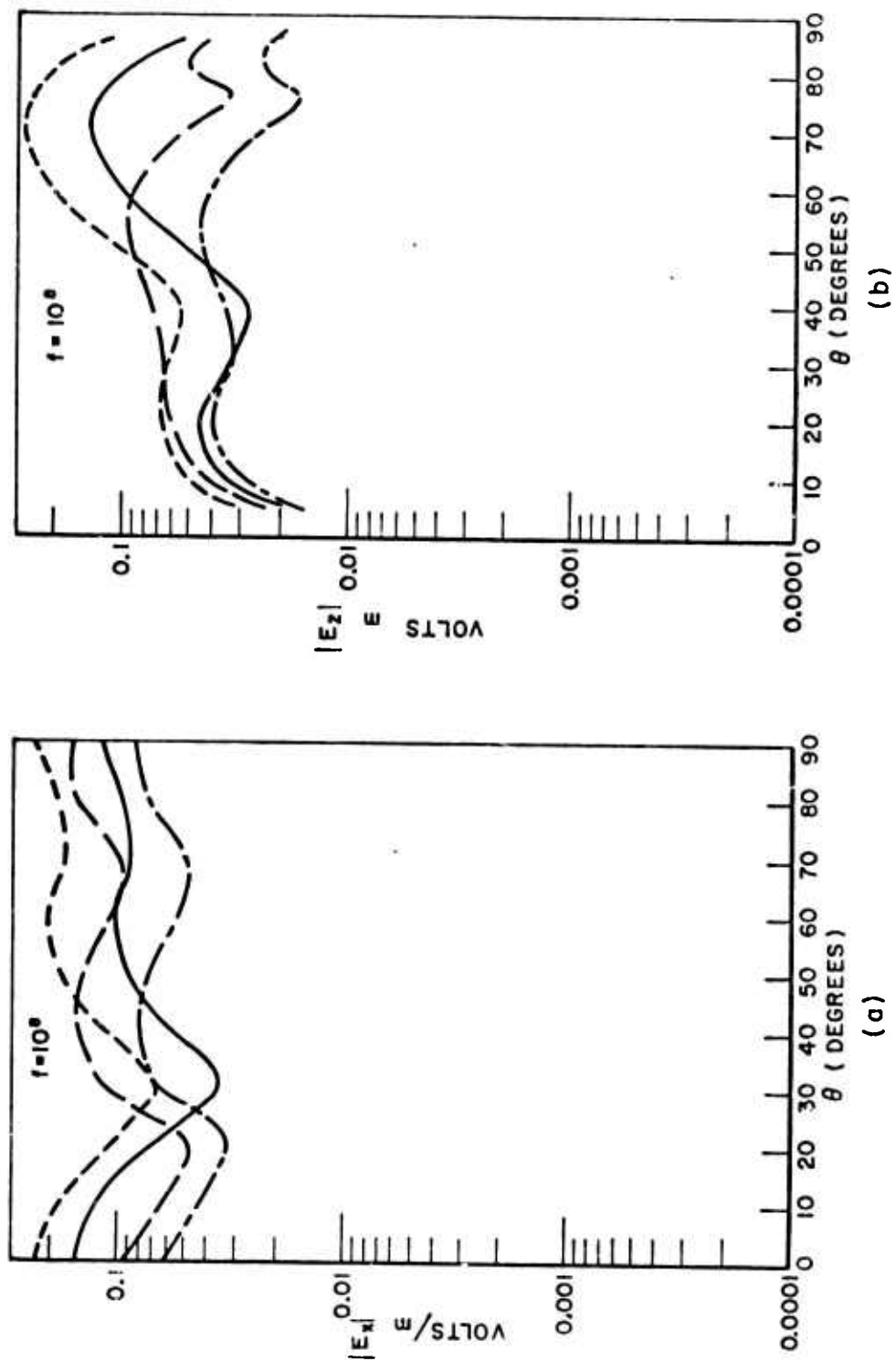
Fig. 51. Subsurface fields of 6 foot dipole, 100 MHz.
(a) x-component (b) z-component.

75

$(E_x)_{H.S.} = 1.38(E_x)_\infty$. Both approximations appear to be yielding reasonably good estimates at low frequencies, considering the assumptions made. At frequencies near 10 MHz and higher, the results can no longer be compared with Wait's data because the displacement currents can no longer be neglected. According to Wait, the z-component should obey the dependence $(E_z)_{H.S.} = 2(E_z)_\infty$. The planewave reflection approximation yields the relationship $(E_z)_{H.S.} \approx 2(E_z)_\infty$ for low frequencies (.1-1 MHz), which agrees with Wait's quasi-static case. The current modification and the current modification with planewave reflection approximations yield, respectively $(E_z)_{H.S.} \approx 0.7 (E_z)_\infty$ and $(E_z)_{H.S.} \approx 1.4 (E_z)_\infty$ for low frequencies (.1-1 MHz). At higher frequencies, there is a slight θ dependence. For angles of $\theta \sim 30°$, however, the above relationships hold for the high frequencies. It appears that for low frequencies, the simple planewave reflection approximation provides the best match to the published results of Wait. For high frequencies, however, the approximation may not be valid and either one of the other approximations could be accurate. Unfortunately, no sources are available for comparison of results.

It is interesting to note that the current modification is advantageous because it also yields a correction to the input impedance of the antenna. The calculated input impedance of the small antenna of Fig. 2b in an infinite medium with a relative dielectric constant of 10 and a conductivity of 0.005 mho/m is 137 ohms at 1 MHz. Using the current modification, an impedance of 275 ohms is calculated. From the direct reflection mode measurements of Chapter III, a measurement of the characteristic impedance at the terminals of the dipole on limestone yielded an effective value of 199 ohms.

Figure 52a shows a comparison of calculated and measured pulses. The measured pulses were transmitted through 20 feet of limestone (see Fig. 26), and the calculated pulse was computed assuming an infinite medium and constitutive parameters that approximated the parameters of limestone. Note that the magnitude of the calculated waveform of Fig. 52a is greater than the magnitude of the measured waveform by a factor of 4, which is the opposite of what is predicted by Wait. Squaring the above value (given by Wait) of

$$1.75 = \frac{(E_x)_{H.S.}}{(E_x)_\infty}$$

to account for both interfaces, the measured pulse should have been greater than the calculated pulse by a factor of 3.03. The difference lies in the fact that the quasi-static approximation used by Wait is not valid at the frequencies of interest in this case, and the similar results should not be expected. Note from Figs. 50a and 51a, which correspond to the frequency range that is of major significance (1-100 MHz), that the field strength for the cases of the modified
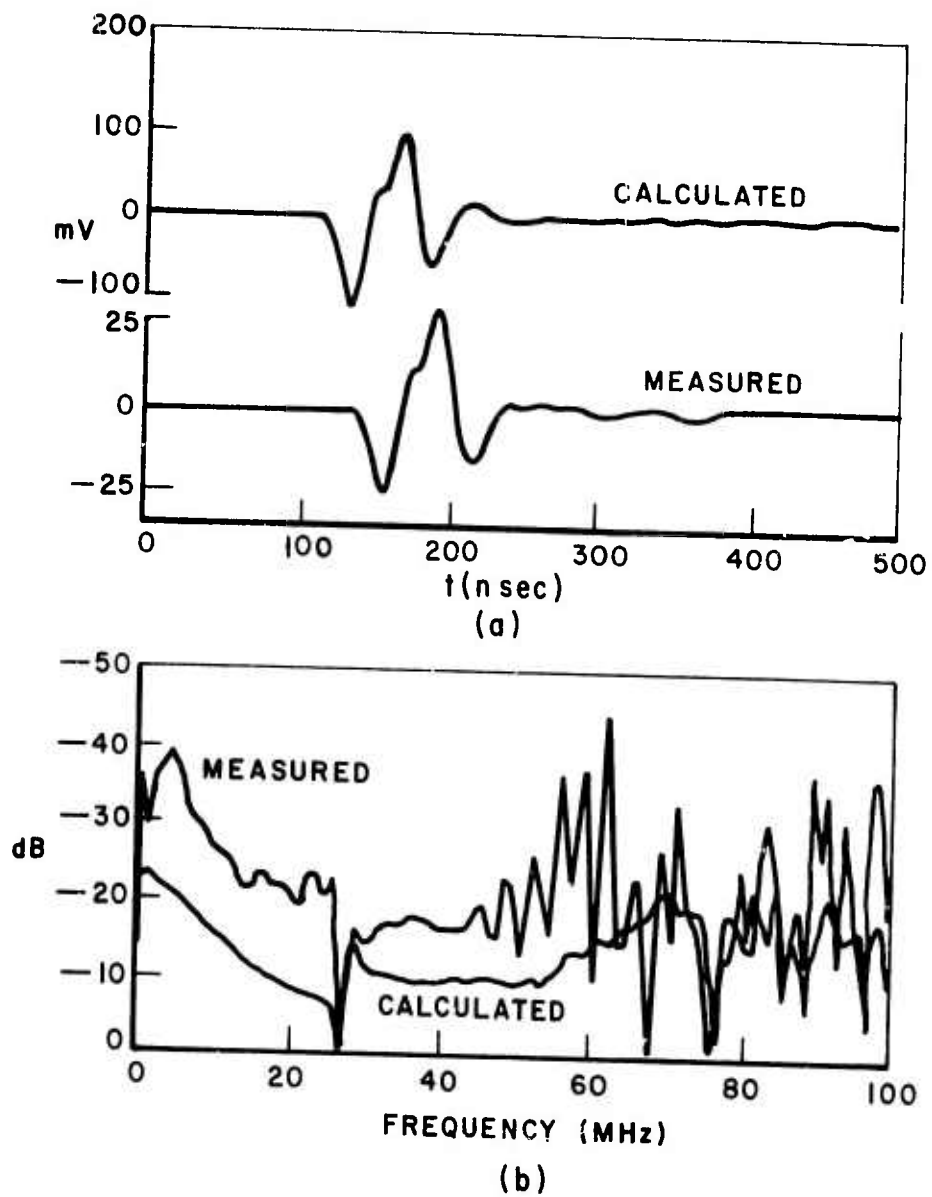
Fig. 52.   Comparison of measured and calculated pulse
transmission waveforms and antenna transfer
functions.
(a) time domain waveforms
(b) transfer function of antennas.

currents and the modified currents with the planewave reflection approximation is smaller than the infinite space field strength. This fact and the fact that the antennas were lying on 2 inches of absorber can account for the factor of 4. While the absorber has very little attenuation on the signal, it does raise the antenna off the rock surface and slightly decouples some of the energy from the medium. Figure 52b shows a comparison of the measured transfer function of Fig. 42b with a similar transfer function derived from the calculated waveform of Fig. 52a. Note that the frequency dependence is the same in both cases, but the magnitude is changed, just as in Fig. 52a, the pulse shape is the same, but the magnitude is scaled by a factor of 4.

VII. EXPERIMENTAL TARGET RESPONSE MEASUREMENTS

A. Soil Medium

As noted earlier, measurements were made on cylindrical targets in soil during the first contract (H0210042) period. These results have been reported previously[8]. Certain of these results are also included in this final report both for completeness and because they illustrate certain characteristics of the system. Orthogonal and direct reflection mode target signature waveforms have been obtained for various targets in three different media. Targets under analysis are a 12 inch diameter infinite metal pipe embedded in limestone, a large cylindrical void (tunnel) in limestone, faults in dolomite, a lithologic contrast and joints in dolomite and metal and dielectric cylinders in soil. Where possible, and of practical interest, the target data were processed at least partially by Eq. (7) to obtain the impulse response of the target.

The targets in soil media consisted of a 4 inch diameter, 3 foot metal cylinder at a depth of 1 foot, and a 2 inch diameter dielectric cylinder at a depth of 2.5 feet. The length of the dielectric cylinder can be considered infinite since it is roughly 100 feet long. Measurements were recorded in the orthogonal mode using the small bow-tie shaped probe of Fig. 2b and the Ikor pulse generator. The absorber used with the antenna on rock media was not used for these measurements, since the vegetation cover of the ground has much the same attenuation effect as the absorber. The top two waveforms of Fig. 53a illustrate the effect of rotating the probe 90° from its standard position (shown in the inserts of Fig. 53) over a 3 foot metal cylinder. The T and R notation in the figure refers to the transmit and receive dipoles. Note that the coupling retains the same polarity, but the polarity of the pipe response is inverted. This demonstrates the use of the polarization properties of the fields in determining the physical nature of the buried target. Note that if the probe were rotated only 45° from the standard position, there would be no target response, ideally. The bottom three waveforms of Fig. 53a show a series of measurements over the 3 foot metal cylinder at a depth of 1 foot for positions over the cylinder, 1 foot offset and 2 feet offset. Observe the manner in which the target response is attenuated and delayed in time as the probe is moved away from the cylinder. An effective refractive index for the medium can be obtained by measuring the delay from the peak of the responses for the 1 foot and 2 foot offset waveforms. The total two-way path lengths are 2.8 feet and 4.46 feet respectively, and the delay is 5 nsec. This corresponds to an effective refractive index of n=3.0, which agrees fairly well with the value of n=3.7 measured in the propagation measurements of Fig. 36, considering that the measurements were recorded on different days. The amplitude spectra of the raw time domain waveforms are shown in Fig. 53b-d.

79
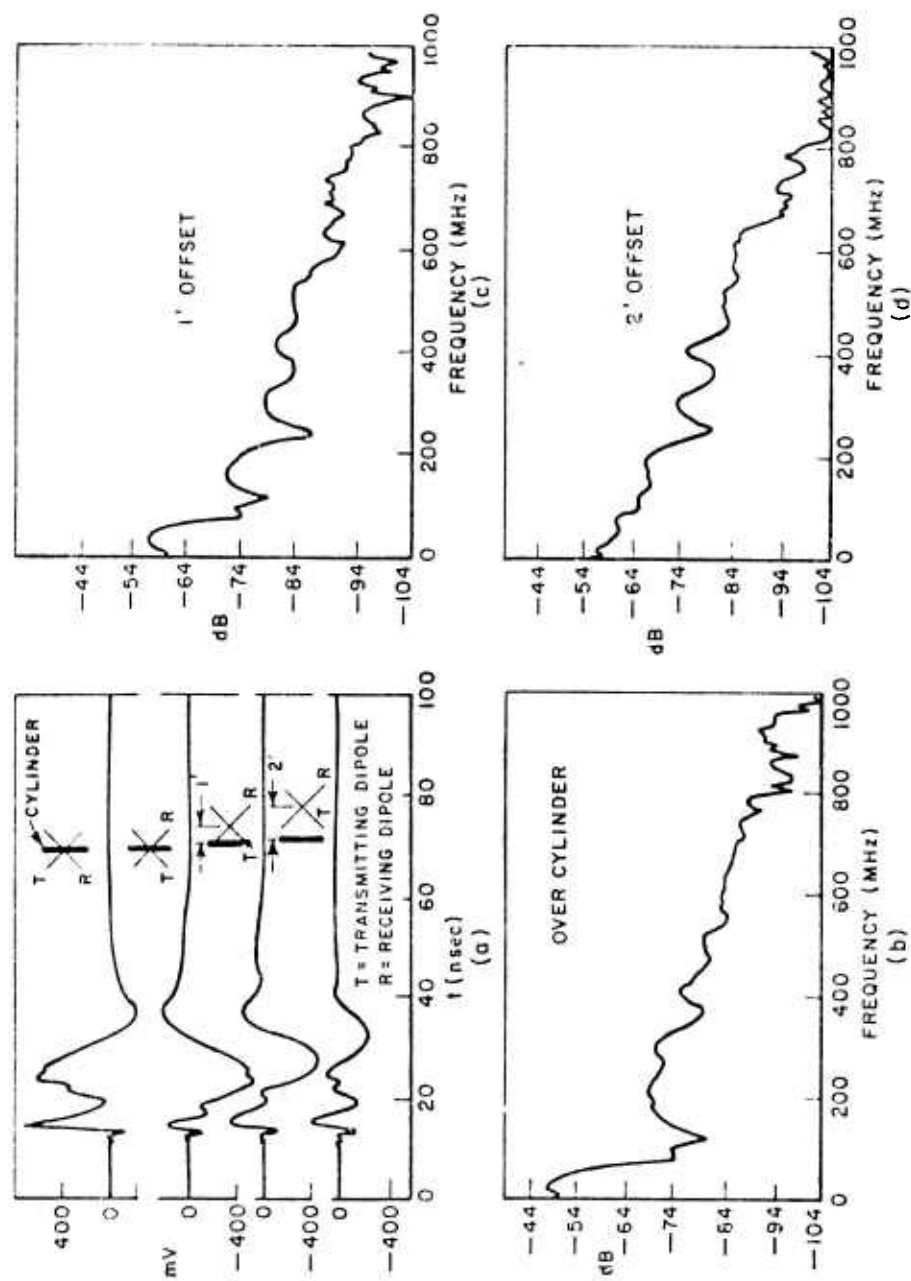
Fig. 53. Orthogonal measurements over metal cylinder in soil.
(a) time domain waveforms (b)-(d) amplitude spectra.

It is interesting to examine this series of target waveforms in more detail. Applying the first of the processing steps of Eq. (7) (which amounts to time window gating to remove the coupling) to the waveforms of Fig. 53a, the target response and spectra of Fig. 54 are obtained. Because of the rather large magnitude of the response, further processing is not necessary for either detection or identification. The period of the first cycle of ringing in the time domain pulse is 16 nsec, which corresponds to a frequency of 59 MHz. A resonance near 50 MHz can clearly be seen as the maximum in the spectra of Fig. 54b. Theoretically, dipole type resonances in the amplitude spectrum can be predicted for cylindrical targets of length L by the formula

$$f_n = \frac{c(2n-1)}{2L \sqrt{\epsilon_r}} \quad \text{Hz.}$$

The first resonance (n=1) predicted happens to be 54.7 MHz, where $\epsilon_r = 9$ has been used to correspond to the measured delay of the soil medium, which agrees very well with the experimental data. Creeping wave type resonances can also be predicted for a 4 inch diameter pipe at frequencies of 286 MHz and 572 MHz, but due to the attenuation properties of soil at these frequencies, it is doubtful that a creeping wave type resonance would be observed.

Figure 55 shows a series of measurements over a 2 inch diameter dielectric cylinder. The cylinder is located at a depth of 2.5 feet and can be considered infinitely long. As in the previous cases the return from the pipe decreases in magnitude and is delayed further in time as the probe is moved away from the pipe. Note that at a horizontal distance of 3 feet from directly over the pipe the probe can be considered out of range of the pipe. The first 18 nsec of the waveforms consist of the direct coupling and ground clutter. The direct coupling is always there and remains roughly the same, except for changes in magnitude due to the nature of the ground in the immediate vicinity of the feed terminals. On the other hand, the ground clutter or antenna clutter is unpredictable and can change with each waveform. It appears to be sensitive to minor variations in the levelness of the ground surface, moisture content of medium, vegetation height and the constitutive parameters of the medium. Reflections from the ends of the antenna can also be a major part of the clutter. Fortunately, the duration of the coupling and clutter is usually not longer than 15 nsec, so that objects buried at sufficient depths can be separated from the clutter by time window gating.

In the case of the buried metal cylinders of the previous discussion, the response from the cylinders was so strong that it simply dominated the clutter signals. After gating the data to obtain only the target pulse responses of Fig. 55b, a definite correlation of the amplitude spectra of Fig. 55c to target and no-target

81
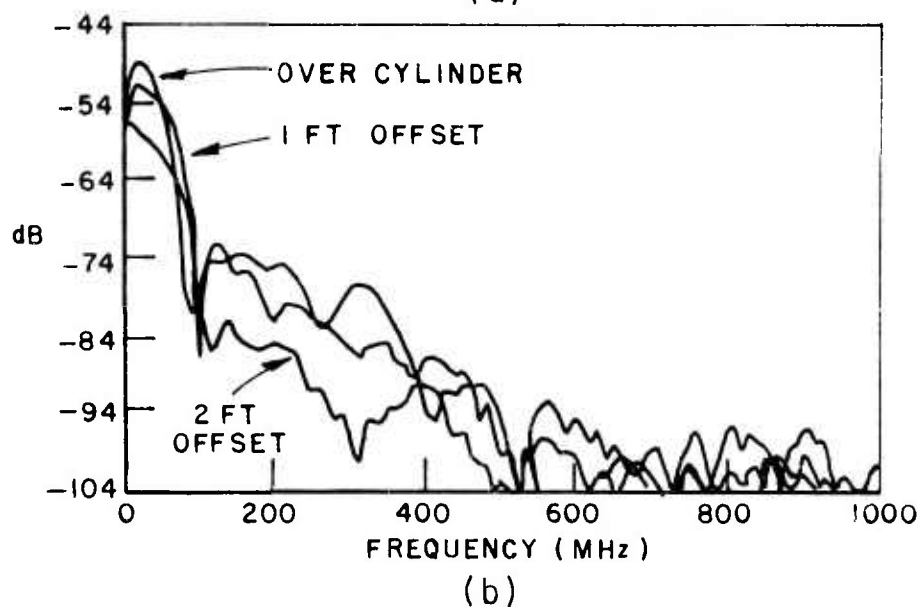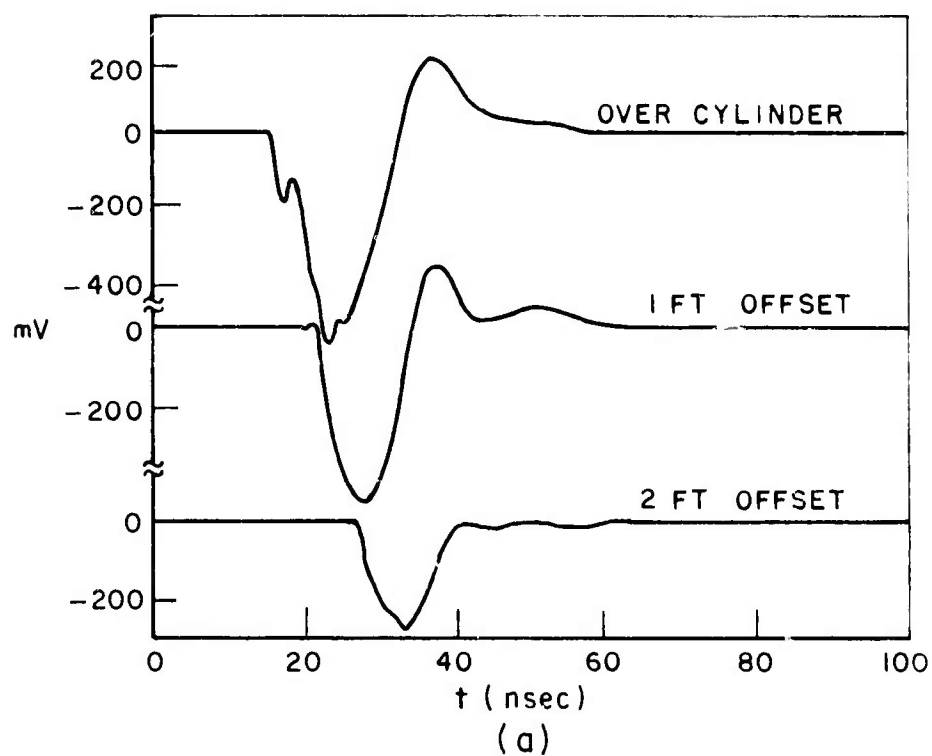
Fig. 54. Gated measurements over metal cylinder in soil.
(a) time domain waveforms
(b) amplitude spectra.

82
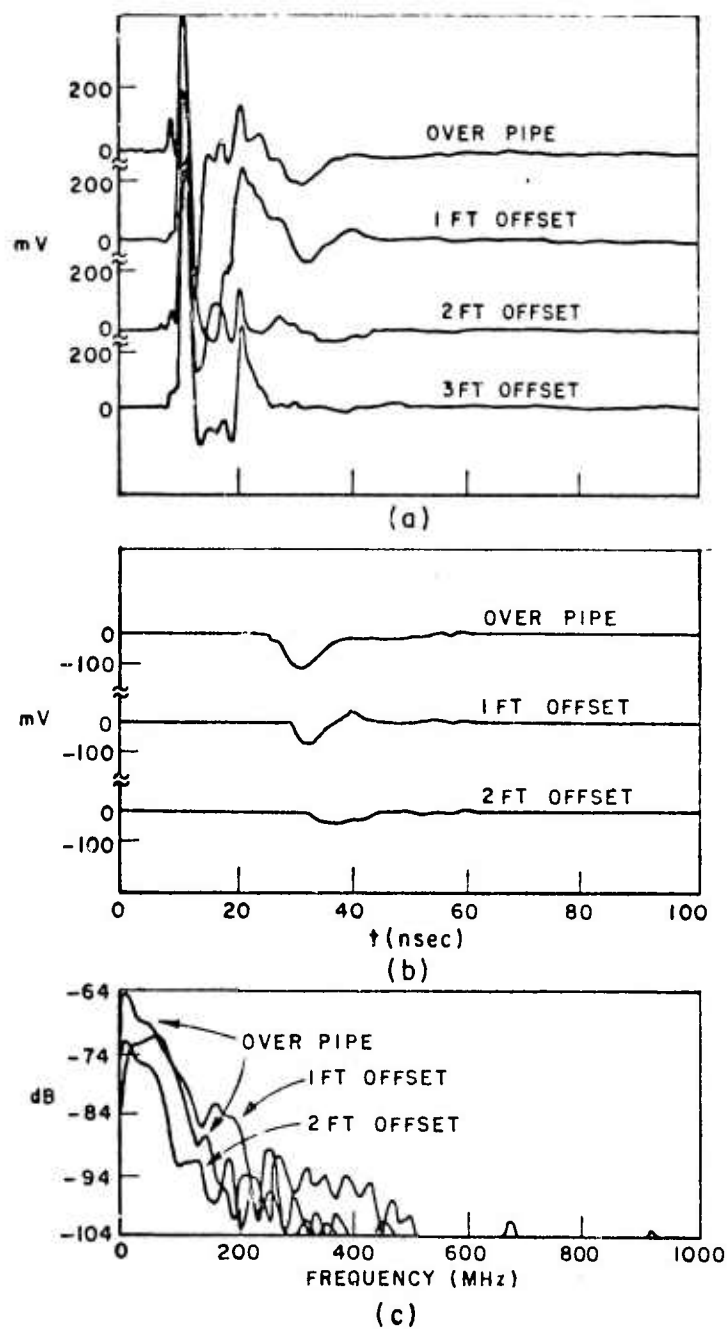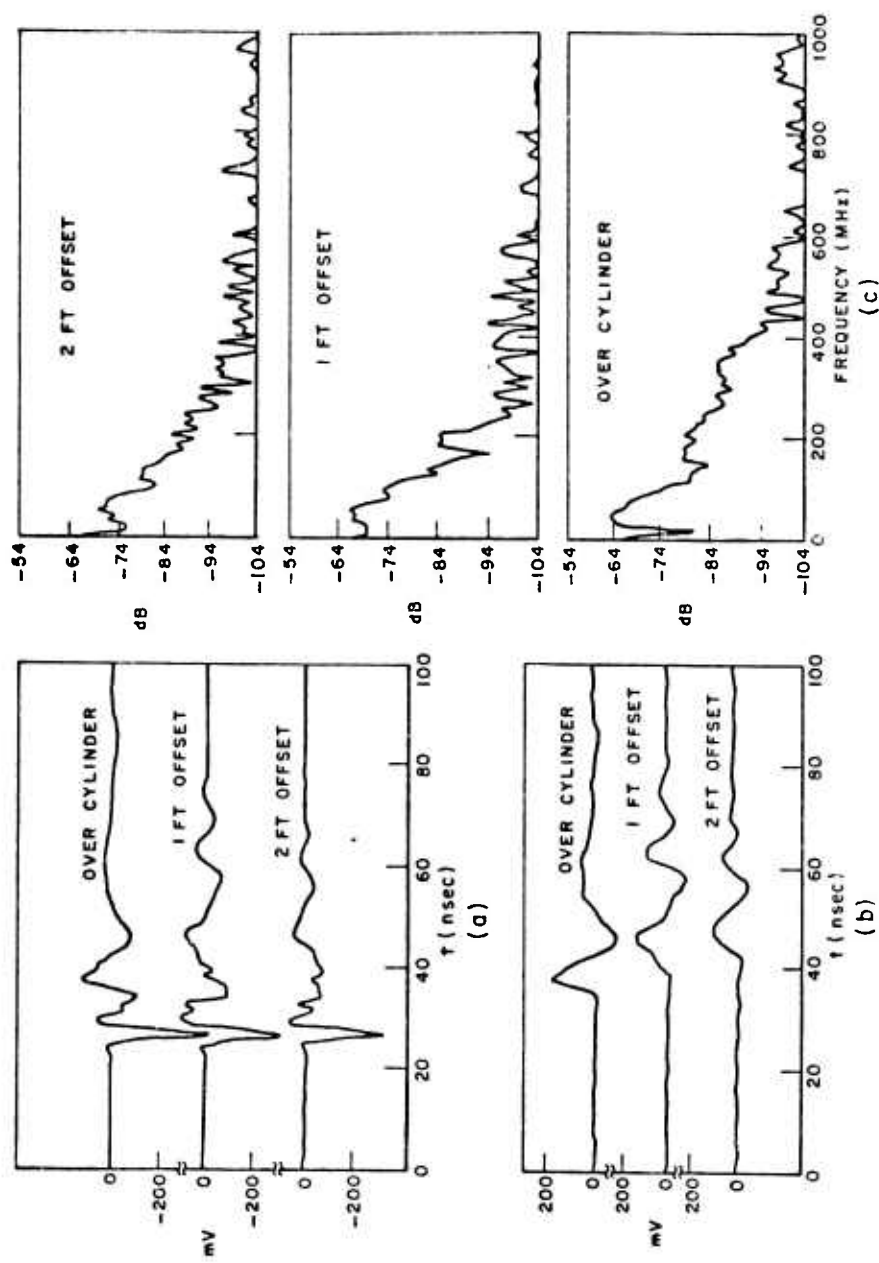
Fig. 55. Orthogonal measurements over dielectric cylinder in soil
(a) time domain waveforms
(b) gated time domain waveforms
(c) gated amplitude spectra.

positions is evident. Before the gating process, however, the coupling and clutter made it difficult to distinguish between the amplitude spectra. Resonances can be predicted for cylindrical dielectric targets, but they are rather complicated, and since the antenna transfer function over soil has not been determined, further processing has not been attempted.

B. Limestone Medium

Figure 56 shows the time domain waveforms using the small antenna (Fig 2b) in the orthogonal mode over a 1 foot diameter metal cylinder in limestone. Since the cylinder was located at the shallow depth of 2 feet, the 1 nsec, 1000 volt Ikor input pulse was used to provide the necessary resolution. The waveforms show the effect of moving the probe laterally away from directly over the pipe, as in the previous pipe measurements. Note that the time delay measured between the feed point coupling and the target responses agrees with the refractive index obtained from the propagation measurements. The propagation data of Fig. 25 yielded an effective refractive index of 3.2 while from these target data a value of 3.3 is measured. Figure 56b shows the gated time domain waveforms after normalization by the attenuation of the limestone. Figure 56c shows the corresponding amplitude spectra.

The first creeping wave resonance for a 1 foot diameter cylinder in limestone (ϵ_r = 3.3) is near 200 MHz. Note that Fig. 56c does show a resonance at 200 MHz for the cases directly over the cylinder and 1 foot offset. This resonance is obviously not the most significant portion of the spectrum, however, since it is roughly 20 dB below the peak (65 MHz) in the amplitude spectrum. The 65 MHz resonance roughly corresponds to a pulse being reflected back and forth between the cylinder and the air-rock interface, which would cause a resonance at 74 MHz.

The second target of interest in the limestone medium was the tunnel that had been used to obtain the propagation data and antenna transfer functions previously described in Chapter IV. Examination of the tunnel from the ledge above the tunnel proved to be very frustrating at first. With the large 28 foot dipoles in the orthogonal mode and with the H.P. pulser, the waveforms of Fig. 57 were obtained for target and no-target cases. Obviously, something had to be causing the large response observed, but the response simply did not correspond to the depth and position of the tunnel. It was later learned that an iron support structure that was visible at the roof of the tunnel actually extended to within a foot of the surface near the antenna, as shown in Fig. 58. With the large antenna in this configuration, the ironwork happened to lie in one quadrant of the probe, causing the responses of Fig. 57. Since operation with the large antenna was obviously not possible in the orthogonal mode, direct mode measurements with the large dipole and orthogonal

Fig. 56. Orthogonal measurements over metal cylinder in limestone. (a) time domain waveforms (b) gated and normalized time domain waveforms (c) gated and normalized spectra.

85
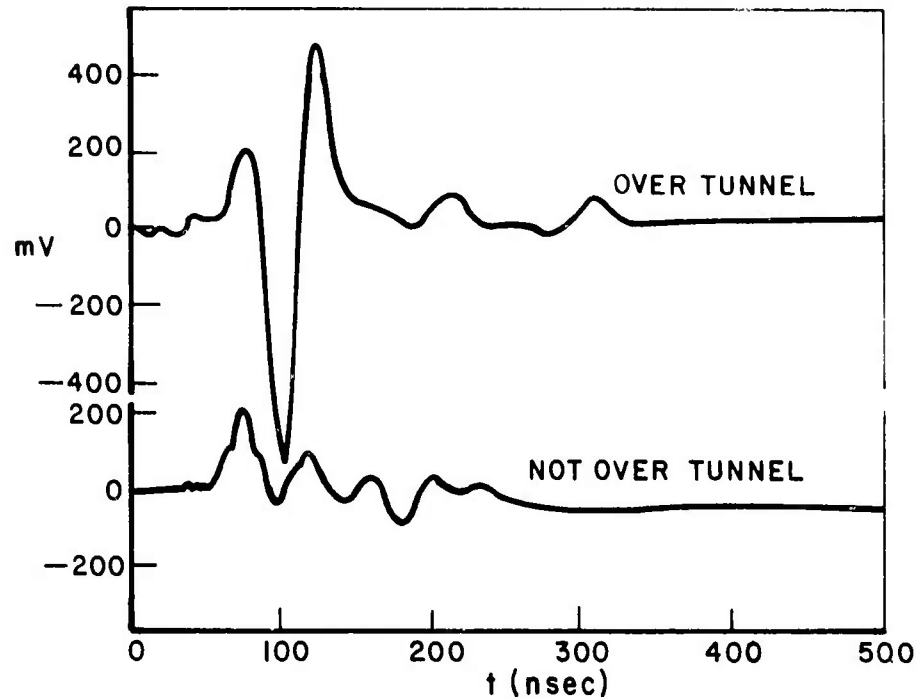
Fig. 57. Orthogonal measurements over tunnel in limestone, using large probe and H.P. generator.

measurements with the small probe were made keeping the probes as far from the ironwork as possible. Figure 59 shows the results using the small probe in the orthogonal mode with the Ikor generator for two positions directly over the tunnel as shown in the inserts. The probe was moved closer to the edge to verify that the response observed at roughly 100 nsec was from the tunnel and not from the ironwork. Note that as the probe was moved closer to the iron, the pulse occurring at roughly 50 nsec from the coupling moved in about 25 nsec, which corresponds to the difference in path length to the ironwork. Figure 60, on the other hand, does display a definite correlation between the distance from the tunnel and the occurrence of the returned signal. The target returns are shown for probe positions directly over the tunnel and 40 feet offset from directly over the tunnel. The refractive index obtained from the delay of the target response, n=2.6 agrees reasonably well with the measured value of 3.2 from the propagation measurement. As in the previous cases, the target measurements were not made on the same day as the propagation measurements, so that a slight variation is to be expected. Figure 60b shows the same waveforms as Fig. 60a after time window gating to remove the direct coupling and clutter. The differences in magnitude and time delay are more apparent in these waveforms. Both the increased path length and attenuation and the relative positions of the probe with respect to the tunnel account for the change in
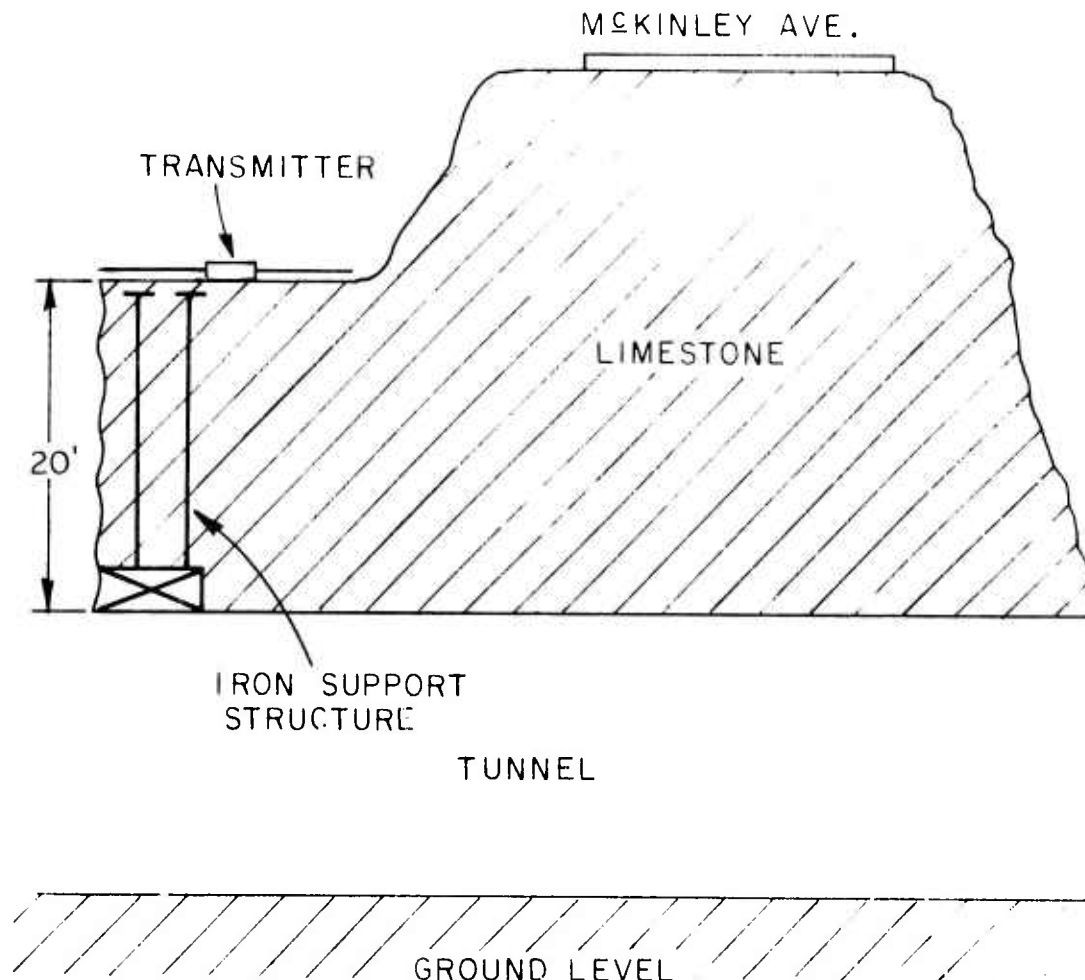
Fig. 58. Sketch of tunnel geometry showing iron
support structure.

magnitude. The increase in path length, on the other hand, implies
that the target being seen in the second waveform is a distance of
25 feet from the probe, which does roughly correspond to the distance
to the tunnel. The amplitude spectra of the waveforms is shown in
Fig. 60c. Figure 61 shows the results of applying the processing of
Eq. (7) to the gated waveform of Fig. 61b directly over the tunnel.
The amplitude spectrum of Fig. 60c was normalized by the attenuation
of the feed system, the attenuation of the medium, and the transfer
function of the cables and antenna to obtain Fig. 61b, which was then
inverse Fourier transformed to obtain the time domain waveform of
Fig. 61a.
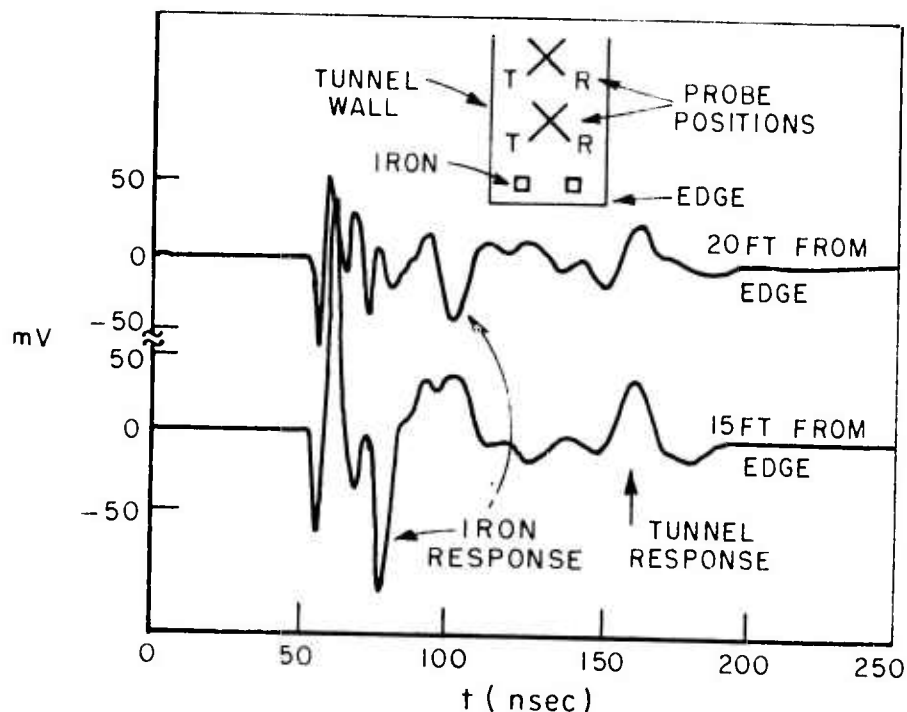
Fig. 59.   Orthogonal measurements over tunnel in limestone using
           small probe and Ikor generator.

Note the sharpening effect that the normalization has on the
target response. The ringing shown in Fig. 61a is a result of the
processing procedure. When normalizing amplitude spectra,
spurious high frequencies are introduced which must be filtered
to obtain the desired response. It is logical to expect that the
signal shown in Fig. 61a is simply the specular return from the
tunnel. Other effects, such as creeping wave or reflections from
the floor of the tunnel have been severely attenuated and hence
will not be observed. If this signal is the specular return the
top waveform of Fig. 60b should roughly correspond to a pulse trans-
mitted through 40 feet of limestone. A comparison between Fig. 60b
and the transmitted pulses of Fig. 25a can be made to substantiate
this claim. Unfortunately, different cable lengths were used for
these series of measurements, so an exact magnitude comparison is
not possible. It is estimated, however, that the loss introduced
by the longer cables used for the measurements of Fig. 25 amounts
to approximately 12 d'   Using this estimate, and a reflection
coefficient of roughly 0.5, the magnitude of the pulse transmitted
through 36 feet of rock does roughly correspond to the magnitude
of the tunnel response of Fig. 60b. The fact that the base width
of the transmitted pulse is wider than the base width of tunnel

88
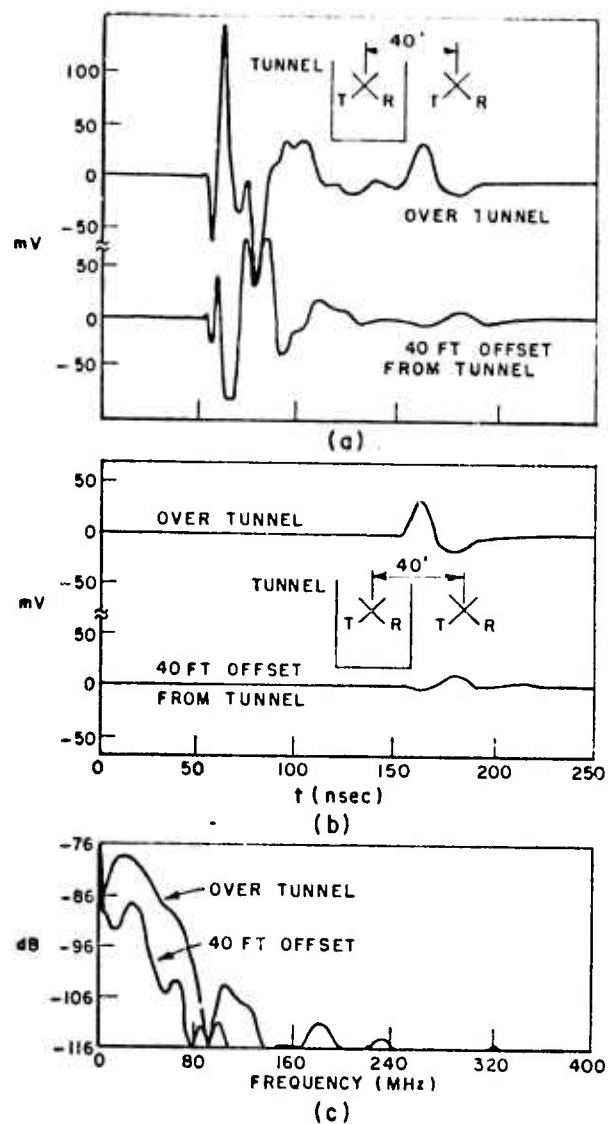
Fig. 60. Orthogonal measurements over tunnel in limestone
using the small probe and Ikor generator.
(a) time domain waveforms
(b) gated waveforms
(c) gated spectra.
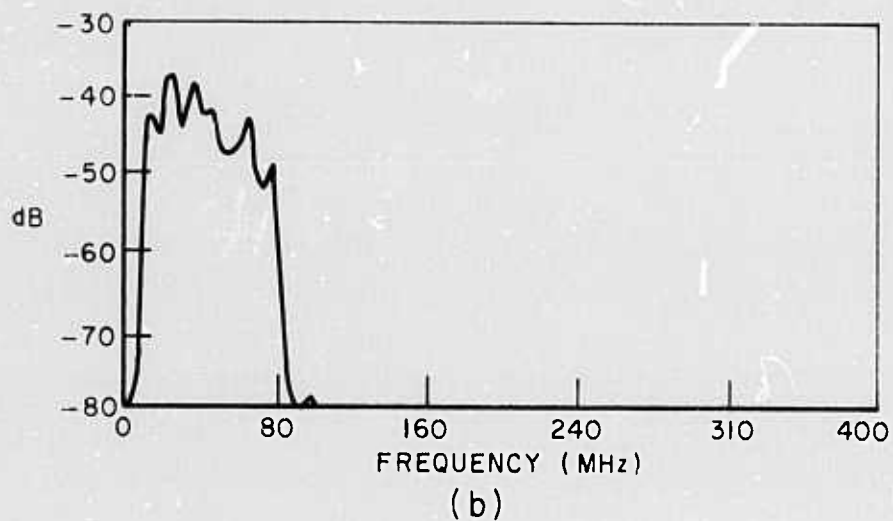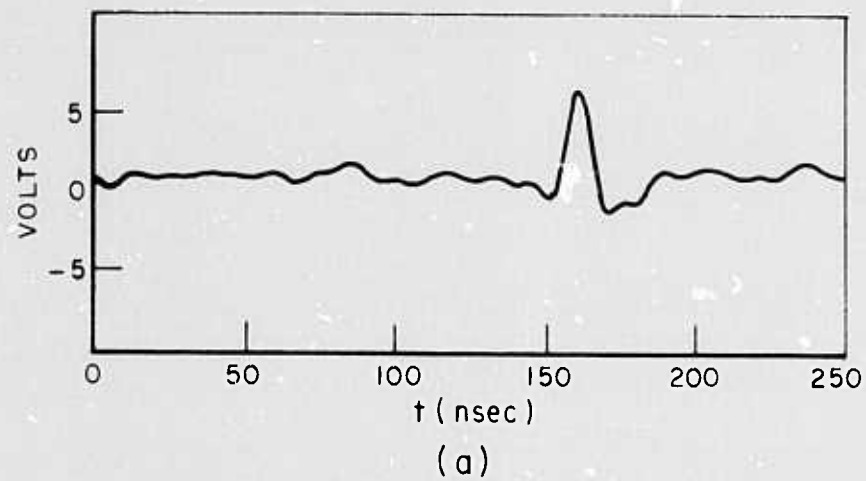
Fig. 61. Processed measurements over the tunnel.
(a) time domain waveform
(b) amplitude spectra.

90

response may be due to the angle of the transmission path between the two dipoles. Note that the difference appears exaggerated because of the difference in the time scales of the two figures.

Figure 62 was obtained using the large 28 foot dipole of Fig. 2a with the H.P. pulse in the direct reflection mode with the limiter. Waveforms are shown for antenna placement directly over the tunnel and roughly 40 feet offset from directly over the tunnel as shown in the insert of Fig. 62. Because of the magnitude and duration of the leading pulse, which is the reflection from the air-rock interface, it is difficult to associate a specific time delay to the beginning of a tunnel response, although the differences are obvious. The duration of the initial reflection is caused by the slow turn-off time of the step recovery diodes used in the limiter.
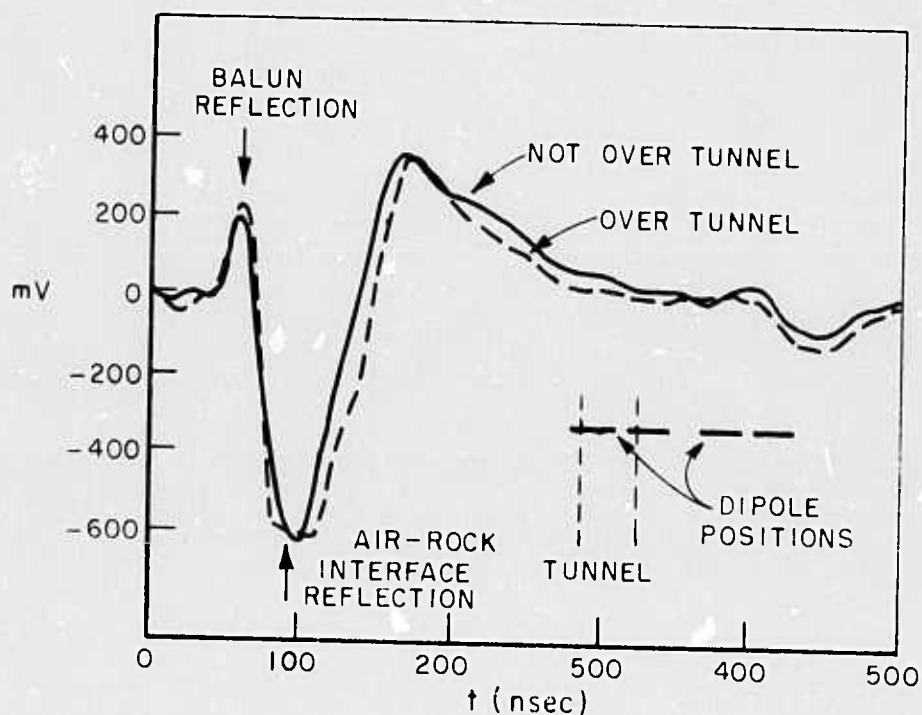
Fig. 62. Measurements over tunnel in limestone using the large dipole and H.P. generator in the direct reflection mode.

C. Dolomite Medium I

Figure 63 shows the results of 4 orthogonal mode measurements made on the floor of the dolomite quarry, which is also referred to as the Lilley-formation. A geological description of the quarry can be found in Reference [18]. The probe was that in Fig. 2b and the Ikor pulse generator was used. The top waveform is a control or no target waveform with the probe located near the center of the floor and no known contrasts beneath the probe to a depth of at least 35 feet. The next three waveforms show the effects as the probe geometry is displaced laterally from a fault occuring along the floor. The fault has a vertical displacement of approximately 13 feet and the probe is on the up side of the fault. The fault was reasonably clean. One can clearly see the correlation between the position of the probe with respect to the fault and the corresponding response waveform. Note that this is using the unprocessed time waveforms. In each of the 4 waveforms shown the first negative spike is the direct coupling across the feed points of the dipoles. Note that the shape of this leading spike is a replica of the pulse shown in Fig. 4. In particular, the base width is roughly 8 to 10 ns. The direct coupling magnitude is quite sensitive to the levelness of the probe. One can anticipate therefore variations in this magnitude throughout a series of measurements. The direct coupling is of no consequence since it can always be gated out, but it does serve as a convenient time reference - that is, it explicitly references in time the arrival of the interrogating pulse at the feed point of the probe. The propagation measurements taken on this day yielded an effective delay for the Ikor pulser in dolomite of 2.17 nsec/ft. When the measurements were taken a light rain was falling and it had been raining steadily for at least 24 hours. It is difficult with this configuration to estimate when the response from the fault actually started. In the normal case, i.e., with the target below the probe plane, it is clear that the shortest path is via feed point - target-feed point with the response via the ends of the dipole arms arriving somewhat later. Consider first the first positive peak and the second negative peak in the fault waveforms. For all three measurements these remain almost constant at delays of 9 and 15 ns, respectively from the start of the direct coupling except at the 5 foot distance where something else has obviously been added to the response. Since these characteristics do not move as the probe is moved, it is contended that they are due to another target beneath the rock whose presence is unknown. On the other hand the second positive peak moves out in time from the direct coupling and occurs respectively at 21, 30 and 49 ns from the direct coupling. With the estimated time delay of the Ikor pulse in dolomite and considering a 2-way path, this means the probe has been moved respectively 2.07 and 6.2 feet away from this target. This agrees reasonably well with the known movement of 2 feet and 5 feet for the last 2 measurements in Fig. 63. The sketch in Fig. 63 may be somewhat misleading. The fault line shown is actually the start of fracturing in the rock - the actual vertical
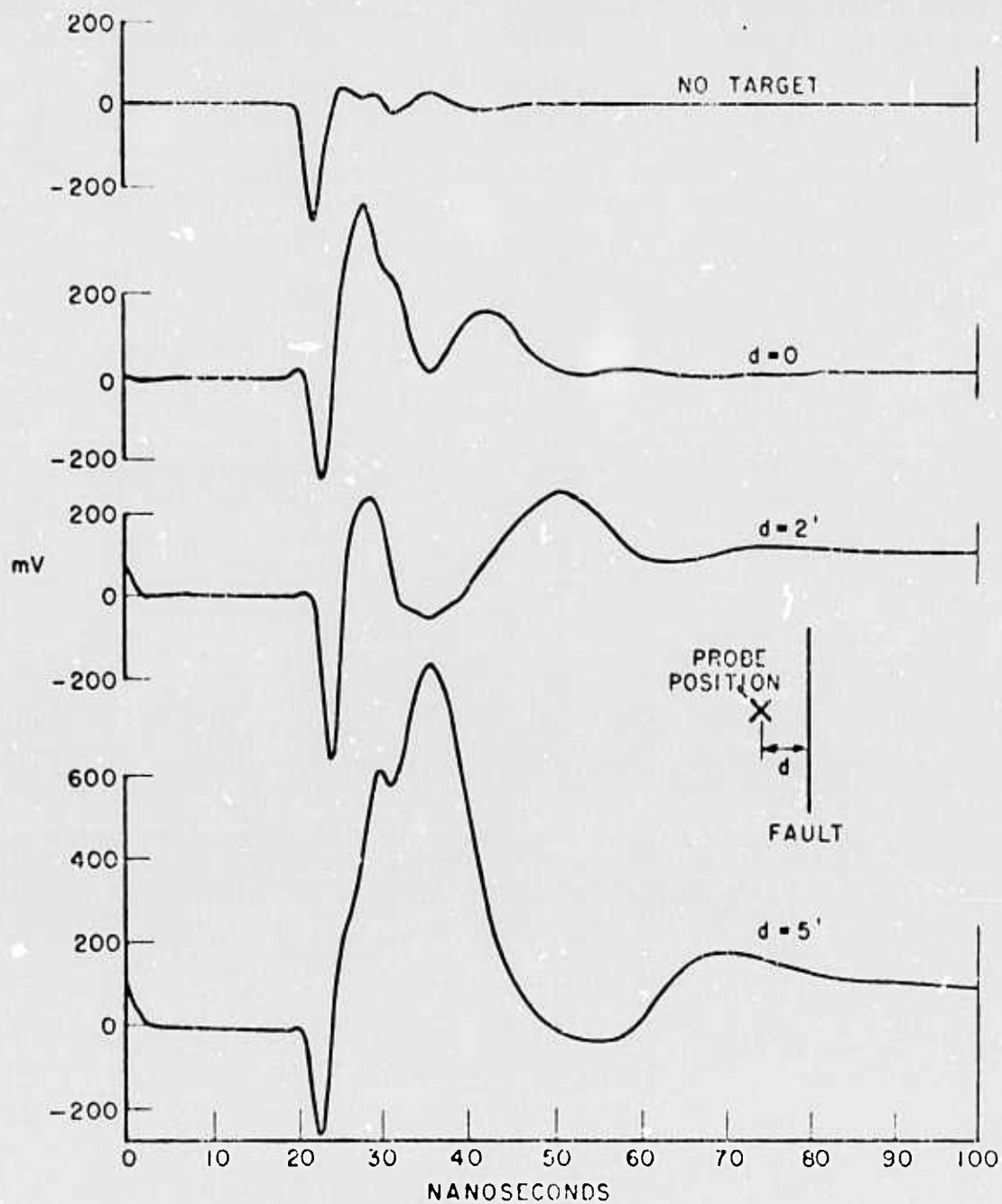
Fig. 63. Orthogonal measurements of fault in dolomite using small probe and Ikor generator.

93

displacement was roughly 2.5 feet to the right of the line shown. Exactly what caused the large target response observed at roughly 18 nsec in the last waveform in Fig. 63 is not known. However, it is unlikely that the response can be attributed to the fault. Apparently the probe had been moved within range of another subsurface target. The amplitude spectra in Fig. 64 also clearly display the presence of the fault when compared to the no-target amplitude spectra (dashed curve in all three). Note the similarities in the low frequency content of the target amplitude spectra, and the peculiar absence of frequency content at approximately 140 MHz in Fig. 64c, which is the spectra of the unexplained target waveform of Fig. 63.

The above set of measurements were repeated with the same probe and the H.P. pulse generator. These response waveforms are shown in Fig. 65. Note in Fig. 65 that while there are differences in the target and no target responses, they are not simply interpreted. This vividly illustrates the advantages of a very narrow interrogating pulse for close in targets. Note also that the addition of a new target in the 5 foot waveform is also evident. It is suspected that the responses occurring near 800 nsec are due to an internal reflection mechanism of the feed system.

Because of the success of the initial fault measurements using the Ikor generator, further fault measurements were conducted in an attempt to locate a minor fault line in a section of the quarry that had not been accurately mapped. With the indispensable help of the quarry geologist*, the fault location was narrowed down to roughly a 75 foot wide strip. Figure 66 shows a sketch of the site with the numbered X's marking the probe positions. As seen in the figure, two sweeps across the strip were made, using the small absorber covered probe and the Ikor pulser. The seemingly random spacing between measurements was necessary because of surface roughness, as it is always desirable to keep the probe as flat as possible on the surface of the rock. Figure 67 shows the time domain waveforms obtained at the 17 probe positions in Fig. 66 and an average of all 17 waveforms which is used as a no-target reference.

---

*Richard Bowman, Head Geologist, Plum Run Stone Division.
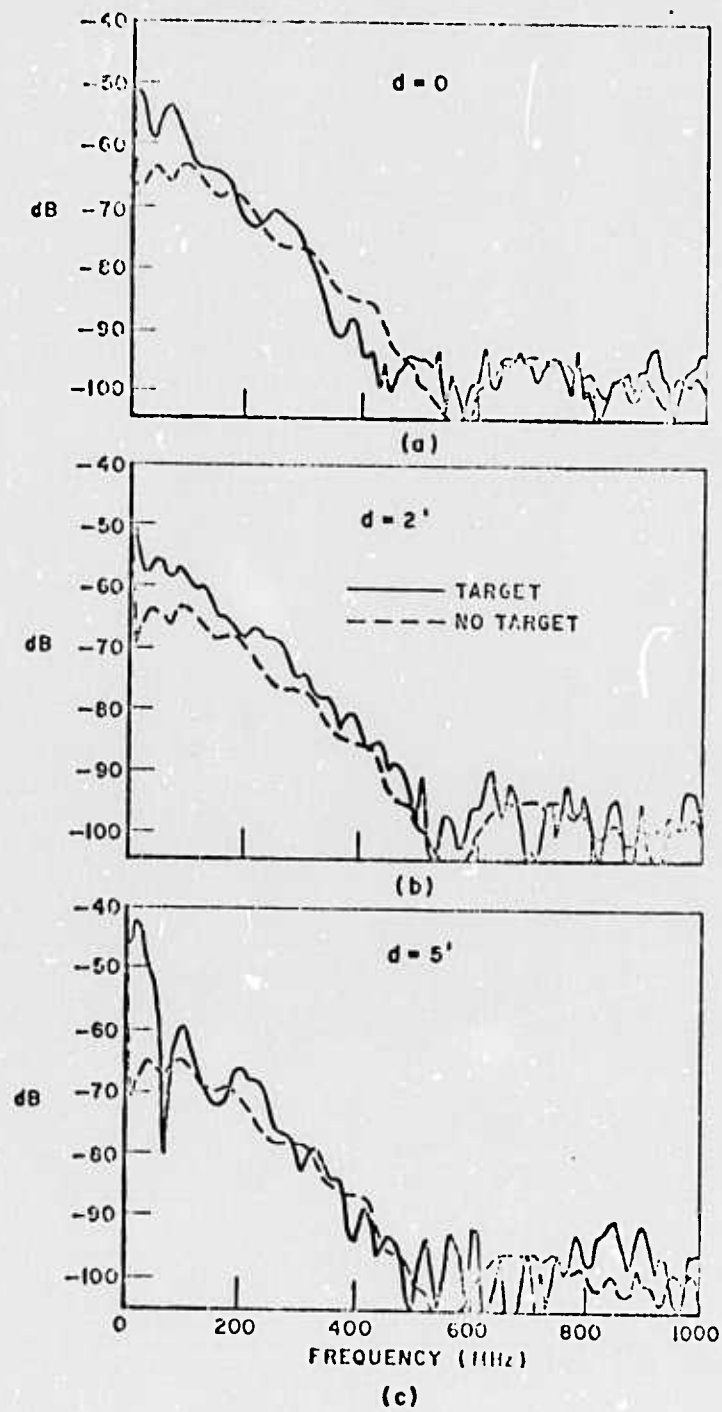
Fig. 64.   Amplitude spectra of fault measurement.

95
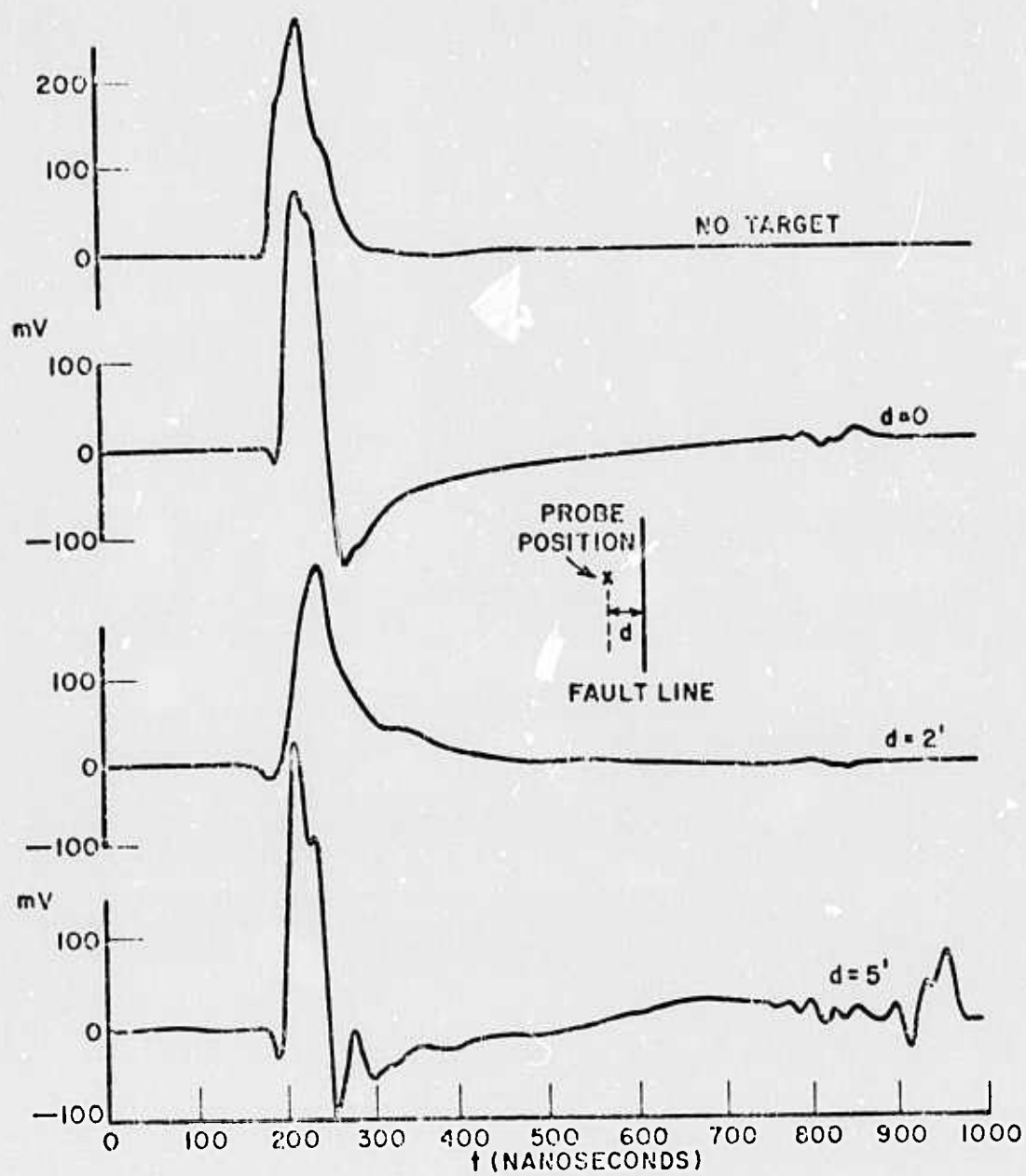
Fig. 65. Orthogonal measurements of fault in dolomite using small probe and H.P. generator.
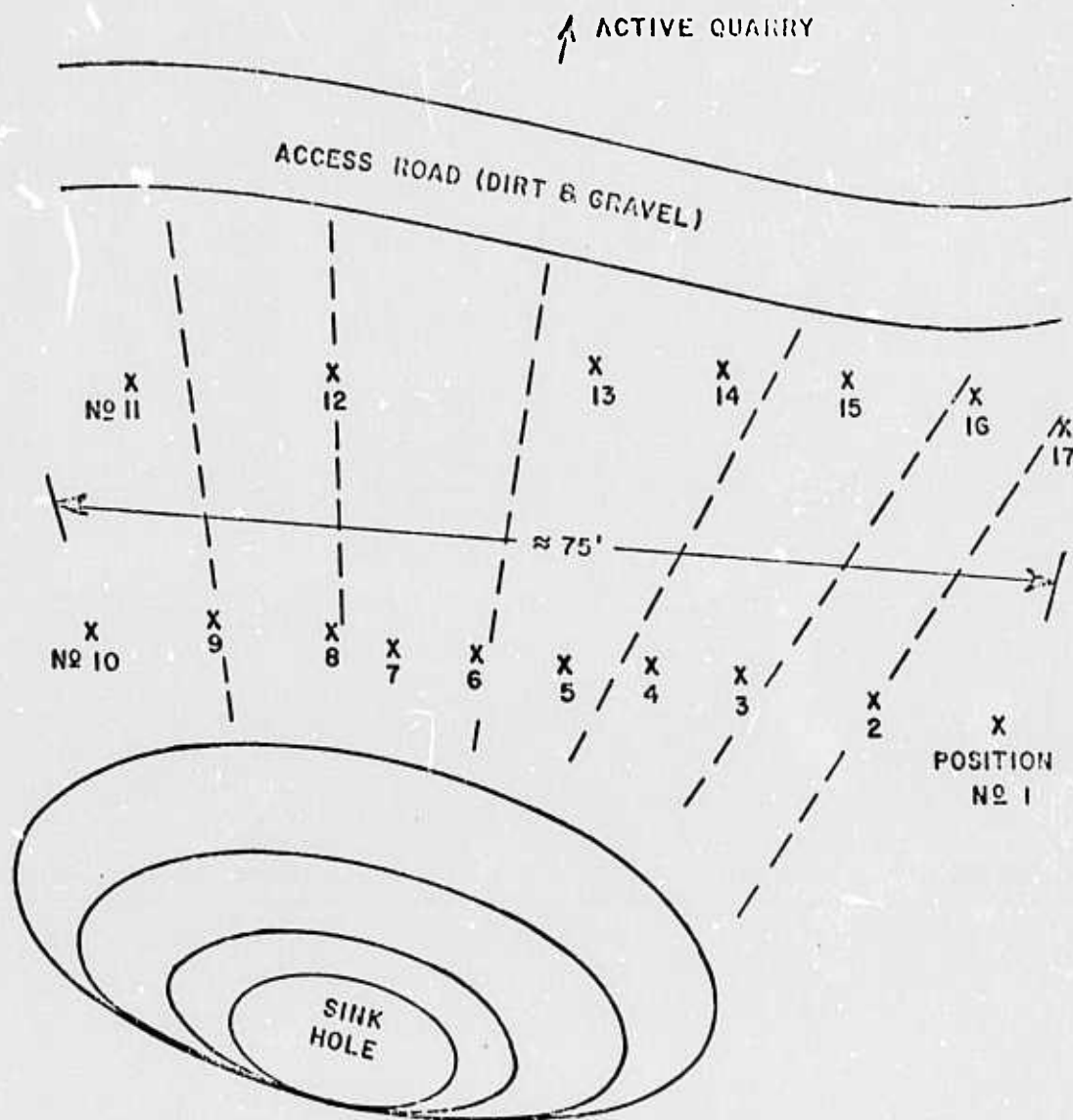
Fig. 66. Sketch of fault location measurement position.
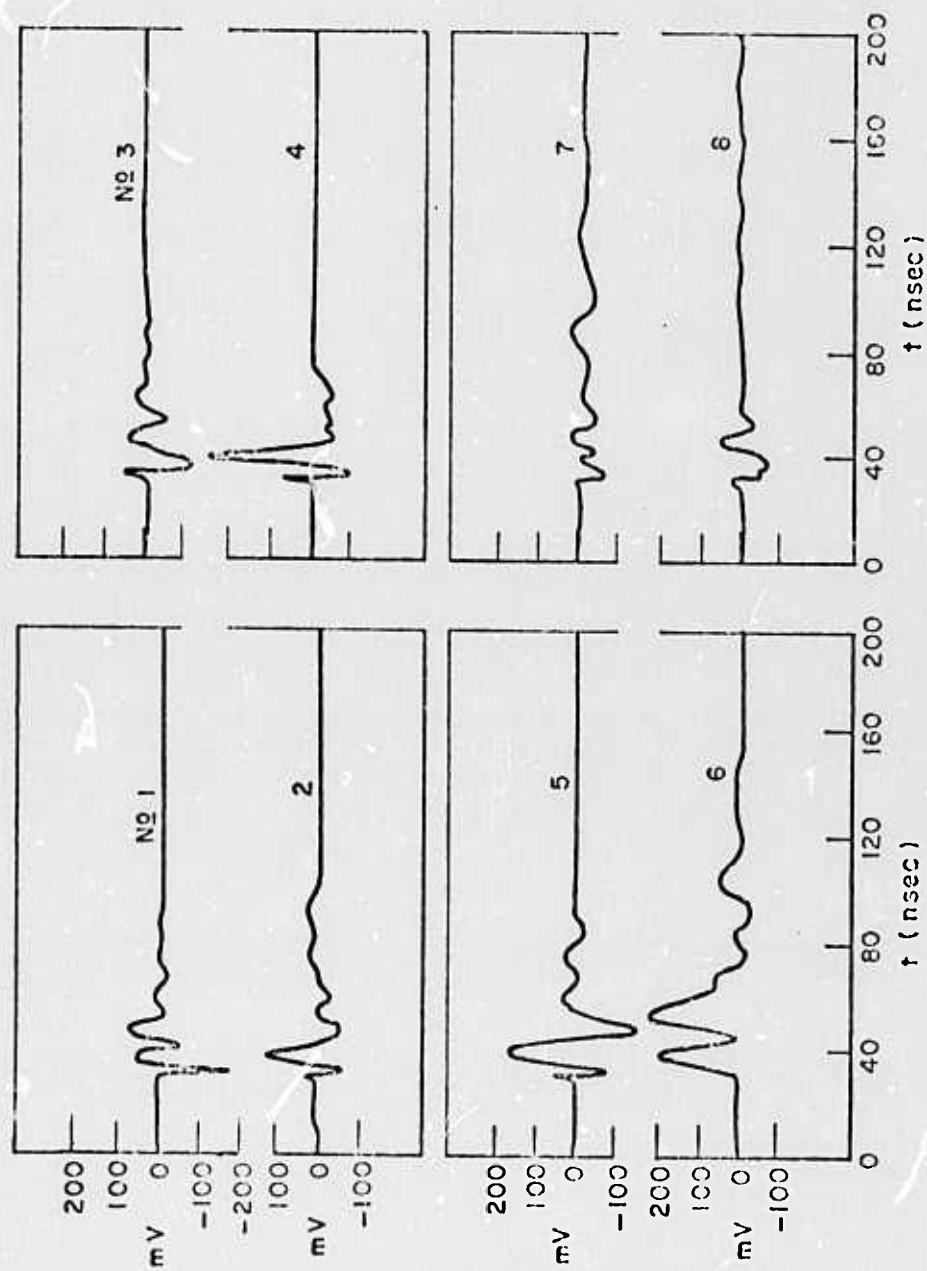
Fig. 67a. Fault location measurements in dolomite, small probe and Ikor generator.
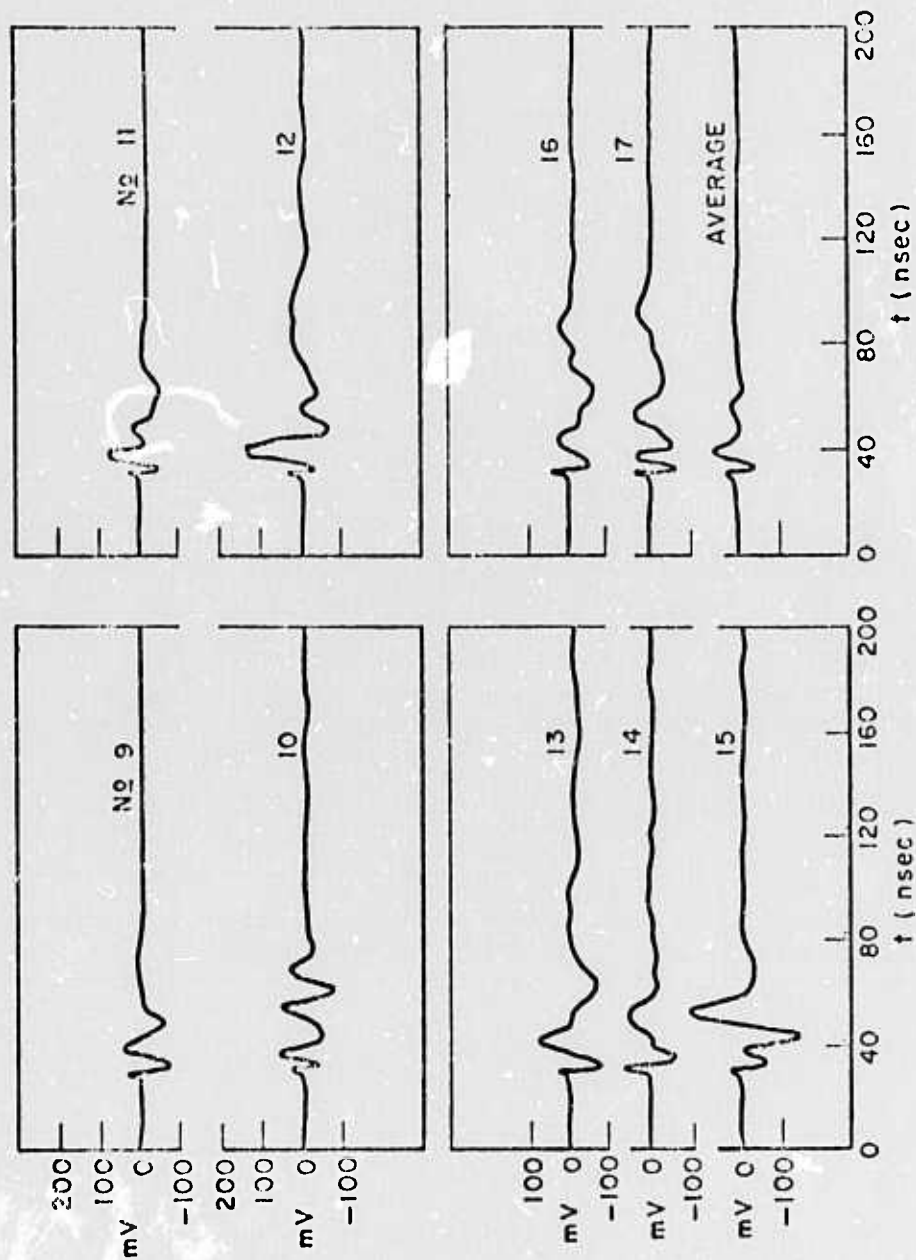
Fig. 67b.. Fault location measurements in dolomite, small probe and Ikor generator.

Observe the large response in Fig. 67, positions 4, 5, and 6, and the manner in which the response is delayed in time as the probe is moved away from position 4. This trend implies that the "target" under observation is very close to position 4. While some evidence of this "target" is apparent in positions 2 and 3, it is rather difficult to associate a similar correlation between the response and distance from target as in positions 4, 5, and 6 and Fig. 63. There were also a number of surface cracks in the vicinity, indicated by the dashed lines in Fig. 66, which are probably responsible for all of the low magnitude responses in Fig. 67. The target in question here is also difficult to describe from a geometrical viewpoint. The fault line need not be perpendicular to the plane of the surface, in fact, it may be tilted at such an angle as to invoke a large response to the probe in position 4 and yet invoke only a minor response to position 3. Note that in the amplitude spectra of positions 4, 5, and 6, shown in Figs. 68a,b,c, respectively, the characteristic low frequency fault response is observed, which is similar to those in Fig. 64. Position 15 contains the maximum response obtained in the second sweep across the fault. Again the amplitude spectrum of position 15 displays the same characteristics. These data, and previous knowledge of the general direction of the fault lead to the conclusion that the fault under investigation follows a line that passes near positions 4 and 15. The precise location of the fault, however, cannot be verified. This section of the quarry has since been worked, and the head geologist generally agreed with our conclusions. However, he stated that so much fracturing occurred in this area that precise location was not possible.

Perhaps the most striking results obtained thus far is the response from a lithologic contrast at a depth of approximately 45 feet. Figure 69 shows the geometry of the measurement. The large (28' dipole) probe with the aluminum sheets is situated on a layer of rock about 45 feet above the quarry floor, and is operated in the orthogonal mode with the 50 volt 45 ns (H.P.) pulse generator. Both rock formations are dolomite, but the upper layer is an open porous reef-type material while the lower layer (quarry floor) is a dense material. Basically there is a large change in the specific gravity of the material, but the contrast is not sharp. The extent of this gradual transition is approximately 3 to 5 feet. On either side of the probe were joints running vertically from the surface near the probe to the quarry floor. The time and frequency domain waveforms for the probe in this position are shown in Fig. 70. Corresponding waveforms for the probe on the quarry floor are shown in Fig. 71 for comparison. From the measurement of the time delay (refractive index) during the transmission measurements, it was found that the large response at approximately 375 nsec corresponded to the lithologic contrast at a depth of 45 feet. The other responses are reflections from the vertical joints, and possibly, the cliff edge. The strong low-frequency content of the H.P. pulse generator is responsible for
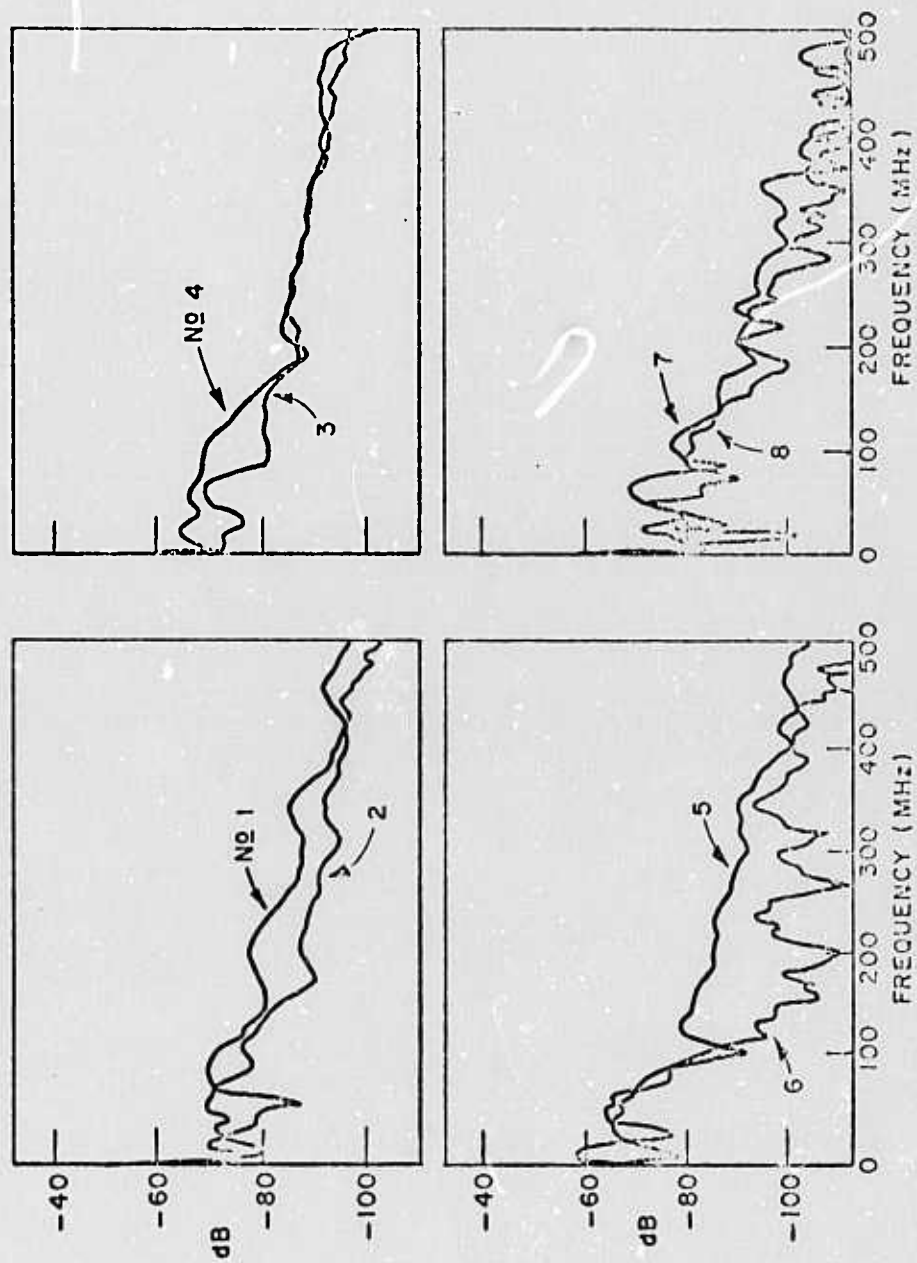
Fig. 68a. Amplitude spectra of fault measurements in dolomite.
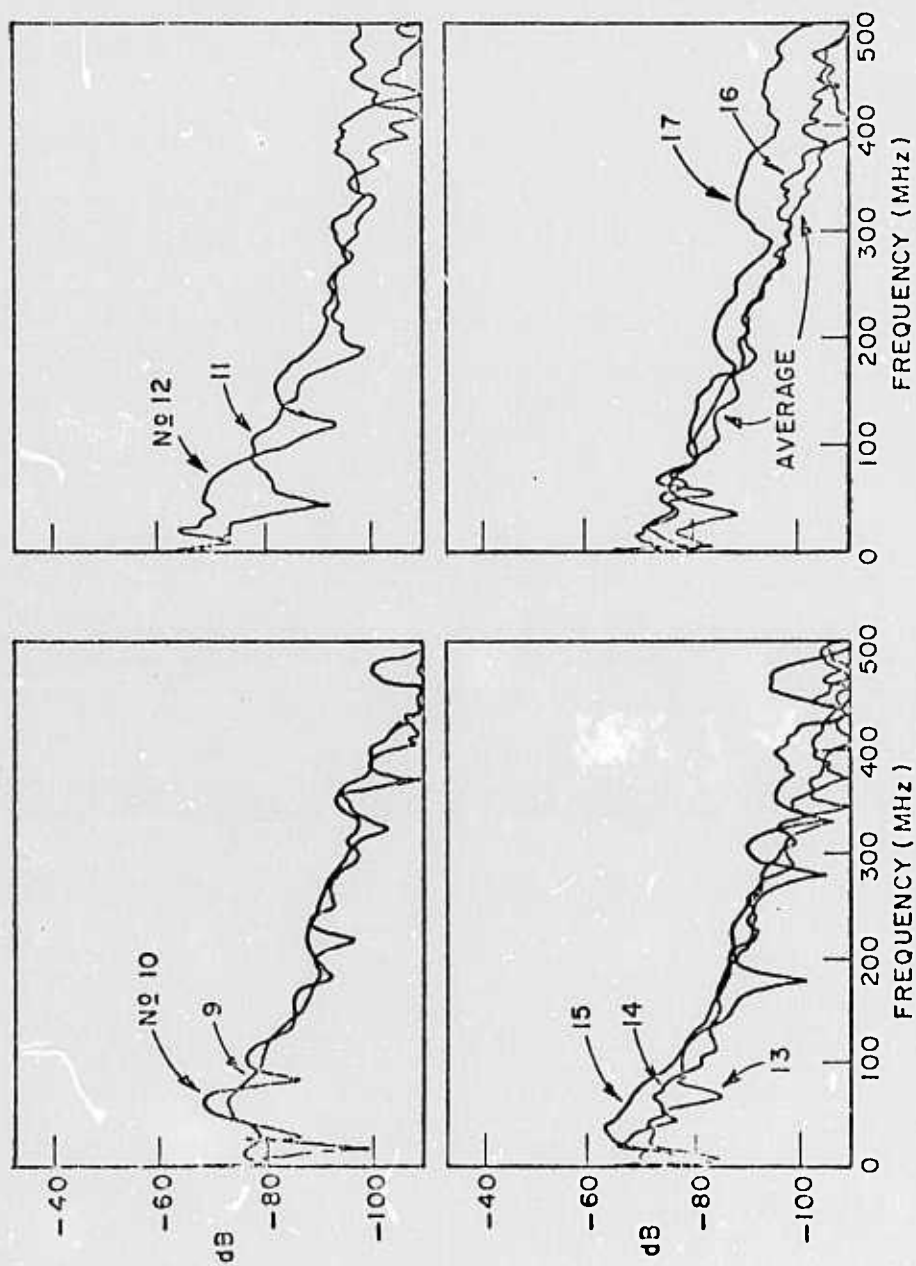
Fig. 68b. Amplitude spectra of fault measurements in dolomite.
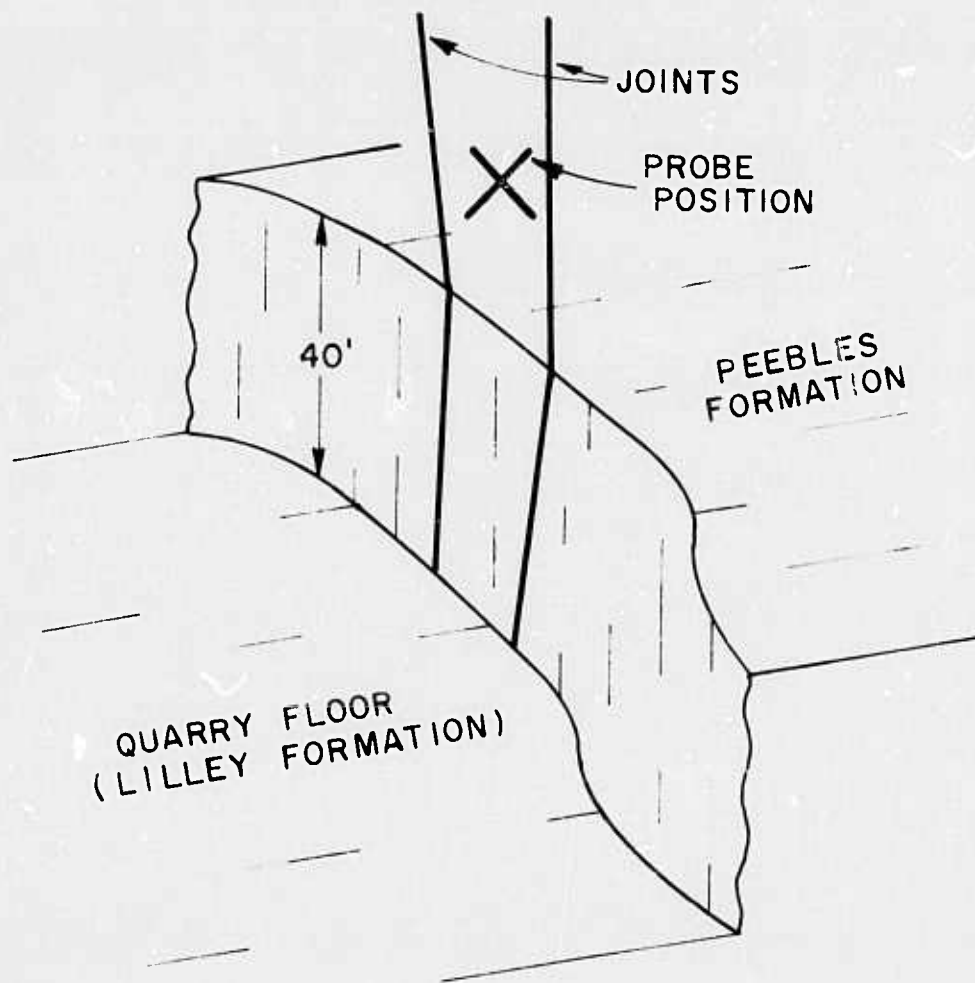
Fig. 69. Geometry of lithologic contrast measurement.

the duration of the ringing. Pulses are apparently being reflected back and forth in the cavity formed by the surface, the contrast, and the joints. Note specifically that cable lengths were varied and it was established that the ringing shown was not due to reflections within the system.
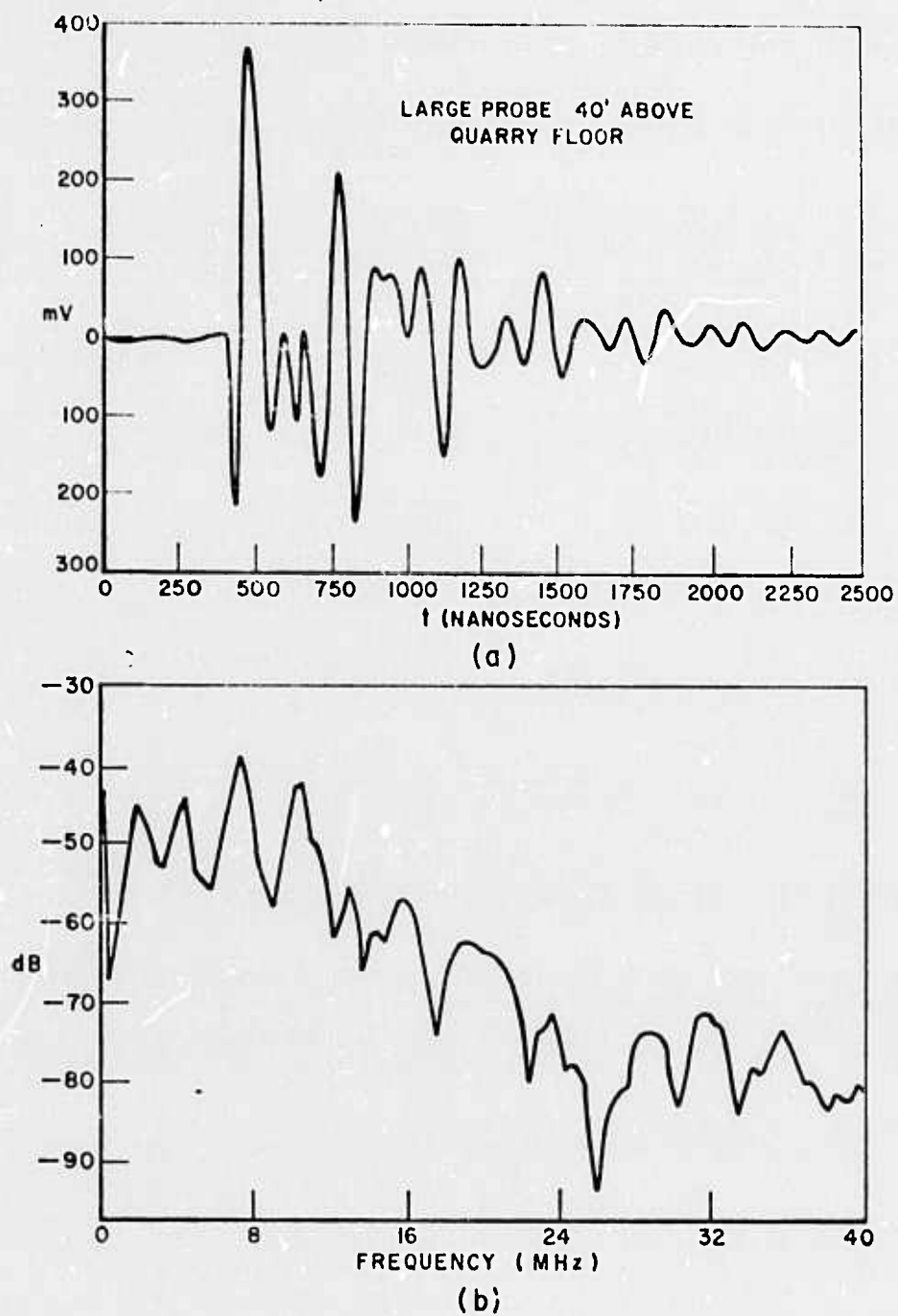
Fig. 70. Orthogonal measurement of lithologic contrast and joint
          using large probe and H.P. generator.
          (a) time domain waveform
          (b) amplitude spectrum.
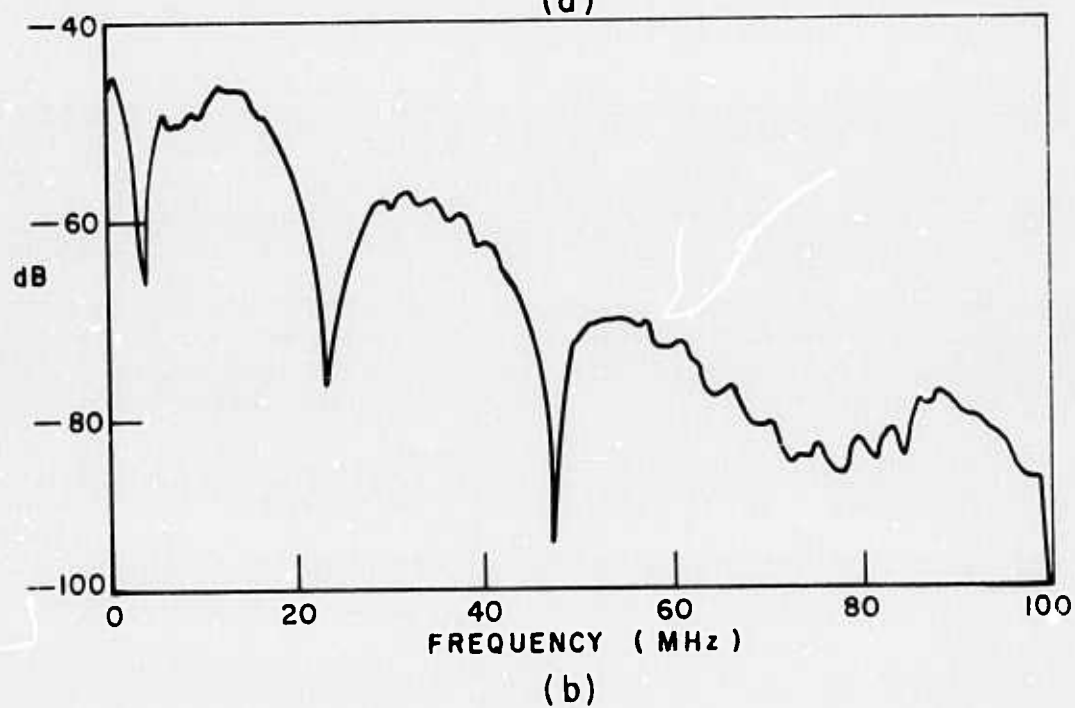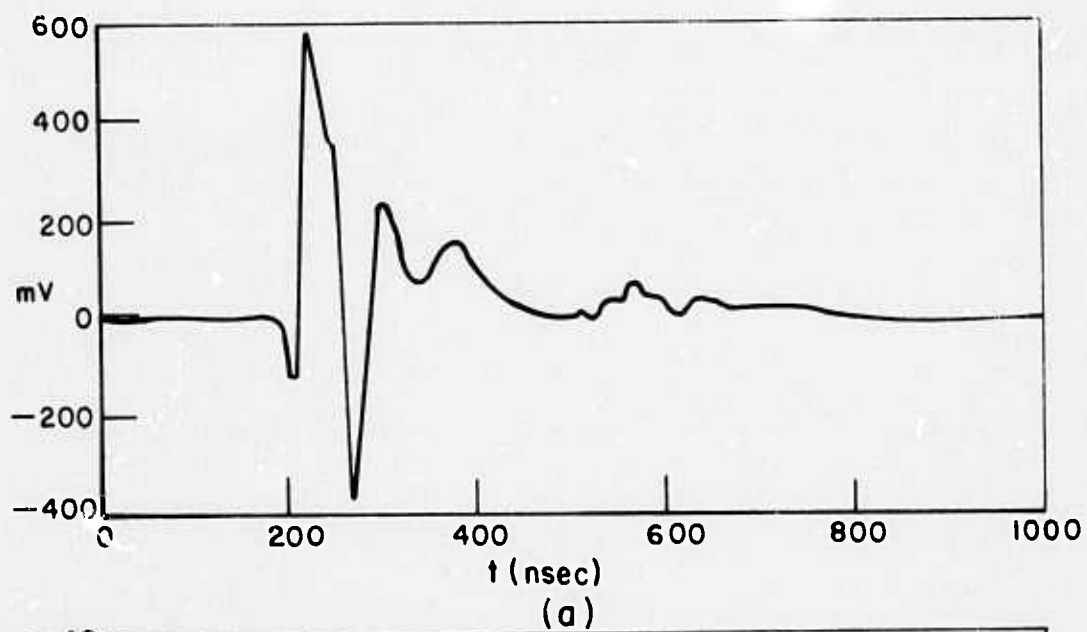
Fig. 71. Orthogonal measurement on quarry floor using large probe and H.P. generator.

D.   Dolomite Medium II

A final series of propagation and scattering measurements were made in the dolomite quarry shortly before the end of the contract. For these last measurements, a large van with a boom[8] was used in order to hold the small probe (Fig. 2b) against vertical cliff walls. It should be noted that the measurements reported in this section (Dolomite Medium II) were made in mid-summer under dry conditions as opposed to those in the previous section where conditions were very wet. One can anticipate therefore changes in the response of repeated targets. Such seasonal or even daily variations in target response would not appear to be a problem in actual deep hard rock probing. On the surface however it would be necessary to monitor a given target over a variety of weather conditions in order to catalog the target.

Extensive dipole-dipole propagation measurements were made holding one small dipole on the cliff face and the other on top of the cliff (Fig. 69). These data would have yielded the differences in electrical properties of the Lilley and Peebles formations. Unfortunately the propagation data were lost due to an undetected failure of the amplifier in one channel of the tape recorder. Time and funds would not permit a return visit to the quarry to repeat these measurements.

For this final series of measurements, the new shielded twin lead transmission line was used. Step reflection measurements using the new line are shown in Fig. 72. Shown are reflection measurements with a short circuit progressively at the end of the coaxial cable, at the output of the balun and at the end of the shielded twin lead and the old 300 ohm line. Also shown is a step reflection measurement with one of the large dipoles (Fig. 2a) on the dolomite quarry floor (Lilley formation). The transmission line is the new shielded line. A comparison of the shielded and unshielded transmission lines in Fig. 72 shows that the shielded line has reduced the mismatch at the baluns. The dipole arms of the large probe can conveniently be made either 14 or 26 feet in length. In Fig. 73, step reflection measurements of a 52 foot dipole, a 28 foot dipole and the 28 foot dipole with metal sheets are compared. The input step level is not the same in Figs. 72 and 73. Note that when surrounding conditions permit, simply extending the length of the dipole arms is one effective way to obtain a "clean" time window.

A series of orthogonal mode measurements were made using the small antenna (Fig. 2b) and the Ikor pulse generator. The antenna was held against the cliff face of the Peebles formation at a distance from the 2 joints shown in Fig. 69. The geometry is shown in Fig. 74 where 2 locations of the antennas are shown. The series of

106
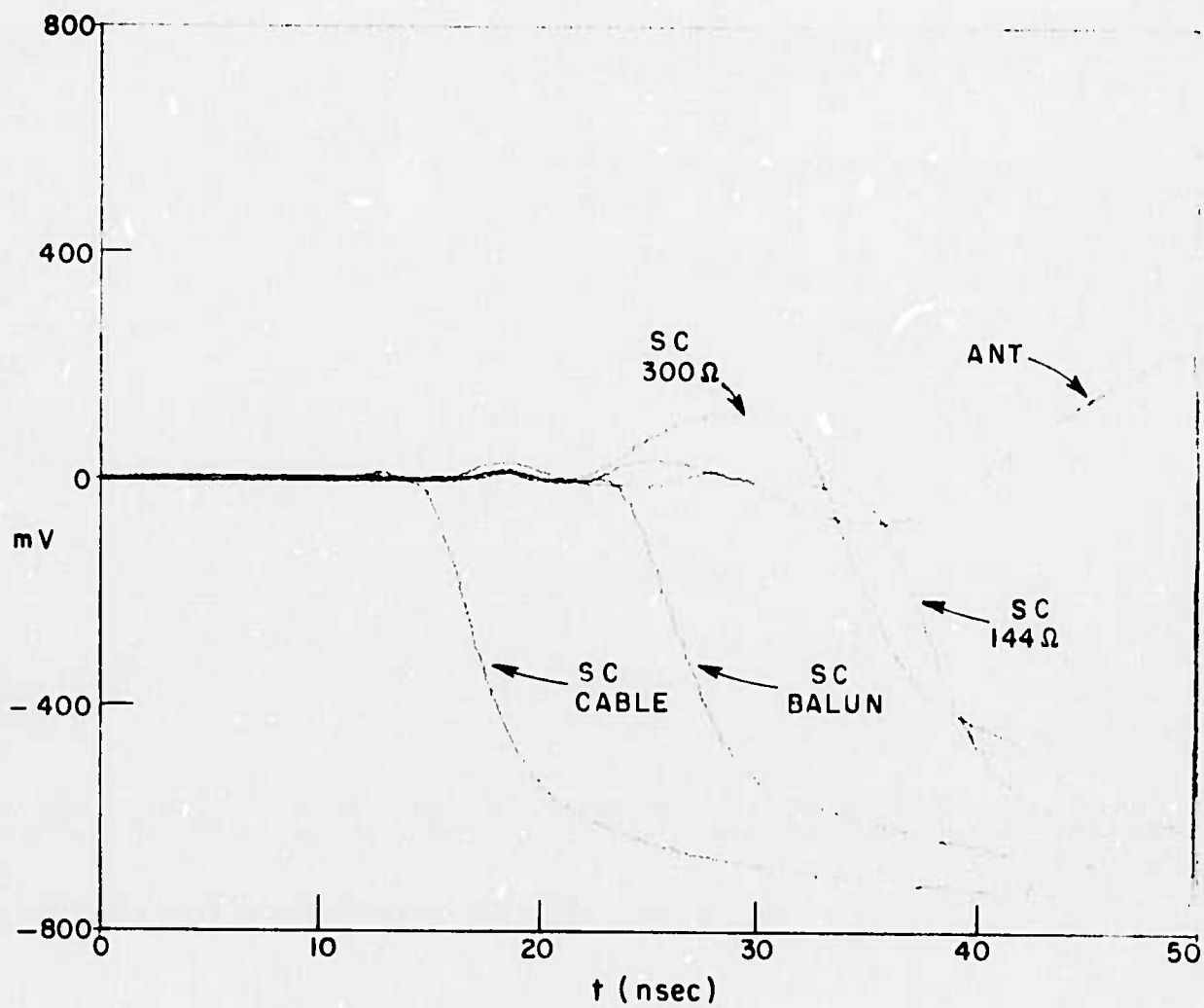
Fig. 72.   Step reflection measurements of large
dipole and with short circuit at
various points along feed system.
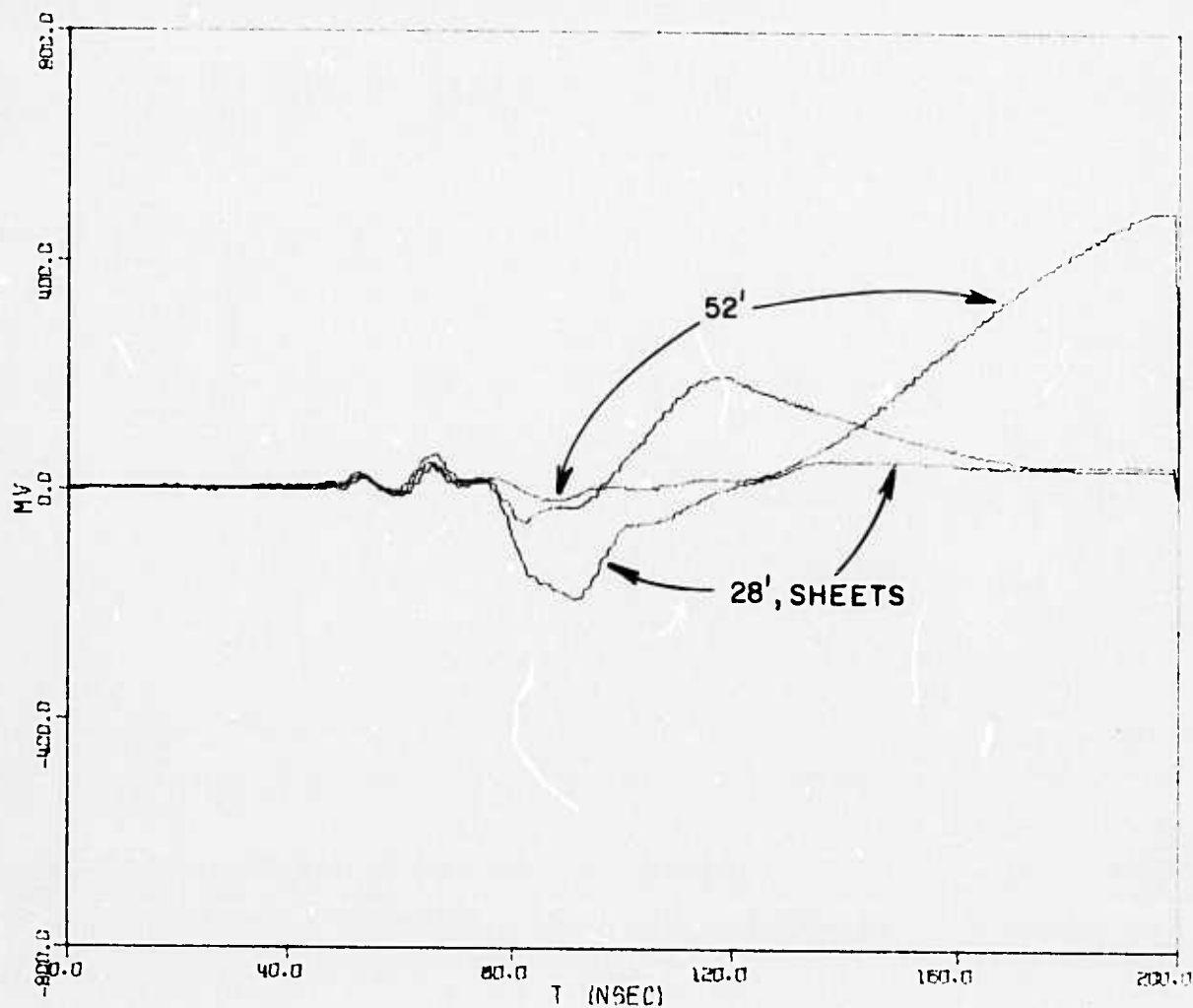
Fig. 73. Step reflection measurements of 52 foot dipole without sheets and 28 foot dipole with and without sheets. Shielded transmission line was used.
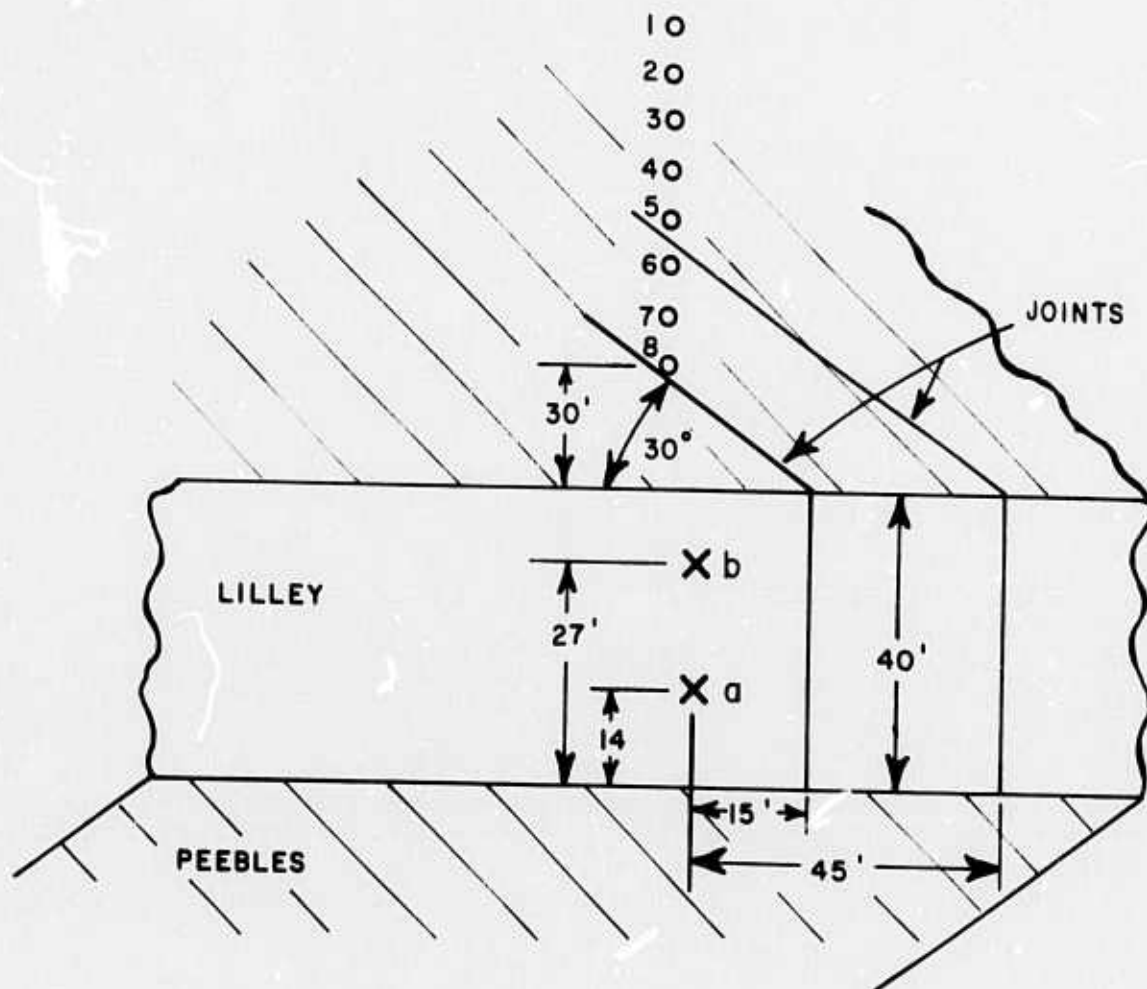
Fig. 74. Geometry of cliff face joint measurements.

109

numbered circles along the top of the Lilley formation have reference
to other measurements discussed later. The absorber pad was located
between the antennas and cliff face in each case. At the site shown,
the cliff face offered the best conditions for placing the antennas
flush with the rock surface. In neither case however were both
antennas ideally located - some portion of one or both of the ends of
the dipole arms were 2 to 8 inches from the rock. The sketch in
Fig. 74 does not show the soil overburden on top of the cliff, i.e.,
the joints are not visible from the top. One can however see a
corresponding joint configuration on the opposite quarry wall along
the line of sight of the joints. This suggests that the joints do
extend some distance as suggested in Fig. 74. The geometry of
positions a and b provides some measure of the possible effect of
tunnel side walls in an actual hazard detection operation in
tunneling, i.e., if the Lilley-Peebles intersection at the base of the
cliff alters the response in position a but not position b.

For all of the orthogonal mode measurements reported in this
section, processing was via Eq. (7) except that the medium, $M^2(s)$,
could not be removed. In addition, the antenna transfer functions
used were those for the limestone medium, i.e., Figs. 42 and 45. It
was not felt that the theoretical calculations had been sufficiently
verified to warrant using a theoretical antenna transfer function.

The unprocessed time waveforms recorded at positions a and b
are shown in Fig. 75. The processed amplitude spectra and corresponding
time waveforms are shown in Figs. 76 and 77 respectively. Also shown
in these figures (75, 76 and 77) is the response from a section of
the cliff face where no jointing or fracturing was visible. Because
of the loss of the propagation data, the effective refractive index
of the Peebles formation at the time the measurements were made is
unknown. Using data from the limestone quarry under dry conditions,
estimates of the arrival time of signals from the joint on paths
perpendicular to the joint and perpendicular to the cliff face are
indicated in Fig. 75. Note that comparing the responses at positions
1 and 2 an effect from the quarry floor is not apparent. Measurements
of a different joint are shown in Fig. 78. In this case only a
single joint was apparent. The geometry is the same as that sketched
in Fig. 74 except that the small probe was held midway between the
quarry floor and the top of the cliff. The joint was approximately
15 and 30 feet along the cliff face from the probe, i.e., the same
15 foot dimension shown in Fig. 74. Note the strong similarity of
the joint responses in Fig. 75 and Fig. 78. Processed amplitude
spectra and time waveforms are shown in Figs. 79 and 80 respectively.

Several points need to be made concerning the processed ampli-
tude spectra and resultant time waveforms. First, as noted previously,
the ringing in the time waveforms (Figs. 77, 80) is the results of
filtering out the high frequencies in the normalized spectrum.

110
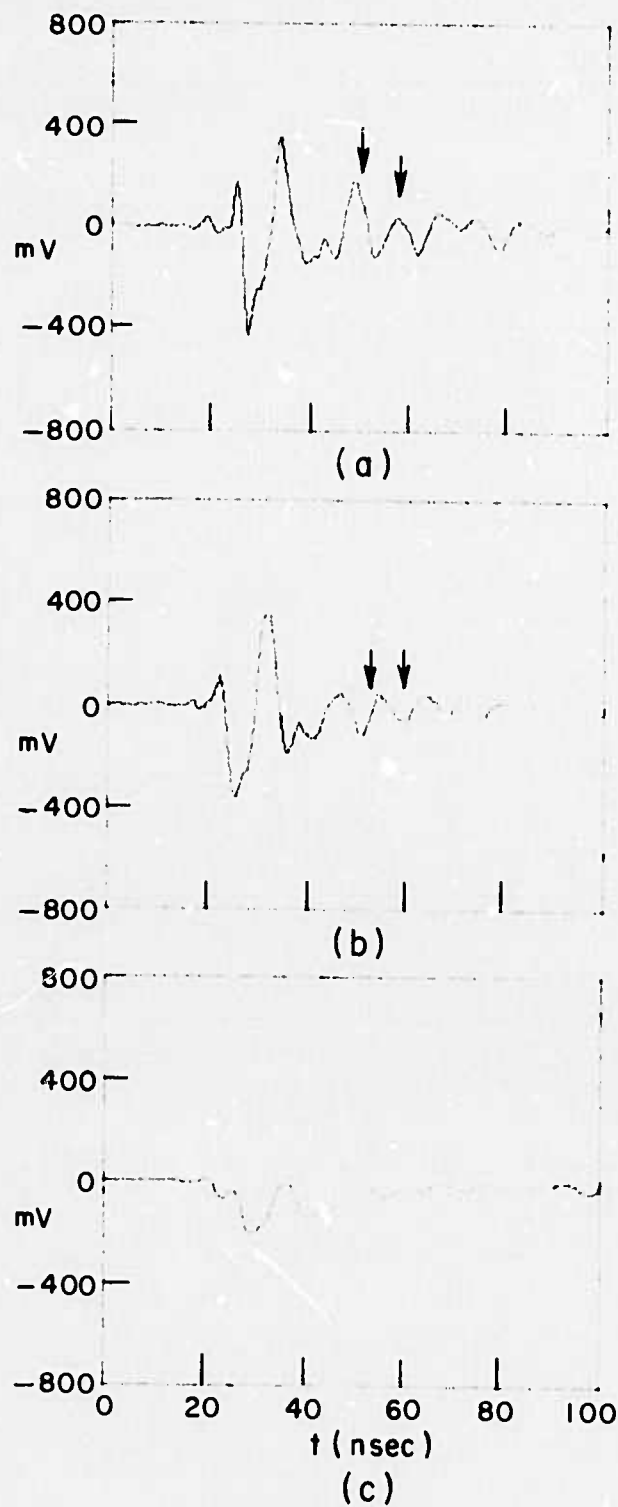
Fig. 75. Double joint measurements.
(a) position 1
(b) position 2
(c) no joint

111
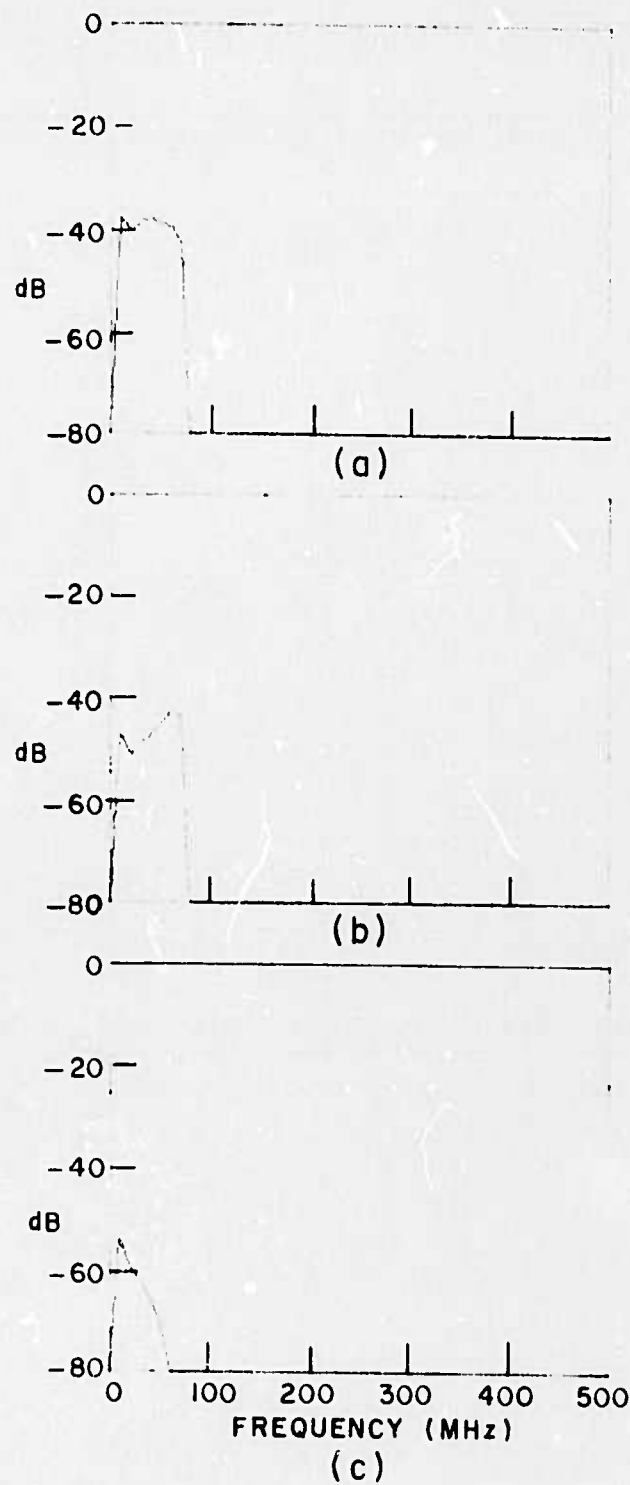
Fig. 76. Normalized (Eq. (7)) amplitude spectra of joint measurements.
(a) position 1
(b) position 2
(c) no joint

112
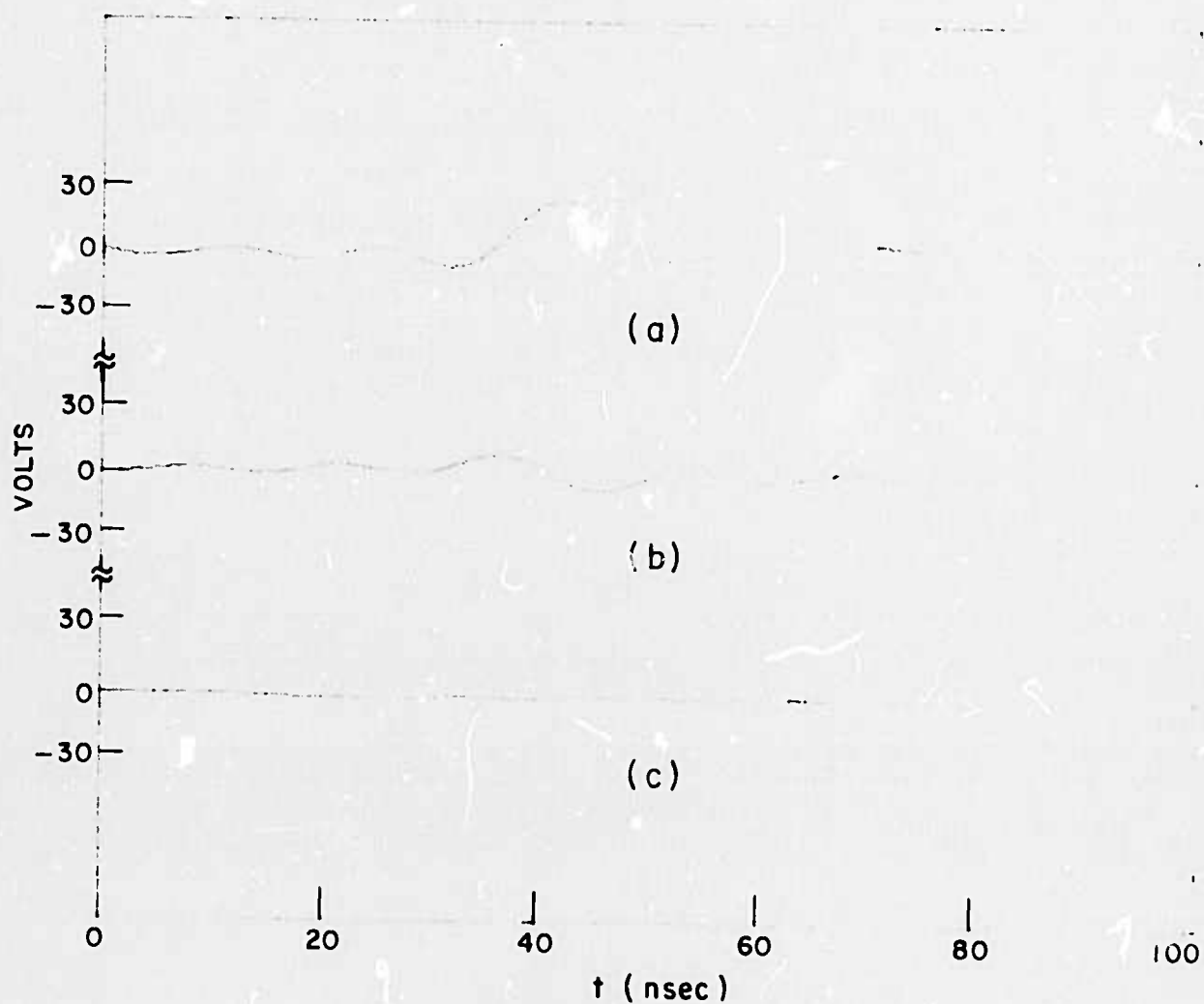
Fig. 77. Normalized time response
waveforms from joints.
(a) position 1
(b) position 2
(c) no joint

113
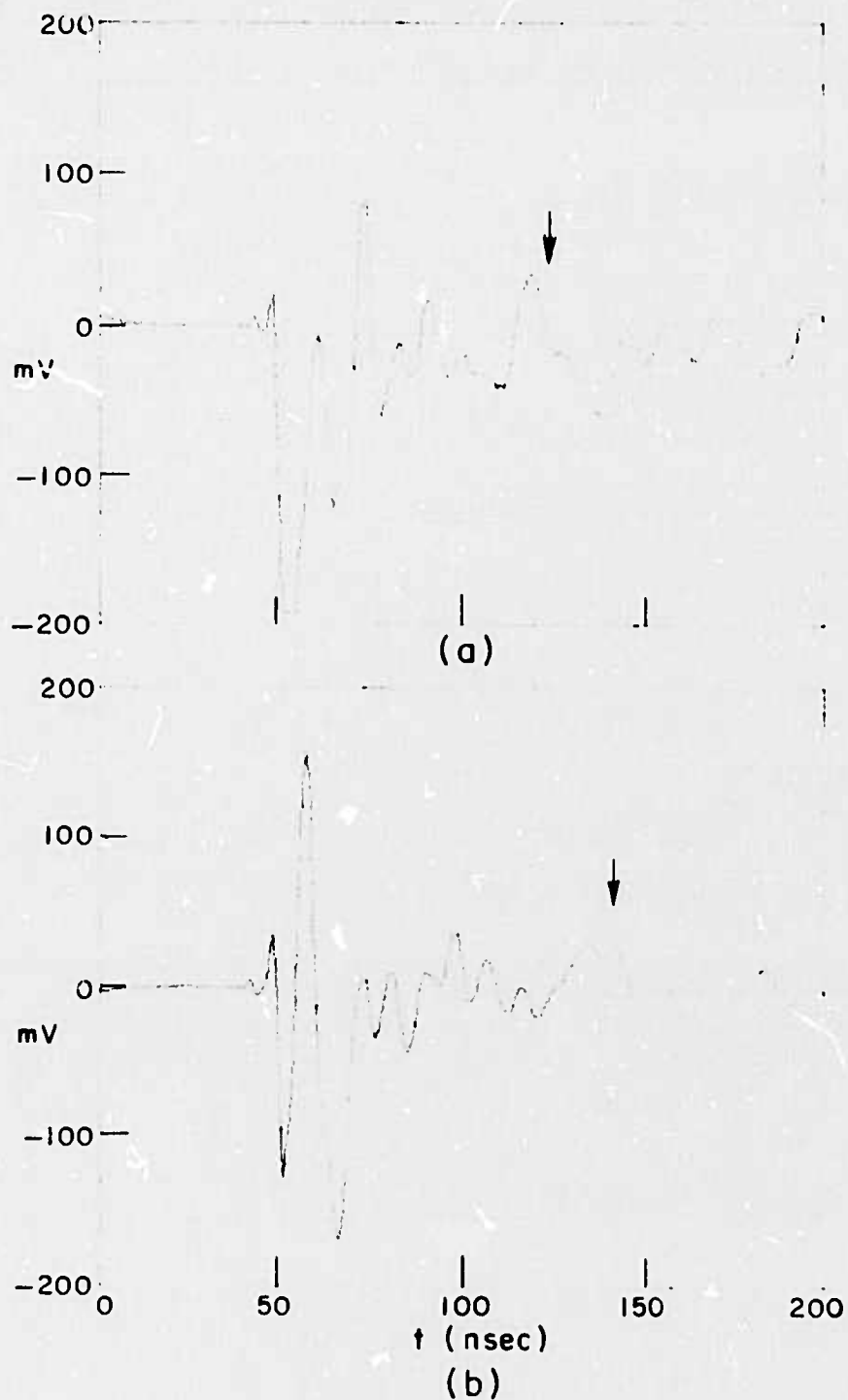
Fib. 78.   Single joint measurements.
(a) 15 feet
(b) 30 feet

114
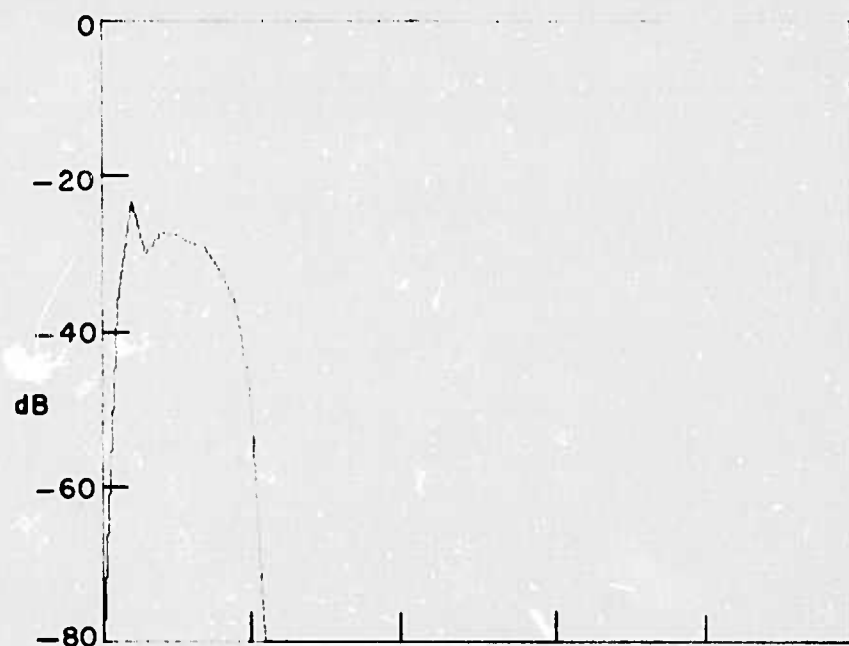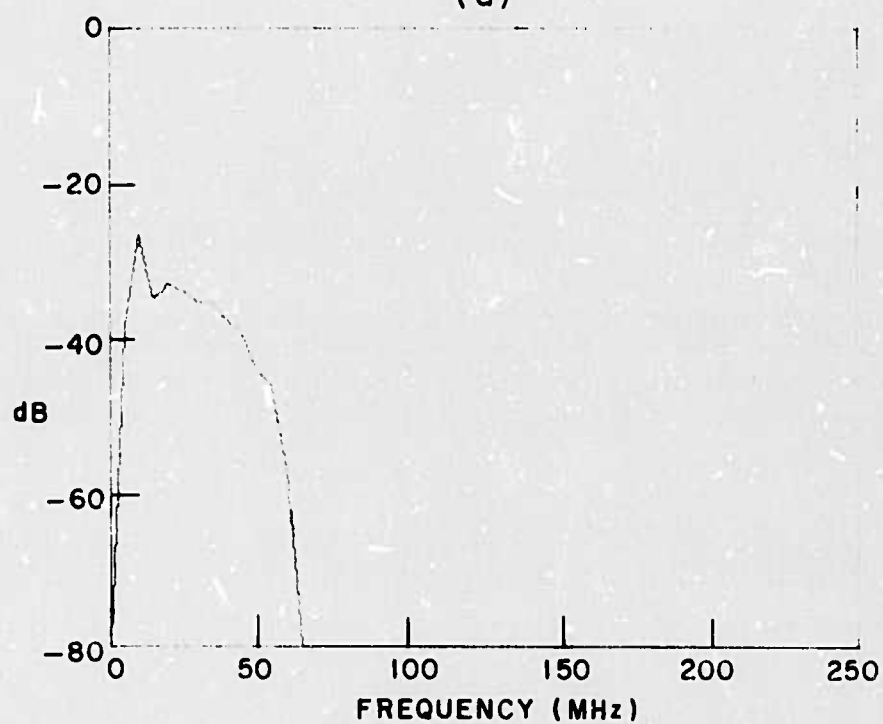
Fig. 79. Normalized amplitude spectra
of single joint.
(a) 15 feet
(b) 30 feet

115
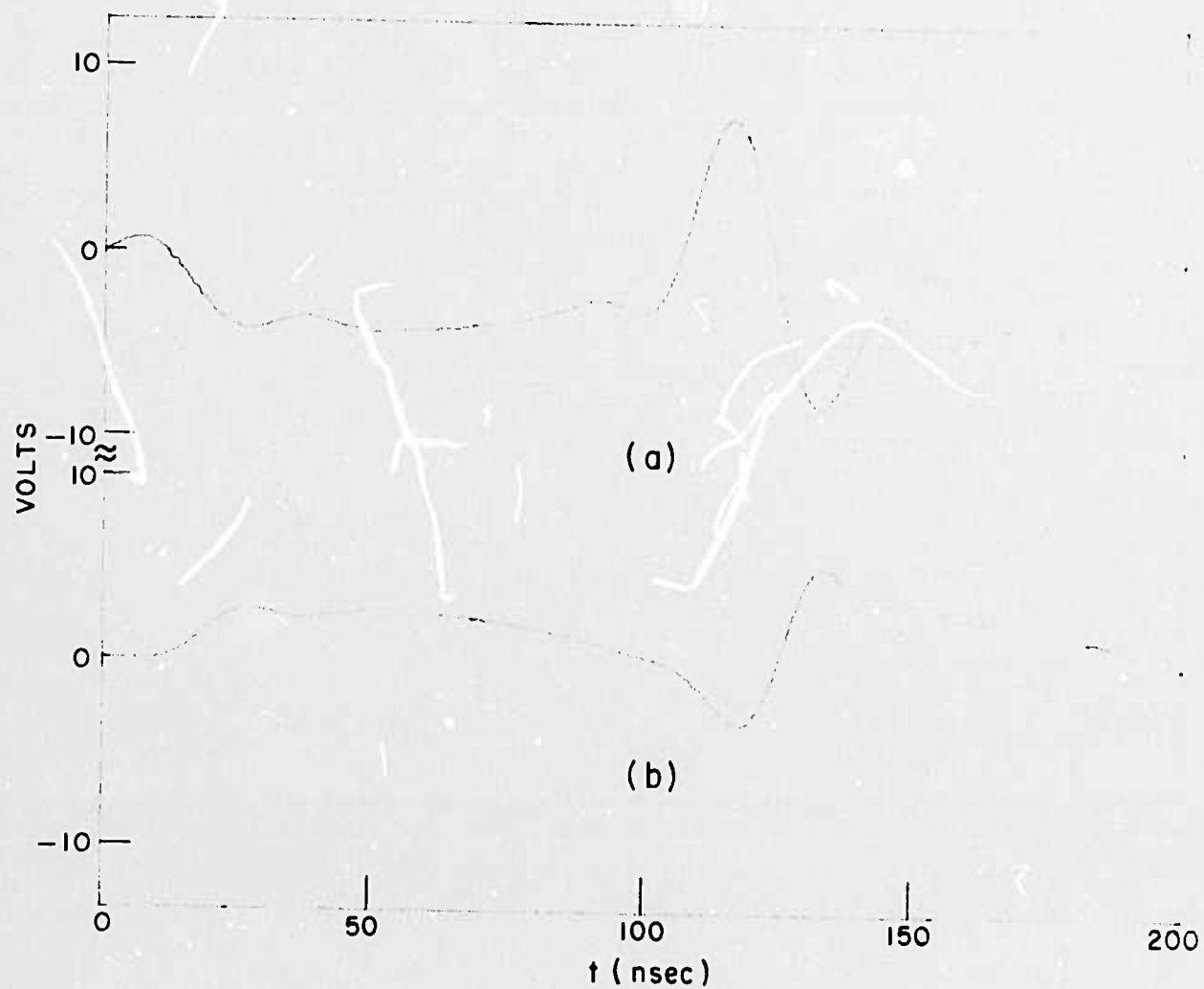
Fig. 80. Normalized time response waveforms
from single joint.
(a) 15 feet
(b) 30 feet

116

Second, because of the uncertainty of pulse velocity, the gate is somewhat broader than usual. Thus the processed waveforms shown may contain more than one return. In an actual hazard detection mission, each significant response would be isolated completely by gating and then processed individually as was done for the tunnel response in Fig. 61a. This was not feasible for the Peebles formation data because of the loss of the propagation data.

The same antennas and pulse generator (Ikor) were used to make a second series of orthogonal mode measurements around the joints of Fig. 74. In this case the probe was moved along the top of the cliff (Peebles formation) along the dashed line in Fig. 74. Positions of the probe are indicated by open dots. The unprocessed time waveforms are shown in Fig. 81. The most dominant features of these waveforms is the very strong response starting approximately 30 to 40 nanoseconds from the direct coupling and the distinct change in the character of the response at positions 5 and 6 over the 10 to 15 nanoseconds immediately following the direct coupling. This time region is usually associated with clutter return, but in this instance appeared to have some significance. Thus in processing the time waveforms in Fig. 81, only the direct coupling was removed by gating. The normalized amplitude spectra and associated time waveforms are shown in Figs. 82 and 83 respectively. Note in Fig. 81 the anomalous character of the waveforms for position 3, and less distinctly in position 5 at approximately 65 nanoseconds. The responses in each waveform in Fig. 81 correspond to the depth of the overburden over the dolomite Peebles formation. A depth calibration is not possible because propagation data are not available. According to the quarry geologist the overburden depth on the Peebles runs from 1 to 10 feet away from the cliff face with approximately a 1% grade. This cover consists partially of residual soil and partially of soil which had been bulldozed into place. In addition, the Peebles surface would be expected to show some undulations. Using data on soil obtained locally an average depth of overburden of 3.75 to 4.0 feet is obtained. The anomalous responses noted earlier could be due to larger pieces of rock or possibly metal objects introduced when fill was added. These same anomalies could easily introduce the noted changes at positions 5 and 6. These latter changes could also be the result of the joint, especially if the visually sighted joint lines were somewhat inaccurate. It is stressed that for the measurements in this section, cable lengths were periodically changed to assure that none of the responses measured were internal reflections. It was originally hoped to make both the cliff top and cliff face measurements at much closer spacings to provide appropriate synthetic aperture processing data. In the time domain, this amounts to a summing and normalization of several adjacent waveforms along a line after time-shifting the waveforms for interrogation at a particular depth. For a soil medium, the 6 foot spacings precludes any dramatic results with such processing. The major element here is time - with

117
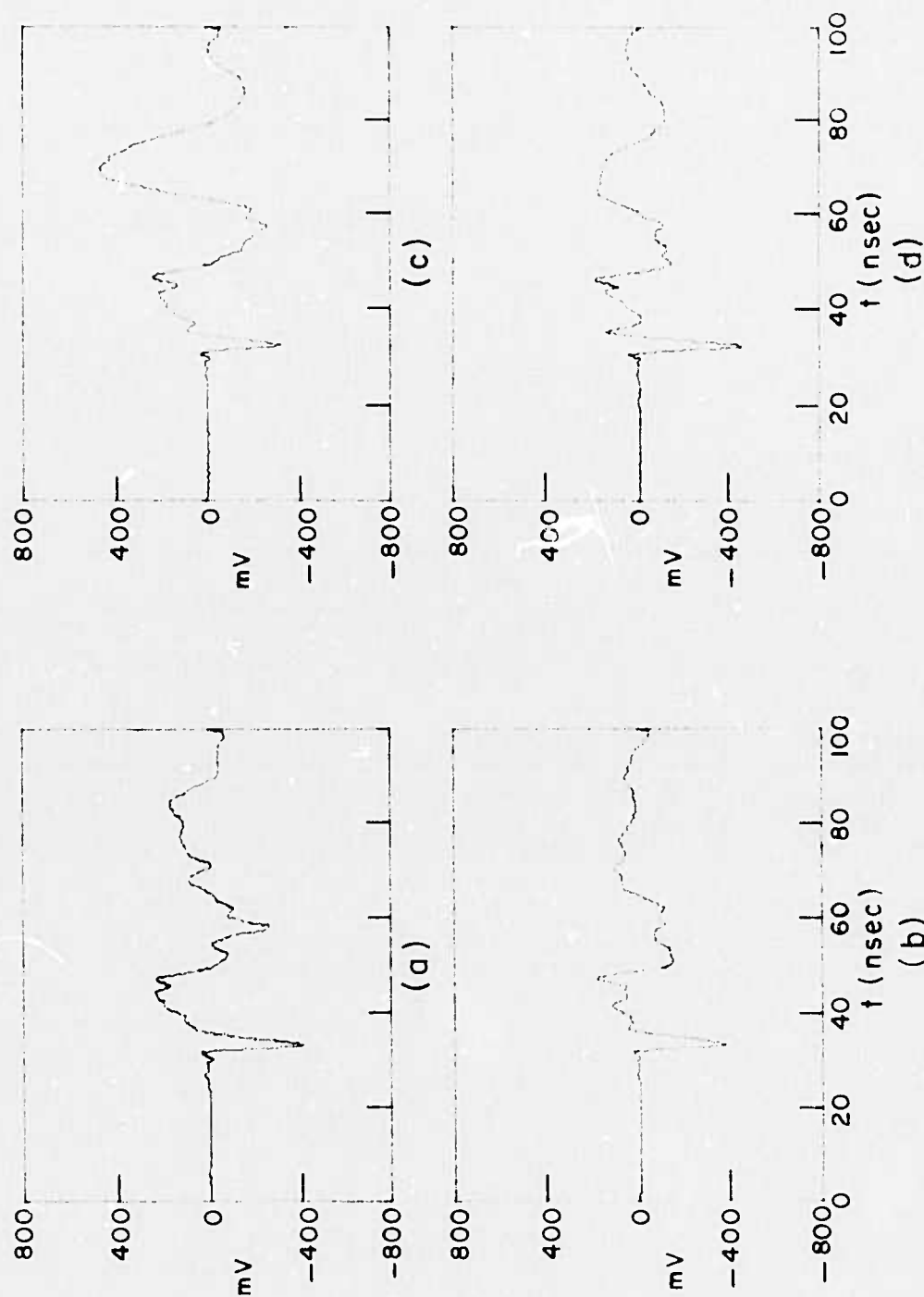
Fig. 81. Joint span measurements.
(a) position 1
(b) position 2
(c) position 3
(d) position 4

118
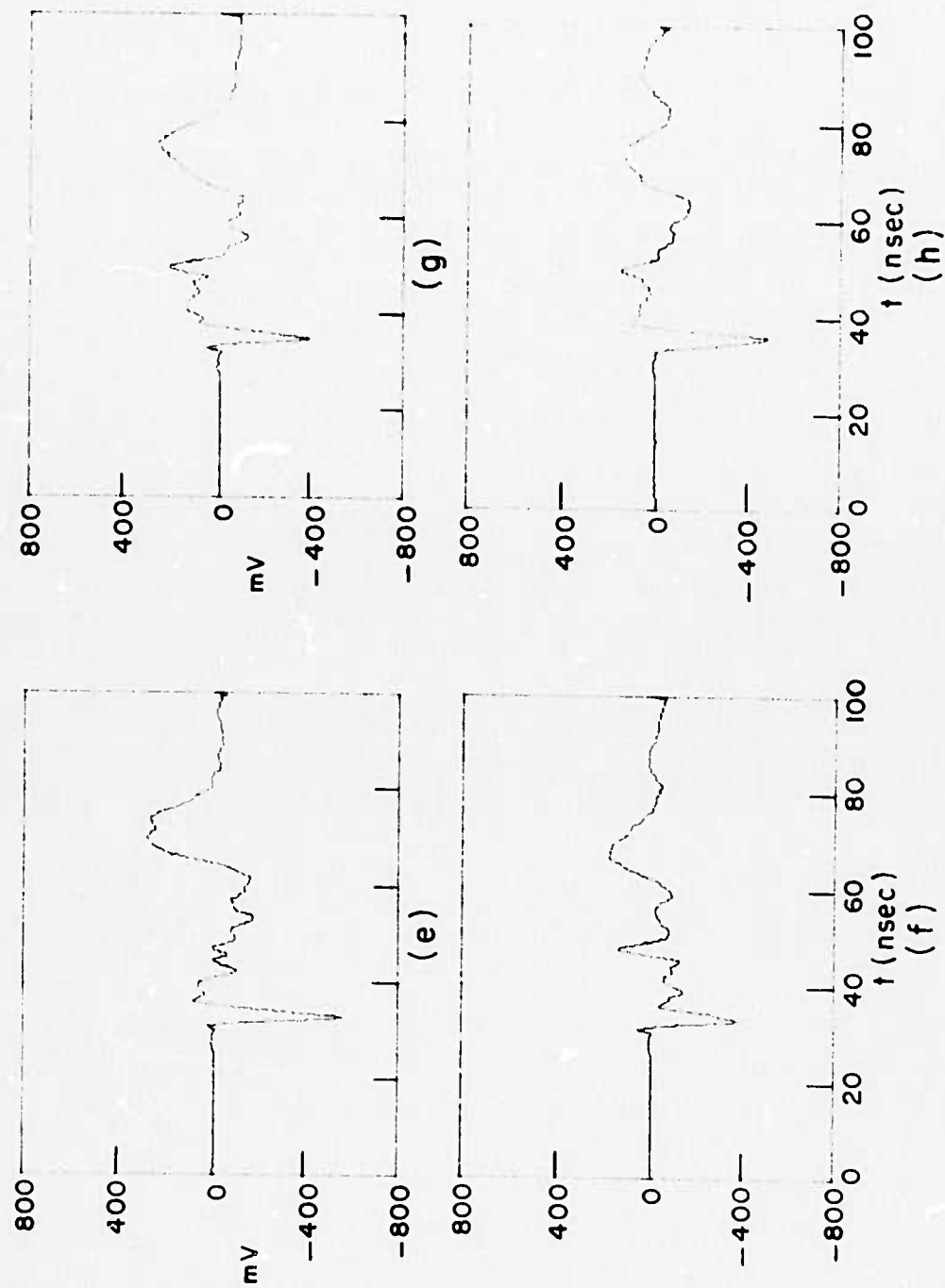
Fig. 81. (Continued)
(e) position 5
(f) position 6
(g) position 7
(h) position 8

119
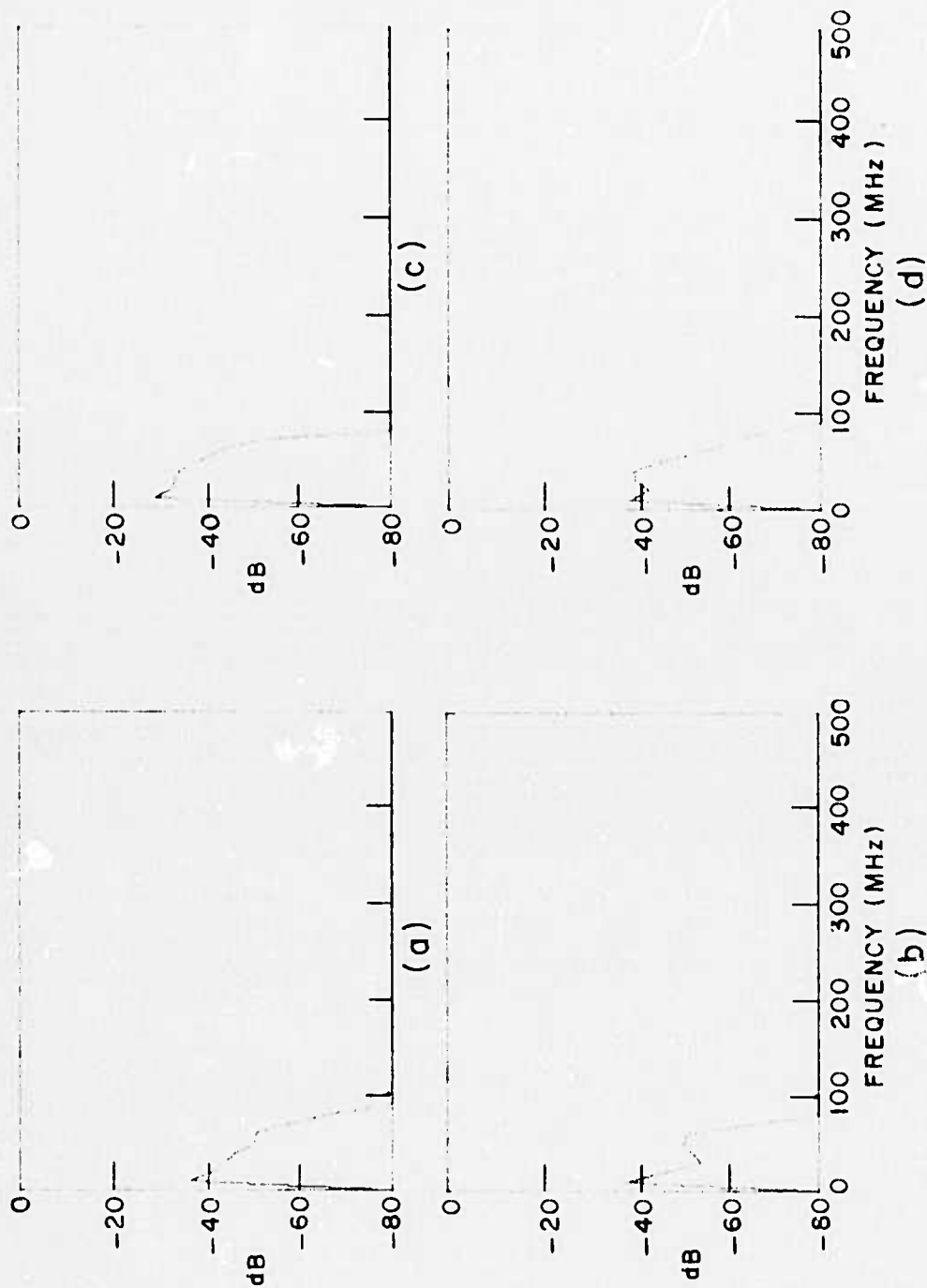
Fig. 82. Normalized amplitude spectra of joint span measurements.
(a) position 1
(b) position 2
(c) position 3
(d) position 4

120
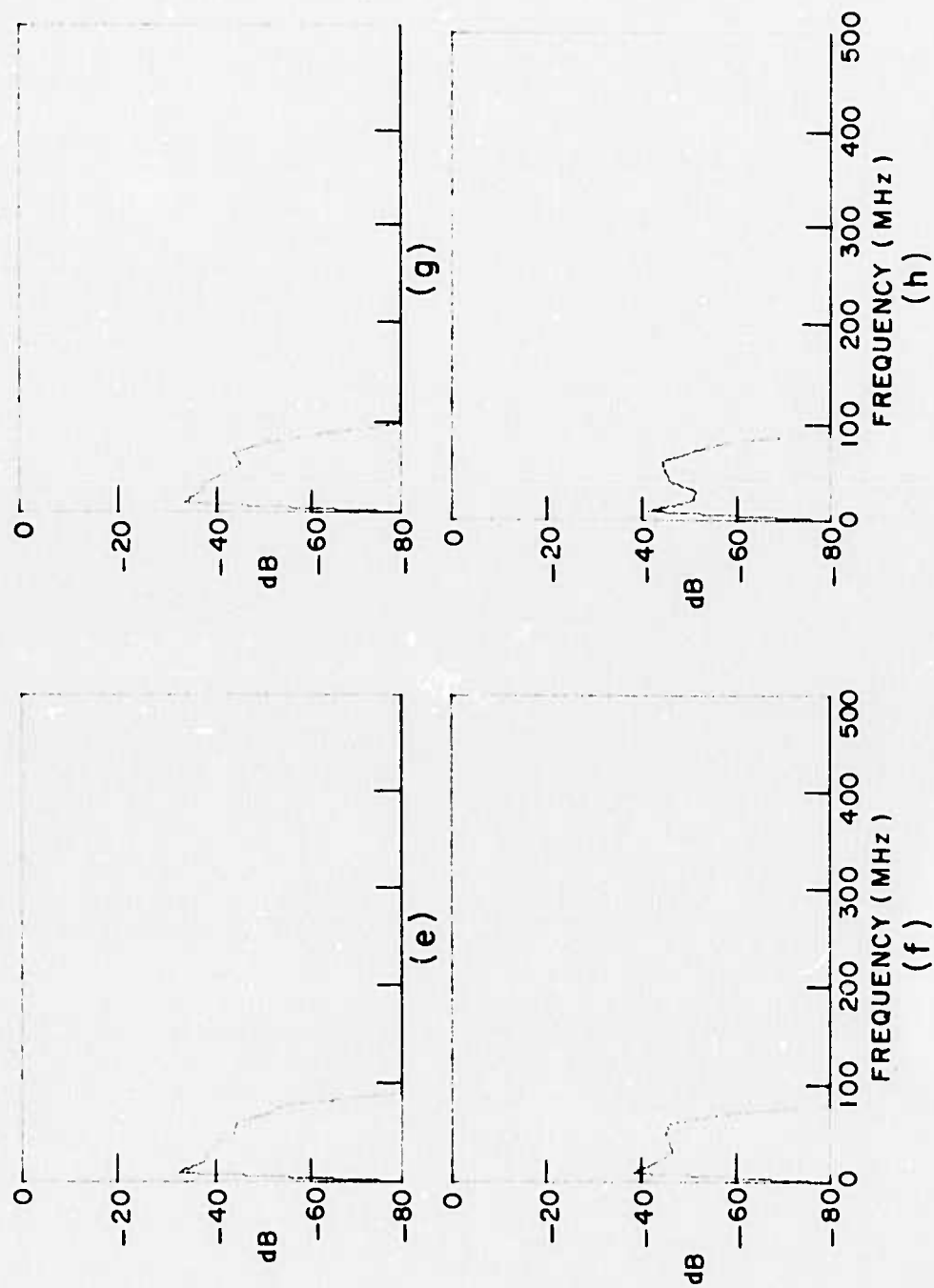
Fig. 82. (Continued)
(e) position 5
(f) position 6
(g) position 7
(h) position 8

121
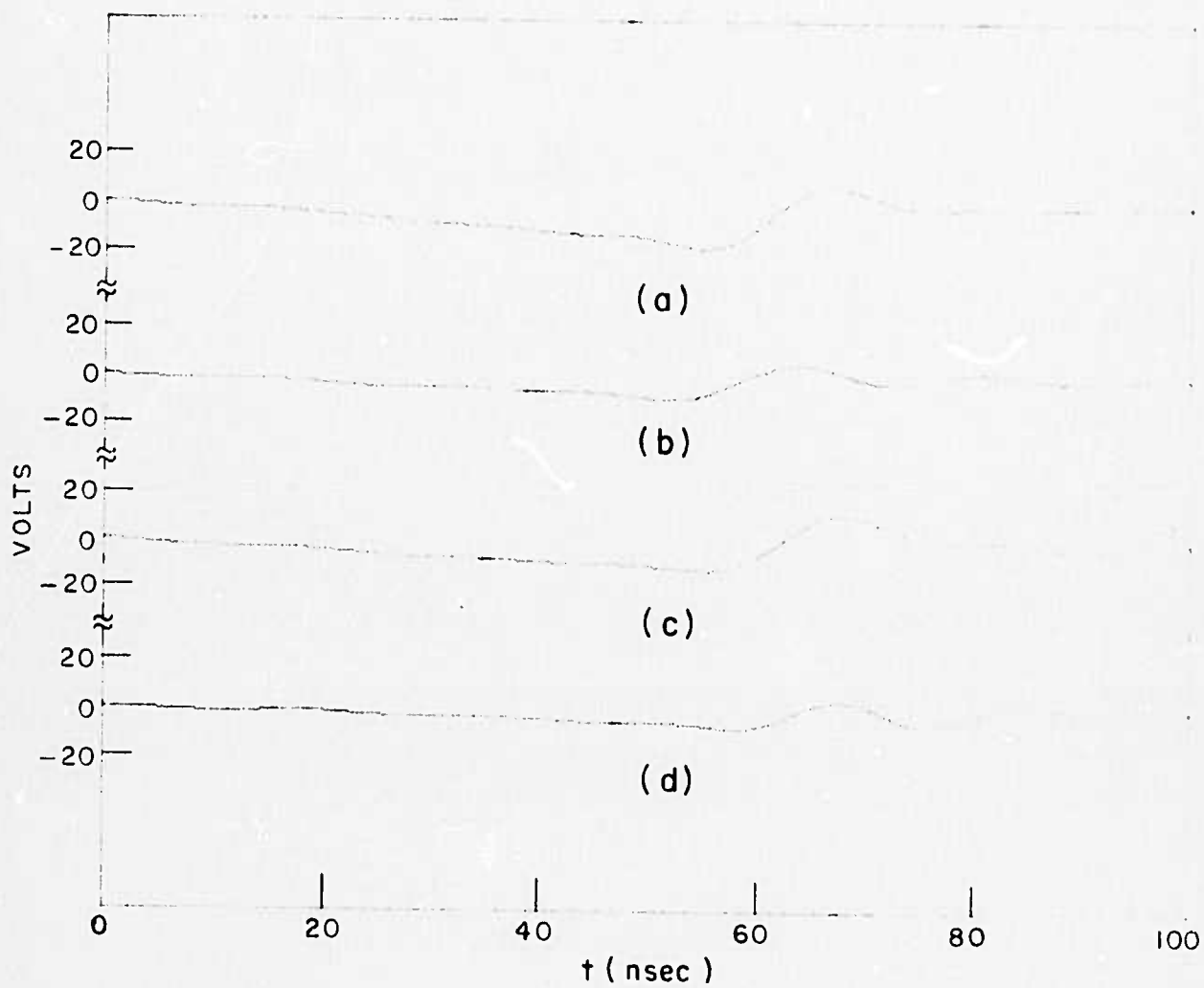
Fig. 83. Normalized time response waveforms
of joint span measurements.

122

Fig. 83. (Continued)

123
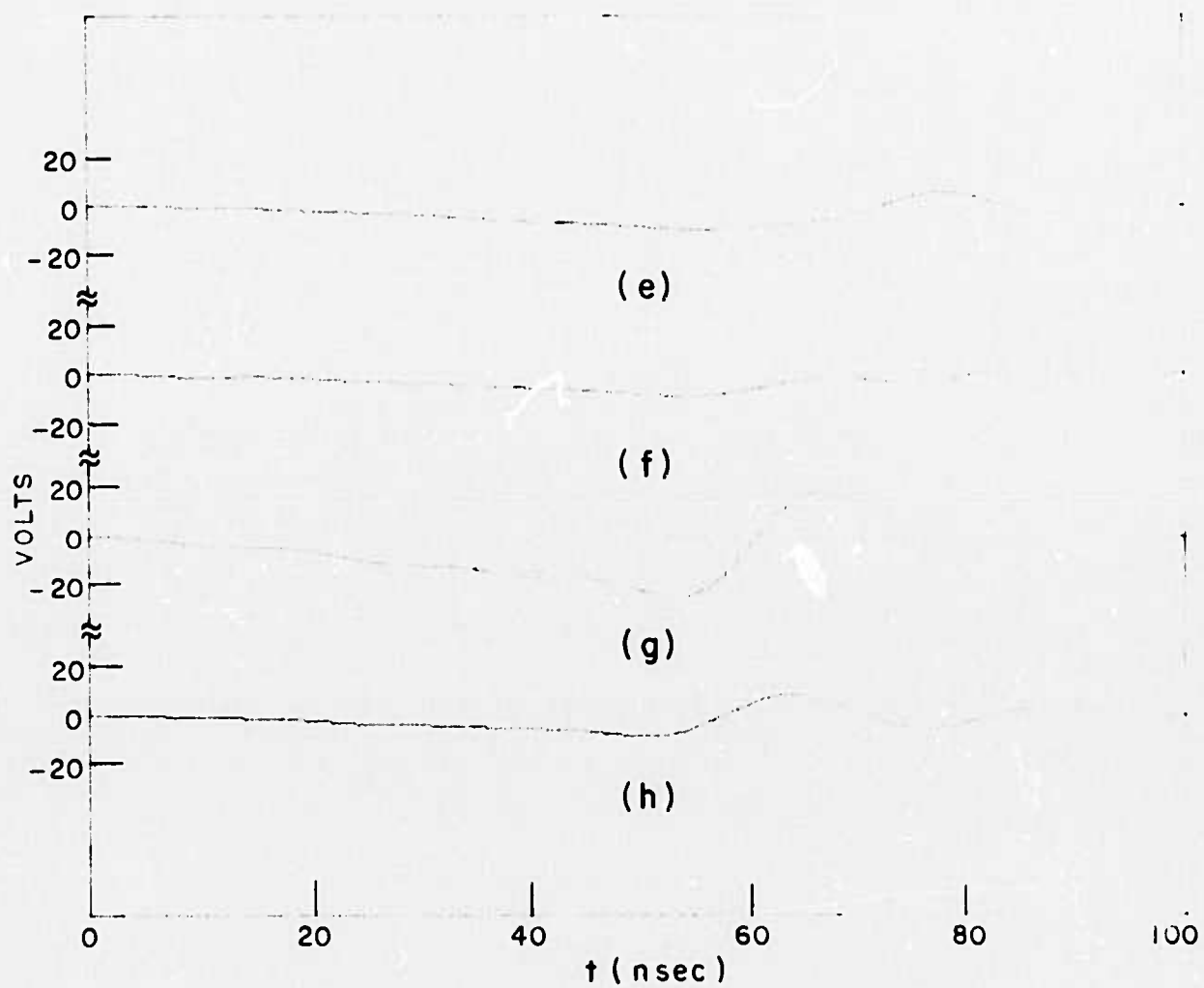
the present laboratory system adapted to field use, a single measurement requires several minutes. This would not be the case for a true field-hardened and adapted system.

The final measurement made on the top of the Peebles formation was approximately a repeat of the geometry in Fig. 69 using the large antennas with sheets and the H.P. pulse generator. The unprocessed time waveform is shown in Fig. 84 and the amplitude spectra in Fig. 85. Again, cable lengths were changed and the response was unchanged. Fig. 84 is to be compared with Fig. 70a. It is stressed that extremely dry and wet conditions respectively prevailed. The duration of the response waveforms, 700 vs. 2500 nanoseconds, is dramatic evidence of the effect of moisture content on the reflection offered by various contrasts. Note that the overburden cover is academic because of the width (45 nanoseconds) of the H.P. pulse. Speculation on the lithologic contrast (Peebles-Lilley formations) is difficult because of the loss of the propagation data, but the response beginning roughly 300 nanoseconds beyond the direct coupling in Fig. 84 indicates a reduction factor of 0.85 in the effective refractive index of the Peebles formation going from wet to dry conditions.

In Fig. 86, the unprocessed time response waveform for the large antenna with sheets (H.P. pulse) on the quarry floor in the orthogonal mode is shown. The amplitude spectra of the waveform in Fig. 86 is shown in Fig. 87. Location of the probe was approximately the same as for the waveform and spectra in Fig. 71. A comparison of Figs. 71a and 86 shows a reduction by 1/2 in the direct coupling for dry conditions (Fig. 86). At the same time, distinct responses at 225, 300 and 425 nanoseconds from the direct coupling in Fig. 86 do not correlate with Fig. 71a. The d.c. offset (beginning vs. end) of the time waveform in Fig. 86 is indicative of equipment rather than target changes. This was confirmed by cable length changes. Thus the shale layer approximately 40 feet below the quarry floor is very suspect inso-far as repeat measurements are concerned.
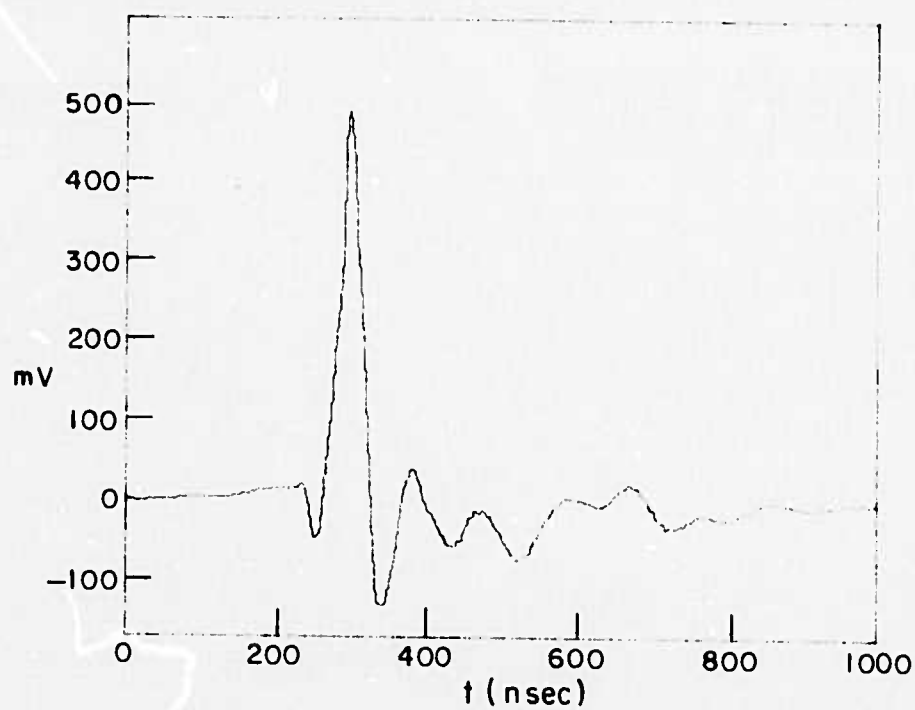
Fig. 84.   Large probe between joints.
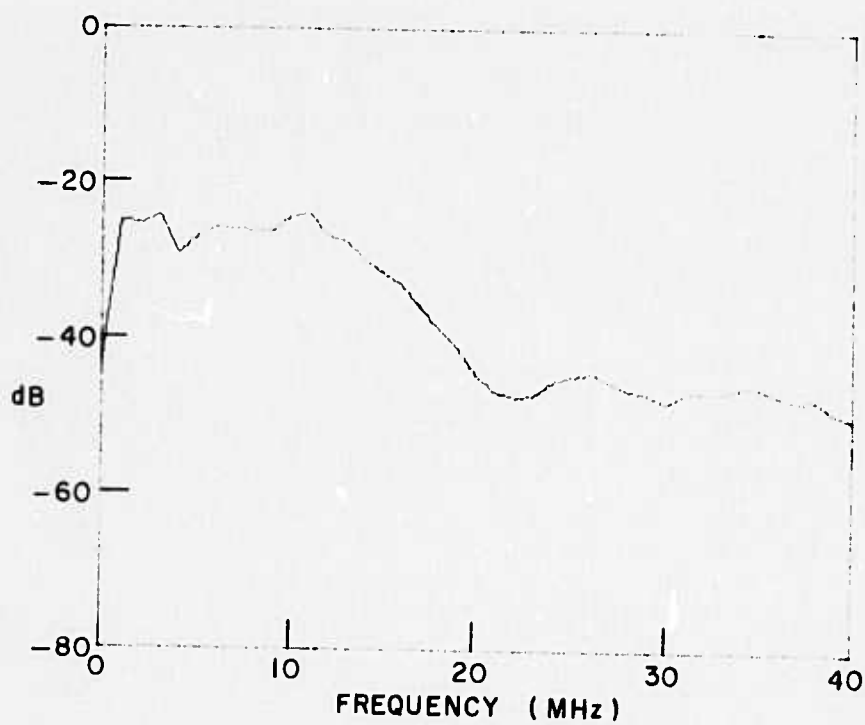
Fig. 85.   Normalized amplitude spectrum
of large probe between joints.

125
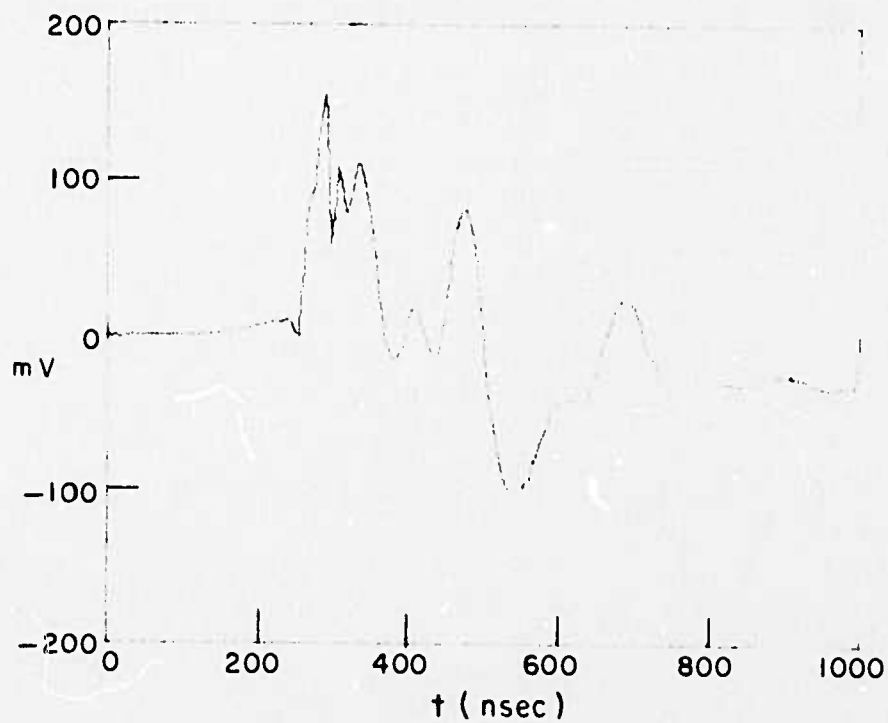
Fig. 86.   Large probe on quarry floor
(Lilley formation).
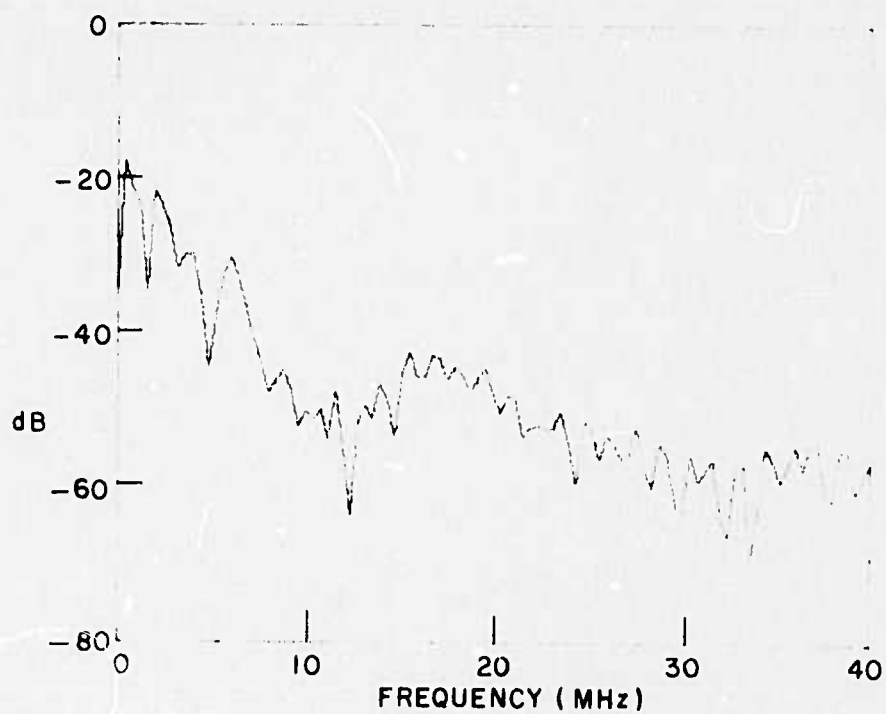
Fig. 87.   Amplitude spectrum of large
probe on quarry floor.

126

VIII. CONCLUSIONS

A unique electromagnetic video pulse sounding system has been developed. In broadest terms the system is an active remote sensor capable of interrogating a medium from the surface of the medium. The system effectively couples electromagnetic energy into the medium and is insensitive to large objects located on the medium surface near the system antennas. The coupling and insensitivity to surface objects have been demonstrated for both soil and soft rock (limestone and dolomite) media using experimental measurements on a full scale version of the system. Modifications of the system to adapt it to a particular medium are minimal and can be easily done experimentally. The size of the antenna structures can be easily adjusted to accommodate a variety of measurement sites and video pulse generators. For example, in this report measurements with 6 foot and 28 foot dipole antennas and with video pulses with 15 nanosecond (10^{-9} sec.) and 150 picosecond (10^{-12} sec.) rise times are shown.

The electromagnetic pulse sounder has the advantage that it can be operated in two modes, one of which (the orthogonal mode) is blind to targets which are symmetric with respect to the system antennas. Thus horizontal stratifications including the air-medium interface are not seen. To see such targets, the other (direct mode) mode is used. Most of the results reported herein were obtained using the orthogonal mode. In the direct mode a limiter must be used to protect the sampling head. The limiter has been built, but the turn-off time of the diodes used was too slow (under high voltages) to permit full power operation without smearing individual responses together. Other diodes are now commercially available which would eliminate this problem.

The electromagnetic pulse sounder has detected 1 inch diameter dielectric cylinders at a depth of 30 inches in soil and 4 inch diameter metal cylinders to depths of 5 feet in soil. In a limestone medium a 2 foot diameter cylinder at a depth of 2 feet and a large cylindrical void (road tunnel) at a depth of 20 feet have been detected. In a dolomite medium the response from faults at a maximum distance of 5 feet, joints to depths of 45 feet and a lithologic contrast at a depth of 45 feet have been detected. For the man-made targets (cylinders and cylindrical void) these results can and have been verified. For the geological targets however it is not possible to obtain a simple verification. Thus the interpretation given these measured data is subject to qualification. None of the data are inconsistent with known geological features however and special care was taken to remove the possibility of internal reflection mechanisms.

It is significant to note that the above results were obtained
in most cases from simply an examination of the temporal and spectral
signatures. That is, it was not necessary to employ complicated
processing procedures in order to detect the presence of the target.
The proper method to process video pulse data is to obtain the band
limited impulse response, temporal and spectral, of the target. To
accomplish this, it is necessary to obtain via theoretical calcu-
lations or experimental measurements the transfer functions of both
the antennas and the medium. To this end, procedures for estimating
the frequency-dependent constitutive parameters of a medium from
measured video pulse propagation data have been developed and
demonstrated. A state-of-the-art analysis and computer program for
arbitrary wire antennas in an infinite homogeneous medium has been
modified to approximately account for an air-medium interface. The
resultant subsurface fields appear to be in agreement with other
results but additional checks are needed. In the long run a more
exact formulation of the half-space problem will probably be needed.
At this stage however it was felt that time and funds were best
devoted to experimental tests of the system. The experimental procedure
for estimating the electrical properties of the medium appears to be
adequate for present purposes. From just 2 propagation measurements
electrical properties spanning the spectral range of interest are
obtained quickly. Undoubtedly more accurate parameters could be
obtained from single frequency measurements but in many applications,
including hazard detection in tunneling, it seems doubtful that the
necessary time would be available.

Specifically in terms of hazard detection in advance of rapid
tunneling in hard rock, the electromagnetic video pulse sounder appears
ideally suited to the task. Responses from certain of the geological
features such as faults, voids and contrasts which would constitute
hazards in tunneling have been obtained in a soft rock medium at
significant depths. Anticipating reductions in medium conductivity
for hard rock by multiplicative factors from 0.1 to 0.01, the sounder,
in its present form, may well approach the stated goal of a 200 foot range.
The size of the antennas which would be mounted flush to the tunnel
working face is easily changed and only a few inches of clearance from
the drilling machine are needed. As presently envisioned, the antennas
would be mounted on the drilling machine and extended forward against
the working face as the machine is withdrawn slightly. Measurements
would be made in the orthogonal mode and in the direct mode on both of
the orthogonally oriented dipoles. In addition, at least 2 different
pulse generators would be used - one with a very fast rise time to
provide a diagnostic capability for close in targets and one with
slower rise time to interrogate further ahead of the working face.
One should also note that pulse generators with significantly greater
power are commercially available. An advantage of electromagnetic
systems is that the coupling of the antenna to the medium is un-
effected by the input power level. With the video pulse system, the

128

only components susceptible to power levels are the baluns which convert an unbalanced line (coaxial cable) to a balanced line (transmission line). Broadband baluns with much greater power handling capacity than those presently used are within the-state-of-the-art.

In summary, an electromagnetic video pulse sounding system has been developed. In its present form, the system is a laboratory instrument, i.e., components are not field hardened. Nevertheless, the system can and has been used in the field to detect geological features which would represent hazards in a tunneling operation. The results in this report fully justify a testing program for the system in an actual hard rock tunnel environment. As a not unexpected side benefit, the electromagnetic video pulse sounding system has appli-cability to a wide variety of other subsurface sensing problems, many of which are directly associated with the expanding national needs of this country. It is strongly recommended that research to refine and test the system be continued.

APPENDIX A
DEEP EARTH PROBING IN LOW LOSS MEDIA

In order to achieve greater depths of penetration, a more directive, higher power radar system is necessary. The video-type pulses presently in use contain energy spanning very wide spectral ranges. It is difficult, therefore, to concentrate power in any given direction to achieve significant depths of penetration.

A pair of S-band horn antennas matched to a soft rock medium (limestone) by dielectric loading were used to couple energy to and from the medium. The dielectric used to load the horns was a fine dry sand with a relative dielectric constant of about 5. Although the mismatch at the rock interface was not completely eliminated, it was significantly reduced by the dielectric loading. A block diagram of the system is shown in Fig. A-1. The microwave source is pulse modulated by a PIN diode to an 80 nsec pulse, and amplified (30 dB power gain) by a TWT amplifier. The received signal is detected using the sampling oscilloscope as a receiver but since the microwave supply is not synchronized with the trigger signal, the recorded waveform looks like a burst of noise. Figure A-2 shows recordings of the input pulse for one oscilloscope sweep only, and for an average of 30 sweeps. Averaging in this case not only reduces the noise level of entire waveform, but also tends to reduce the magnitude of the signal. To prevent signal loss by the averaging process, a simple diode detector was constructed to detect the envelope of the received pulse. The third waveform in Fig. A-2 shows an example of an average of 30 sweeps on the envelope detected pulse.

Calculations of attenuation and depth penetration as functions of frequency and the constitutive parameters of realistic media were made to estimate the performance of the system. Figures A-3 and A-4 show the effect of conductivity, relative dielectric constant and frequency on the attenuation and depth penetration of a time-harmonic field in a homogeneous medium. The depth penetration was calculated assuming that a 5 mV signal could be detected with a 50 Volt signal as the input voltage level, or a total gain of 80 dB. The two way path is accounted for and a reflection coefficient magnitude of unity is assumed. Note from Fig. A-3 that, as the medium approaches a perfect dielectric, the penetration depth increases without limit. For realistic values of conductivity less than .002 mho/m, depths of up to 40 meters can be probed at 2 GHz. Obviously, as the relative dielectric constant is increased, the depth of penetration increases, and the attenuation decreases. Figure A-4 illustrates the effect of frequency on the attenuation and depth of penetration. As the frequency is lowered, the depth penetration increases and attenuation decreases substantially, however, at lower
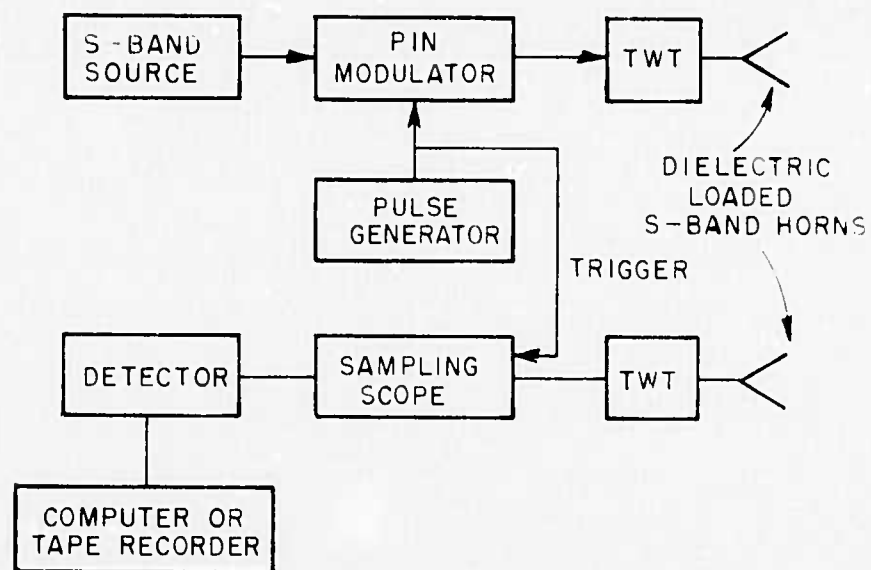
Fig. A-1. Block diagram of radar-type probe system.
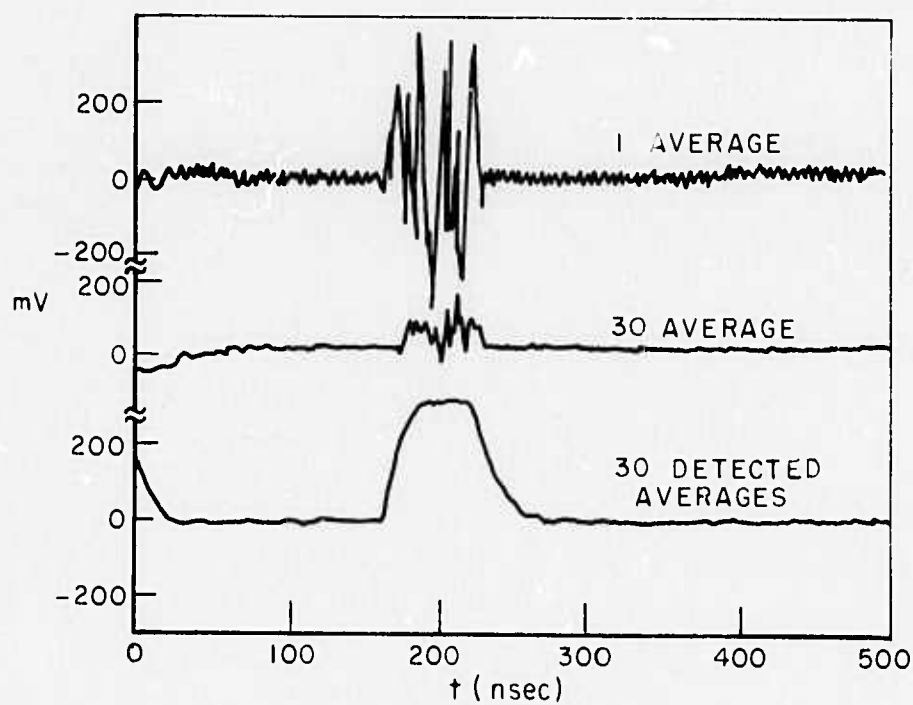
Fig. A-2. Probe modulated S-band signal.

131
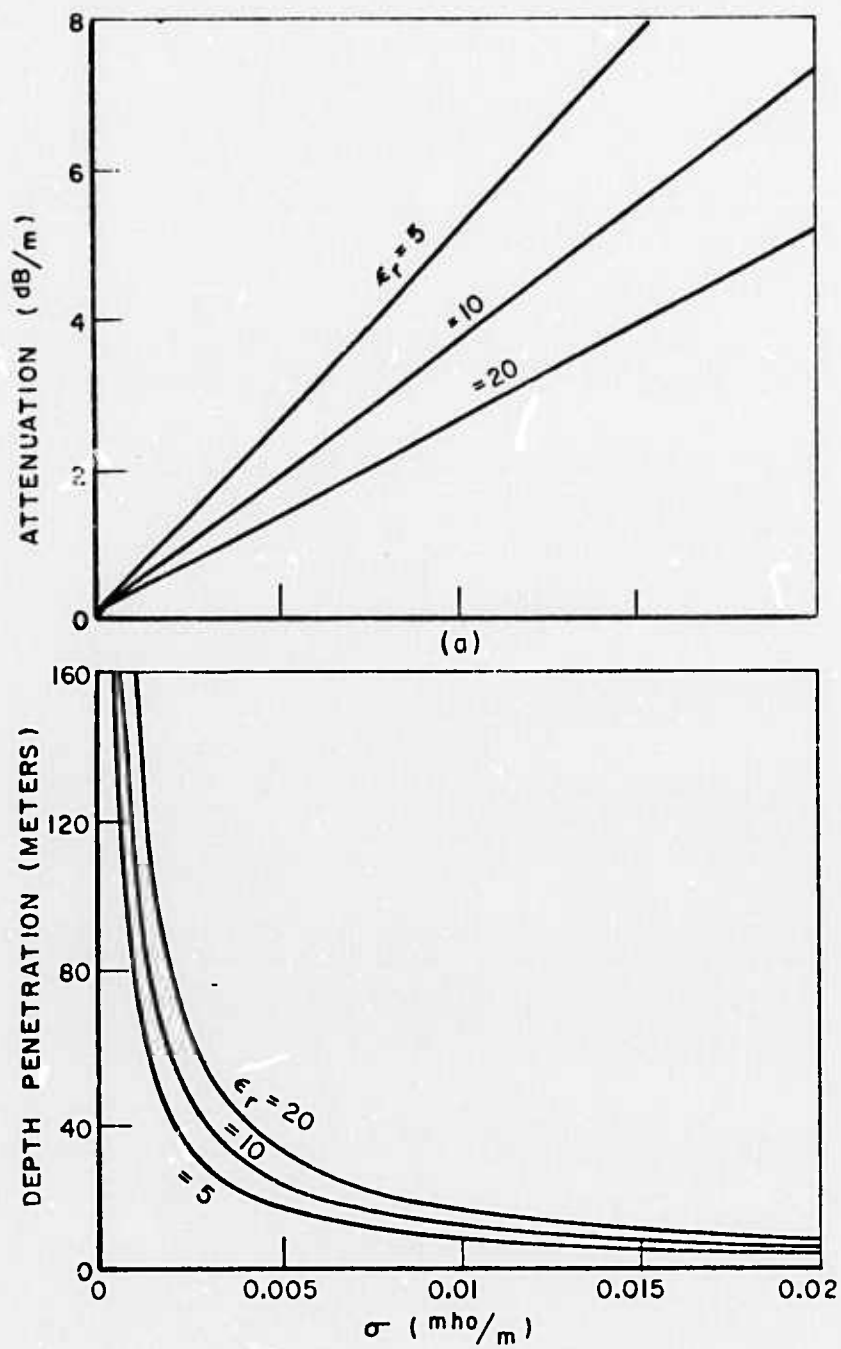
Fig. A-3. Attenuation and depth penetration
versus conductivity.
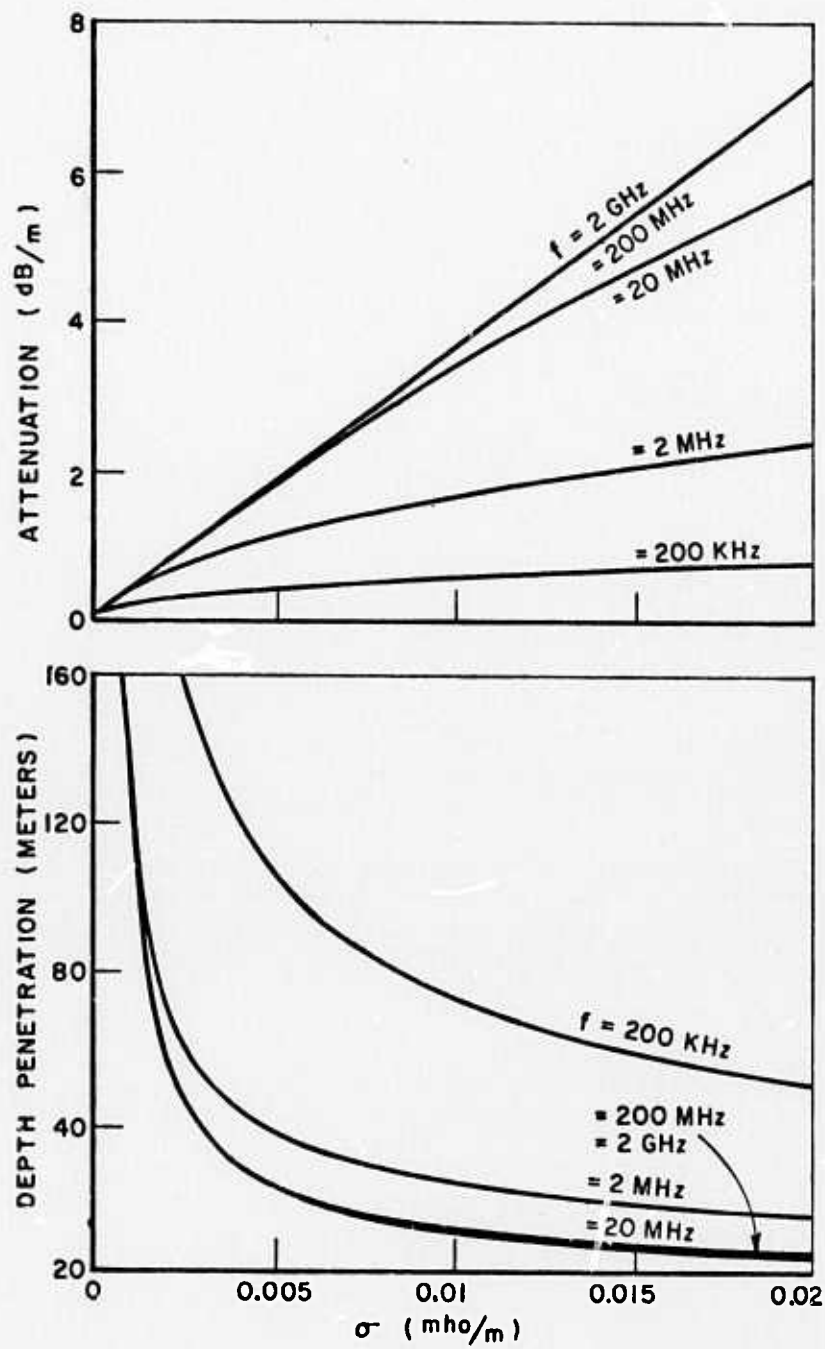
Fig. A-4.   Attenuation and depth penetration
versus conductivity.

133

frequencies, it becomes difficult to obtain a directive, yet compact and portable system. For very low loss media, (σ .002 mho/m) such as igneous type hard rock, the present system operating at 2 GHz appears to be capable of acheiving significant depth penetration.

Experimental testing of the system in the limestone quarry was unsuccessful. Measurements through a small slab of rock showed that the attenuation of the limestone at 2 GHz was roughly 6 dB/ft. Figure A-5 shows the recorded waveforms. Referring to Figs. A-3 and A-4 and extrapolating, this value of attenuation corresponds to a conductivity of roughly .05 mho/m, and a depth penetration of less than 10 feet.
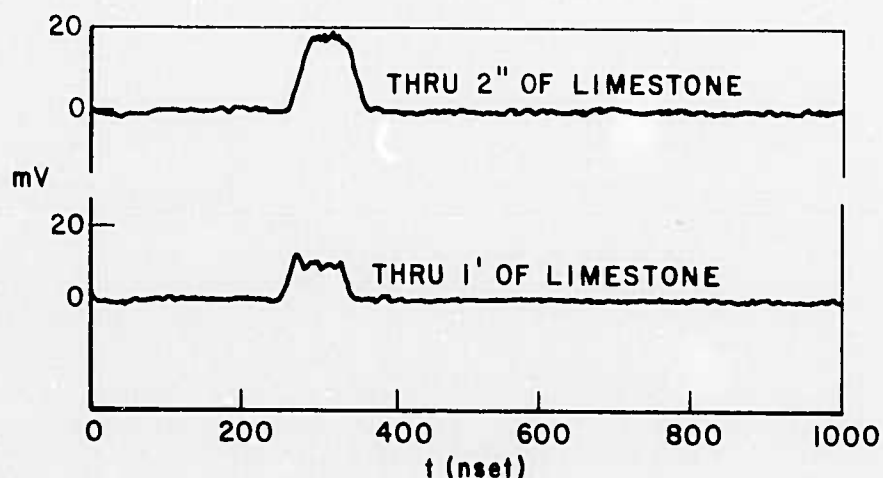
Fig. A-5. Pulse modulated signal through limestone.

134

APPENDIX B
PHASE SPECTRA

As noted in the text, phase spectra of video pulse soundings are not as yet sufficiently well referenced to warrant analysis. To satisfy a contractual obligation, phase spectra corresponding to amplitude spectra given in the text are included in this appendix. The figure numbers in the appendix are the same as those for the amplitude spectra in the text, e.g., Fig. 3b of this appendix is the phase spectrum for the amplitude spectrum shown in Fig. 3b of the text.
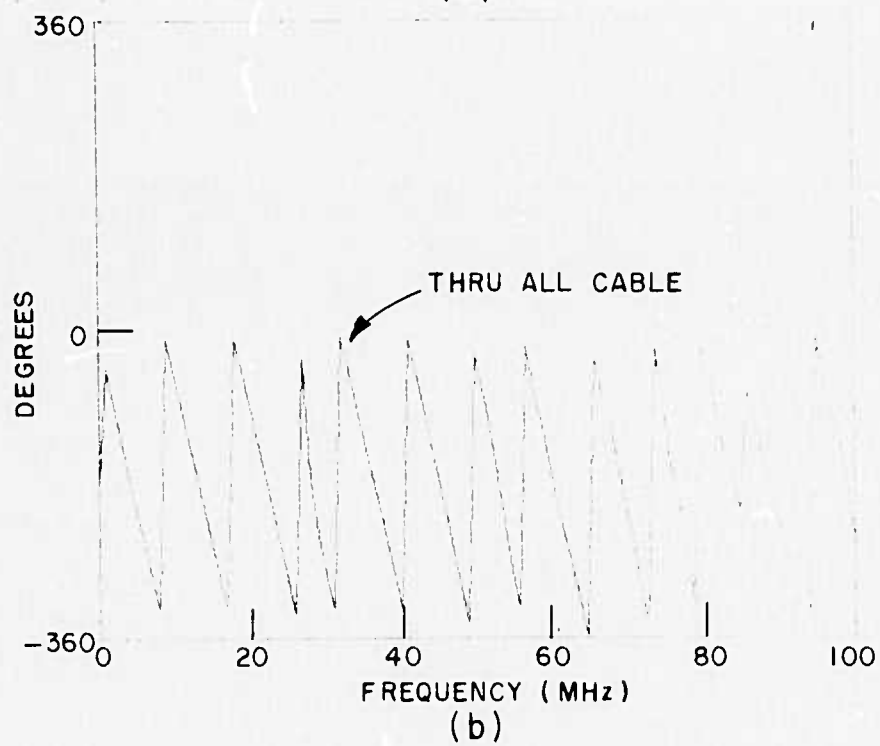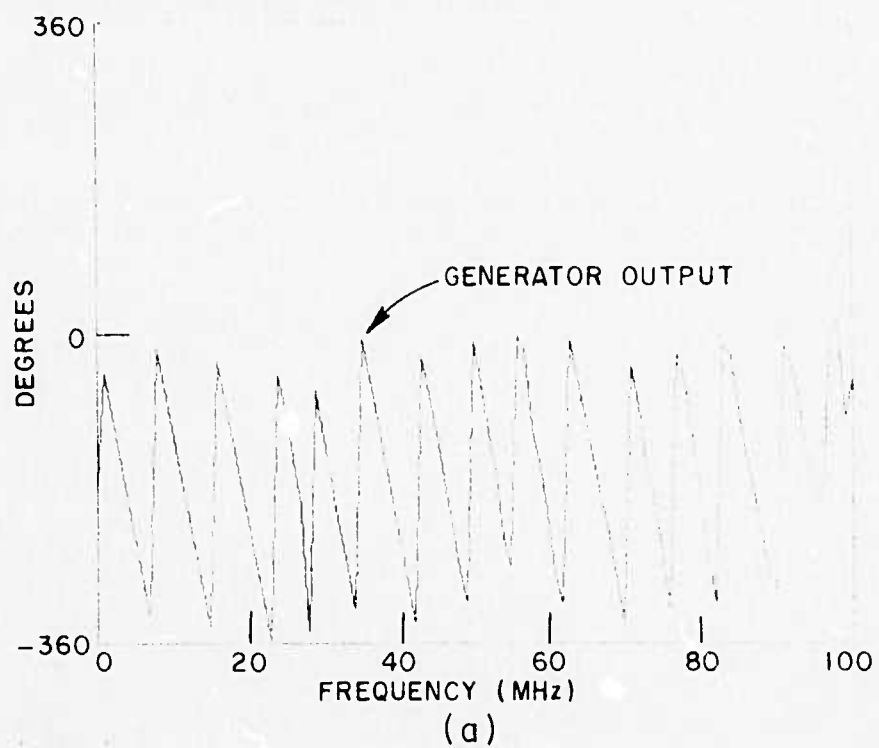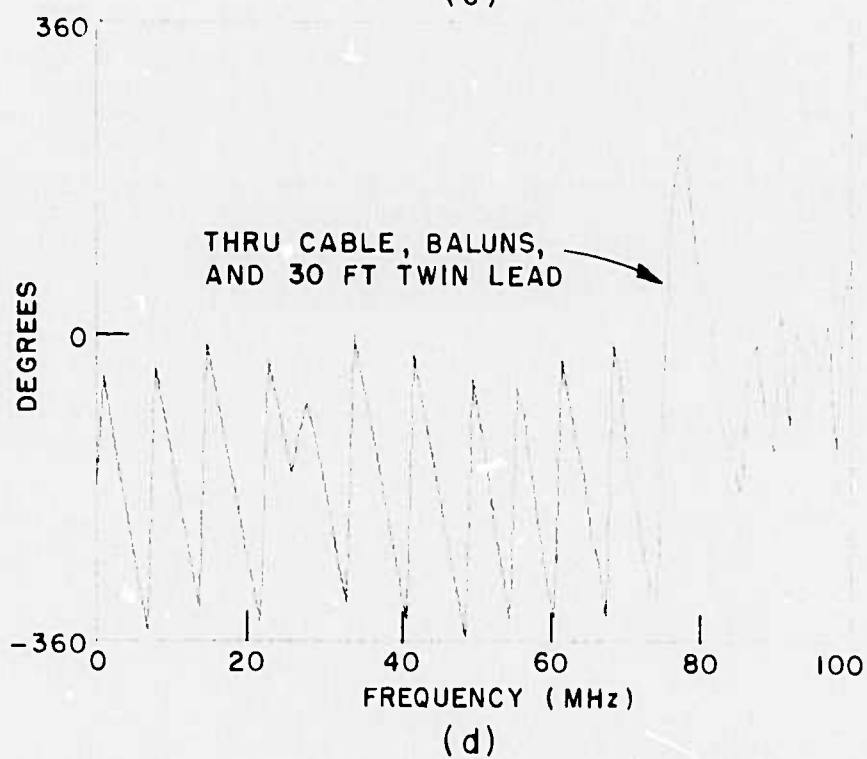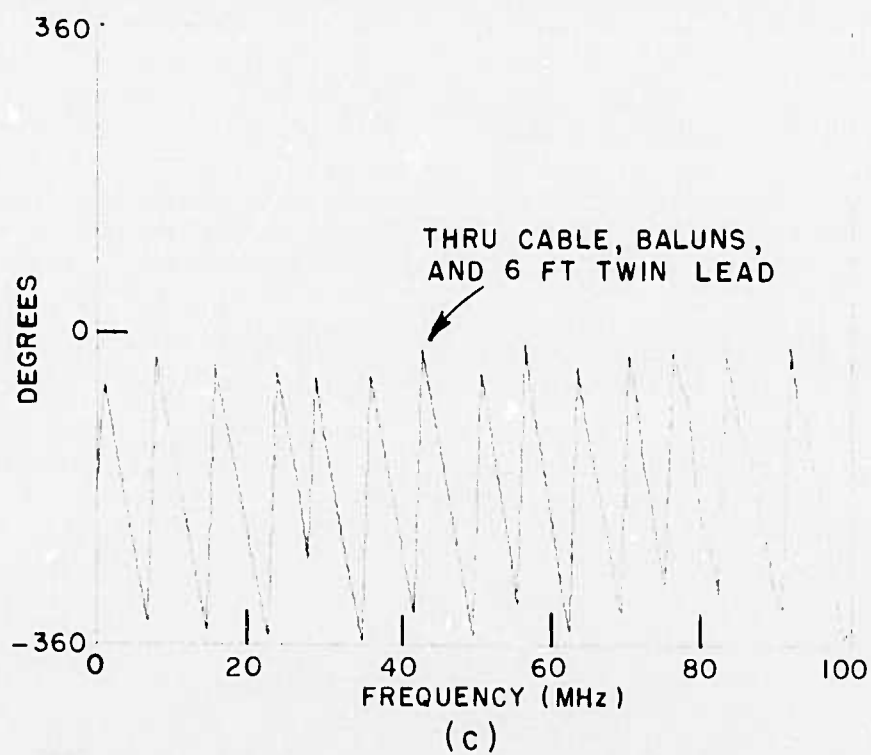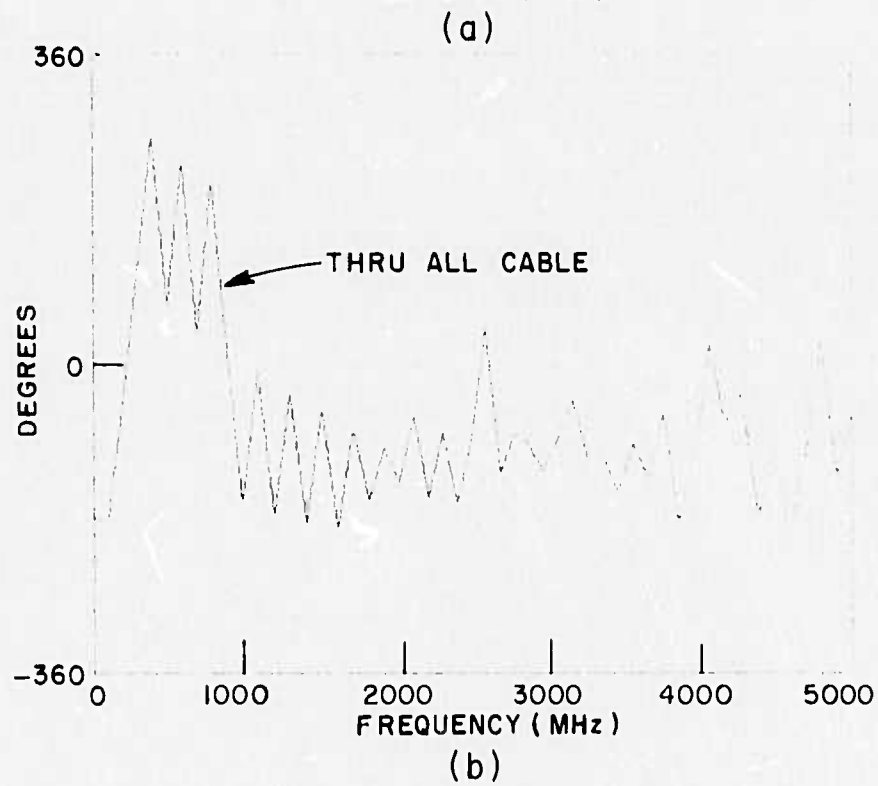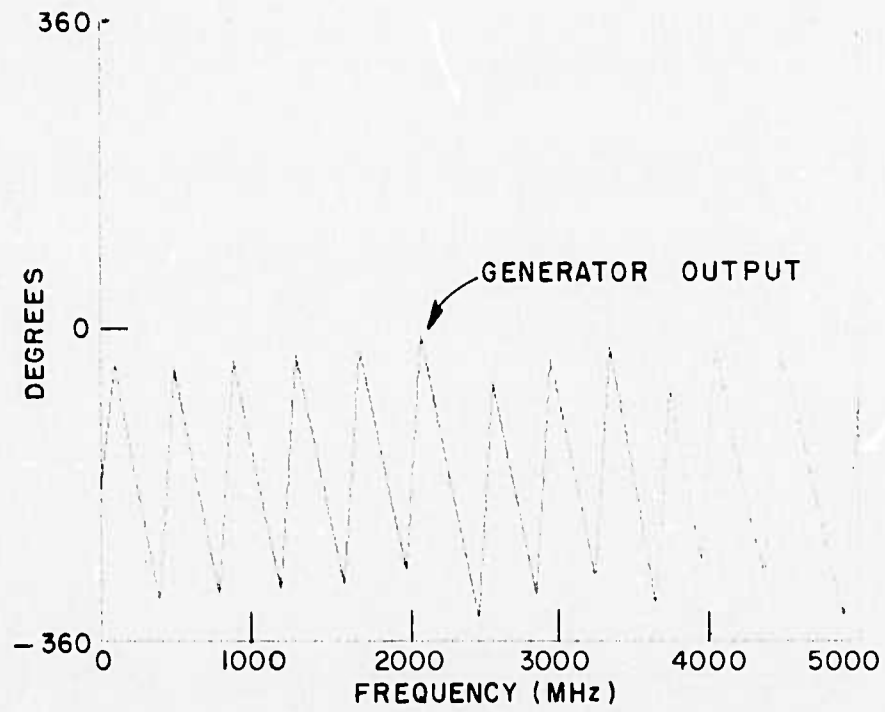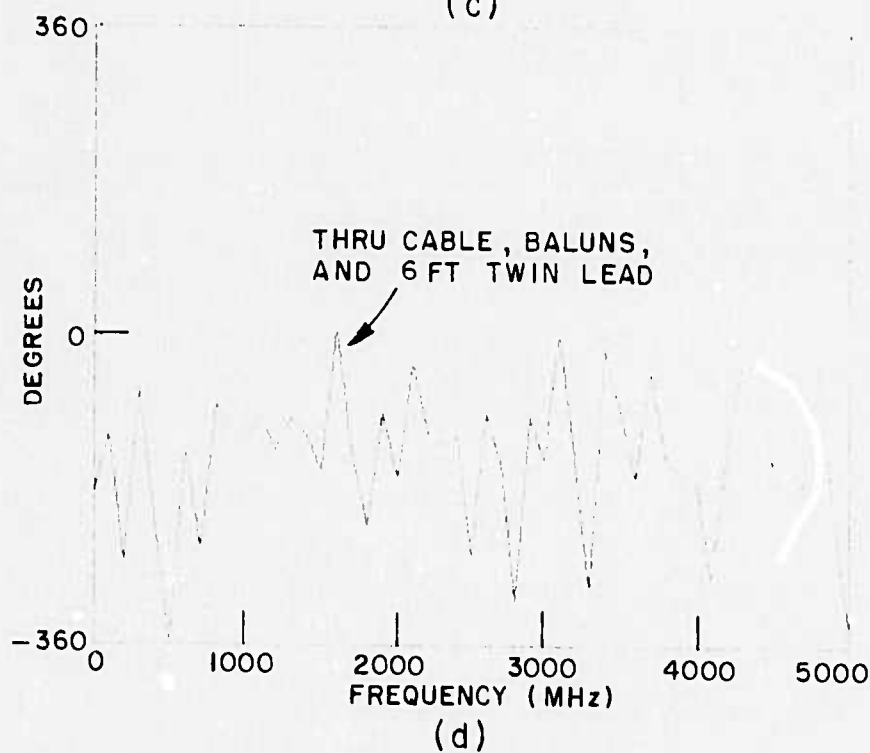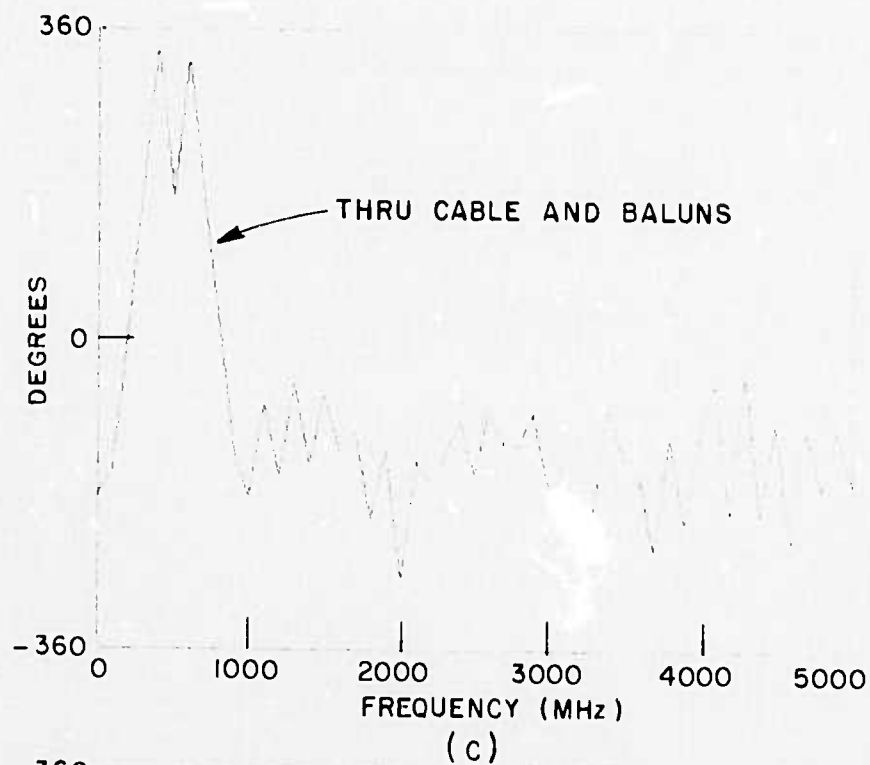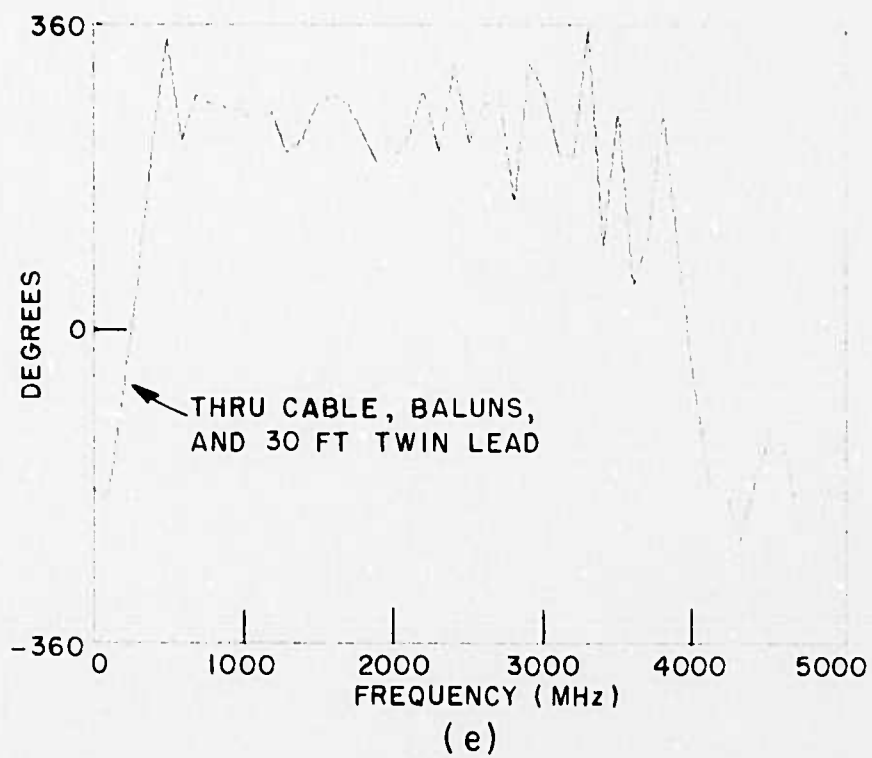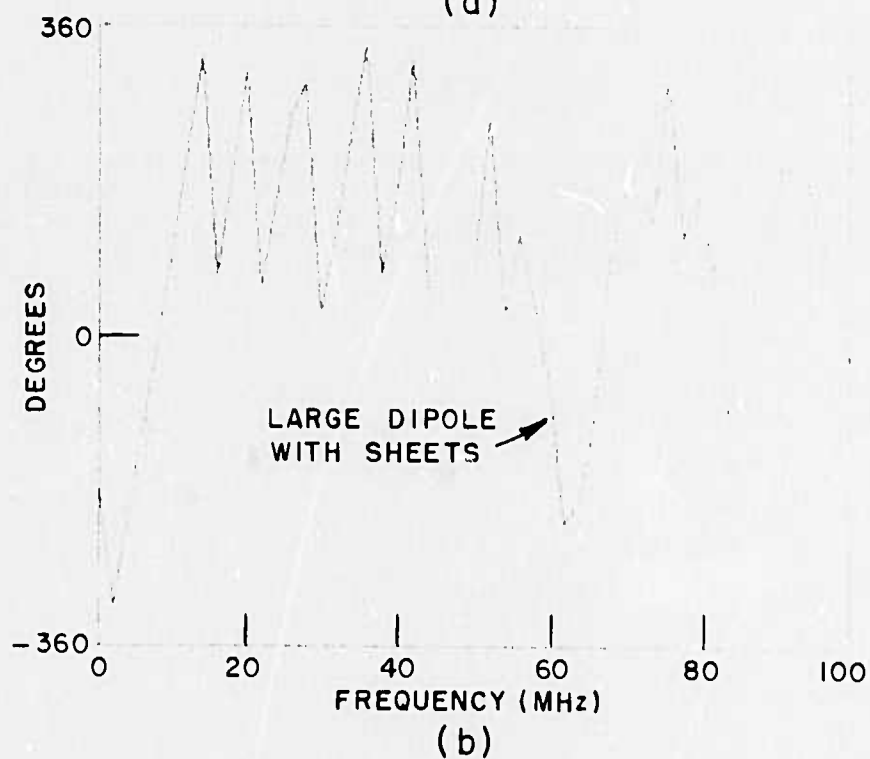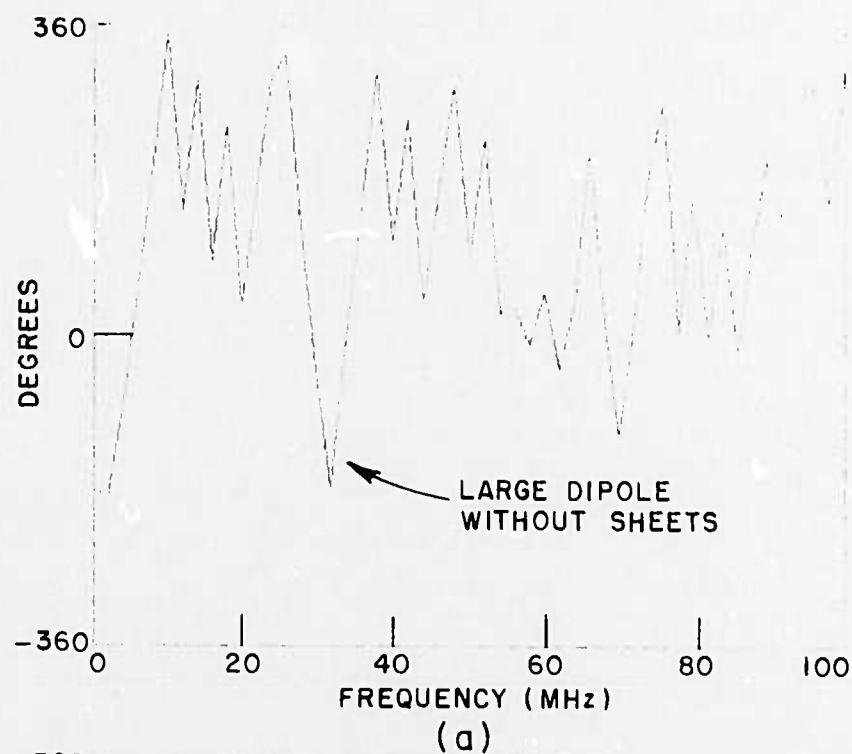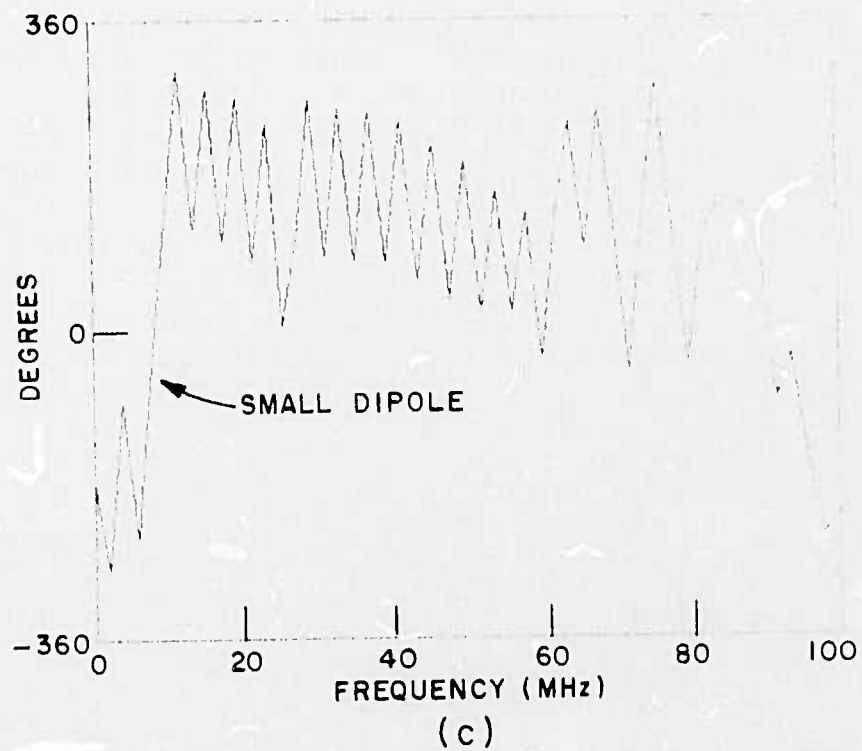
135

Fig. 3b.

136

Fig. 3b. (Continued)

137

Fig. 4b.

138

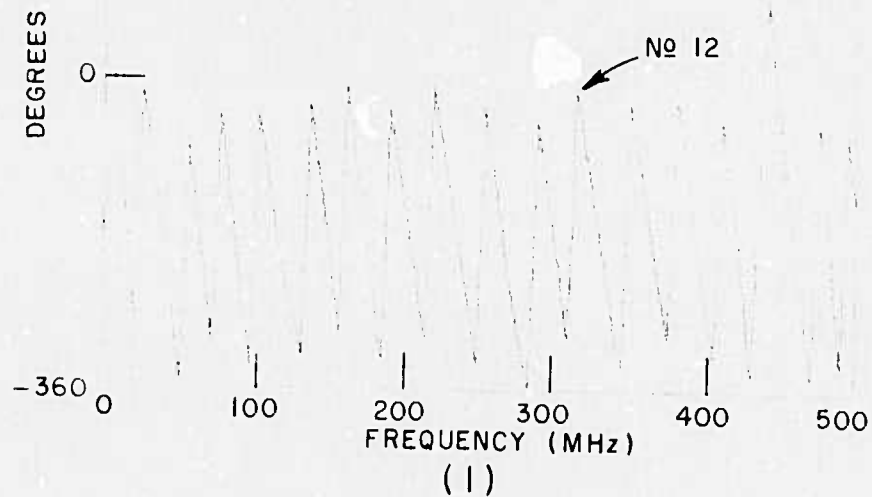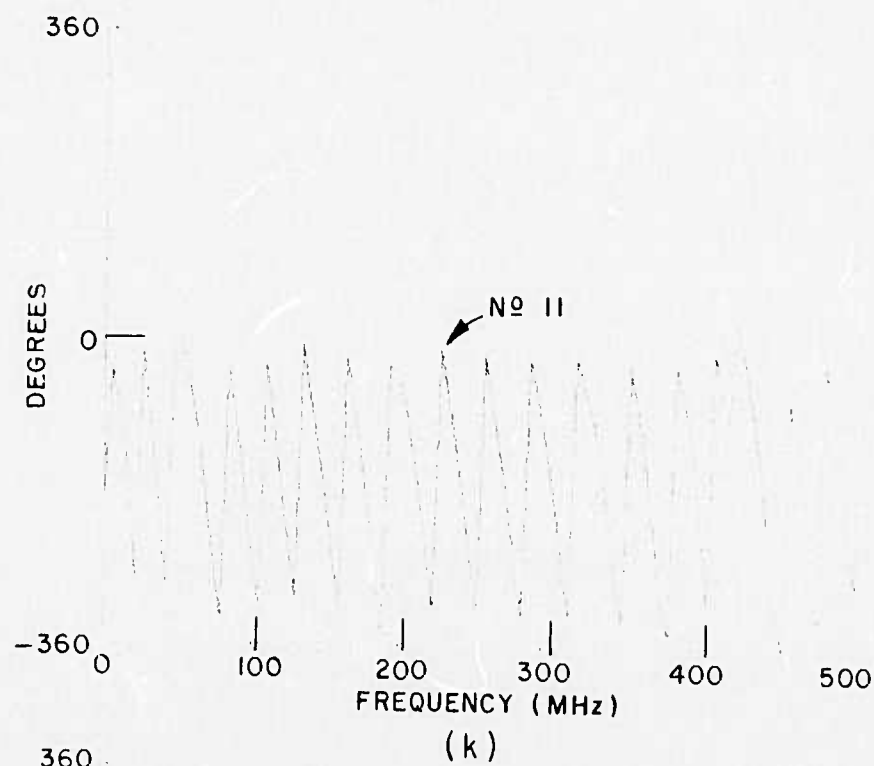THRU CABLE AND BALUNS

(c)

THRU CABLE, BALUNS,
AND 6 FT TWIN LEAD

(d)

Fig. 4b. (Continued)

139

Fig. 4b. (Continued)

140

Fig. 12b.

141

Fig. 12b. (Continued)

142

Fig. 13b.

143

Fig. 13b. (Continued)

144

Fig. 30b.

145

Fig. 31b.

146

Fig. 43b.

Fig. 44b.

147

Fig. 46b.

Fig. 47b.

148

Fig. 60b.

149

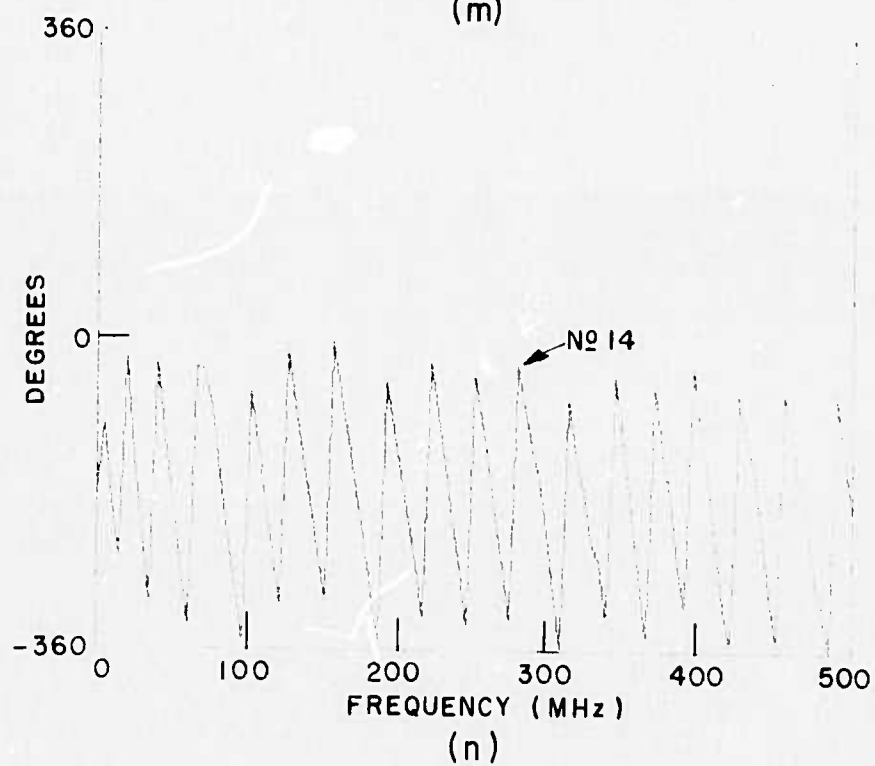Fig. 61b.

Fig. 64b.
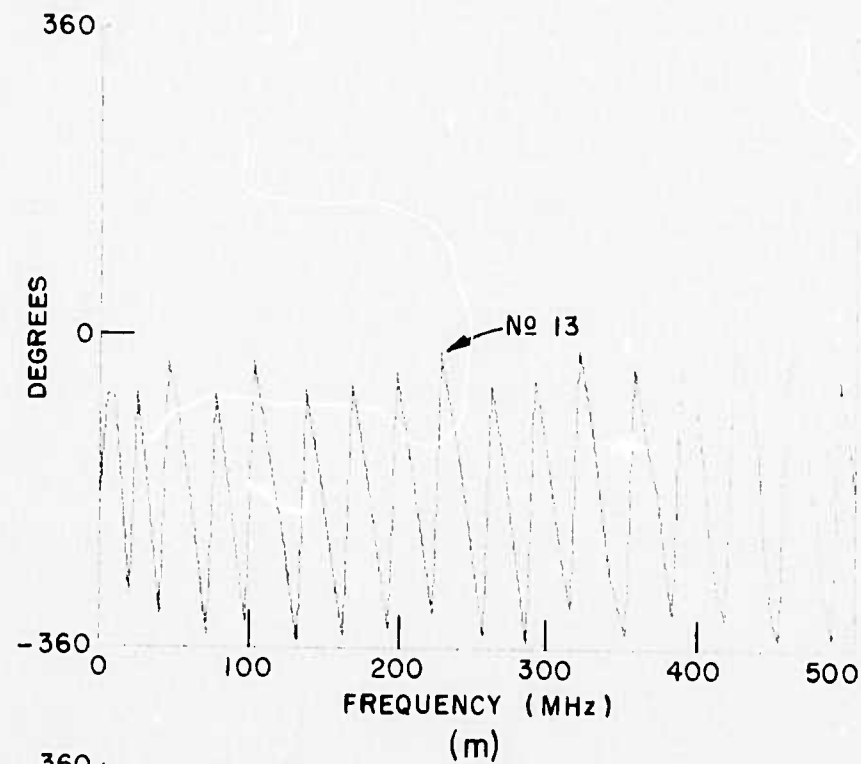
151

Fig. 64b. (Continued)

152

Fig. 67a.

153
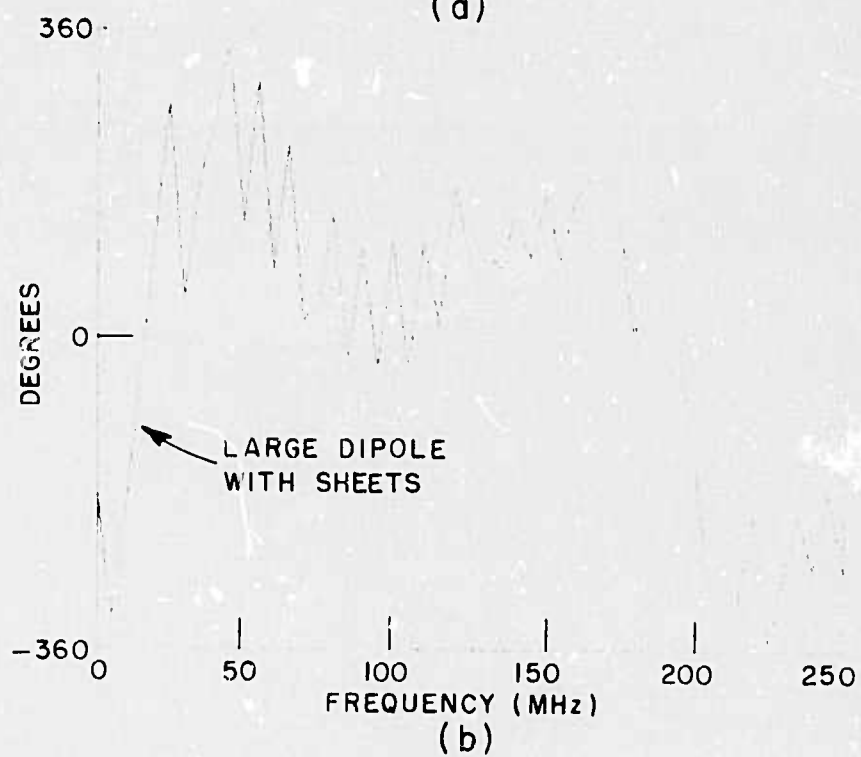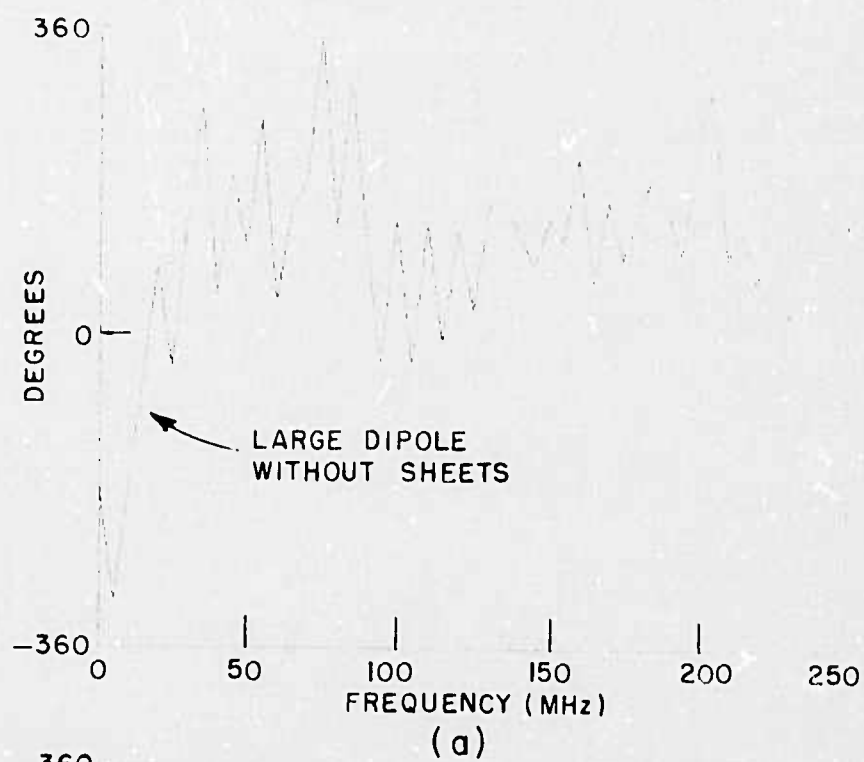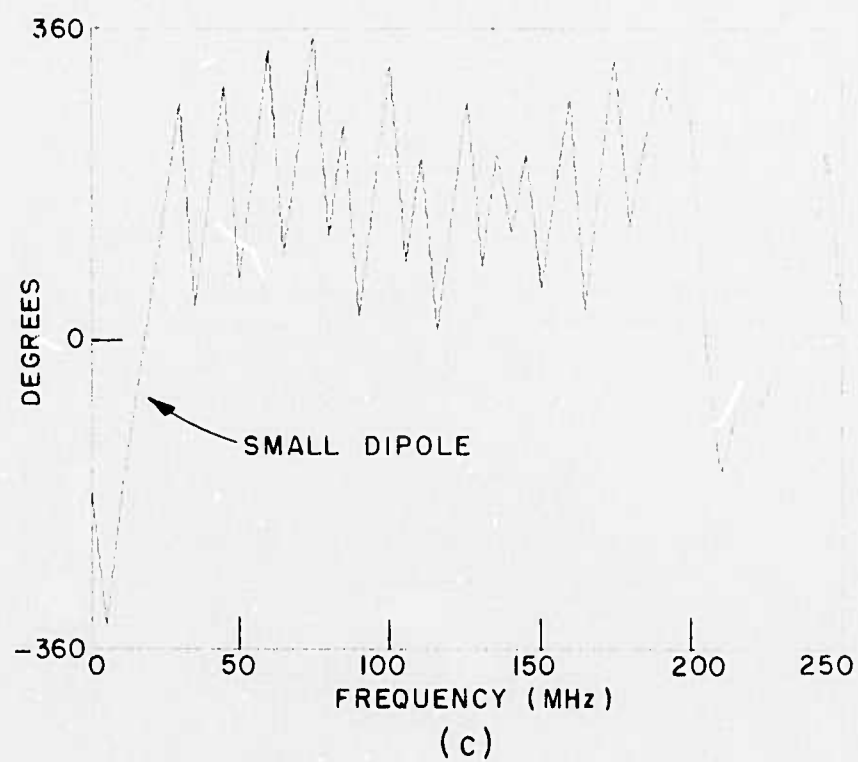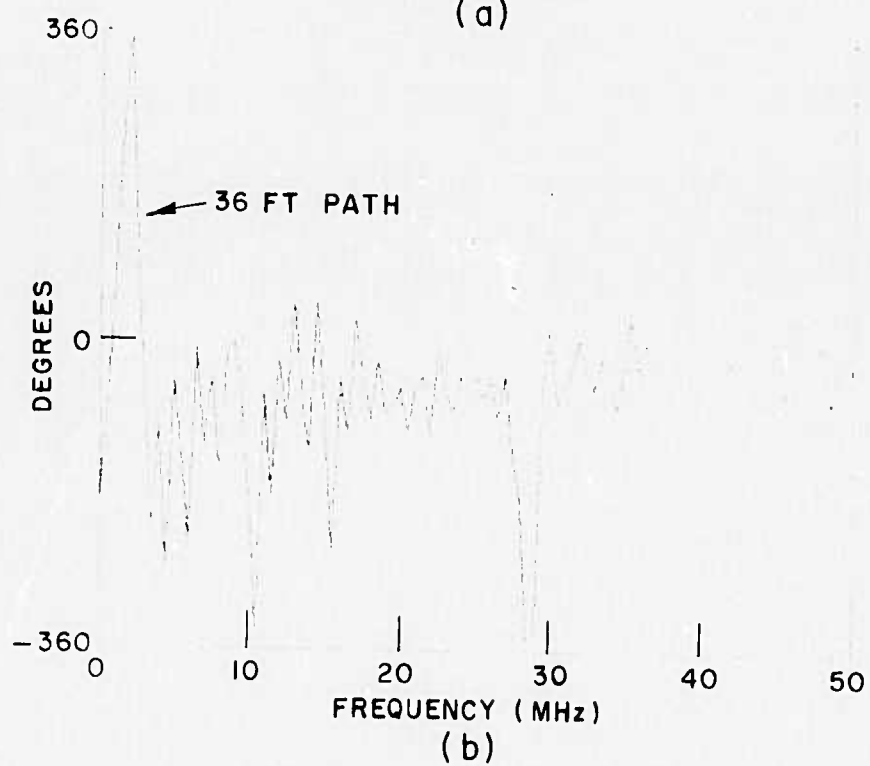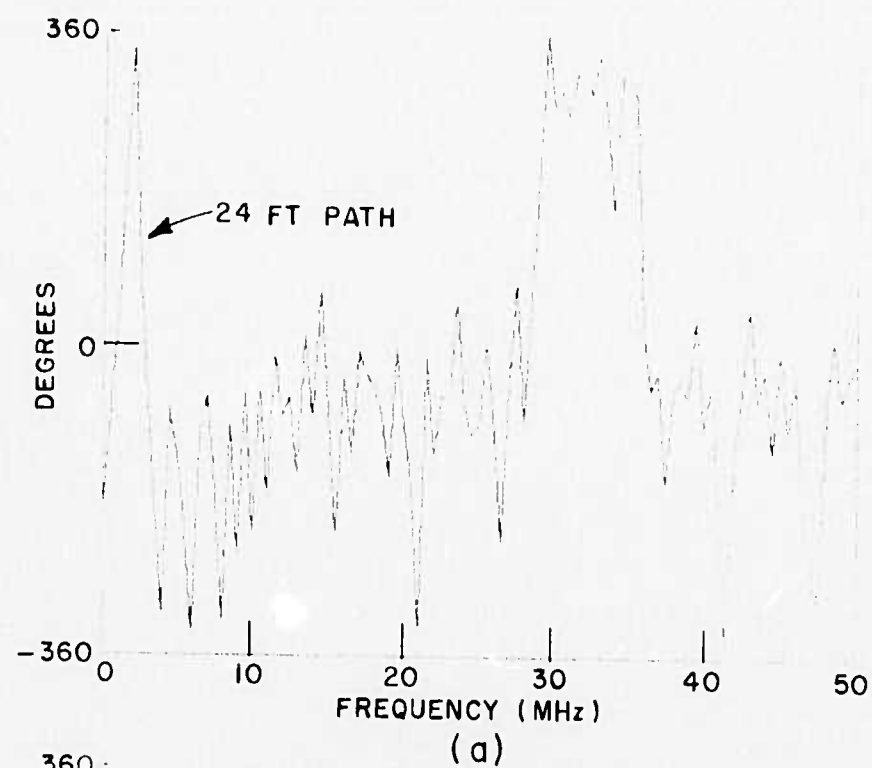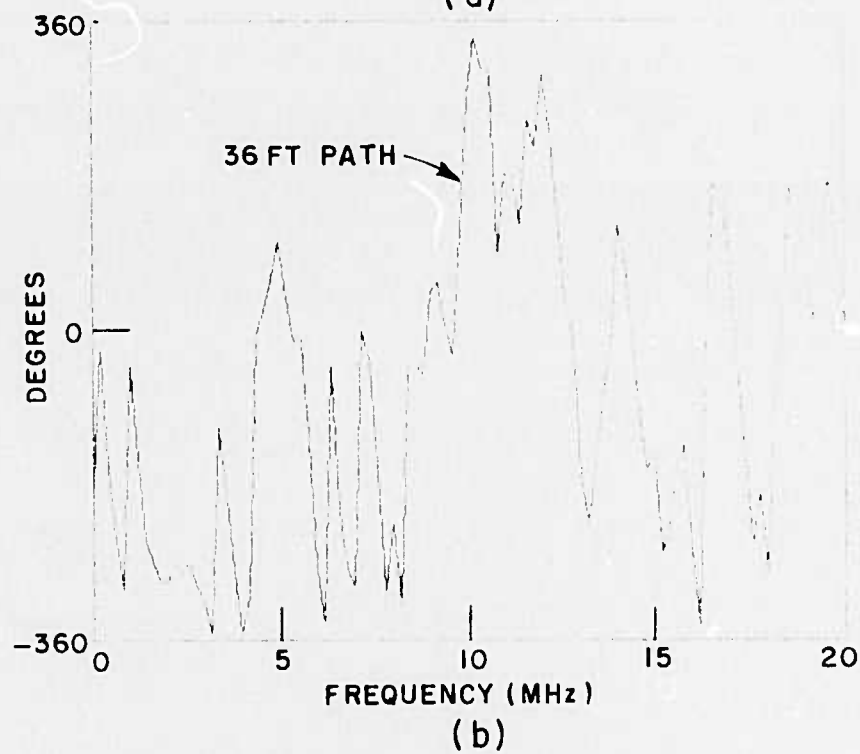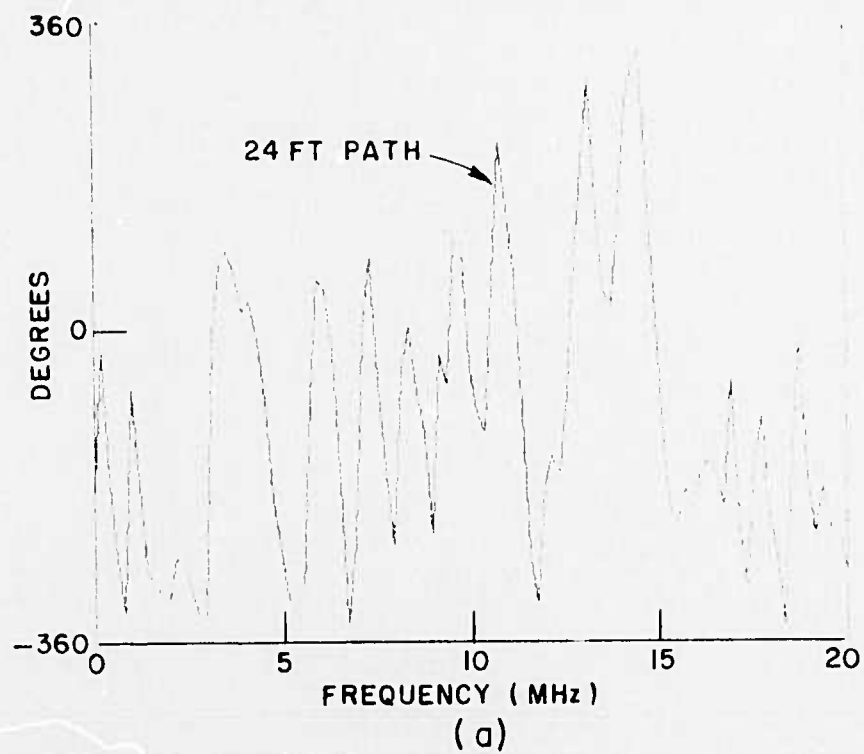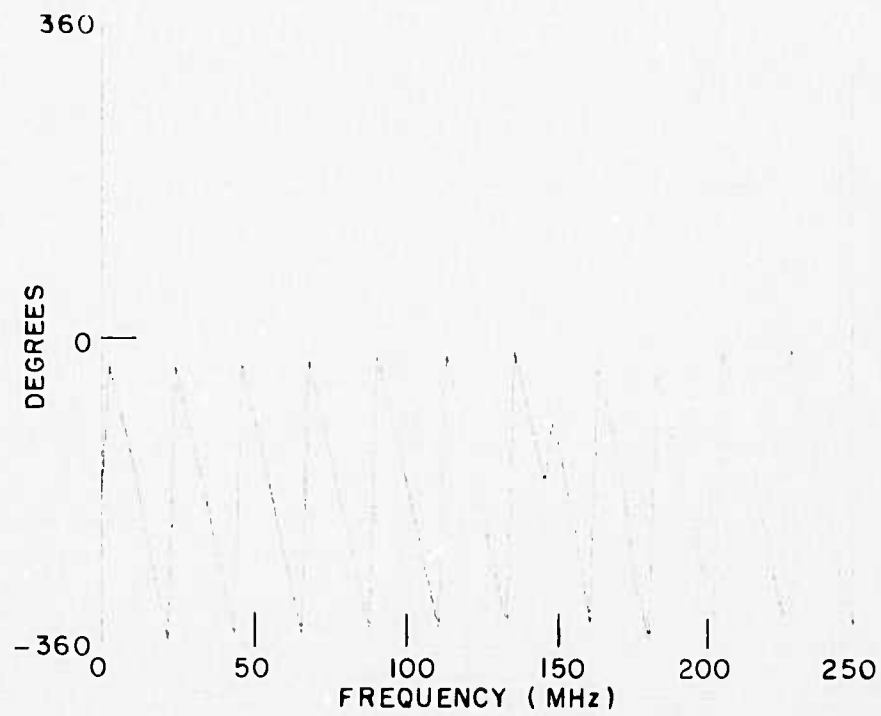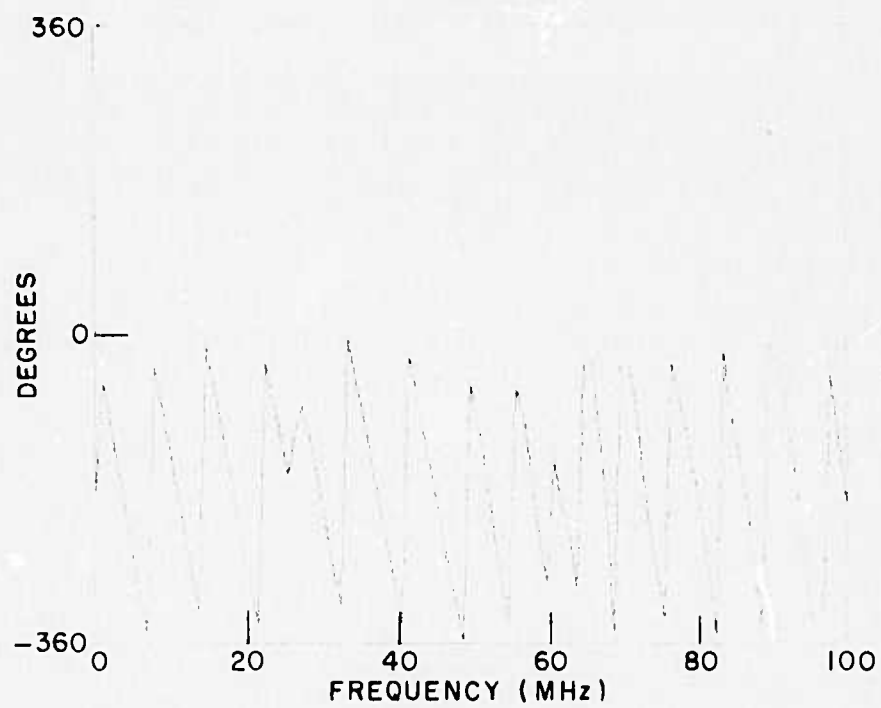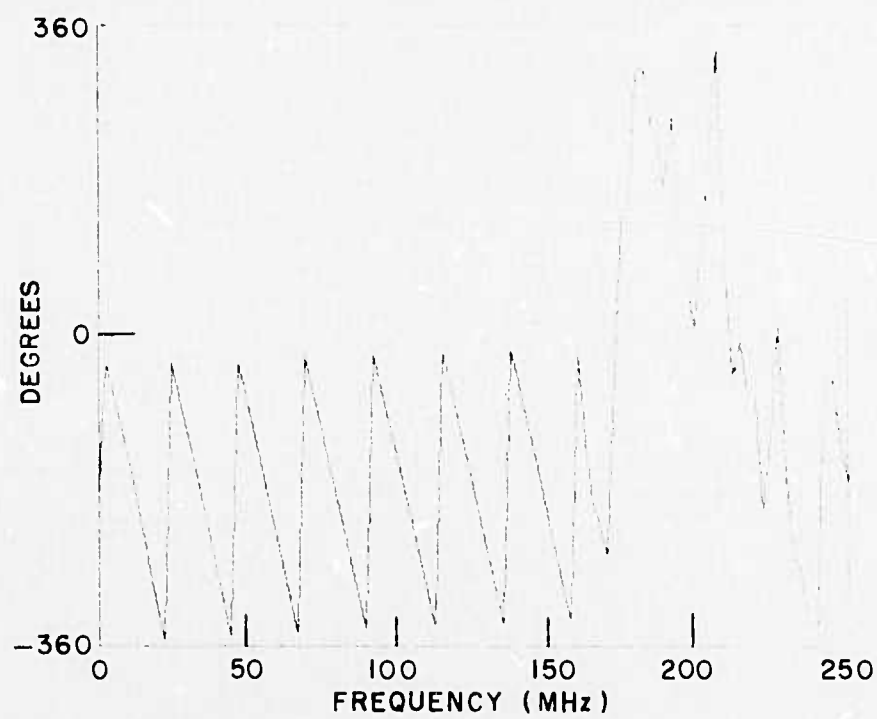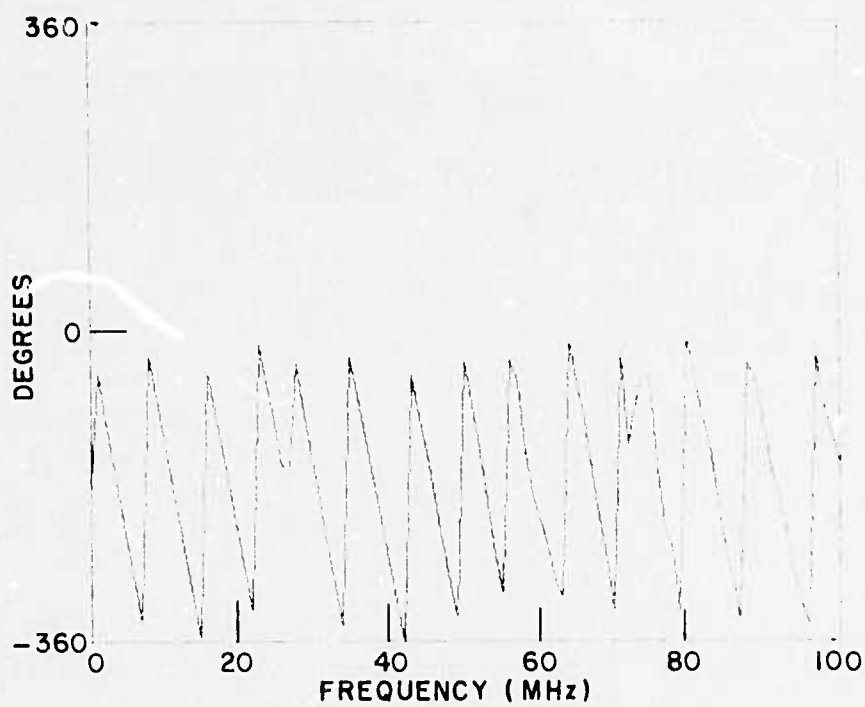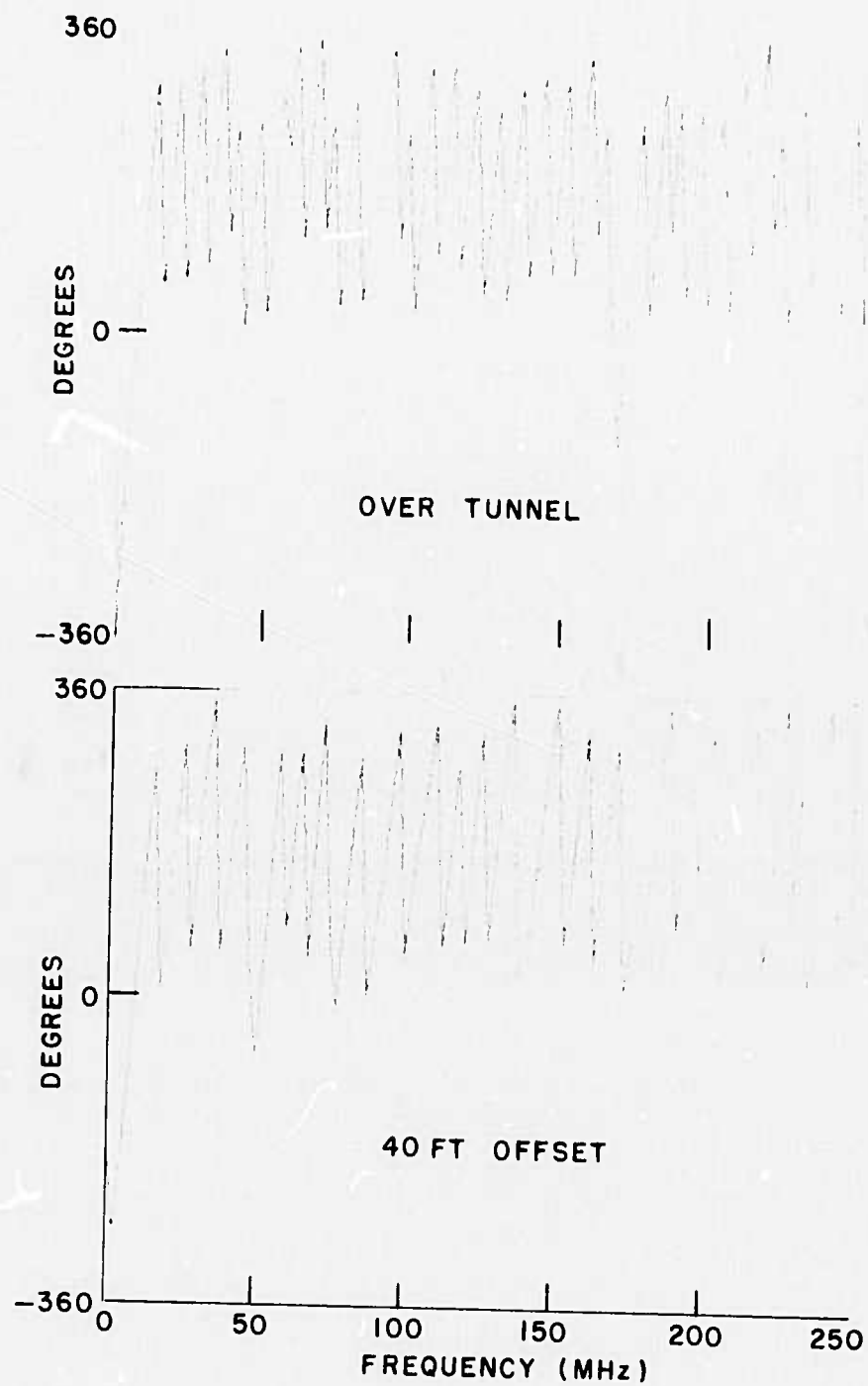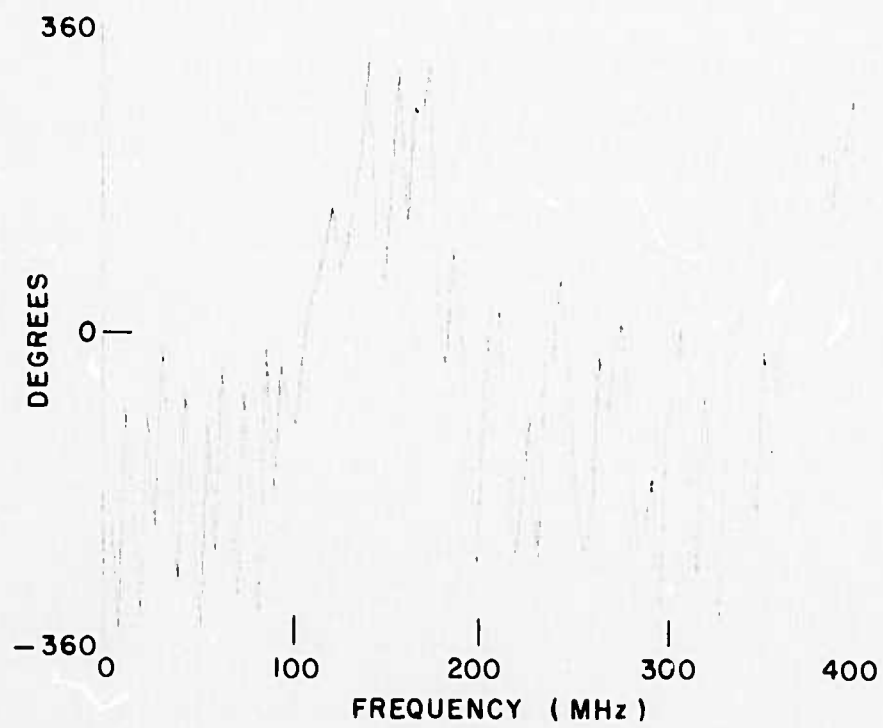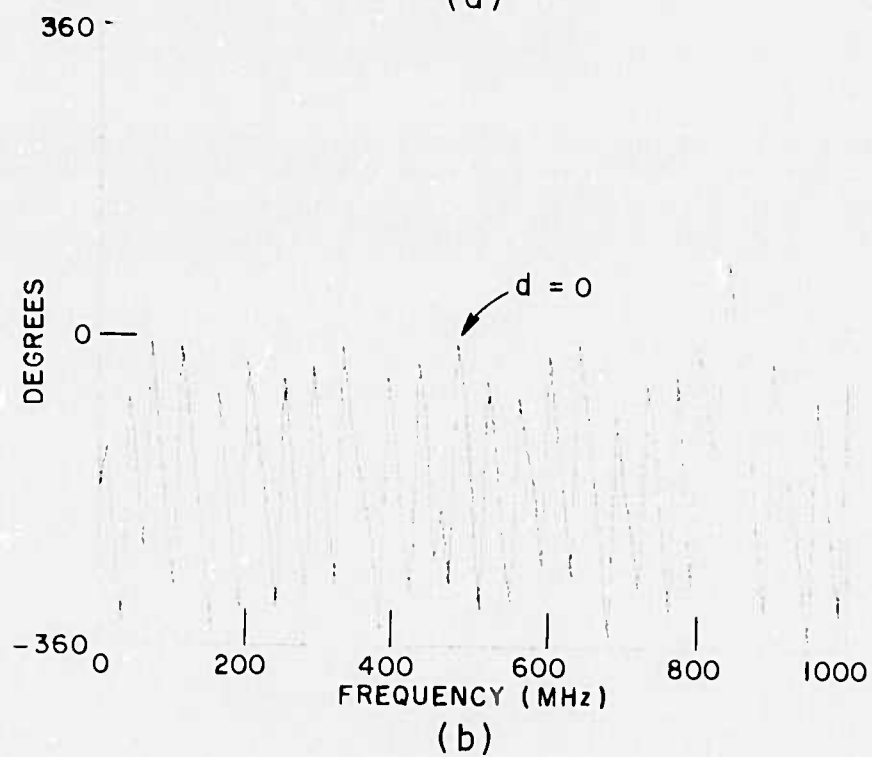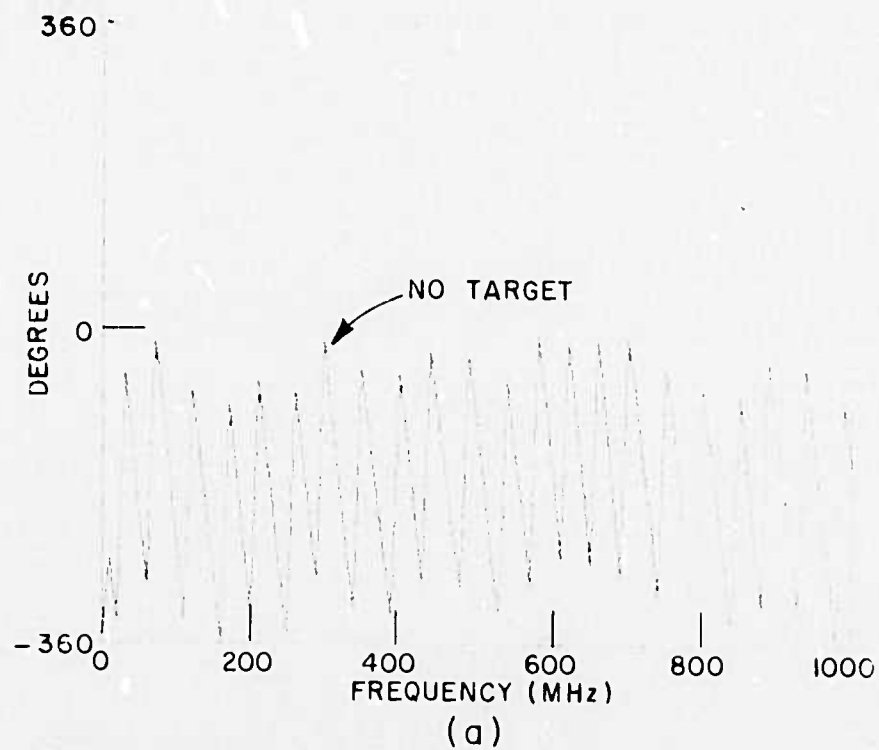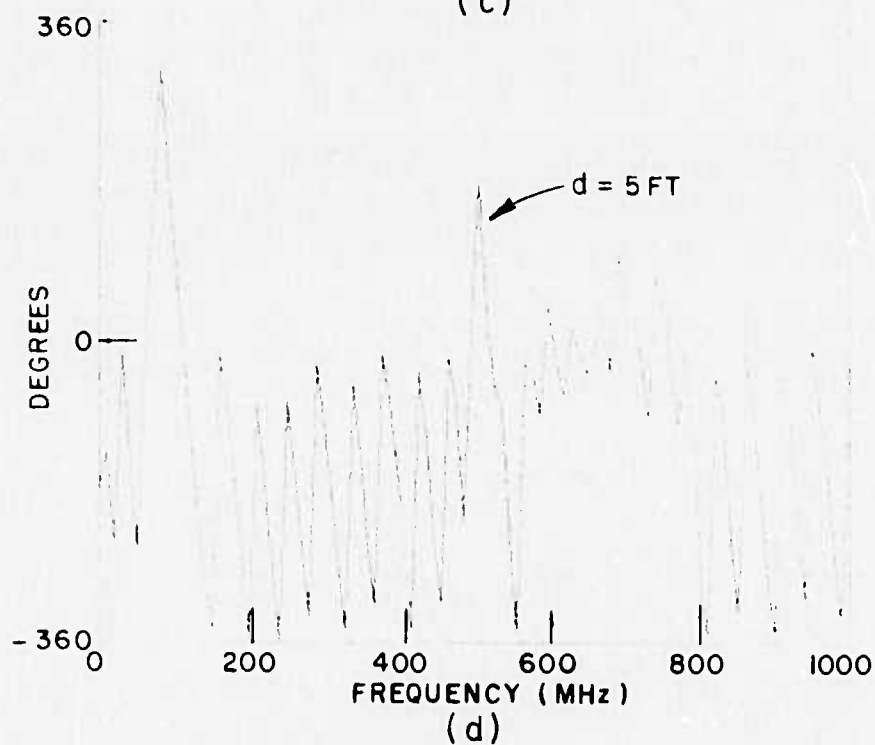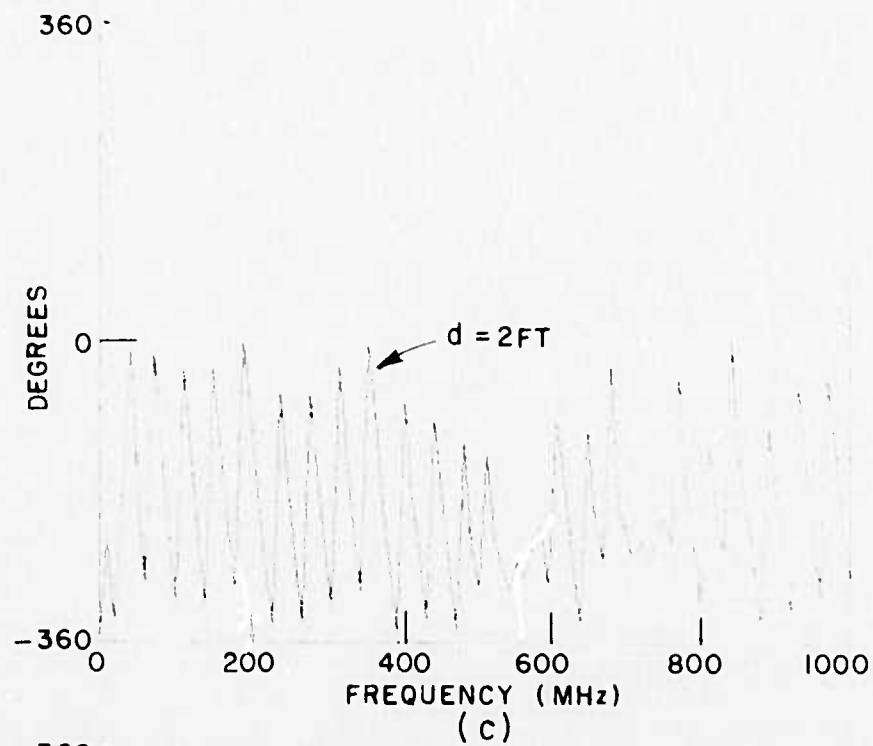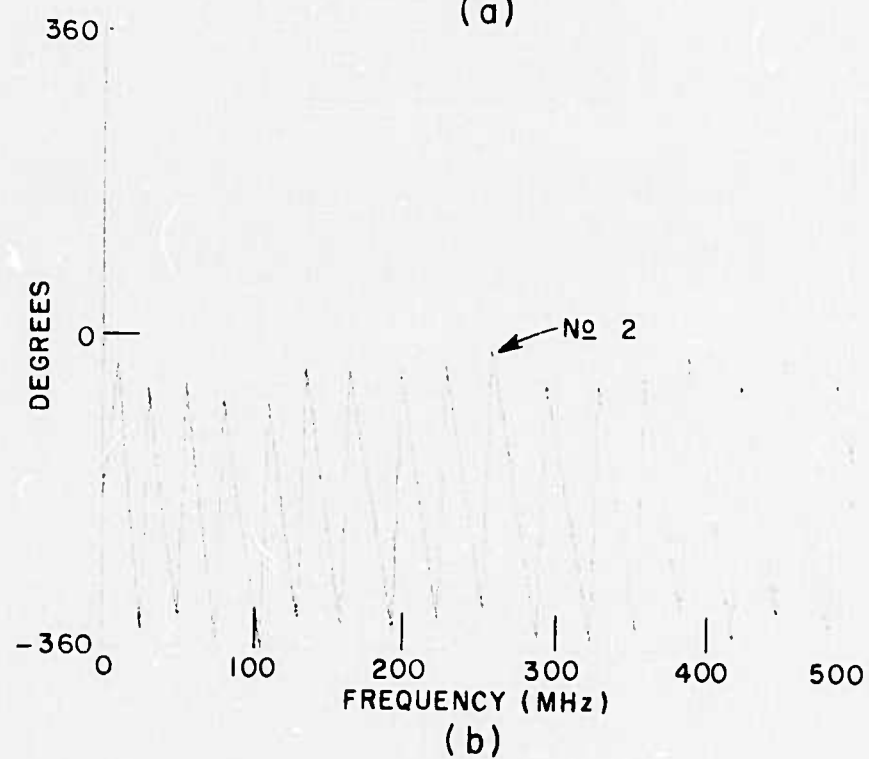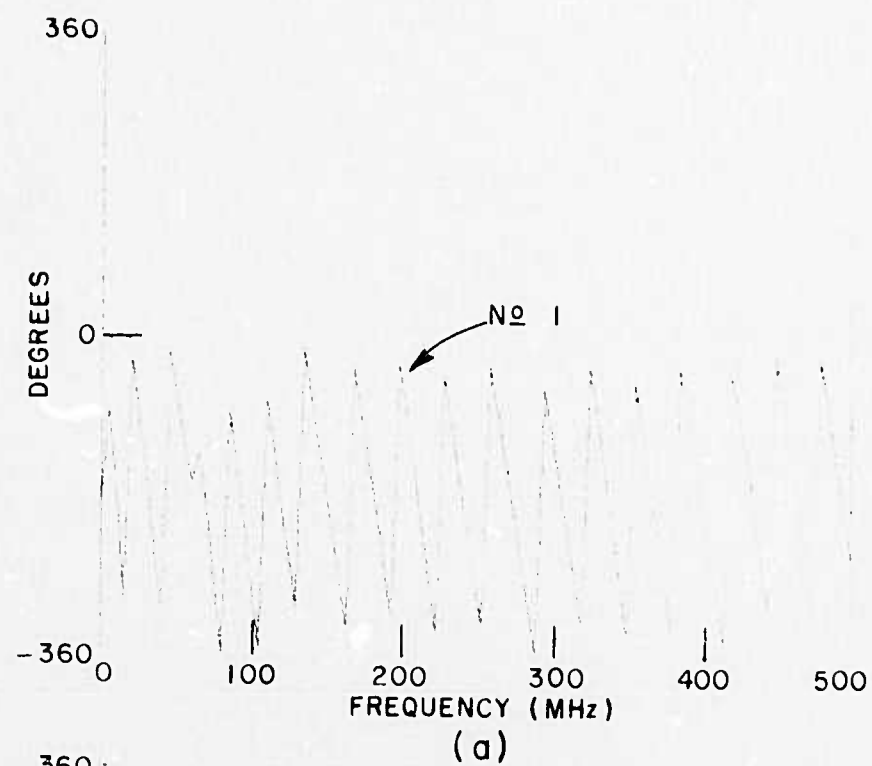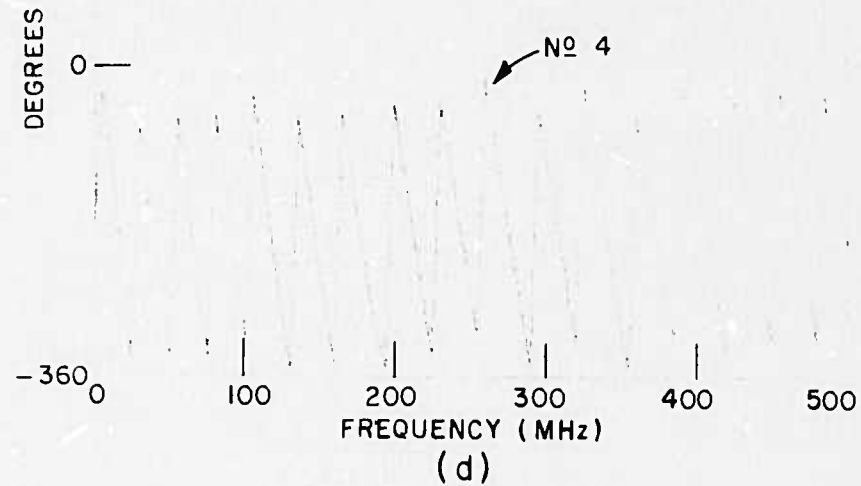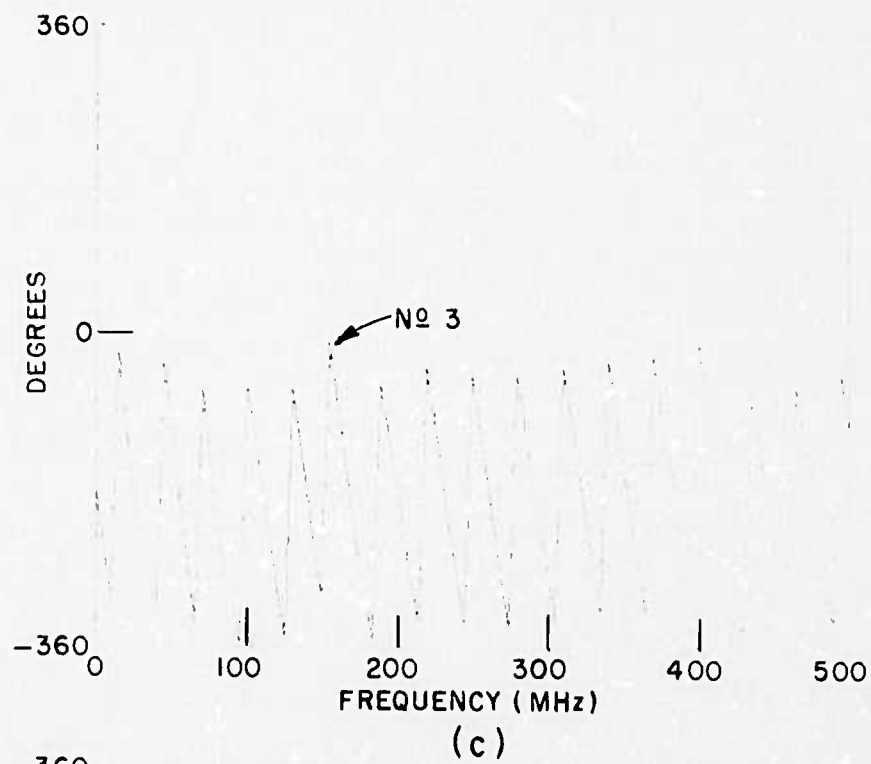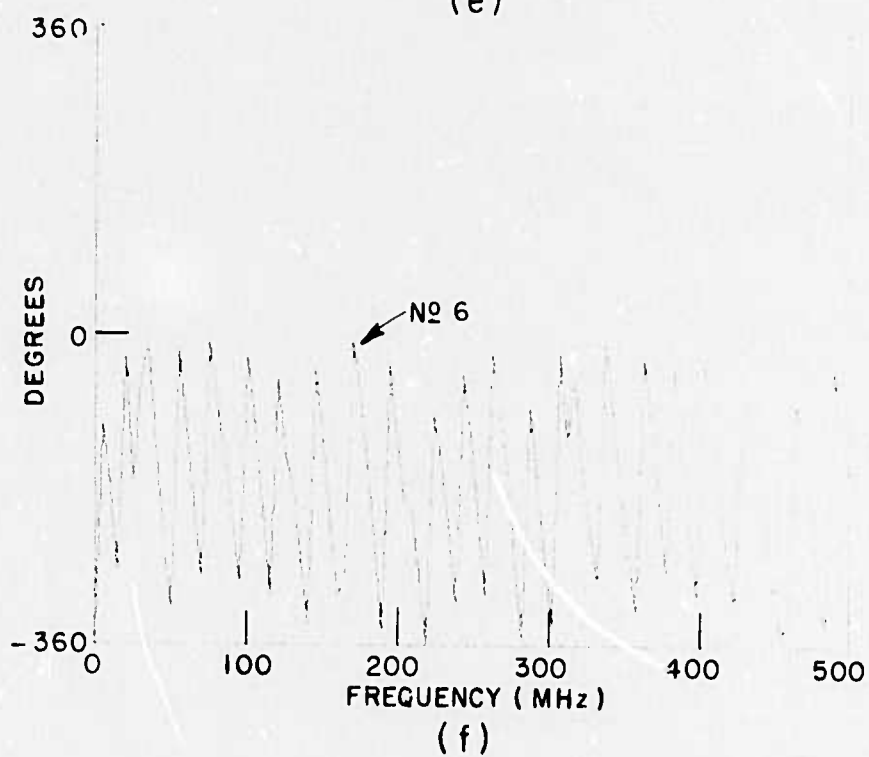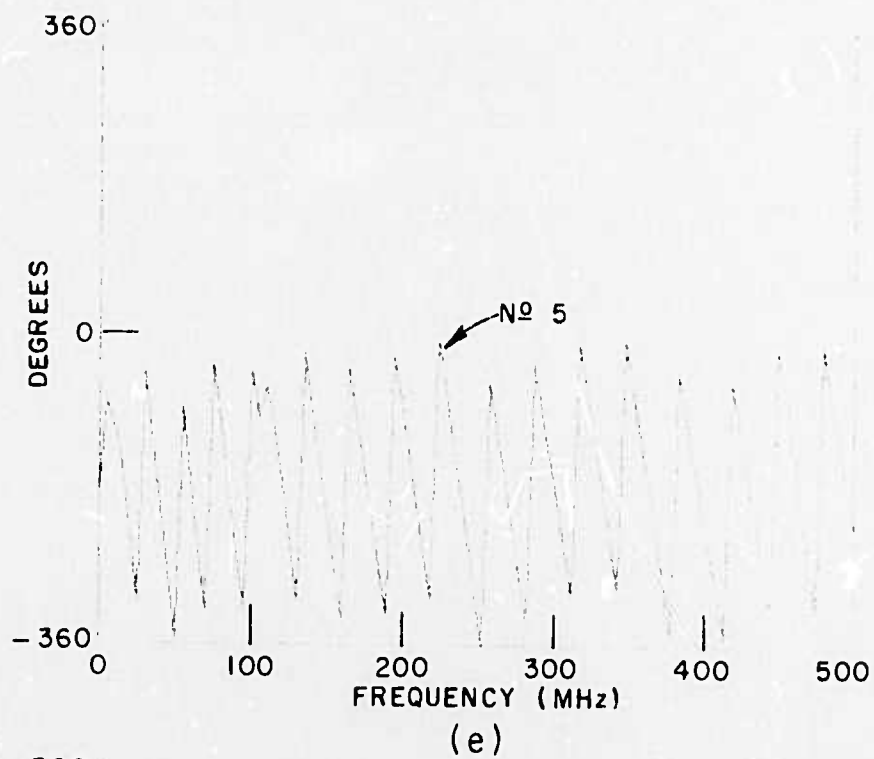
Fig. 67a. (Continued)

Fig. 67a. (Continued)

155

Fig. 67a. (Continued)

156

Fig. 67b.

157

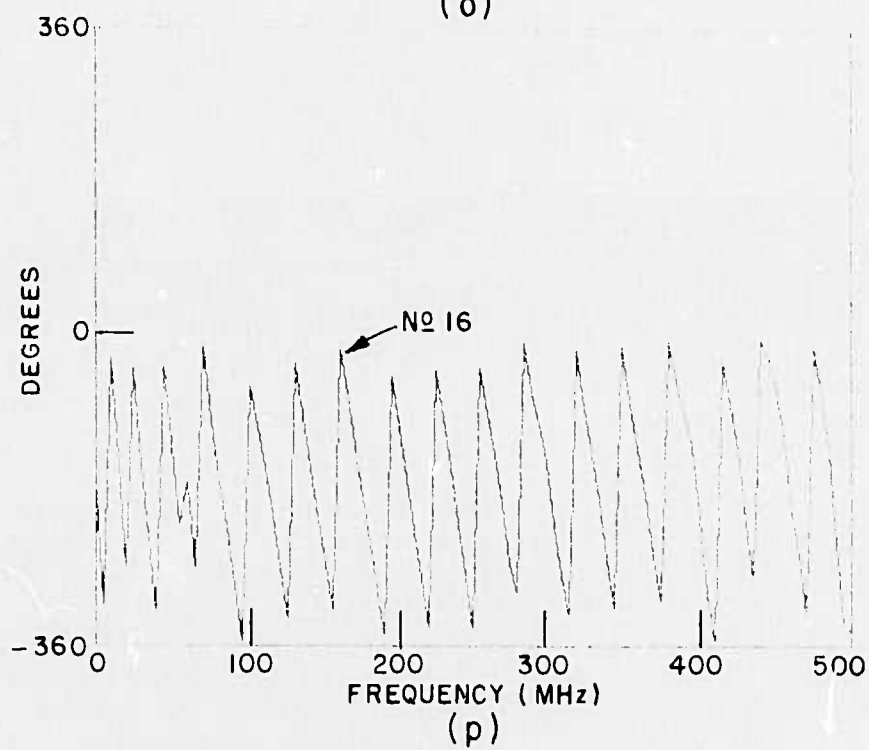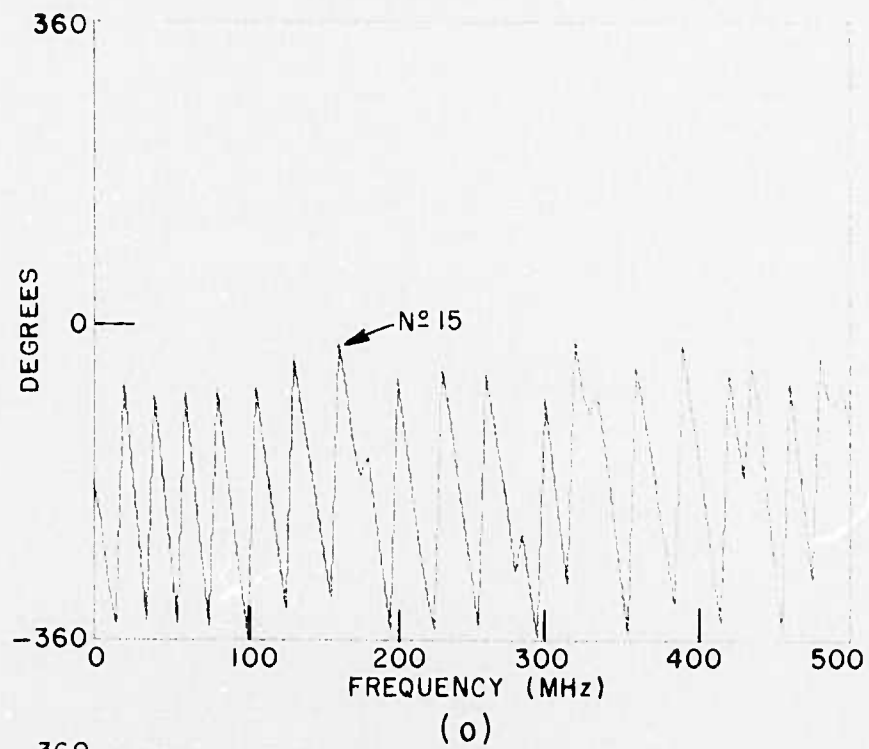Fig. 67b. (Continued)

158
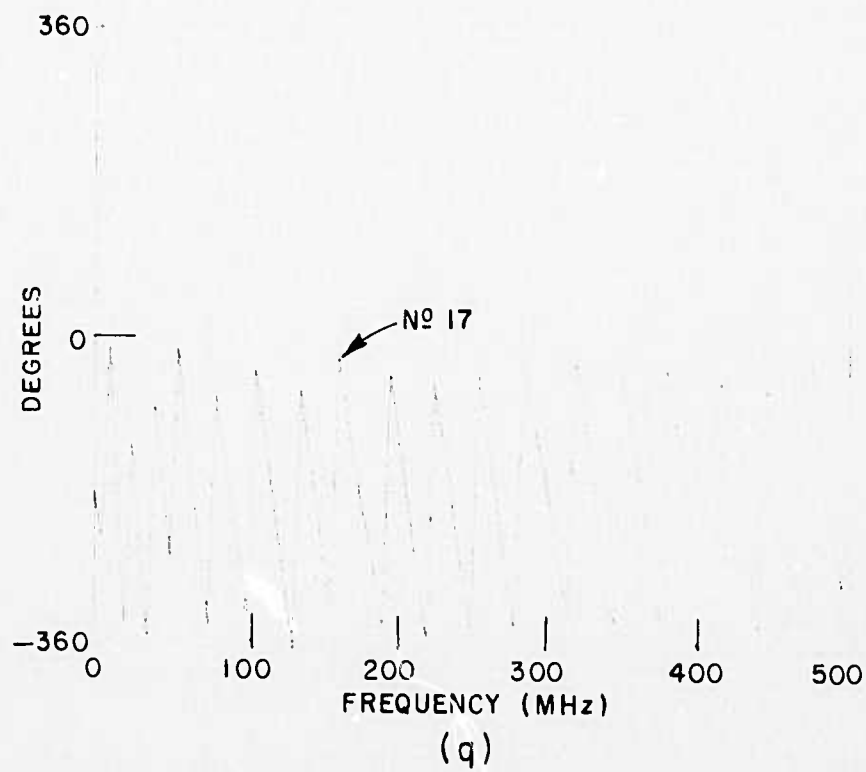
Fig. 67b. (Continued)
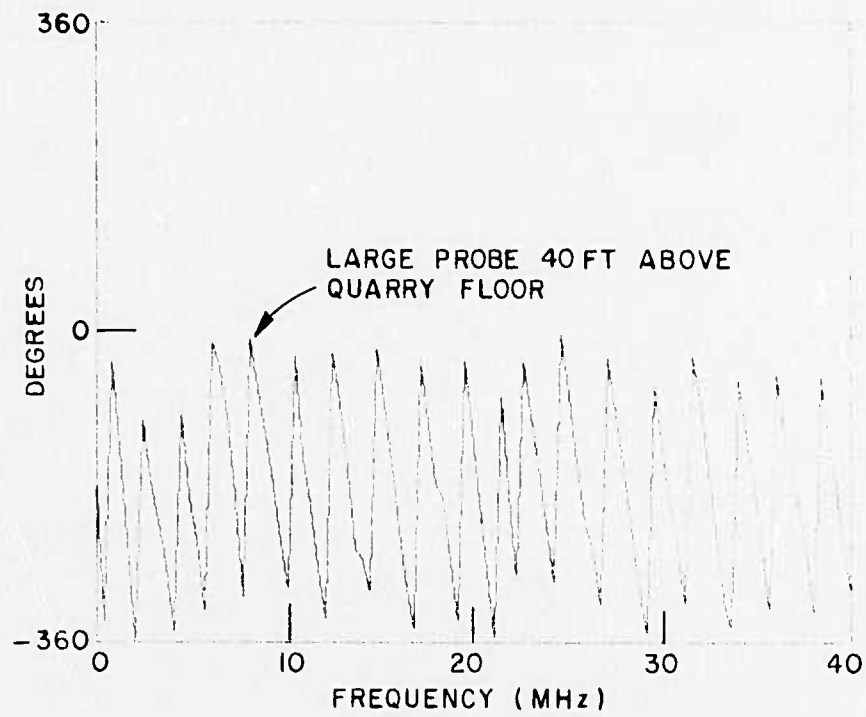
159

Fig. 67b. (Continued)

160
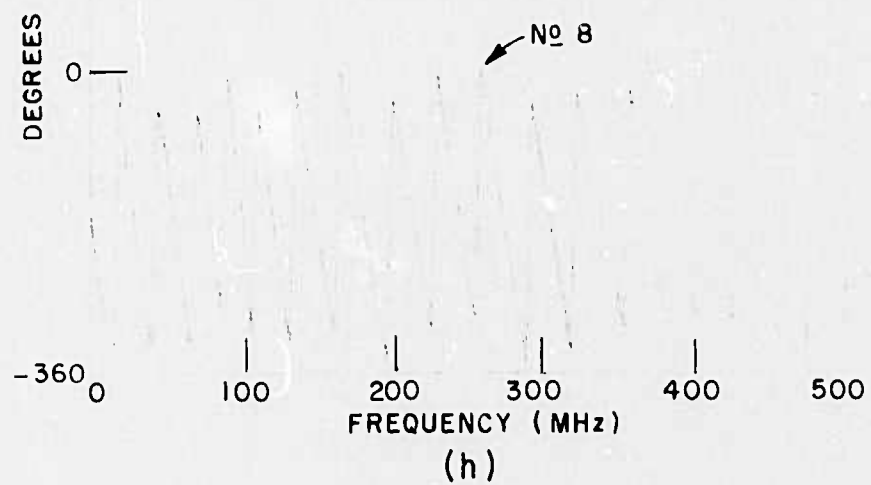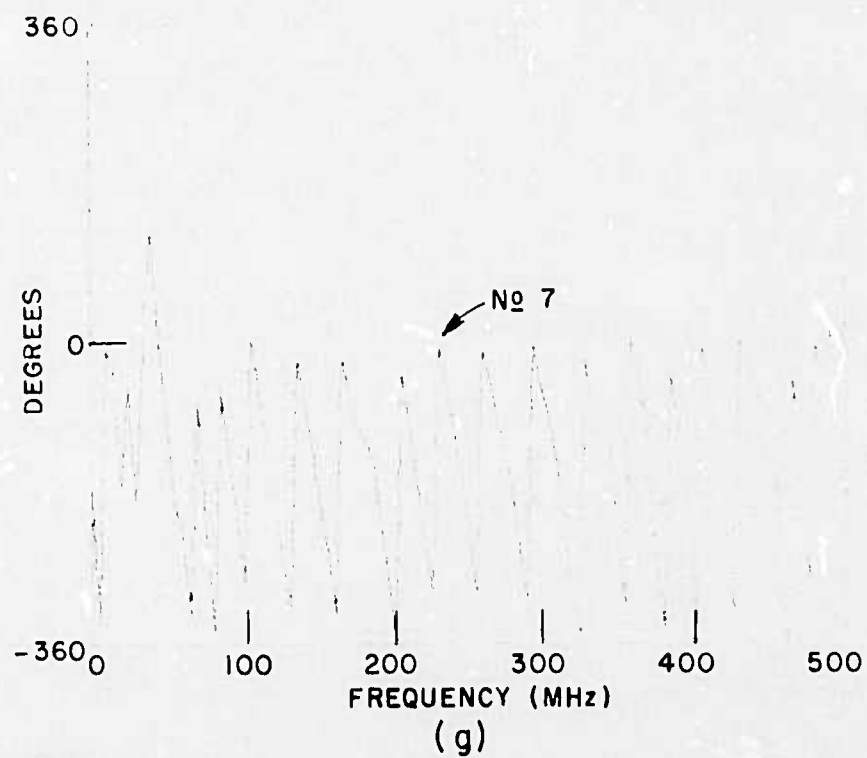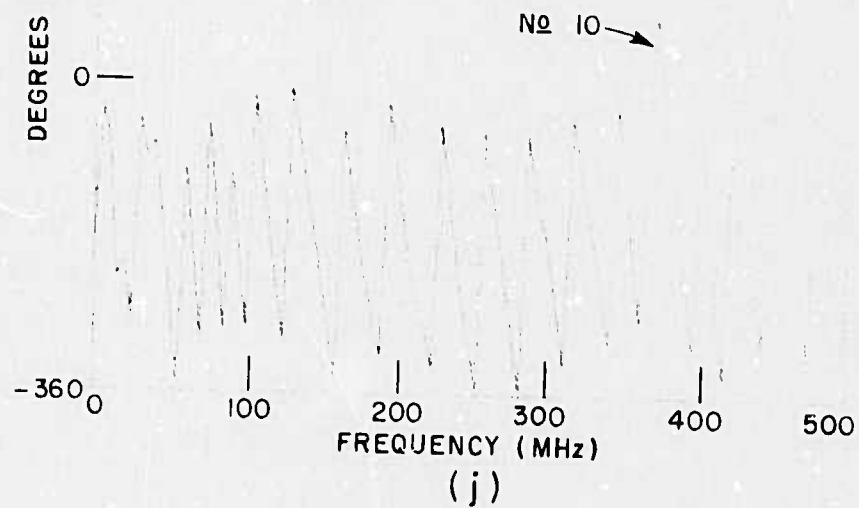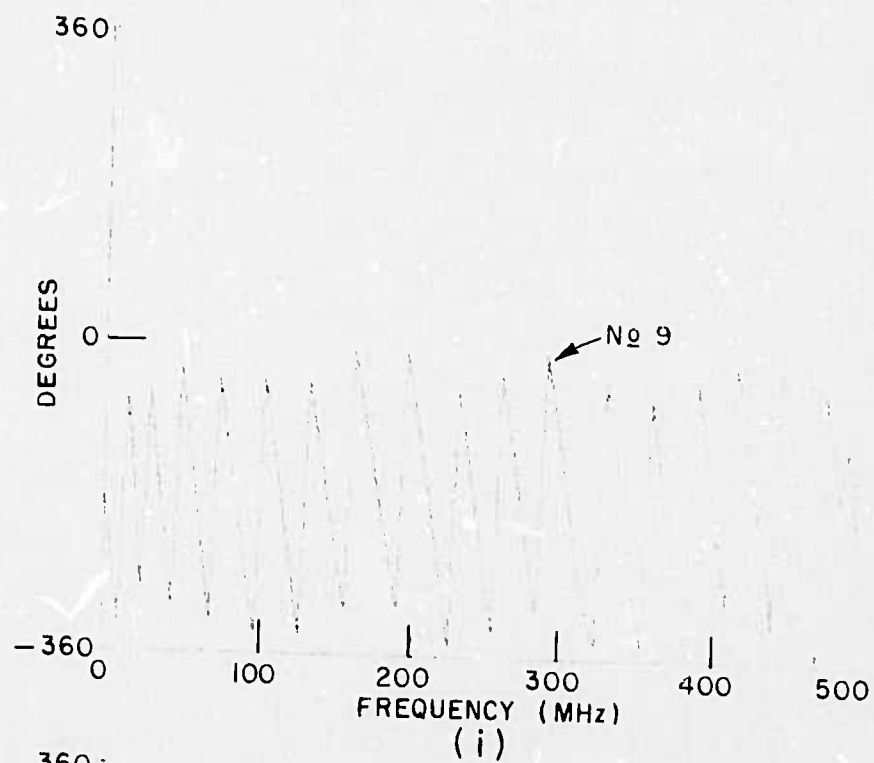
Fig. 67b. (Continued)

Fig. 70b.

Fig. 71b.

162
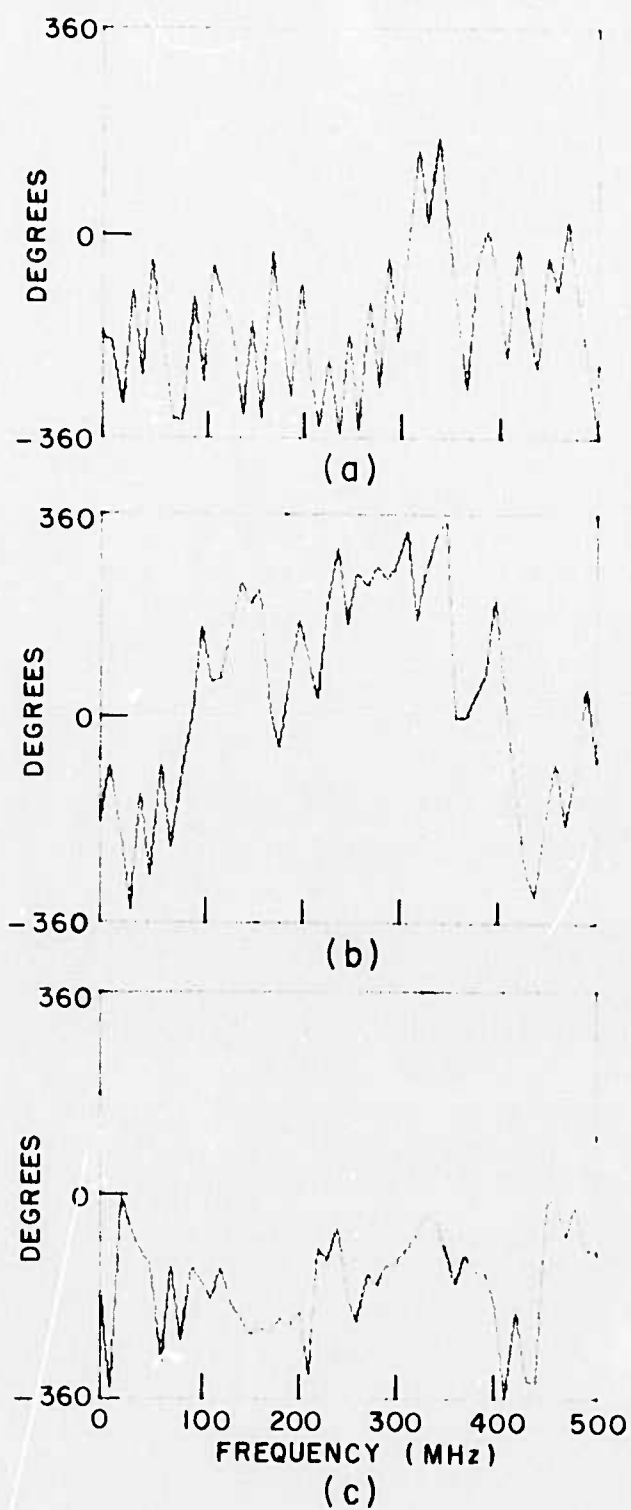
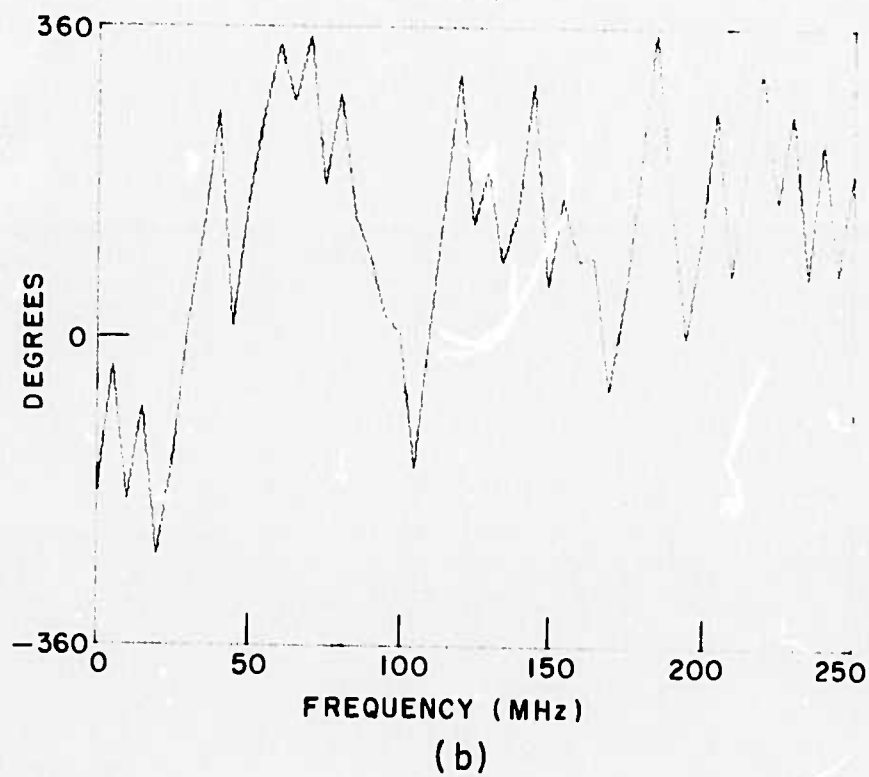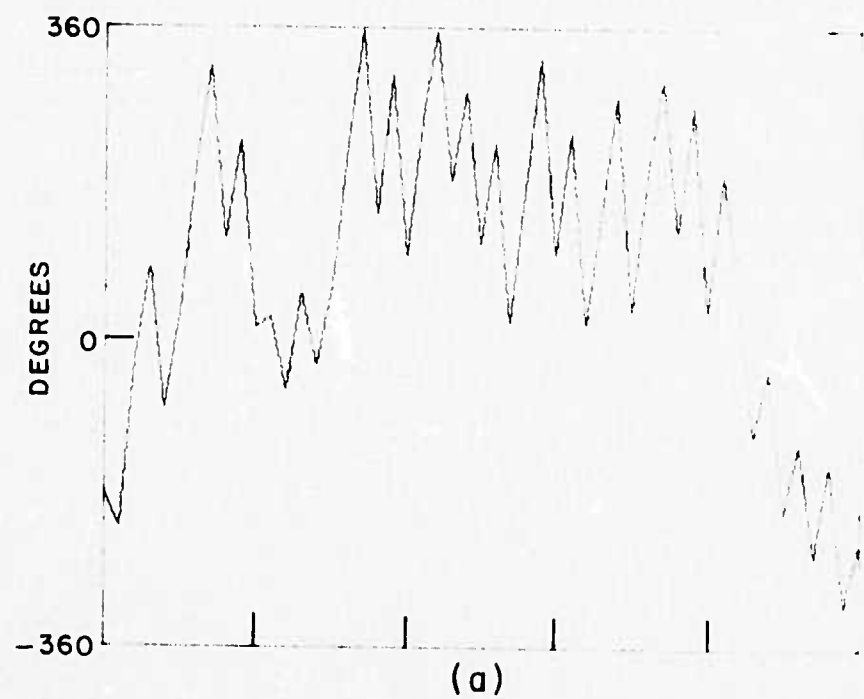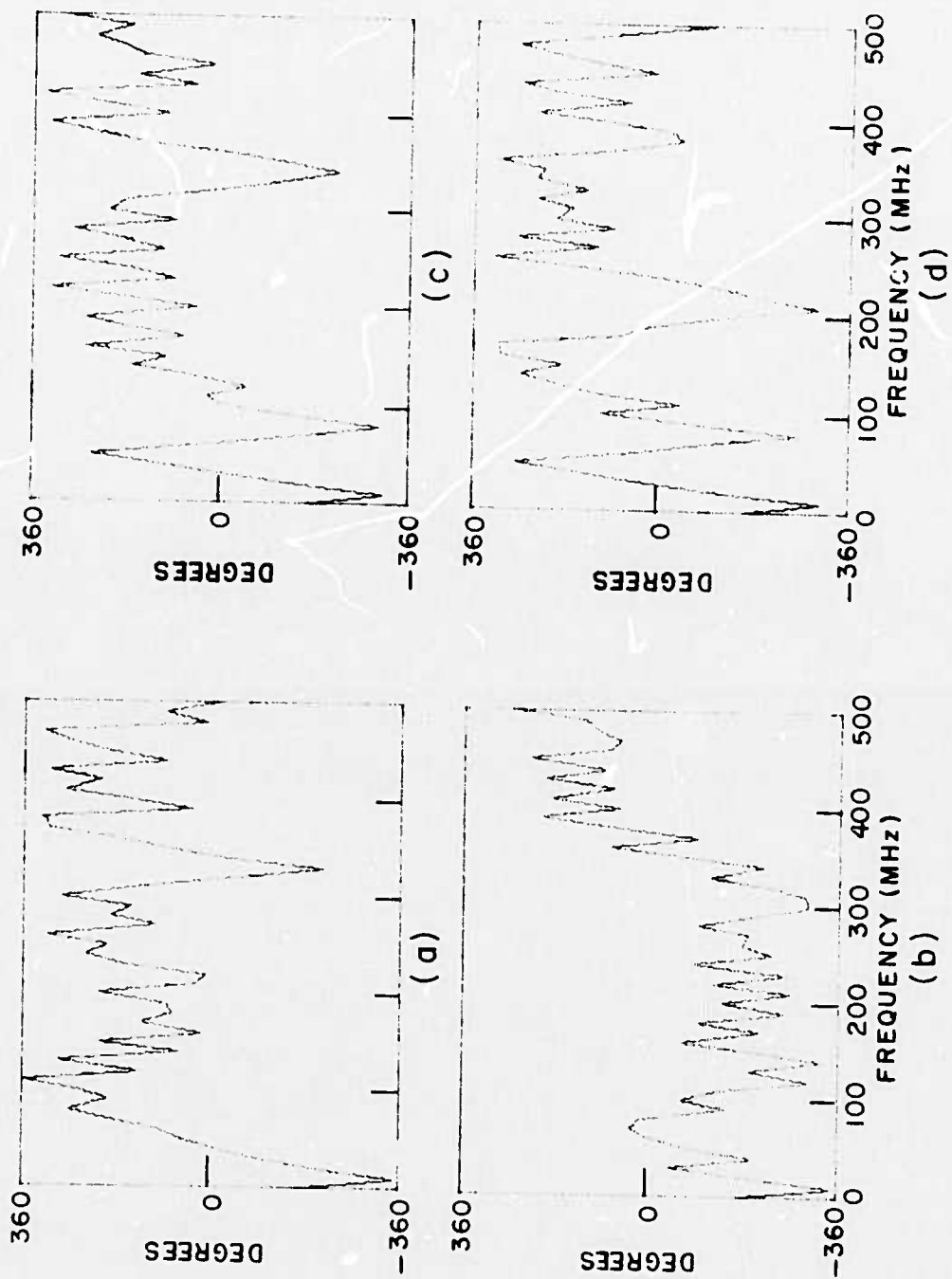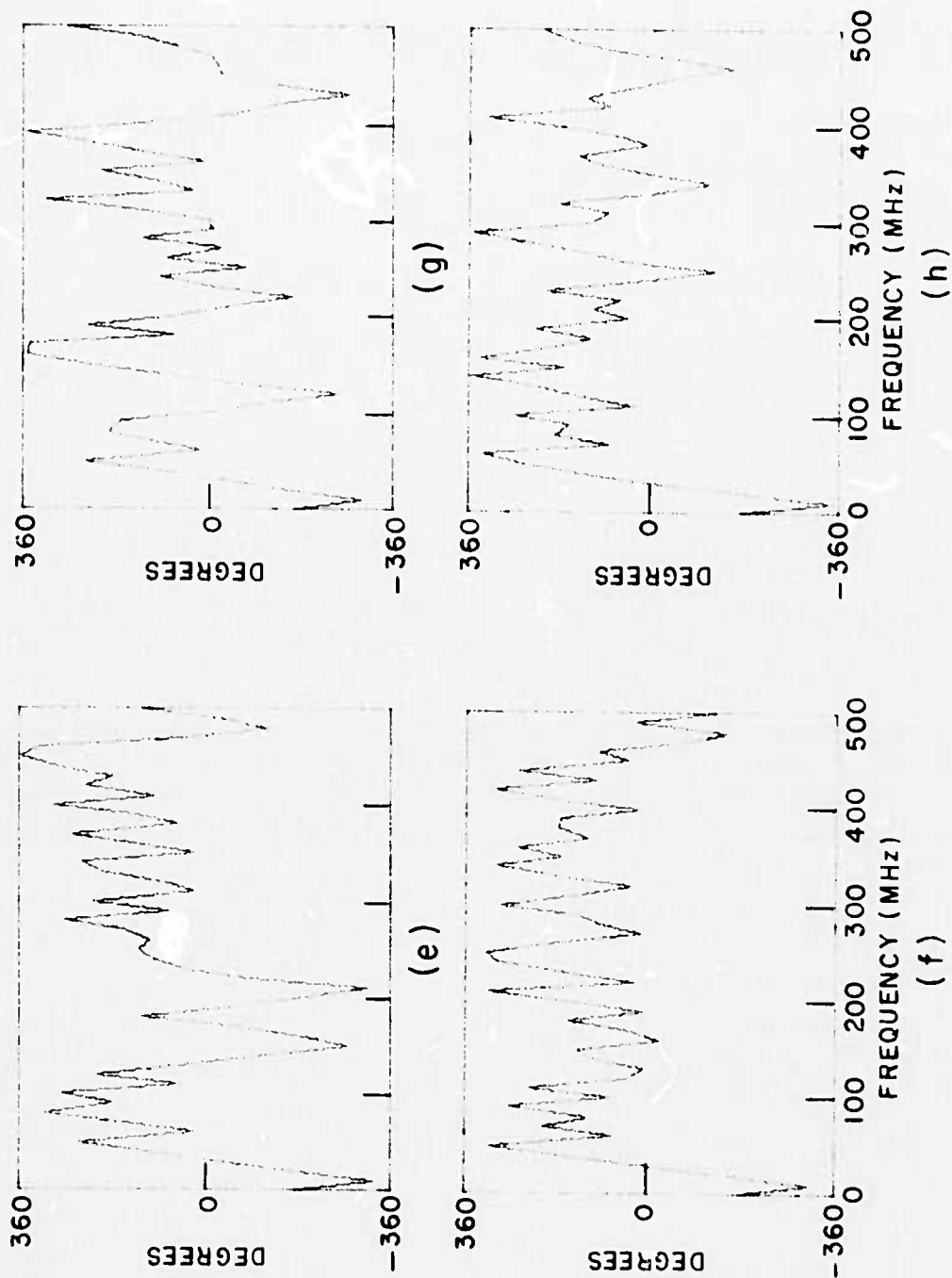Fig. 76b.

163

Fig. 79b.

164

Fig. 32b.

165
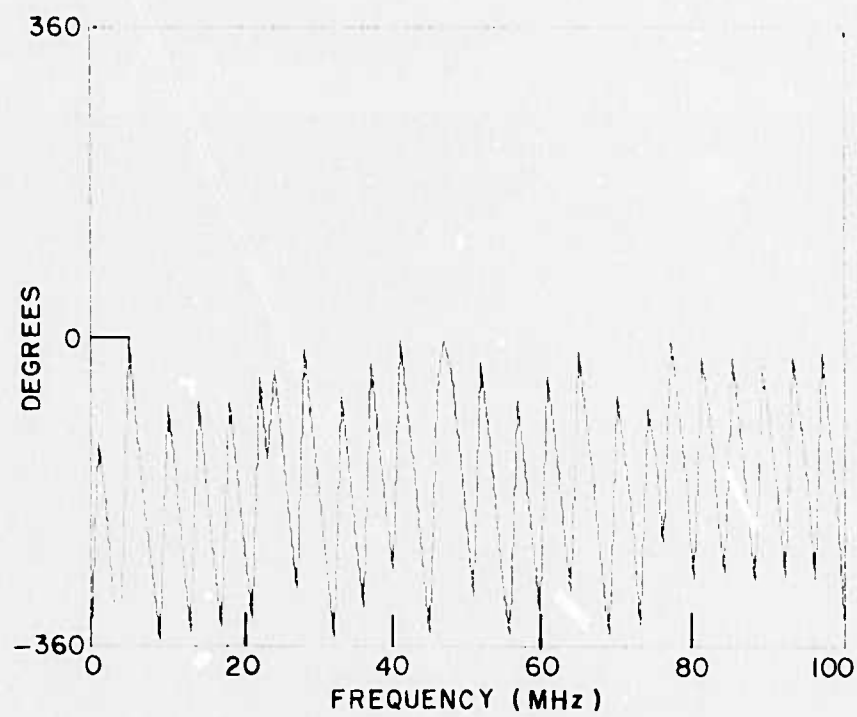
Fig. 82b. (Continued)

APPENDIX C
TUNNEL EFFECTS AND SYSTEM PERFORMANCE

In an actual hard rock tunnel geometry, 2 possible deleterious influences on performance of the electromagnetic probe are apparent. The first is the presence of large mining equipment a few inches from the probe on the working face and the second are the walls, roof and floor of the tunnel. It was documented in an earlier report[11] that the presence of an automobile actually within one quadrant of the large probe had absolutely no effect on the measured response waveforms. This was a reconfirmation of results reported even earlier[8]. We conclude without qualification that the mining equipment will not be a problem. Both the joint measurements reported in Section VII-D (Fig. 74) and the tunnel measurement in Section VII-B (Fig. 58) were made in the presence of a wall-type surface perpendicular or nearly perpendicular to the probe working surface. In particular the tunnel measurement (Fig. 58) was made quite close to a wall without any noticable effect of the wall. We conclude again that the walls, roof and floor of the tunnel should not interfer with operation of the electromagnetic video pulse sounder on the tunnel working face.

Documentation of the system performance is covered in Sections IV and VI. Section IV demonstrates the individual temporal and spectral effects of the coaxial feed cable, broadband impedance matching network (balun), twin lead transmission line and the antenna in a direct reflectometry mode. Results of tests on a new shielded transmission line are given in Section VII-D. Overall system performance is detailed in Section VI, where in particular the video pulses actually transmitted into the medium are given for both antenna structures and both video pulse signal generators.

It should also be noted that no computer programs were developed specifically on this program. As noted in Reference [8], the basic control and processing programs for video pulse signals were developed on earlier programs. The antenna programs utilized in Section VI were developed by Professor Richmond on other programs[14]. The basic computer program is detailed in Reference [20].

167

REFERENCES

1. Wait, J.R., "On The Theory of Transient Electromagnetic Sounding Over a Stratified Earth," Canadian Journal of Physics, Vol. 50, No. 11, 1972.

2. Vanyan, L.L., Electromagnetic Depth Soundings, Translated from Russian by George V. Keller, Consultant Bureau, 1967.

3. Kennaugh, E.M. and Moffatt, D.L., "Transient and Impulse Response Approximations," The Ohio State University Electro-Science Laboratory, reprinted from the Proceedings of the IEEE, Vol. 53, No. 8, August 1965.

4. Moffatt, D.L., "Time Domain Electromagnetic Scattering from Highly Conducting Objects," Final Report 2971-2, May 1971, The Ohio State University ElectroScience Laboratory, Department of Electrical Engineering; prepared under Contract F19628-70-C-0125 for Air Force Systems Command, Bedford, Massachusetts. (AFCRL-71-0319) (AD 885 883)

5. Irons, D.A., Jr., "Characteristic Spectra of the Electromagnetic Field Scattered by a Buried TMDB Mine," Report 2857-7, 15 March 1971, The Ohio State University ElectroScience Laboratory, Department of Electrical Engineering; prepared under Contract DaaK02-C-0693 for U.S. Army Mobility Equipment Research and Development Center, Fort Belvoir, Virginia.

6. Sullivan, W.B., "Short Pulse Measurements of Targets Immersed in a Lossy Half-Space," M.Sc. Thesis, The Ohio State University Electro-Science Laboratory, Department of Electrical Engineering, 1970.

7. Caldecott, R., Irons, D.A., Jr., Moffatt, D.L., Peters, L., Jr., Puskar, R.J., Toth, J.F., and Young, J.D., "Electromagnetic Pulse Sounding for Surveying Underground Water," Report 401X-1, October 1972, The Ohio State University ElectroScience Laboratory, Department of Electrical Engineering; prepared under Contract N00019-72-C-0184 for Naval Air Systems Command.

8. Peters, L., Jr. and Moffatt, D.L., "Electromagnetic Pulse Sounding for Geological Surveying with Application in Rock Mechanics and Rapid Excavation Program," Report 3190-2, September 1972, The Ohio State University ElectroScience Laboratory, Department of Electrical Engineering; prepared under Contract H0210042 for Bureau of Mines, Dept. Interior (ARPA).

9. Moffatt, D.L. and Peters, L., Jr., "An Electromagnetic Pulse Hazard Detection System," The Ohio State University Electro-Science Laboratory, reprinted from the Proceedings of the 1972 North American Rapid Excavation and Tunneling Conference, June 1972.

10. Young, J.D., et al, "A Memorandum on Buried Pipe Measurements," The Ohio State University ElectroScience Laboratory, Department of Electrical Engineering, Technical Note #4, July 1972.

11. Moffatt, D.L., Puskar, R.J., and Peters L., Jr., "Electromagnetic Pulse Sounding for Geological Surveying With Application In Rock Mechanics and the Rapid Excavation Program, Semiannual Technical Report 3408-1, The Ohio State University ElectroScience Laboratory, Department of Electrical Engineering; prepared under Contract H0230009 for U.S. Department of Interior, Bureau of Mines.

12. Irons, D.A., Jr., "A Computer Assisted Measurement System for Electromagnetic Impulse Sounding," M.Sc. Thesis, The Ohio State University ElectroScience Laboratory, Department of Electrical Engineering, December 1972.

13. Hewlitt-Packard Application Note 918.

14. Richmond, J.H., "Radiation and Scattering by Wire Structures in Active and Passive Media," Report 2902-10, The Ohio State University ElectroScience Laboratory, Department of Electrical Engineering, prepared under Grant Number NGL 36-008-138 for National Aeronautics and Space Administration, (in process).

15. Parkhomenko, E.I., Electrical Properties of Rocks, Plenum Press, 1967.

16. Wait, J.R., "Theory of Wave Propagation Along a Thin Wire Parallel to an Interface," Radio Science, Vol. 7, No. 6, June 1972.

17. Wait, J.R., "Propagation of Electromagnetic Pulses in a Homogeneous Conducting Earth,"Applied Scientific Research, Vol. 8, 1960.

18. Guidebook for Field Trips, The Geological Society of America, Cincinnati Meeting, 1961.

19. King, Ronold W. P. and Harrison, Charles W., Jr., Antennas and Waves, A Modern Approach, MIT Press, 1969.

20. Richmond, J.H., "Computer Program For Thin-Wire Structure in a Homogeneous Conducting Medium," Report 2902-12, August 1973, The Ohio State University ElectroScience Laboratory, Department of Electrical Engineering; prepared under Grant NGL 36-008-138 for National Aeronautics and Space Administration.